THE UNIVERSITY
of EDINBURGH

The Role of Natural Organic Matter in Binding Uranium and Incorporating Radiocarbon in Soils and Sediments

THE UNIVERSITY *of* EDINBURGH

Michael R. Muir

PhD

The University of Edinburgh

2017

Declaration

I certify that the work described in this thesis is my own, except where otherwise stated and has not been previously submitted for any other degree at this, or any other university.

Michael R. Muir

Acknowledgements

There have been many people involved in helping me to bring this project to completion and I would like to offer them my thanks.

Firstly, my supervisor Dr Margaret Graham who was always able provide help and encouragement, as well as offering her vast experience and insight into the technical details of the subject. The tireless dedication, energy and enthusiasm that Dr Graham puts into her work serves as an inspiration for those who work with her, and I have much gratitude for all she has done for me. I would also like to thank my supervisors Dr Gillian MacKinnon and Dr Dušan Uhrín who gave me great assistance with planning experiments and sample analysis.

I am very grateful to Dr Lorna Eades, Dr Clare Peters, Dr Nicholas Odling, Mr Jim Smith, Dr Juraj Bella and Dr Lorna Murray of the University of Edinburgh for sharing their expertise and training me in the use of the various preparative and analytical instruments I required for this project.

I would like to thank Professor Gordon Cook, Dr Graham Muir, Mrs Caroline Donnelly and others at SUERC who helped me with the analysis of radiocarbon and other radionuclides. I would also like to extend my thanks to Dr Gareth Law and Dr Adam Fuller of Manchester University and Professor Fred Mosselmans and others at the Diamond Light Source Synchrotron for their help with the analysis of my samples by X-ray absorbance spectroscopy.

I gratefully acknowledge the Natural Environment Research Council, Radioactive Waste Management and the Environment Agency for their funding of this project and the whole RATE program.

The support, insight, entertainment, help and friendship provided by Kenny, Ellen, Gavin, Andrew, John, James, Sarah, Sam and the others with whom I shared Lab 293 cannot be overstated. I feel very lucky to have had the opportunity to work alongside you all.

Finally, I would like to thank my family for their encouragement throughout and Rachel for her support, love and most importantly, patience.

Abstract

The impact of long-lived radionuclides on human health depends on their behaviour in near-surface soils and sediments and the LORISE project aims to define the key controlling physical, chemical and biological processes at a number of 'natural laboratories' around the UK. Within this PhD project, the role of natural organic matter (NOM) is of especial importance because NOM can potentially facilitate the transport or attenuation of radiologically significant elements such as U and radiocarbon (^{14}C).

Peaty soils in the vicinity of natural uranium mineralisations are often highly enriched in U with concentrations of up to 3000 mg kg^{-1}, 4000 mg kg^{-1} and 2500 mg kg^{-1} having been found in the US (Owen and Otten, 1995), Switzerland (Regenspurg *et al.*, 2010), and the UK (Xu, 2013), respectively. The NOM within these soils has been implicated in U retention but the controlling processes and the nature of interactions are poorly characterised. The Needle's Eye natural mineralisation, SW Scotland, provides a rare opportunity within the UK to investigate long-term U-NOM interactions.

Similarly, the well characterised inputs of radiocarbon into the Irish Sea from the Sellafield nuclear reprocessing facility since the mid-1960s present an opportunity to investigate the transfer of anthropogenic ^{14}C between environmental pools and trace its incorporation into coastal sediments. While the enrichment of sediment organic matter with anthropogenic ^{14}C has been identified, (MacKenzie *et al.*, 2004), the chemical and physical characteristics of NOM enriched with ^{14}C have not been investigated.

Currently, there is not a good understanding of which NOM components govern U binding or incorporate ^{14}C, and therefore the implications of the influence of NOM on radionuclide mobilisation or immobilisation are hard to assess.

In this study, the characteristics of organic matter from the Needle's Eye natural analogue site have been examined and the relationship with the geochemical properties of the site and U binding have been investigated. Further to this, NOM extracted from the Needle's Eye peat bog and from sediments of the Solway coast at the Southwick Merse has been fractionated and characterised using a range of spectroscopic techniques to identify the components of NOM which are responsible for binding U and those which incorporate anthropogenic ^{14}C.

The investigation of the properties of NOM at the Needle's Eye natural analogue site showed a high degree of spatial heterogeneity over a relatively small area, with variation in NOM characteristics seen between samples collected from different zones of the site, particularly evident in the transition from the highly organic, reducing peat bog to the inner saltmarsh. This was signified by an increase in aromaticity and humic character due to the change in vegetation from deciduous tree cover to dense saltmarsh grasses. NOM analysed in depth profiles from the highly organic, U-rich bog showed characteristics consistent with ageing and microbially driven humification processes, with an increase in humic acid content, decrease in oxygen containing functional groups and increased aromaticity with depth.

The analysis of U and other elements in the same samples showed that while the character of NOM is not the dominant factor in U accumulation, the characteristics of the NOM in the U-enriched zone, particularly the high amounts of aliphatic and oxygen containing NOM, are ideal for U binding. Analysis of Fe(II) and Fe(III) in porewaters suggest highly dynamic redox properties in the zone of U accumulation, first seen by Xu, (2013) and confirmed by this study. The variability in redox conditions is likely to lead to Fe-humic colloid precipitation and co-precipitation of U, acting as a mechanism of U removal to the solid phase. Analysis of samples from the Needle's Eye bog by x-ray absorption spectroscopy (XAS) confirmed, for the first time at this site, that the U was present in the

U(VI) oxidation state and was directly bound to the oxygen functional groups of organic matter.

The application of multiple NOM fractionation and characterisation techniques has made it possible to draw robust conclusions about the properties of NOM samples. The results showed the differences in NOM qualities between physically and chemically separated samples and samples of different origin.

Analysis of U in characterised NOM samples showed that it was preferentially bound in the large size fraction, which had more humic and aliphatic character, while smaller size fractions of more fulvic and aromatic character had a lesser association with U. These results showed that the type of NOM with U associated had relatively lower mobility and can therefore effectively retard U mobility for as long as the geochemical conditions remain favourable. Changes in pH or redox conditions could increase the mobility of NOM associated U.

Characterisation of NOM from the Southwick Merse salt marsh sediment using spectroscopic techniques and $\delta^{13}C$ analysis showed variation with depth due to the origin of NOM, with a greater proportion of marine NOM at depth which decreased towards the surface due to terrigenous inputs. NOM in the depth profile and in separated size fractions showed the increasingly aromatic character of terrigenous NOM compared to that of marine origin. ^{14}C analysis of extracted NOM showed ^{14}C concentrations enriched above background levels due to the anthropogenic inputs from Sellafield reprocessing facility. Analysis of extracted and fractionated NOM showed that the 0.1 M NaOH extractable NOM had increased ^{14}C activity compared to the non-extractable sediment organic matter. Analysis of NOM separated into size fraction showed that the NOM which was more enriched in ^{14}C was found in the larger size fraction, and was characterised by a more aliphatic character. The results of $\delta^{13}C$ analysis showed that this fraction, relatively enriched in ^{14}C, is of marine origin.

Lay Summary

Natural organic matter (NOM) is formed by the degradation of biological material of plant or animal origin once it is no longer living. It is a major component of soils at varying concentrations and is also found in surface waters and the marine environment. NOM is formed of a complex mixture of degradation products which are significantly different to the material from which they originated and has many different properties affecting the way it behaves in the environment. NOM is known to have a large capacity for binding metals and radionuclides and this process can cause the metals to be immobilised in the soil. However, certain components of NOM are highly soluble, reactive and mobile and can therefore enhance the mobility of metals or radionuclides they are associated with. This is a potential risk to plants, animals and humans who could be exposed to the potentially dangerous radionuclides if their mobility is promoted by association with NOM.

In this study, the properties of NOM are investigated to develop an understanding of which types of NOM could enhance or decrease the mobility of certain potentially dangerous radionuclides which are major components of nuclear waste. The investigation focuses on NOM collected from two natural settings which have higher than normal concentrations of particular radionuclides. The first is The Needle's Eye natural analogue site in South West Scotland, an area where uranium from a natural mineral vein has leached into a highly organic soil where it has become concentrated over a timescale of thousands of years. Although this is a natural occurrence, uranium is a radionuclide commonly found at high concentrations in nuclear waste, so analysing the processes controlling its mobility at this site can help to understand processes which might control its mobility elsewhere.

The results of this investigation show that the uranium is directly bound to organic matter and not mineral components of the organic soil. Further results show that the type of NOM

involved in uranium binding is likely to be stable and immobile, and not promote the mobility of uranium unless there is a large change in the soil conditions at the site.

A second radionuclide investigated is radiocarbon, or carbon-14 (^{14}C). Radiocarbon is potentially dangerous as it can be incorporated into biological material and is radioactive. Radiocarbon is discharged into the Irish Sea from the Sellafield nuclear waste reprocessing facility. In the Irish Sea it becomes incorporated into organic matter which is deposited in coastal sediments. Sediment samples from the Solway coast near Dalbeattie were collected and analysed, and the results show that the highest concentration of radiocarbon in coastal sediment NOM is found in a type of organic matter with large size and properties that make it unlikely to be reactive or mobile. This suggests that the radiocarbon incorporated into sediments is likely to remain stable without a great risk of coming into contact with plants, animals or humans.

Table of figures

Foreword

Project background: Introduction to the NERC – RATE consortium

This project forms one part of a Research Council UK (RCUK) programme "Radioactivity And The Environment" (RATE), a multi-disciplinary undertaking aiming to provide insight into the environmental behaviour of radionuclides. The programme, funded by the Natural Environment Research Council (NERC), Environment Agency (EA) and Radioactive Waste Management Limited, was commissioned to provide research relevant to the assessment of long-term nuclear waste storage. The research programme also has wider applications to the fields of nuclear power generation, long-term environmental radiation protection and radionuclide biogeochemistry. The RATE consortium comprised three groups each with their own theme:

- HydroFrame: "Hydromechanical and Biogeochemical Processes in Fractured Rock Masses in the Vicinity of a Geological Disposal Facility for Radioactive Waste"

- TREE: "TRansfer - Exposure – Effects: Integrating the science needed to underpin radioactivity assessments for humans and wildlife."

- Lo-RISE: "Long-lived Radionuclides in the Surface Environment: Mechanistic Studies of Speciation, Environmental Transport and Transfer"

This PhD project is part of the "Lo-RISE" consortium which includes academics, researchers and students from 10 UK institutions. The research carried out as part of Lo-RISE investigates processes controlling the transport of radionuclides in soils and sediments, the marine environment and the biosphere. Results from the Lo-RISE project are intended to complement modelling assessments of environmental radionuclide transport in the development of a long-term geological repository for radioactive waste.

1. Uranium and radiocarbon in the environment

Uranium-238 (^{238}U) and radiocarbon (^{14}C) are naturally occurring radionuclides with significantly different sources, physical properties and geochemical behaviour that, mainly due to human activities, pose a significant potential risk to human health and the environment. Uranium-238 is a "primordial" radionuclide, one which has been present since the formation of the Earth, and is relatively uniformly dispersed in the Earth's crust at a concentration of 1 – 3 mg kg^{-1} (Heier, 1965). Radiocarbon is a "cosmogenic" radionuclide which is constantly formed in the upper atmosphere by the interaction of fast neutrons with ^{14}N. It has a half-life ($t_{1/2}$) which is approximately 6 orders of magnitude lower than ^{238}U. Anthropogenic nuclear activities have created pathways for the release of high concentrations of these radionuclides to the environment, predominantly as a by-product of energy production and weapons manufacture and testing, and have thereby increased the potential risk to human health and the environment over the last century (UNSCEAR, 2008; Ewing, Runde and Albrecht-Schmitt, 2010).

The key factor in estimating radiological risk is understanding the pathways from sources to receptors which are controlled by the environmental behaviour of the radionuclide, specifically its mobility through different environmental pools, such as transfers from geological materials to surface waters and uptake by biota. The mobility of radionuclides in the environment is complex and dependent on many factors such as the chemistry of the radionuclide and the chemical and physical characteristics of its local environment (M. Eisenbud and Gesell, 1997b; Till, 2008).

In this chapter properties, sources, geochemistry, mobility in the surface environment and the risks posed to human health and the environment are discussed; first for U and then for ^{14}C. A description of the sources, structure and properties of natural organic matter (NOM) is presented and its interaction with ^{14}C and U is discussed.

1.1. Properties and natural sources of uranium

Uranium exists naturally as three isotopes, all of which are radioactively unstable and decay primarily by emission of an α (alpha) particle. The most common is ^{238}U which has an abundance of 99.28% (Table 1.1). (Holden, 1981; Rumble, 2017)

Table 1.1. Isotopes of uranium with their natural abundance and half-life (Holden, 1981; Rumble, 2017).

Natural isotope	Natural abundance	Half-life ($t_{1/2}$)
^{238}U	99.28 %	4.47×10^9 years
^{235}U	0.72 %	7.037×10^8 years
^{234}U	0.0055 %	2.45×10^5 years

Uranium-238 and ^{235}U have been present on the Earth since its formation, around 4.6×10^9 years ago, and have not yet completely decayed as they each have a very long $t_{(1/2)}$ of billions and hundreds of millions of years, respectively (Table 1.1). The other natural isotope, ^{234}U, is the product of α decay of ^{238}U and the subsequent β (beta) decay of ^{234}Th and ^{234}Pa (Kirby, 1954; Eisenbud and Gesell, 1997; Alloway, 2013; Rumble, 2017). The position of each of these U isotopes within the natural decay series is shown in Figures 1.1 and 1.2. Uranium-238 and ^{235}U are the parent nuclides in the uranium and actinium series, respectively.

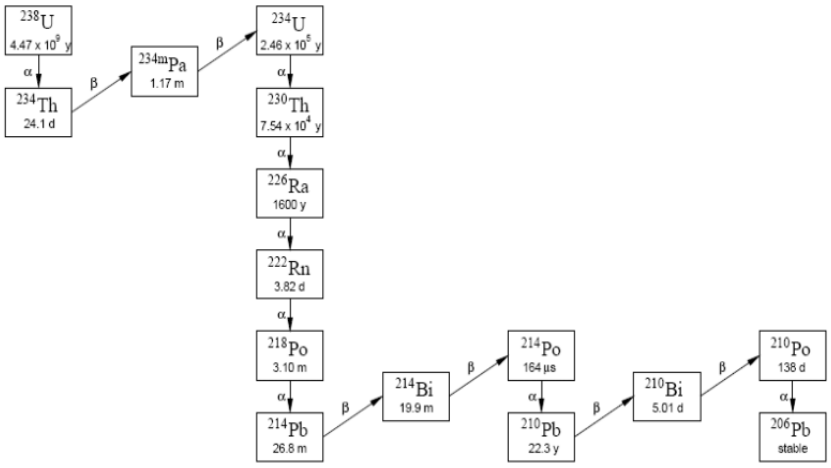

Figure 1.1. Uranium series natural decay chain (IAEA, 2010).

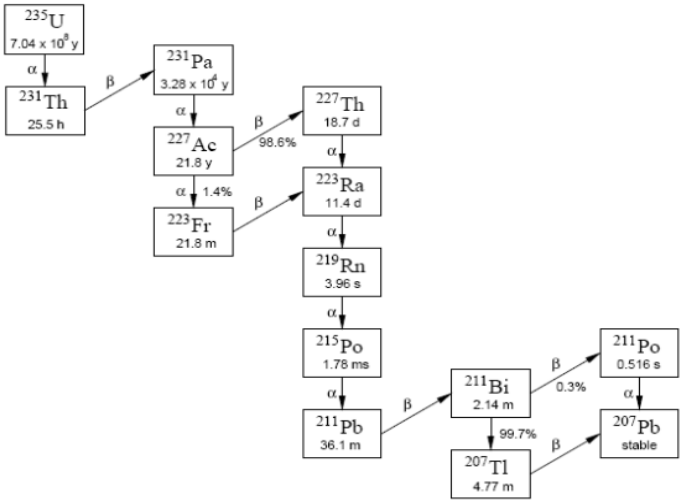

Figure 1.2. Actinium series natural decay chain (IAEA, 2010).

The parent nuclides in the natural decay chains slowly decay via α emission, thereby transmuting to the first daughter nuclide in the chain. The daughter nuclides decay sequentially by α or β emission over variable lengths of time ranging from fractions of a second to hundreds of thousands of years. Often the nuclear decay is also accompanied by the emission of high energy γ (gamma) radiation as the nucleus of the daughter nuclide decreases from an excited state to a more stable state by emission of a photon of energy. Each decay chain ends when a stable isotope of Pb is formed, i.e. ^{206}Pb and ^{207}Pb in the uranium and actinium series, respectively (Figures 1.1 and 1.2).

Table 1.2. Uranium minerals mined as a source of U (Ritcey, 1996).

Type	**Mineral**	**Formula**
Oxides	Uraninite	UO_2
	Pitchblende	$(U^{IV}_{1-x}U^{VI}_{x})O_{2+x}$
	Gummite	
	Becquerelite	$7UO_3.11H_2O$
Mixed Oxides	Brannerite	$(U, Ca, Fe, Th, Y)(Ti, Fe)_2O_6$
	Davidite	$(Fe, Co, U, Ca, Zr, Th)_6(Ti, Fe, V, Cr)_{15}(O,OH)_{36}$
	Pyrochlore	$(Na, Ca, Fe, U, Sb, Pb, Th, Zr, Ce, Y)_2(Nb, Ta, Ti, Sn, Fe)_2 O_6 (O, OH, F)$
Silicates	Coffinite	$U(SiO_4)_{1-x}(OH)_{4x}$
	Uranophane	$Ca(UO_2)_2 (SiO_3)_2(OH)_2.5H_2O$
	Uranothorite	$(Th,U)SiO_4$
Phosphates	Autunite	$Ca(UO_2)_2(PO_4)$ 10 to 12 H_2O
	Torbernite	$Cu(UO_2)_2 (PO_4)_2$. $12H_2O$
Vanadates	Carnotite	$K_2 (UO_2)_2(VO_4)_2$. 1 to 3 H_2O
	Tyuyamunite	$Ca(UO_2)_2(VO_4)_2$ 2.5 to 8 H_2O
	Thucholite	

N.B. No formulae for gummite or thucholite are given as these exist as non-crystalline amorphous mixtures.

Uranium is present at elevated levels in granites and phosphate rocks (Ritcey, 1996; Pulford, 2010). Uranium tends to form secondary minerals along the crystal boundary of

mineral phases as it doesn't readily fit into the crystal structure of other minerals and tends to stay in solution in magma or aqueous solution until the final stages of solidification occur (Wilson, 1996).

Approximately 200 uranium minerals have been identified of which around 15 are mined to produce uranium for use in the nuclear fuel cycle. The latter are listed in Table 1.2, reproduced from Ritcey (1996).

Uranium is also dispersed throughout soils and the surface environment. The concentration of U in soil is highly variable, but generally less than 10 mg kg^{-1} is considered to be a "background" concentration (Pulford, 2010; Alloway, 2013).

1.1.1. Geochemistry of uranium

Uranium can exist in oxidation states of +IV, +V or +VI with +IV and +VI being the most important. Uranium(V) may exist as the UO^{2+} ion, however the U(V) oxidation state only tends to form at low pH values and intermediate redox potentials and is much less stable than the U(IV) or U(VI) species (Langmuir, 1997; Renshaw *et al.*, 2005). The oxidation state of U is a major factor controlling its environmental mobility as U in the VI oxidation state is highly soluble whereas the reduced form, U(IV), is insoluble. Uranium is sensitive to redox changes and U(IV) can readily undergo chemical oxidation when subjected to aerobic conditions. The opposite reaction of U(VI) reduction is most often facilitated by microorganisms but can also take place abiotically with various mineral forms of Fe(II) as the reducing agent (Liger *et al.*, 1999; Behrends and Van Cappellen, 2005; Suzuki and Suko, 2006; Fox *et al.*, 2013; Veeramani *et al.*, 2013; Hyun *et al.*, 2014). Bioreduction of U(VI) is an important mechanism of U immobilisation by the formation of insoluble U(IV) compounds (Renshaw *et al.*, 2005; Newsome *et al.*, 2014). Highly organic soils accumulate high concentrations of U and effectively act as a U sink and a barrier to its mobility (e.g.

Read *et al.*, 1993; Bordelet *et al.*, 2013). The mechanisms involved in U accumulation in organic soils are still not well understood. These are discussed in more detail in section 1.7.1.

1.1.1.1. Analysis of U oxidation state

The importance of the oxidation state of U in controlling its solubility and adsorption properties means that it is one of the key parameters to analyse when assessing mechanisms of U mobility. However, the sensitivity of U(IV) to oxidation on exposure to air means that it is important that samples are handled carefully. Uranium oxidation state is tricky to measure directly and there are only a few techniques which can be used.

A popular method of U oxidation state analysis is x-ray absorbance spectroscopy (XAS) (e.g. Warren and Haack, 2001; Kelly, 2010; Fox *et al.*, 2013; Veeramani *et al.*, 2013; Li *et al.*, 2014). This technique is described in detail in section 2.3.

1.1.2. Uranium speciation in soils and surface waters

The pH and redox conditions have a large impact on the speciation and associations of U in the environment, as do the U concentration in solution, the ionic strength, temperature, pressure and carbonate concentration. These variables influence the aqueous speciation of U which in turn affects the ability of U to bind onto mineral and organic phases (Garrels, 1953; Li *et al.*, 1980; Echevarria *et al.*, 2001; Lesher and Honeyman, 2009; Chew, 2013; Cumberland *et al.*, 2016).

In an aqueous system with CO_2 excluded and a low U concentration of 10^{-8} M the dominant dissolved species at a pH of 5 or lower is UO_2^{2+} (figure 1.4). An increase in pH causes hydrolysis to occur and the U speciation to change to $UO_2(OH)^+$ at a pH of around 5.5 – 7 while from pH 7 -8 $UO_2(OH)_2^0$ is the dominant species. Increasing the U concentration to 10^{-4} M (figure 1.5) increases the importance of the $(UO_2)_3(OH)_5^+$ ion, making it the dominant species from pH 5 - 8. With this increase of U concentration from 10^{-8} to 10^{-4} M comes a change of charge of the dominant species above pH 7 from neutral to positive. However, such simple systems are not found in the environment and in the presence of air the formation of carbonate complexes influences the U speciation, as can be seen in figures 1.6 and 1.7.

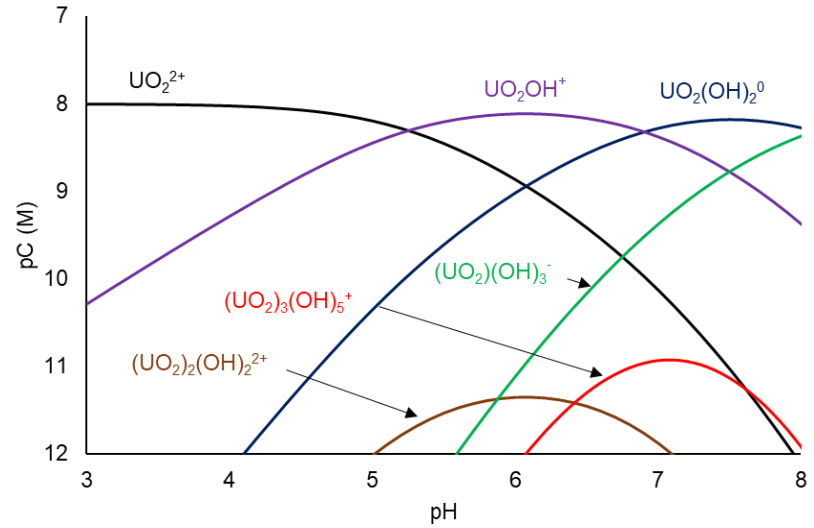

Figure 1.4. Uranium(VI) speciation in an aqueous system with changes in pH and the exclusion of CO_2. Uranium(VI) concentration = 10^{-8} M. Speciation modelled using Visual Minteq 3.1 (Gustafsson, 2014) with reference to Waite et al., 1994.

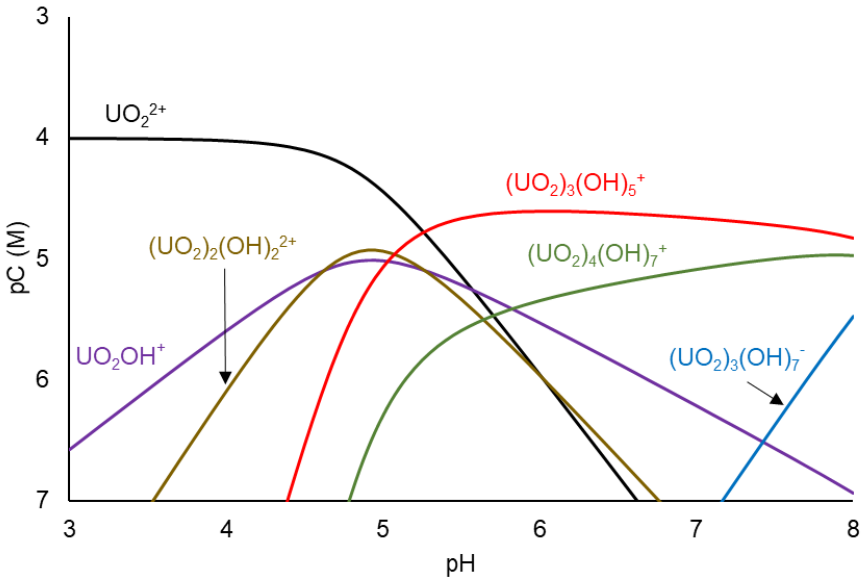

Figure 1.5. Uranium(VI) speciation in an aqueous system with changes in pH and the exclusion of CO_2. Uranium(VI) concentration = 10^{-4} M and ionic strength (I) = 0.1. Speciation modelled using Visual Minteq 3.1 (Gustafsson, 2014) with reference to Waite et al., 1994.

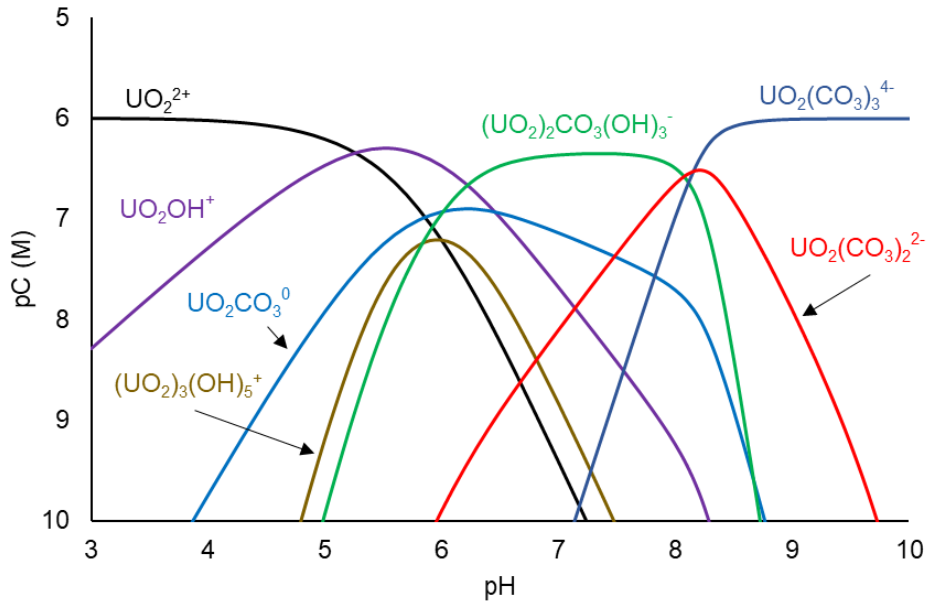

Figure 1.6. Uranium(VI) speciation in an aqueous system with changes in pH in the presence of CO_2 at a partial pressure of $10^{-3.5}$ atm. Uranium(VI) concentration = 10^{-6} M. Speciation modelled using Visual Minteq 3.1 (Gustafsson, 2014) with reference to Waite et al., 1994.

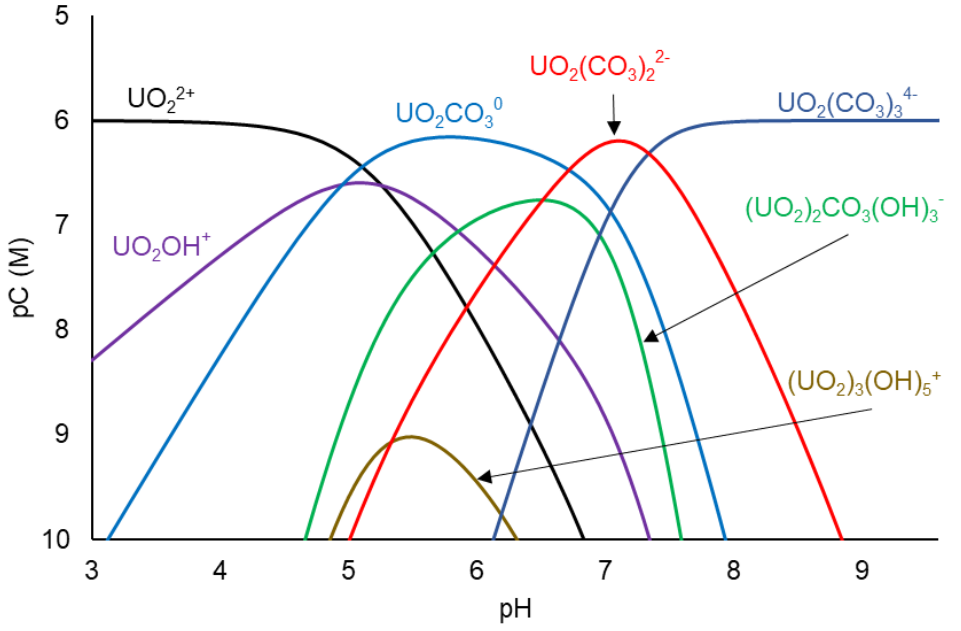

Figure 1.7. Uranium(VI) speciation in an aqueous system with changes in pH in the presence of CO_2 at a partial pressure of 10^{-2} atm. Uranium(VI) concentration = 10^{-6} M. Speciation modelled using Visual Minteq 3.1 (Gustafsson, 2014) with reference to Waite et al., 1994.

Dissolved CO_2 in solution has a significant effect with U-hydroxy-carbanato complexes forming at low CO_2 partial pressure. At increased partial pressure carbonate complexes are the dominant species at pH>5 (Waite *et al.*, 1994).

The variation in speciation affects the sorption of U onto soil binding surfaces such as minerals and organic matter due to the changing charge of the U species and the pH dependent charge of adsorbent surfaces. The negative charge of species formed by U at higher pH, such as $UO_2(CO_3)_3^{4-}$ at pH > 8 (Waite *et al.*, 1994), inhibit the binding of U onto negatively charged functional groups of Fe-oxides, and humic substances. Uranium species with positive or zero charge, formed at near neutral pH or below, can take part in adsorption processes on negatively charged surfaces. This leads to the formation of a variety of U(VI) complexes with carbonates, bicarbonates, minerals and humic substances (Read *et al.*, 1993; Braithwaite and Livens, 1997; Zhou and Gu, 2005; Graham *et al.*, 2011; Wang *et al.*, 2013; Yang, Saiers and Barnett, 2013; Fan *et al.*, 2014).

Uranium has maximum adsorption onto Fe oxide minerals at a pH range between 5 and 8.5 in a system open to atmospheric CO_2 (Waite *et al.*, 1994). Li *et al.*, (1980) showed that the association of U with OM is pH dependent and that the characteristics of the OM involved are important, finding that U dissociates from fulvic acid at a pH of 5, while it remains associated with humic acid down to a pH of 4. Echevarria *et al.*, (2001) showed that there is a linear relationship between soil binding of U and pH over the range 5.5 to 9.0 with U preferentially binding to soils below pH 7. It is clear from these results that U speciation and pH are important factors in U adsorption onto soil surfaces.

1.1.3. Uranium isotope fractionation

If a parent nuclide has a much longer half-life than its daughter then, if left undisturbed, a state of secular equilibrium will be reached, a point at which the activity (in Becquerel, Bq, where 1 Bq = 1 disintegration per second) of both the parent and daughter nuclide is equal. This process takes around 7 half-lives of the daughter nuclide (Bourdon *et al.*, 2003; Murray and Holbert, 2015). The natural decay series are useful in assessing geochemical processes because chemical reactions can cause isotope fractionation which creates a deviation in the activity ratio from unity. In rocks which have been stable for more than 10^6 years the ratio of $^{234}U/^{238}U$ should have reached secular equilibrium and be unity. However, when rock containing mineralised uranium is exposed to weathering processes chemical and radiological processes can affect a specific isotope. For example, when an atom of ^{238}U decays to ^{234}U by emission of an α particle the force of the ejection causes "alpha recoil," the simultaneous recoil of the ^{234}U atom in the opposite direction to the α emission. If the atom is within around 200 Å of a mineral surface, including internal fractures and pore space, then it can be directly ejected from the rock. A secondary mechanism occurs due to the etching of the mineral structure around where the α particle is emitted which allows chemical weathering to degrade the mineral and release the ^{234}U into solution. The ^{234}U is ejected as a free radical which makes it likely to oxidise to U(VI) and thereby remain soluble in solution and be transported away from the original source rock (Aitken *et al.*, 1980). This causes a decrease of the $^{234}U/^{238}U$ ratio in the rock as ^{234}U is preferentially removed and also causes the ratio to increase in the soil or water environment outside the mineral (Tokarev *et al.*, 2006). The $^{234}U/^{238}U$ ratio can therefore be used to assess whether U is stable or being mobilized from a site.

1.2. Properties and natural sources of radiocarbon

Radiocarbon (^{14}C) is a natural cosmogenic isotope formed in the upper atmosphere when a nitrogen atom is bombarded with cosmic radiation and absorbs a thermal neutron. In this process a proton is lost from the nucleus so the overall mass, 14, remains the same but the atomic number decreases by 1 from 7 (N) to 6 (C) (Eisenbud and Gesell, 1997b; Balonov *et al.*, 2004). The production of ^{14}C is summarised in equation 1.1:

$$^{14}_{7}N + {}^{1}_{0}n \rightarrow {}^{14}_{6}C + {}^{1}_{1}p \qquad \textit{Equation 1.1}$$

This reaction produces ^{14}C, the only radioactive isotope of C, which has a $t_{1/2}$ of 5730 ± 40 years, and a natural abundance of 1 atom of ^{14}C for every 10^{12} atoms of ^{12}C. Radiocarbon is a low energy beta particle emitter and as such does not pose a great radiological risk at natural background concentrations. At elevated concentrations, however, it is a significant radiological hazard (Balonov *et al.*, 2004) (See section 1.4.).

The half-life of ^{14}C and the fact that it is ubiquitous in the natural world makes it a very useful tool in tracing global carbon processes and calculating the age of archaeological materials up to 60,000 years old (IAEA, 2002; Cook, Scott and Harkness, 2010; Taylor and Bar-Yosef, 2014). A figure for the background level of natural ^{14}C in living organisms and the atmosphere is around 250 Bq of ^{14}C per kg of stable carbon. This value is used by the National Radiological Protection Board in the UK, as well as authorities in France and Switzerland, to determine the impact of sources of ^{14}C other than that which is cosmogenically created in the upper atmosphere (Eisenbud and Gesell, 1997b; Balonov *et al.*, 2004; Magnusson, 2007).

1.2.1. The global carbon cycle: Carbon in aqueous and terrestrial environments

As this study aims to investigate the character and mobility of OM from terrestrial, fresh water and marine environments it is important to understand the movement of C between global reservoirs and the processes that affect the mobility or stability of C. The transfer of C between the lithospheric, atmospheric, biospheric, terrestrial and marine pools is described by the global carbon cycle. The major reservoirs of the global carbon cycle are summarized in table 1.3.

Table 1.3. Reservoirs in the global carbon cycle (Sundquist *et al.*, 2009)

Environmental Carbon Reservoir	**Approximate duration of storage**	**Gigatons of carbon stored, (GtC)**
Atmosphere	Years	590
Vegetation	Decades	680
Soils	Centuries	3,200
Ocean	Centuries	37,000
Reactive Sediments	Millenia	3,000
Fossil fuels	Millenia	>6,000
Geologic	Millenia	78,000,000

The largest amount of carbon is held in the lithosphere which contains around 78 million gigatons of carbon (GtC), although this is predominantly inert as it is resistant to most of the key biological breakdown processes. The oceans are the next greatest reservoir of carbon, storing around 37,000 GtC. In comparison, the amount of C in soils, 3200 GtC, is relatively small. Carbon in soils, oceans and surface waters is in constant exchange with atmospheric CO_2, either through biota via respiration and photosynthesis or through gas exchange as gaseous CO_2 dissolves into, or is evolved from aqueous solution. An important aspect of the behaviour of C is its ability to exist in both inorganic and organic forms, and transfer between the two.

Inorganic carbon can form soluble or insoluble mineral species which may be readily characterised and provide a vital role in many environmental processes, for example pH buffering and formation of complexes.

The dissolution of CO_2 in water and subsequent ionisation to bicarbonate and carbonate anions takes place in the following sequence:

$$CO_2\,(g) \rightleftharpoons CO_2\,(aq) \qquad \text{Equation 1.2}$$

$$CO_2(aq) + H_2\,O\,(l) \rightleftharpoons H_2\;CO_3\,(aq) \qquad \text{Equation 1.3}$$

$$H_2\,CO_3\,(aq) \rightleftharpoons H^+(aq) + HCO_3^-\,(aq) \qquad \text{Equation 1.4}$$

$$HCO_3^-\,(aq) \rightleftharpoons H^+(aq) + CO_3^{2-}(aq) \qquad \text{Equation 1.5}$$

The dominant species present in solution changes as the pH is increased. This is shown in the speciation diagram below (figure 1.9).

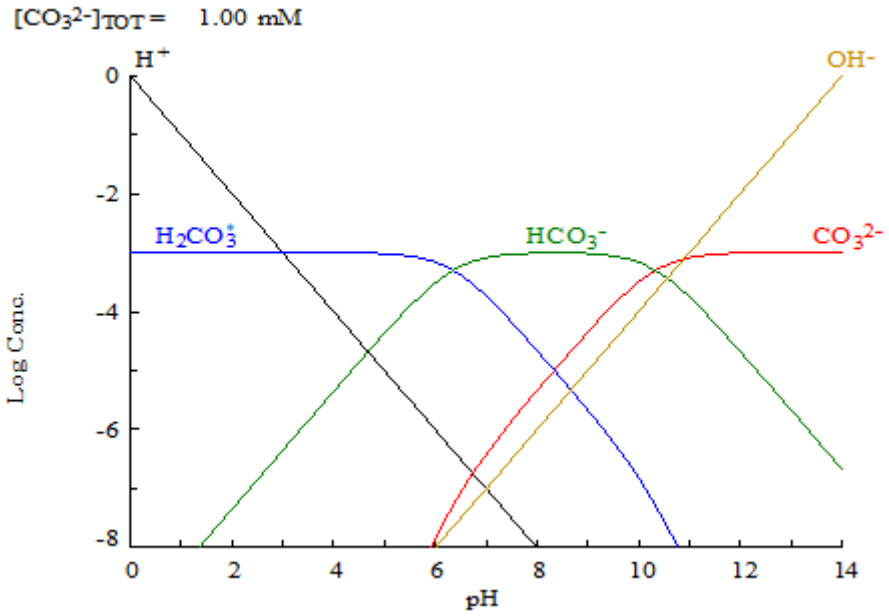

Figure 1.9. Speciation of bicarbonate ions in aqueous solution at different pH calculated using Hydra-Medusa Speciation software (Puigdomenech, 2013).

At a pH between 3 and 6 the dominant species of C is $H_2CO_3^*$, which is the sum of dissolved CO_2 and H_2CO_3 in solution. This is predominantly truly dissolved $CO_{2\ (aq)}$. A low pH of < 4 favours the evolution of gaseous CO_2 which escapes to the atmosphere. Bicarbonate is the most important species between pH 6 and 10 while at high pH of 10 or above carbonate dominates. The speciation of inorganic carbon, affected by pH, temperature and ionic strength, is important when considering the of solution chemistry of metals due to the range of complexes that can be formed under different conditions as is shown above for U, in section 1.1.2.

The dominant transfer of C from inorganic to organic forms occurs via photosynthesis in plants. In the terrestrial environment atmospheric CO_2 is incorporated into plants while in freshwater and marine systems dissolved C in the form of HCO_3^- is incorporated into plants by photosynthesis. Bicarbonate can also be mineralized as $CaCO_3$ by molluscs and other organisms in shell forming processes (Fabry *et al.*, 2008). Carbon incorporated into plants, in both the terrestrial and marine environments, can then in turn be incorporated into the cells of heterotrophic organisms. When organisms die their remains are decomposed into CO_2 and increasingly stable forms of carbon such as peats, humic substances and eventually fossil fuels (e.g. Stevenson, 1982). Organic C incorporated into soils, for example in the form of humic substances, may be stable and immobile for thousands of years, however it could also become incorporated into biota, dissolved in surface waters or transferred to the marine environment (Battin *et al.*, 2009; Sundquist *et al.*, 2009). Rivers carry C of terrigenous origin into the oceans as truly dissolved or suspended particulate material. This C may be used up rapidly as a substrate for microbial respiration or accumulate in seabed and coastal sediments (Hedges, Keil and Benner, 1997). The accumulation in sediments can act as a long-term sink for C, however in highly dynamic coastal or marine environments sediments and the C within them are subject to erosion and transport

(MacKenzie *et al.*, 1994). Organic forms of C in the environment are involved in a wide range of environmental processes and are not straight forward to characterise due to the complex mixtures they form comprising thousands of interacting organic molecules with diverse physical and chemical properties (see section 1.6).

1.2.2. Carbon isotopes as tracers of organic matter origin

Although the isotopes of carbon can be used interchangeably in chemical and biological processes their very small difference in mass does lead to fractionation during certain reactions. This can be exploited to ascertain the origin of organic molecules which have undergone natural degradation and mobilisation processes. The differences in the concentration of ^{13}C in a sample relative to an international standard can occur as a result of the carbon source ($CO_{2(g)}$ or $HCO_3^-{}_{(aq)}$) and photosynthetic pathway (e.g. C_3 or C_4) a plant uses (Hackney and Haines, 1980; Maberly, Raven and Johnston, 1992). This property has been successfully employed to trace the origin of organic C in water and sediments as marine or terrestrial (e.g. MacKenzie *et al.*, 2004; Chikaraishi *et al.*, 2005; Abdulla *et al.*, 2010).

1.3. Anthropogenic sources of U and ^{14}C

1.3.1. Uranium

Uranium is often introduced to the environment at concentrations higher than natural levels due to anthropogenic activities. These include mining and milling of U ore, use of depleted uranium in armouries manufacture, storage and reprocessing of nuclear waste, accidents at nuclear facilities, nuclear weapons manufacture and testing, dispersal of fly ash from coal power plants and use of phosphate fertilizers over long timescales (e.g. Pulford, 2010). With so many potential sources it is no surprise that environmental contamination with uranium is a problem seen in locations worldwide. Mobilisation of U from mining activities has been reported in Portugal (Favas *et al.*, 2016; Viseu, Carvalho and Oliveira, 2016), the USA (Dias da Cunha *et al.*, 2014), France (Phrommavanh *et al.*, 2013), China (Wang *et al.*, 2016) and the UK (Miller *et al.*, 1994) to name just a few. Uranium contamination is found at military test sites where depleted uranium munitions are used (Johnson *et al.*, 2004; Oliver *et al.*, 2008) and phosphate fertilizer use acts as a diffuse U source due to the high concentrations of U found associated with phosphate rocks (Ritcey, 1996; Pulford, 2010).

1.3.2. Radiocarbon

The main contaminant sources of radiocarbon are from the operation of nuclear power plants (Yim and Caron, 2006; Magnusson, 2007), nuclear waste reprocessing such as that at Sellafield reprocessing facility (Cook *et al.*, 1995; Bracke and Müller, 2008), and the atmospheric detonation of nuclear weapons which approximately doubled the global atmospheric radiocarbon concentration (Levin and Kromer, 2004; Currie *et al.*, 2009). In the following sections some sources of U and ^{14}C to the environment arising from the nuclear industry are described.

1.3.3. Nuclear waste: characteristics, disposal and long-term fate

In the pioneering early days of nuclear research and innovation in the UK, the rush to develop technology capable of harnessing the energy of radionuclides outpaced the understanding of how to deal with waste material generated. The first development of nuclear weapons in the 1940's and the inception of the civilian nuclear power programme in 1955 led to the creation of large amounts of nuclear waste, much of which has remained unprocessed and remains part of the 4.5 million m^3 UK nuclear waste inventory (Collingridge, 1984; NDA and DECC, 2014). The subsequent growth of nuclear power as an energy source in the UK and globally caused a concurrent growth in nuclear waste production and, although management of this waste is much improved since the early days, only a single long-term waste storage facility is operational worldwide, in the USA (US Department of Energy, 2017). Many unique issues are involved in the storage of nuclear waste which add to the complexity of developing a long-term storage solution. These include the long timescales involved, the dangers of handling radioactive material, the large volumes of poorly characterised legacy waste and the complicated mixture of radionuclides involved. The choice of materials involved in the construction of such storage facilities is also an important consideration as some materials may cause changes which could influence radionuclide mobility, for example by the increase in pH associated with use of cement (Stockdale and Bryan, 2012; Bots *et al.*, 2014). Since its first proposal in the late 1950's, (US National Research Council/ National Academy of Sciences, 1957) there is a general consensus in the scientific community that the safest and most practical method of storing nuclear waste is in a deep underground repository, built in a stable rock formation with adequate barrier controls in place to prevent radionuclide escape to the environment. However, due to the number of confounding factors involved in implementing such a plan, detailed investigations and a thorough understanding of processes which could occur under storage conditions are necessary. The importance of a thoroughly reviewed "safety case"

for any possible geological storage facility is highlighted in a report by the International Atomic Energy Agency (IAEA, 2003), which states the necessity for understanding the radionuclide transport processes involved on both the near and far field scales. This includes the mechanisms that could affect the mobility of radionuclides in the surface environment.

Nuclear waste is categorised according to its activity into one of four main groups, described below (Health and Saftey Executive, 2001; Bayliss and Langley, 2003a; IAEA, 2009):

High Level Waste (HLW)- Waste with high activity (10^4 – 10^6 TBq/m^3) predominantly from a high concentration of long lived radionuclides which will pose a risk to health long after the effectiveness of engineered barrier systems can be guaranteed. Temperature increase must be taken into consideration for the storage of this waste as the high activity can generate significant amounts of heat. The main type of waste which fits into this category is the liquid residue from reprocessing fuel rods. This liquid is vitrified into a borosilicate glass substance and clad in steel before long term sequestration at depths of hundreds of meters. (DEFRA, 2008)

Intermediate Level Waste (ILW) – Waste which contains a high concentration of long-lived radionuclides with a high activity, but does not produce large amounts of thermal energy. This waste mostly arises from the reprocessing of fuel rods and can be in a solid or liquid state. The proposed storage method is to contain in cement in steel barrels which can then be stored below ground. Depths of tens to hundreds of meters are recommended.

Low level waste (LLW) – Low radionuclide concentration waste which has an activity of no more than 4 GBq/tonne of alpha radiation or 12GBq/tonne of beta and gamma radiation. This waste tends to be disposed of by super compaction in steel drums and

storage a few meters below the ground surface. Most LLW comes from sources other than power generation, such as hospitals, universities and industry. It has a high volume but accounts for only a tiny fraction of the total radioactive waste inventory for the UK.

Very low level waste (VLLW) – Waste which requires no special disposal protocol and can be disposed of as landfill as it contains less than 400 kBq β or γ activity per 0.1 m^3 of waste.

Some components of nuclear waste are subject to specific controlled disposal licenses, for example liquid effluent containing ^{14}C is discharged into the Irish Sea from the Sellafield reprocessing facility up to a limit of 21 TBq per year (Sellafield Ltd, 2011).

Since uranium is the fuel used in almost all operational nuclear power plants, it is found in high volumes in waste streams. Fuel rods typically contain enriched uranium comprising ~97% ^{238}U and ~3% fissile ^{235}U. Only 1 – 3% of a uranium fuel rod is used up in a thermal nuclear reactor and what is left is predominantly ^{238}U contaminated with small amounts of un-used ^{235}U, other actinides, e.g. isotopes of Pu, Am, and fission products. The spent fuel rods may be reprocessed to extract ^{235}U and ^{239}Pu which can be used again, but even after reprocessing there is a large amount of uranium-containing waste generated which requires disposal as high level waste due to the high temperatures and high radioactivity caused by the short lived fission products it contains (Wilson, 1996; Wallbridge, Banford and Azapagic, 2012; NDA and DECC, 2014).

Radiocarbon is also a very significant component of nuclear waste and is considered to be the highest contributor of radiation dose to the global population from anthropogenic nuclear activities (Jones *et al.*, 2013). Radiocarbon is generated in nuclear reactors by the interaction of ^{13}C, ^{14}N, ^{15}N, ^{16}O and ^{17}O with fast neutrons. The isotopes of C, N and O listed above occur as impurities in the fuel, in structural material or in cooling water (Balonov *et al.*, 2004; Magnusson, 2007). The amount of ^{14}C created by a nuclear power

plant is highly dependent on the type of reactor and fuel used, with magnox fuel gas cooled reactors creating the highest volume and fast breeder reactors the least, generating around 30 times less GBq of ^{14}C per GW of energy per year. Much of the ^{14}C from nuclear facilities is produced as CO_2 gas which is either vented to the atmosphere or precipitated as barium carbonate to limit releases of radioactive material (Wilson, 1996). Some of the ^{14}C is released as a liquid effluent under license, for example Sellafield discharged 6.4 TBq of ^{14}C to the Irish Sea in 2011 and only 0.4 TBq to the atmosphere (Sellafield Ltd, 2011). However, prior to a change in discharge policy in 1994 atmospheric discharges were the primary route for Sellafield radiocarbon (Tierney *et al.*, 2015).

The effects of being in the vicinity of operational nuclear facilities and waste stores have been seen all over the world with increased incorporation of radionuclides into biota which can accumulate throughout the food chain and increased radiation dose to people living in the area (Nedveckaite, Gudelis and Vives i Batlle, 2013; Sohrabi *et al.*, 2013; Muir *et al.*, 2017; Tierney *et al.*, 2017). The potential risks to human health, organisms and the environment U and ^{14}C pose because of their mobility and their chemical and radiological toxicity (section 1.4) means that it is of the utmost importance to understand how they behave over long timescales in the natural environment (Bryan *et al.*, 2012). This understanding will help with the development of safe long-term geological sequestration facility, inform the regulation of very low-level radioactive waste discharges and, ultimately, minimise the health risk to future generations.

1.3.4. Radioactive waste from the Sellafield reprocessing facility: Discharges to the Irish Sea

The Sellafield nuclear reprocessing facility has discharged nuclear waste to the Irish Sea since the site began generating nuclear power in 1951. Formal regulation of the discharge was not put in place until 1954 with the introduction of the Atomic Energy Authority Act, 1954. The discharges consisted of a concentrated solution of medium activity effluent

which was the product from two reprocessing systems in operation, along with untreated fuel storage tank water. This liquid effluent was discharged directly into the Irish Sea via a system of pipes which extended approximately 2.5 km from the high-water mark. The opening of a fuel storage water treatment plant at the end of the 1970s and the termination of discharging reprocessing plant effluent in 1980 contributed to a large decrease in the activity of waste discharged to the Irish Sea from 1975 onwards (Gray, Jones and Smith, 1992) The commissioning of the Enhanced Actinide Removal Plant (EARP) further reduced radionuclide discharges into the Irish Sea (Vintró *et al.*, 2000).

Environmental monitoring is a requirement of the Radioactive Substances Act, 1993 (DEFRA, 2011) which are implemented in England and Wales as the Environmental Permitting (England and Wales) Regulations, 2010, (DEFRA, 2013). Sellafield Ltd. produces an annual report of all environmental discharges that take place over a year and compares them to the limits imposed by the Environment Agency (Sellafield Ltd, 2011). This includes a detailed evaluation for each radionuclide, which allows easy comparison with the discharge limits and the data collected from previous years. The annual reports list all radioactive material discharged to the Irish Sea, to the atmosphere and taken to specialist landfill, as well as the potential radiation dose that residents in the vicinity of the site could be receiving from activities at the facility. The accumulation of some radionuclides in certain organisms, seawater and sediments is also reported. The reports are a valuable source of information that can be included in environmental studies.

A wide range of radionuclides are discharged at variable concentrations. These nuclides exhibit radiological and chemical toxicity which makes understanding their mobility in the environment particularly important, in order to limit their paths to receptors. Discharged radionuclides become dispersed throughout the Irish Sea and eventually become incorporated into coastal sediments. It is possible to see elevated levels of ^{14}C as well as

other radionuclides in sediments the Southwick Merse due to these discharges. (Kershaw et al., 1990)

1.3.4.1. Inputs to the Irish Sea from the Albright and Wilson "Marchon" Phosphate Plant

The "Marchon" factory was opened in Whitehaven in 1941 and initially produced detergents which had high phosphate content. In the 1950s, the factory started production of phosphate fertilisers and, at a later stage, high purity phosphoric acid, both of which involved importing phosphate-rich rock from overseas as the feedstock for the chemical manufacturing processes. The reason that the plant is of interest from a radionuclide perspective is because phosphate-rich rocks have high concentrations of U associated with them, of up to 152 mg kg^{-1} (ARPANSA, 2005). A large volume of waste from the processing of the phosphate was discharged into the Irish Sea which led to the average input of around 40 tonnes U per year, 10 times that of Sellafield origin. McCartney *et al.* (1990) attribute the high concentrations of unsupported ^{210}Pb in the Irish Sea basin to the natural decay series nuclides discharged into the water from the Marchon phosphate plant. Over the nearly 70 year lifetime of the plant, which ceased phosphate activities in the year 2000 (Kennedy and Atkinson, 2006), this input represents a considerable inventory of uranium and its daughter nuclides in the Irish Sea, which can become deposited in coastal and sub-tidal sediments, remain in solution or become incorporated into biota.

1.3.4.2. Input from Chernobyl fallout

Following the catastrophic failure of the Chernobyl nuclear power plant, Ukraine, in 1986 a large plume of radioactive particles was released into the atmosphere. The prevailing weather conditions at the time of the accident directed the plume over south-west Scotland and north-west England where rainfall caused a large amount of radioactive material to be washed out of the atmosphere and deposited. In particular, this led to elevated concentrations of ^{137}Cs and ^{210}Pb, especially in upland areas of these parts of the UK (McKenna and Longworth, 1995; Bell and Shaw, 2005). Despite the significant concentrations of radionuclides that were deposited over the UK, for example the 100 – 10,000 Bq m^{-2} of ^{137}Cs deposited on grass in the UK as the contaminant cloud passed over (Clark, 1986; Bell and Shaw, 2005), the signal from Chernobyl fallout in Irish Sea coastal sediments is swamped by the radionuclide inputs from Sellafield (Thomson, Dyer and Croudace, 2002).

1.4. Health risks associated with uranium and radiocarbon

1.4.1. Types of ionising radiation

Ionising radiation is the term for a particle or wave which has the ability to cause ionisation of atoms it comes into contact with. There are three mechanisms by which radiation can be released from the nucleus of a radionuclide: α, β and γ, decay, each characterised by the emission of an energetic particle or photon. In α decay a particle equivalent to a He nucleus, consisting of two protons and two neutrons, is ejected from the nucleus of the radionuclide. The relatively large α particle has a high ionisation energy over a short distance. A nucleus which has emitted an α particle has a reduction in mass of 4 amu (atomic mass units) for example ^{238}U to ^{234}U. The short distance that α radiation can travel in air means that it only poses a radiological risk when an α emitting radionuclide is taken into organisms and is in

close proximity to sensitive tissues, in which case it can cause large amounts of damage to cells and DNA.

Beta radiation is the emission of an electron at high speed from the nucleus. The small size of an electron means that it is less likely to interact with the nuclei of other atoms and therefore can travel longer distances of up to10 m in air and around 1 cm in a solid. This greater degree of penetration increases the radiological health risk to organisms as the β particle can get through barriers like skin and have damaging ionising effects on sensitive organs. Ejecting an electron from the nucleus changes the charge of a nucleus but only has a tiny effect on the mass so a radionuclide which decays by β emission transmutes into a different element, as is shown in the case of ^{14}C below (equation 1.6):

$$^{14}_{6}C \rightarrow {}^{14}_{7}N + e^{-} \qquad \text{Equation 1.6}$$

Finally, γ radiation is the term for emission of a high energy photon when a nucleus in an excited energy state, usually following α or β decay, loses energy to return to a stable ground state. The photon has very high penetration ability and can pass through organisms without any interaction occurring (Bayliss and Langley, 2003b; Keith, Doyle and Harper, 2012).

1.4.2. Uranium: Risk to health

^{238}U and ^{235}U decay via α-emission therefore are a radiological health risk to organisms only if ingested or inhaled. Perhaps more significantly, uranium also has acute chemical toxicity. This is exemplified in the World Health Organisation recommended upper limit for U in drinking water, which is only 30 μg L^{-1} (WHO, 2012). Uranium is not essential for any biological processes and the health effects of chronic U ingestion are varied, with impact on the reproductive system, nervous system, brain and links to birth defects (Taylor and Taylor, 1997; Brugge and Buchner, 2011). Chronic exposure of up to 9 μg kg^{-1} body

weight is known to result in kidney toxicity (Zamora *et al.*, 1998), however, studies of communities in Finland with water supplies contaminated with up to 1,500 µg L^{-1} U have shown that the toxicity is strongly related to the U speciation and oxidation state, with high concentrations of calcium uranyl carbonate species not showing a toxic effect, highlighting the importance of understanding the chemistry of U in the environment (Kurttio, Harmoinen, *et al.*, 2006; Prat *et al.*, 2009). Uranium is also a radiological hazard and around 30% of internal radiation dose received by UK residents is from nuclides in the U and Th natural decay series, equating to approximately 3.7% of the total natural radiation dose (Watson *et al.*, 2005). In parts of the world where people are exposed to high U concentrations (> 100 µg L^{-1} in drinking water) due to contamination of food and water there is a link to increased instances of cancers such as bladder cancer and leukaemia (Kurttio, Salonen, *et al.*, 2006; Winde, Erasmus and Geipel, 2017).

In the environment, U has been shown to have the ability to be taken up by certain plants and in some cases bioaccumulate to very high concentrations and have significant phytotoxicity in soils with high U concentration (Sheppard, Evenden and Anderson, 1992; Babula *et al.*, 2010). Plants can also aid in the transfer of U to herbivores as it becomes enriched in the upper parts of some plants which are then eaten (Gramss and Voigt, 2014). The US Environmental Protection Agency (USEPA) and US Geological Survey (USGS) use an estimate of toxicity of chemicals in the aquatic environment termed the "effect concentration" (EC), which for U in surface waters is 2.7 µg L^{-1} (Kostich *et al.*, 2017). This relatively low value shows the potential risk of elevated uranium concentrations to the environment in contaminated areas where U concentrations can be up to three orders of magnitude higher (Read *et al.*, 1993; Graham *et al.*, 2008; Prat *et al.*, 2009; Xu, 2013).

The chemical toxicity of U and the potential mobility of U throughout the environment makes the ingestion or uptake of contaminated water or contaminated foodstuffs a significant potential risk to the health of organisms, including humans.

1.4.3. Radiocarbon: Risk to health

The decay of ^{14}C to ^{14}N by β-emission has a relatively low energy (0.157 MeV, (Wilson, 1996)) and therefore it does not pose a great radiological risk unless it is taken into the body by ingestion or inhalation, or becomes incorporated into biological tissue. Inside the body, the beta radiation has the potential to cause damage to cells which can lead to adverse health effects (Lemotte and Little, 1984; Watson *et al.*, 2005; Jones *et al.*, 2013; Nedveckaite, Gudelis and Vives i Batlle, 2013). Radiocarbon is considered to be the single greatest contributor to the human radiation dose due to anthropogenic activity in the UK and on a global scale (Watson *et al.*, 2005; UNSCEAR, 2008).

1.5. Components and characteristics of soils and sediments

1.5.1. Soil formation

The fundamental building block of any soil is the parent material: the inorganic mineral component on top of which the soil forms. The parent material is usually an underlying bed rock but can also be a deposited sediment. Physical and chemical weathering processes, driven by climate, topography, and biota, cause the gradual breakdown of parent material into smaller and smaller particles which combine with organic material and begin to take on the characteristics of a soil. In a developed soil, the solid material, consisting of organic matter, parent material and secondary minerals, is around 50% of the total soil volume with the remaining 50% comprising water and air. The parent material influences the physical condition of the soil, e.g. soil texture, and chemical conditions within the soil, e.g. nutrient status, pH and cation exchange capacity (CEC). These factors are important not only when considering soil fertility but also when contaminant mobility is to be investigated.

As soils age, they tend to get deeper as the weathering of parent material progresses. Soils exhibit changes in physical and chemical conditions throughout a depth profile due to changing composition. The changes are classified into horizons which are commonly recognisable in soils globally and can be used to determine the soil type. A simplified soil profile showing the major horizons is presented below (figure 1.10). The soil surface is generally covered with an organic rich layer which receives fresh inputs of organic matter from dead plants and other organisms. This O horizon can be further classified into the litter layer (L) found on the surface where organic material which has undergone little or no degradation, the fermentation layer (F) comprised of partially degraded organic material in which the source material is still recognisable and the humus layer (H) that contains humic substances which have been well degraded and contains no recognisable material. Below the O horizon is the A horizon, a layer where humified organic matter is well mixed with weathered soil minerals. Below comes the B horizon, a zone of mineral material which

has a small amount of organic matter mixed in which has been illuvially deposited from above. This layer marks the beginning of the transition to the C horizon, where parent material is clearly recognisable, and finally to the D horizon which is the parent material (McKinney and Schoch, 2003; Pulford and Flowers, 2006b; Hanrahan, 2012). A peat soil is one that has an O horizon of greater than 40 cm depth and is usually forms in cold wet conditions. The poor soil texture due to lack of mineral material usually leads to waterlogging and reducing conditions in the soil (Pulford and Flowers, 2006b; Huang *et al.*, 2009).

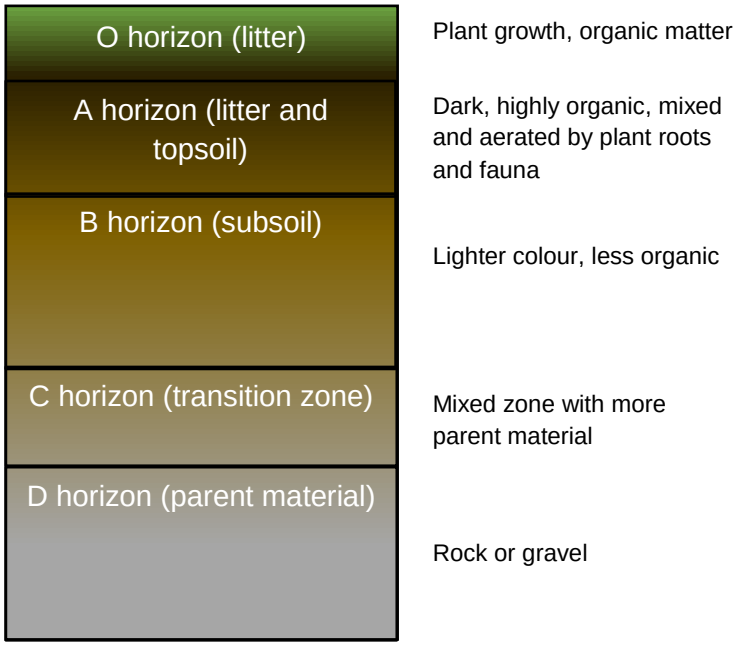

Figure 1.10. The horizons which form the basis of most soils, after McKinney & Schoh (2003)

1.5.2. Saltmarsh sediments: Formation and processes

Like soils, sediments are composed of a mixture of inorganic and organic material with pore spaces containing air and water. However, unlike soils, the solid material in sediments has been transported and deposited by water with consecutive layers building on top of the previous ones. Saltmarshes are areas of marine sedimentation characterised by terracing, deep creeks with steep banks and salt-tolerant vegetation. They can develop in estuaries, coastlines with low tidal energy and around barrier islands as these systems cause a decrease in water flow and cause particles, picked up and transported in fast flowing and energetic waters, to be deposited (Adam *et al.*, 2008). The regular inundation of an area of saltmarsh is a controlling factor in its properties as a low zone which is regularly inundated will accrete faster and only be hospitable habitat for hardy, salt tolerant plants. As the saltmarsh height increases, inundation decreases, leading to slower accretion and increasing diversity of plant life with distance from the water's edge. The main saltmarsh zones are summarised in figure 1.11 below.

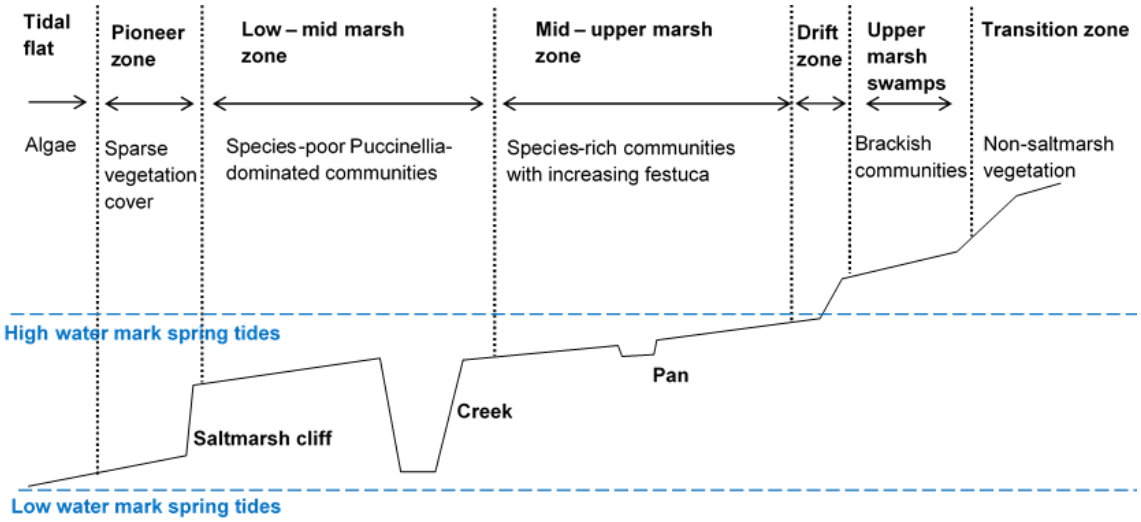

Figure 1.11. A schematic diagram of Saltmarsh zones (not to scale), after Burd, (1989).

The continual growth of sediments also leads to compaction in the deeper layers which causes a greater density and reduced water holding capacity. In addition, sediments tend to become anaerobic over time due to the frequent inundation and compaction. Vertical zonation can occur in sediments with a more oxic upper layer, characterised by a higher concentration of Fe in the solid phase where it precipitates as Fe(III). Below the solid phase Fe(III) peak reduced Fe(II) increases with depth in the profile, often evident by the occurrence a dark grey/black colour. Solid phase Mn can exhibit a peak above the Fe(III) peak as the redox change occurs at a lower Eh (Pulford and Flowers, 2006a).

1.5.3. Mineral components of soils

The inorganic components of soils can be described as primary or secondary minerals. Primary minerals are those which are recognisable in the parent material while secondary minerals form from the weathering and chemical alteration of the parent material. The composition of primary minerals affects the nutrient status of the soil, for example sandstone and granite primary minerals produce soils which are low in essential plant nutrients such as Ca and Mg whereas basalt and shale can produce soils rich in nutrients (Pulford and Flowers, 2006b). The mineral composition influences other soil properties such as the cation exchange capacity (CEC). This is a measure of the capacity a soil has for adsorption of positively charged metal ions from aqueous solution. The CEC is a pH dependent property as H^+ ions in solution competitively sorb onto available binding sites. Clays and Fe oxyhydroxides are important minerals which have a large influence on CEC due to their surface oxygen functional groups, such as carboxylic acids, which can protonate and de-protonate as pH decreases and increases respectively. Organic matter also affects the CEC and is discussed in detail in section 1.7 (Hanrahan, 2012).

pH dependent surface charge isn't the only controlling factor in CEC as the formation of secondary minerals which have high CEC can only occur in specific conditions. Fe and Mn form insoluble oxyhydroxides with high CEC in aerobic conditions but under anaerobic conditions these phases can be reduced to Fe (II) and Mn (II) which are both highly soluble and therefore don't have the same capacity to retain ions on the solid phase. The dependence of the speciation of Fe on the redox potential and pH is shown in a pourbaix diagram below, (figure 1.12).

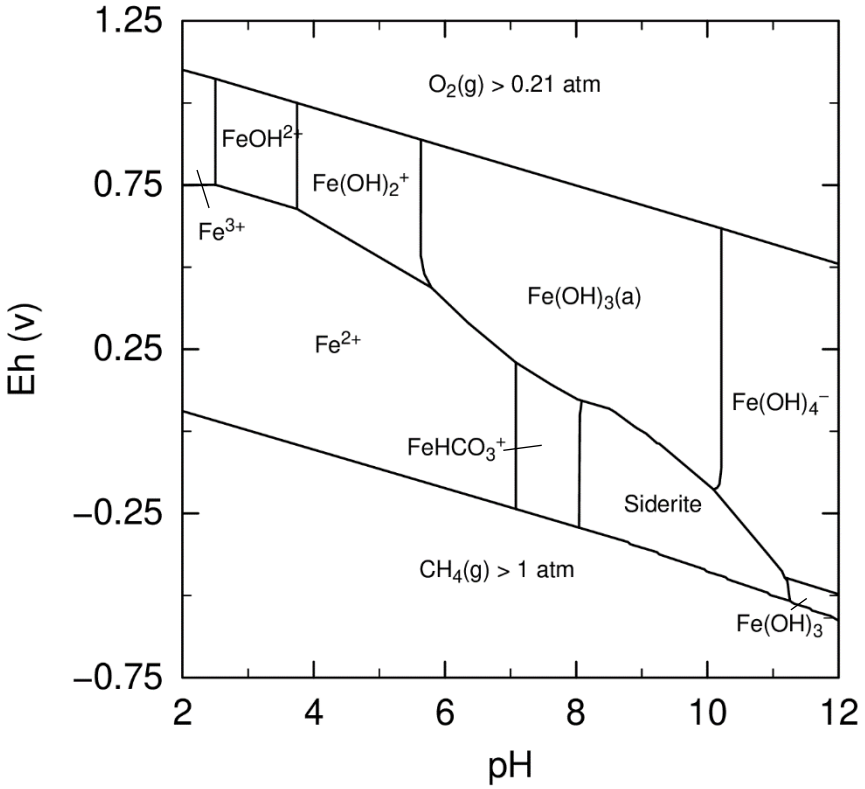

Figure 1.12. Eh-pH diagram of Fe speciation in aqueous solution modelled using PhreePlot (Kinniburgh and Cooper, 2011). The phases considered are ferrihydrite ($Fe(OH)_3(a)$), siderite and $Fe(OH)_2$ in a solution with a ΣCO_2 concentration of 10^{-2} mol/kg and Fe activity in solution of 10^{-6}.

The Pourbaix diagram (figure 1.12) shows that at conditions relevant to natural waters and pore waters, in a pH range of around 5.5 – 7.5, the Fe speciation is very sensitive to changes in the redox potential. At a pH of 6.5 a change in Eh from around 0.25 V – 0.5 V would result in the oxidation of Fe(II) in solution to the solid, amorphous Fe(III) mineral ferrihydrite which has a large CEC. In an area sensitive to redox changes the reverse

reaction could also occur potentially releasing trace elements bound to the Fe(III) mineral into solution. Equally, a small change in the pH can have the same effect. This highlights the importance of having a good understanding of the underlying geochemical processes when investigating the properties of a soil with relation to trace element adsorption and mobility.

1.5.4. Influence of pH on soil properties: point of zero charge

The ability of surfaces within soils to adsorb ions from solution is not uniform, with different materials having varying affinity for particular ions (Covelo, Vega and Andrade, 2007). pH conditions also affect the ability of a material to sorb ions due to the protonation and deprotonation of surface functional groups with decreases and increases of pH, respectively. The protonation and deprotonation of functional groups leads to a variation in the charge of a surface, with acidic conditions causing protonation and an overall positive charge and the opposite effect seen in basic conditions, leading to an overall negative surface charge. The surface charge of a material dictates its ability to bind ions from solution, as dissolved cations are attracted to negatively charged surfaces and anionic species in solution are attracted to positively charged surfaces. The opposite case is also in effect, with cations and anions repelled from positively and negatively charged surfaces, respectively. On a material surface the overall charge is a balance of the protonated and deprotonated sites. If the positively and negatively charged sites exactly cancel each other out then the overall surface charge is 0, and the point of zero charge (PZC) is reached. Different materials exhibit a different range of PZC, with crystal structure and other components in solution influencing PZC (Schwertmann, 1982). Bakatula *et al.*, (2018) determined the PZC of several organic and inorganic materials and found they increased from kaolinite (~3.0) < peat moss (~3.4) < maple saw dust (~4.7) < brown algae (~6.1) < green compost (~7.7) < wood ash (~9.5) < goethite (~10.9). Schwertmann, (1982), found that the PZC of natural ferrihydrites (5.3 – 7.5) were lower than those of synthetic

ferrihydrites. Naganuma *et al.*, (1993) demonstrated that the PZC of two tropical peat samples was ~3.4. The PZC of a material and the pH of the soil solution determine the ability of an ion to bind onto the material surface. For example, as is shown in figure 1.6, in a solution with U(VI) concentration of 10^{-6}M and pCO_2 of $10^{-3.5}$ atm the dominant U species in solution between pH 5 and 6 is UO_2OH^+. Using the PZC values for materials calculated by Bakatula *et al.*, (2018) shows that at a pH of 5.5 the sorption of this U species to peat moss (PZC = ~3.4,) would be favourable as the peat surface would be negatively charged, whereas the sorption to goethite (PZC = ~10.9) would not as the surface would be positively charged and would repel the positively charged UO_2OH^+ species. The PZC values of organic substances and clays tend to be lower than those of Fe oxides (Schwertmann, 1982; Naganuma *et al.*, 1993; Helmy, Ferreiro and Bussetti, 1994; Appel *et al.*, 2003; Bakatula *et al.*, 2018). Thus, the pH of soils and natural waters is fundamental to the binding of dissolved species, earning it the title of "master variable" (Sposito, 1998).

1.6. Natural Organic Matter (NOM): Characteristics and properties

1.6.1. Environmental role of organic matter

The organic component of soils and sediments plays a pivotal role in their biogeochemistry. Fundamental soil properties influenced by organic matter include water holding capacity, pH, buffering capacity, redox chemistry, metal binding ability and fertility. Soil classification depends on the amount of organic matter it contains, for example in the UK soil classification system an organic horizon (O horizon) is one that contains >30% or >20% organic matter in a soil which has a clay content in the mineral fraction of >50% or 0% respectively, and a peat soil is one that has an O horizon of greater than 40 cm depth (Pulford and Flowers, 2006b; Huang *et al.*, 2009). However, it is important to consider the properties of organic matter and not just the total amount present when assessing its role in the environment as NOM of different types can exhibit different environmental behaviour which in turn influences chemical processes involving other soil components. This is exemplified by looking at organic matter solubility. The presence of dissolved organic matter can promote mobility of metals, including contaminant heavy metals, by forming soluble complexes or colloids which are stable in solution and are mobile over long distances. (Jackson *et al.*, 2005; Graham *et al.*, 2008; Schijf and Zoll, 2011). On the other hand, NOM which is part of the soil solid phase or associated with mineral phases can bind and retain metals which might otherwise be mobile, thus causing them to be retained in the soil and decreasing mobility (Tack, 2010). For this reason, it is important to understand the properties of organic matter when assessing its role in environmental processes at a particular site.

Organic matter impacts the physical and chemical properties of soil. For example, soil with a NOM content of around 5-6% will have improved physical structure, water retention, nutrient content and nutrient availability compared to a sandy soil with a NOM content of

~1%. Too much organic matter in a soil can also be detrimental to soil structure and a NOM content of ~10% or higher can lead to poor drainage and therefore poor aeration. Many aspects of the environmental behaviour of NOM are well understood, but only relatively recently have the details of the structure of molecules within the complex mixture of NOM been identified. This has been driven by advances in technology involved in complex mixture separation and characterization, particularly in nuclear magnetic resonance (NMR) and mass spectrometry (Jawinski, 2002; Simpson *et al.*, 2002; Stenson, Marshall and Cooper, 2003; Tremblay, 2006; Stenson, 2009; Bell *et al.*, 2014, 2015; Minor *et al.*, 2014).

1.6.2. Organic matter structure and properties

NOM is a complex, heterogeneous mixture of organic molecules derived from biological decay processes of fresh organic material such as leaf litter or animal cells. The molecules that make up NOM are from all stages of the degradation process. When the organic material has decayed to the extent where it is no longer obvious what parent material it is derived from it is called "humus" or "soil organic matter" (SOM). Soil organic matter includes all organic matter present in the soil apart from any undecayed plant or animal material, or living biomass. SOM can be simply divided into two categories: "non-humic substances" and "humic substances." Non-humic substances are recognisable common biological chemical classes, for example amino acids, carbohydrates, polysaccharides, lipids and proteins. These tend to be good substrates for biological activity and therefore are broken down quickly, meaning that any present in the soil are likely to have been introduced recently and are younger than other soil components. Structural components of plant cells like cellulose and lignin are also found in this fraction and can remain stable in soils for a longer time as they are more resistant to microbial decay processes (Stevenson, 1982; Brady and Weil, 1996). Humic substances are often classified according to their solubility into operationally defined fractions. "Humic acids" are insoluble at acidic pHs of 2 or below. "Fulvic acids" are soluble over the entire pH range. The residual organic

fraction, which is not soluble in acid or alkali is known as “humin” (Jones and Bryan, 1998). Soil organic matter has been widely studied since the early days of agricultural science and humic substances have been further divided into a number of fractions according to their solubility in different reagents as can be seen in figure 1.13 (adapted from Stevenson, 1982). The application of modern spectrometric techniques to NOM analysis is enhancing the understanding of the composition of the complex mixture of molecules that make up NOM.

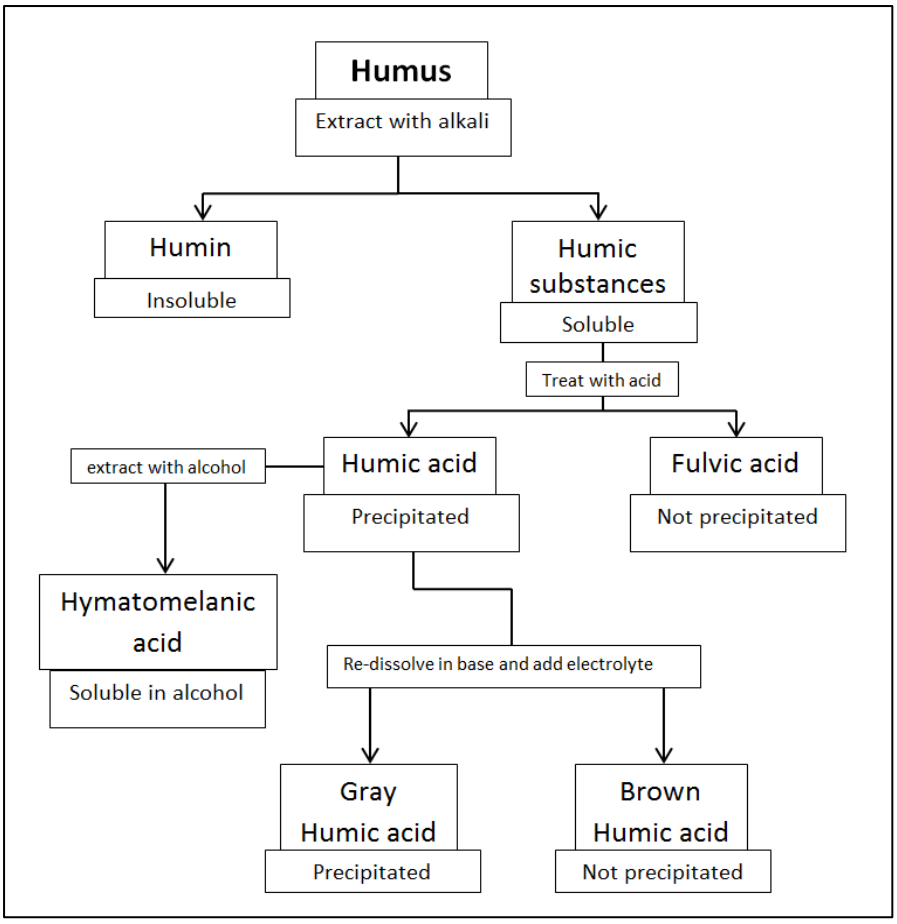

Figure 1.13. Definitions of fractions of NOM in soil, defined by their chemical characteristics. Figure adapted from (Stevenson, 1982)

1.6.2.1. Progress in Organic Matter Analysis

The study of organic matter over many years using many techniques has built up a very large body of published data concerning the structure and composition of major types of organic matter. The techniques used can be generally categorized into two broad groups:

1) Those which are common and readily available, tend to have a low running cost and require little sample preparation.

2) Those which are less commonly used in routine analysis, require specialist equipment and careful sample handling and preparation and generate very high-resolution data.

Techniques which fall into the first group include elemental analysis, UV/Visible spectroscopy analysis (UV/Vis), fourier transform infrared spectroscopy (FTIR), fluorescence spectroscopy, 1-dimensional NMR spectroscopy and chromatographic techniques. These are common laboratory techniques that can be readily applied to NOM analysis to obtain information on the composition and chemical behavior of mixtures of organic molecules within operationally defined fractions. The second group is comprised of multi-dimensional NMR experiments, very high-resolution mass spectrometry techniques such as Fourier Transform Ion Cyclotron Resonance Mass Spectrometry (FT-ICR-MS) and microscale analysis techniques like Transmission Electron Microscopy (TEM). Multi-dimensional NMR and FT-ICR-MS are powerful techniques which can be used to obtain very detailed structural analysis of samples to the individual molecule level (Hertkorn *et al.*, 2013). TEM has been used to analyse individual organic matter colloids at a nm scale and can be coupled with elemental analysis techniques such as Energy Dispersive X-ray (EDX) spectroscopy and Electron Energy Loss spectroscopy (EELS) to investigate the quantity and oxidation state of associated metals (Wang *et al.*, 2013).

1.6.2.2. Comparison of NOM properties

Commonly reported important properties of NOM fractions are the elemental compositions and the relative abundance of specific functional moieties such as aromatic rings, carbonyl and carboxyl groups and aliphatic chains. A statistical evaluation of published elemental analysis data by Rice and MacCarthy (1991) showed that humic acids have significantly higher C and lower O content than fulvic acids and that fulvic acids are likely to be less aromatic than humic acids (based on the H/C ratio). The comparison of humic acids and humin shows that the elemental composition of the two fractions are not significantly different (based on a relatively small amount of humin data). The source of the organic matter (soil, freshwater or marine) also resulted in significant differences in the elemental composition, with soil humic acids having higher C and lower O content than freshwater humic acids. Other studies have also shown that soil fulvic acids tend to have higher O content than soil humic acids and that this is likely to be due to their higher carboxylic acid content (Thorn, Folan and MacCarthy, 1989; Ritchie and Perdue, 2003; Chang *et al.*, 2013).

The chemical changes occurring during ageing of organic matter have been investigated by examining NOM characteristics with depth in peat and soil profiles. The main changes with depth are a decrease in oxygen and increase of aromaticity and condensation. These compositional changes can be attributed to the ongoing microbial degradation of organic molecules in soils as increasingly stable organic molecules are used as a metabolic substrate in biological processes. Organic matter at greater depth has been present in the soil for a longer period of time and therefore has undergone much more microbial degradation than newer organic matter inputs at the soil surface (Stevenson, 1982; Rashid, 1985; Purmalis and Klavins, 2012).

Until recently humic substances were considered to be very large molecules with a high degree of cross linking and many varied functional groups consisting of cyclic and aromatic groups with carboxyl and phenolic functional groups as well as other varied functionalities (Stevenson, 1982; Schulten and Schnitzer, 1993). It is now more widely accepted that rather than very large individual molecules the fractions of NOM are formed from a large number of heterogeneous smaller molecules which are closely linked and tightly bound together forming a mixture which is difficult to separate using traditional chemical methods (Piccolo, 2002; Duarte, Barros and Duarte, 2012).

The idea that humic substances are not composed of few very large molecules of >100,000 Da size but an aggregating mixture of molecules of <2000 Da size was first conceived and tested through changing the elution pattern of humic substances in chromatography experiments by varying the ionic strength and composition of the eluent (Piccolo, Nardi and Concheri, 1996a, 1996b; Piccolo, 2002). Application of multidimensional NMR techniques and high resolution mass spectrometry has confirmed the likelihood that this interpretation is correct and gone further to describe the components of NOM. (Simpson *et al.*, 2002; Steelink, 2002; Kim, Kramer and Hatcher, 2003; Hertkorn *et al.*, 2013) Using these methods, a complex mixture of NOM can be separated not only into common organic compound classes of polysaccharides, polypeptides, aliphatic chains, aliphatic and aromatic acids and lignin derived structures, but into individual molecule structures. Samples of DOM have been separated into over 1000 individual peaks with unique m/z (mass to charge) ratios by FT-ICR-MS (Blackburn *et al.*, 2017). The structural formula of the molecule corresponding to each peak can be calculated by exact mass determination with an error of < 1 ppm. FT-ICR-MS has subsequently been used to characterize NOM from different sources (marine, freshwater and soil), analyze degradation of DOM and investigate reactions involving organic matter in the environment (D'Andrilli *et al.*, 2010; Mead *et al.*, 2013; Lu *et al.*, 2015; Lv *et al.*, 2016).

1.6.3. Organic matter in solution: dissolved or colloidal?

Soil pore waters can contain high concentrations of organic matter that interact with other components of the soil solution. The organic matter can be in the truly dissolved fraction or present as colloids with a diameter of 1 – 1000 nm which can be separated by use of specialist filters. The process of colloid formation begins with the breakdown of the host rock or the mineralization of truly dissolved species due to a change in chemical conditions (Takala and Manninen, 2006) causing small particles to be suspended in solution. Dissolved organic matter can bind with inorganic colloidal material generating a larger, heterogeneous colloid with the surface properties of both its mineral and organic components. These colloids can stay in solution due to their surface charge properties and small size, however changes in soil solution conditions, such as pH and ionic strength, can influence the stability of colloids (Lead *et al.,* 1997). Six interactions between organic matter and minerals were identified by Gu *et al.*, (1994) with the two most important being electrostatic attraction and ligand exchange between oxygen containing functional groups on the mineral and organic matter surfaces. The adsorption of organic acids by Fe minerals is by electrostatic attraction which is most favourable at a pH of ~4–5. Humic substances which are more hydrophobic, indicative of a more humic acid like character, are preferentially bound to Fe oxide minerals as their lower surface charge compared to hydrophilic humic substances means they are not repelled by hydroxyl groups on the Fe mineral surface (Gu *et al.*, 1994; Vindedahl *et al.,* 2016). The properties of the organic matter can affect the way it behaves in solution. Carboxylic-rich organic matter has been shown to bind irreversibly to soils when other organic matter is readily desorbed (Oren and Chefetz, 2012). Silver has been shown to bind to more strongly to humic substances with higher aromaticity (Settimio *et al.,* 2015). Other reactions involving DOM, mineral surfaces and inorganic contaminants include competitive sorption onto mineral binding sites, reduction of oxidized mineral phases and contaminants facilitated by electrons

donated from DOM, and DOM – metal complexation leading to the increased solubility of contaminants (Polubesova and Chefetz, 2014). Colloid transport is a well-known mechanism of contaminant mobilization (McCarthy and McKay, 2004) and colloid formation has been implicated as the first step to contaminant concentration in soils as colloids react with metals in solution, grow and precipitate or block soil pores (Graham *et al.*, 2011; Gavrilescu, 2014).

1.7. Organic matter and radionuclides: Mechanisms of interaction

Interactions between NOM and radionuclides are varied and can be complex due to the range of environments where the two are found. Primary processes involving NOM are direct binding or incorporation (for example of ^{14}C) leading to mobilization or immobilization, and reduction of oxidized chemical species. Secondary effects can be due to the influence NOM has on soil pH and redox chemistry and facilitation of microbially mediated reduction reactions (Landais, 1996).

NOM plays an important role in the mobility of radionuclides in the environment due to its high surface area and pH dependent negative charge which is attributable to dissociated acidic functional groups. These also give NOM a very high cation exchange capacity (CEC), generally equal to or greater than that of silicate clays (Brady and Weil, 1996). These properties allow metals including radionuclides to become strongly bound to NOM (Fesenko *et al.*, 2014). The binding of radionuclides with solid phase NOM can retard their mobility. This can result in their accumulation, as has been seen in natural settings, such as at the Needle's Eye Natural Analogue site in SW Scotland (section 2.1.2), or in areas with anthropogenic contamination such as firing range soils in SW Scotland and NW England (e.g. Oliver *et al.*, 2008). Competition for binding sites may affect the capacity of organic matter to bind radionuclides in a dynamic equilibrium between ions in solution and organic

binding sites which is affected by solution ionic strength, pH-dependent charge of solid surfaces and the characteristics of solution species. Although solid phase organic matter can remove radionuclides and other elements from the solution phase, microbial degradation of the organic matter may lead to the re-release of bound elements into solution (Neagoe, Iordache and Fa, 2012). The immobilisation in the presence of organic matter is also strongly pH-dependent, with acidic conditions usually leading to an increase in metal binding by mineral phases in the presence of organic matter, and an increasing pH leading to a decrease in metal binding. A pH of 6 or below is likely to favour metal binding to organic matter due to the presence of carboxylic acid groups, while between 6 and 8 mineral phases like Fe-oxides and hydroxides are more important due to their hydroxyl functional groups (Warren and Haack, 2001). The following sections include more detailed consideration of interactions between organic matter and the radionuclides relevant to this study, U and ^{14}C.

1.7.1. Uranium and organic matter

Uranium interacts with organic matter in both of its common oxidation states, U(IV) and U(VI)(Lenhart *et al.*, 2000; Bone *et al.*, 2017a). In areas where uranium accumulates to high concentrations organic matter can play an important role by: (i) directly binding U(VI) or U(IV); or (ii) stabilizing redox processes allowing U(IV) minerals to form. The former case is seen in highly organic soils where U immobilization is due to removal and concentration of U(VI) from pore waters by binding to solid phase humic substances (Read *et al.*, 1993; Regenspurg *et al.*, 2010; Bordelet *et al.*, 2013; Li, *et al.*, 2014; Li *et al.*, 2015). An example of the second case is seen in U deposits in New Mexico, USA, where the NOM stabilizes the mineral coffinite by inhibiting its oxidation in the presence of oxidizing groundwater (Deditius, Utsunomiya and Ewing, 2008). In areas with a high U solid phase concentration, e.g. >500 mg kg^{-1}, a correlation is often seen between U and organic carbon regardless of the immobilisation pathway (Landais, 1996). Reduction of U(VI) to U(IV) is seen as an important mechanism in limiting U mobility and organic matter can contribute to this end by facilitating microbial U(VI) reduction leading to U mineralization as poorly soluble uraninite, UO_2 (Fredrickson *et al.*, 2000; Perminova, Hatfield and Hertkorn., 2002; Newsome, Morris and Lloyd, 2014). Humic substances with a more condensed and humic acid character have been shown to be more effective in mediating the microbial reduction (Perminova, Hatfield and Hertkorn., 2002; Chen *et al.*, 2003; Gu and Chen, 2003; Gu *et al.*, 2005). Recently U(IV) has been shown to bind to organic phases in anoxic sediments and thereby resist mineralization to UO_2, but still be immobilized (Bone *et al.*, 2017b). By different mechanisms the same result, of reductive U immobilisation, is achieved. On the other hand, U(IV) bound to organic matter has been shown to be more susceptible to oxidation and therefore remobilization (Gu *et al.*, 2005). The redox reactions involving uranium are further complicated by the presence of high concentrations of Ca^{2+} and HCO_3^- as these have been shown to inhibit U(VI) reduction, even in highly reducing conditions

(Brooks *et al.*, 2003; Suzuki and Suko, 2006). The two opposing influences OM has on the redox chemistry of uranium highlights the importance of understanding soil chemical processes when trying to predict U mobility.

Uranium has also been observed to be transported with Fe-humic colloids in highly reducing conditions which would otherwise be expected to immobilize uranium by the reduction pathways described above (Wang *et al.*, 2013). Colloid transport is often an important mechanism of U mobility and it has been observed in peats and highly organic soils (Pokrovsky, Dupré and Schott, 2005; Graham *et al.*, 2008; Xu, 2013), contaminated surface water (Phrommavanh *et al.*, 2013) and sediments (Jackson *et al.*, 2005). However U is not universally associated with colloids in solution and has also been found associated with humic complexes smaller than colloidal size (Jackson *et al.*, 2005) and in the "truly dissolved" fraction of pore water (Williams, Hooker and Brightman, 1990; Graham *et al.*, 2011). Moreover, the colloidal or truly dissolved nature of U can be very localised and is dependent on the immediately surrounding geochemical conditions with speciation changes seen over spatial scales of centimetres to metres (Xu, 2013).

Laboratory studies have highlighted how the interaction with NOM can both enhance and retard the mobility of U. Mibus *et al.* (2007) showed in column experiments that the presence of humic acid enhanced the mobility of U(VI) eluted through a sand column as it combined with humic colloids; at the same time a portion of the U(VI) was immobilized in the column as colloids were filtered out. This agrees with Tinnacher *et al.*, (2013) who showed that varying the fulvic acid concentration or pH can have a large effect on the elution of U(VI) in a similar column system, enhancing or decreasing U(VI) sorption to silica. Lesher *et al.*, (2013) showed enhanced mobility of U through a sand column after equilibration with fulvic acid. Yang *et al.*, (2012) showed that hydrophobic and higher alkyl content organic matter promotes U(VI) elution and mobility in a sand column. An SEC column investigation of humic substances with a naturally elevated U concentration by

Zhang *et al.*, (1997) showed that U eluted with the smallest fraction of NOM. These experiments highlight that organic matter can both enhance and retard U mobility, and often both effects occur simultaneously in a single system.

The complexity of U-NOM interactions in the environment cannot be solely described by using binary interaction models. Extra inputs must be included to explain the environmental behaviour of U. In lab experiments ternary interactions have been investigated, usually involving U, humic substances and Fe oxides, for example Murphy *et al.* (1999) showed that the presence of fulvic acid enhances the absorption of U(VI) to hematite at acidic pHs while Yang *et al.*, (2013) showed that U(VI) strongly binds to humic and ferric oxide colloids by inner sphere binding and the presence of humic substances in solution promoted the desorption of U(VI) from Fe oxide colloids. Similar ternary interactions have been observed in the analysis of natural samples. U can be associated with Al-humic colloids in contaminated sediments (Jackson *et al.*, 2005) and has been observed to be associated with Fe-humic colloids in soil pore waters (Graham *et al.*, 2008; Xu, 2013). Pédrot *et al.*, (2008) went further and stated that in heterogeneous colloids U appears to be directly bound to an Fe phase stabilised by NOM in colloid form and not directly bound to organic matter.

It is clear that U binding to NOM is an important process in the environment, and many studies have investigated the nature of the binding to discover attributes of organic matter that promote U binding. Carboxylic acid functional groups are seen as important in humic binding of uranium (Munier-Lamy *et al.*, 1986) by the dehydrogenation and substitution complexation shown below (Equation 1.7) (Landais, 1996).

$$2RCOOH + UO_2^{2+} \rightarrow RCOO - (UO_2) - OOCR + 2\,H^+ \qquad \text{Equation 1.7.}$$

R= an extended organic structure

COOH = carboxylic acid functional group

The complex can take the form of a 2:1 RCOOH: UO_2 complex, or a 1:1 complex. Carboxylic acid content has been implicated in the binding of U in highly organic soils (Read *et al.*, 1993) and humic acids have been shown to form stronger complexes with U(VI) than fulvic acids (Lenhart *et al.*, 2000). In sediments, degraded organic matter has been seen to bind more U(VI) than fresher OM inputs with U fixation onto particulate organic carbon being more prevalent than U mobilization by DOC (Schaller *et al.*, 2008). Overall, organic matter binding of U can be through strong, inner sphere bonds with oxygen rich functional groups, weak surface adsorption interactions or incorporation into the matrix of colloids and solid phases with iron oxides and organic matter which associate due to hydrophobic interaction. The conclusions that can be drawn from the aspects of U-NOM interactions discussed above are as follows:

1) NOM can both promote and impede the mobility of uranium in soils and sediments

2) Colloidal transport is an important mechanism promoting U mobility, and colloid removal can act as a mechanism of U immobilisation

3) Redox chemistry has a large impact on U mobility as U(VI) is highly soluble and U(IV) is very insoluble in aqueous solution.

4) Oxygen containing functional groups, in particular carboxylic acids, are important for binding U to humic substances

5) NOM, Fe oxides and U are often found in association together

1.7.2. ^{14}C incorporation into marine NOM

Organic matter in the marine environment comes from distinct sources: terrestrial DOM discharged into the sea globally by rivers, the decaying remains of marine macro-organisms including fish and seaweeds, and marine phytoplankton and other micro-organisms (Hedges, Keil and Benner, 1997; Benner, 2004). Radiocarbon incorporated into marine NOM from its natural production in the troposphere and from atmospheric nuclear weapons testing can be used as a tracer to follow the circulation of ocean currents, with deep waters ranging from around 100 years old in the North Atlantic to around 2000 years old in the North Pacific (IAEA, 2002). Particulate organic carbon in rivers is depleted in ^{14}C relative to DOC, suggesting that it is older and more stable carbon that has undergone microbial degradation processes (Raymond and Bauer, 2001) however POC in the Irish Sea is enriched in ^{14}C with respect to background levels, due to the inputs of ^{14}C from the Sellafield nuclear reprocessing facility (Tierney *et al.*, 2015; Muir *et al.*, 2017). Radionuclides in the Irish Sea are transported up the west coast of Scotland via the North Channel (MacKenzie, Scott and Williams, 1987) and sediments within the Irish Sea basin are enriched with organic and inorganic ^{14}C. The enrichment of ^{14}C in different pools of the Irish Sea shows seasonal variation and the likely mechanism of Sellafield derived ^{14}C transfer between them is shown below (Cook *et al.*, 1995):

DIC → biota → POC → DOC

Dissolved Inorganic Carbon (DIC), enriched in Sellafield-derived ^{14}C, is incorporated into marine plants and phytoplankton by photosynthesis. As these organisms die they break down to Particulate Organic Carbon (POC) and Dissolved Organic Carbon (DOC). Incorporation of organic matter into on-shore sediments has been seen to provide a source of Sellafield-derived ^{14}C which can be traced in the sediment depth profile (MacKenzie *et*

al., 2004). Radiocarbon is not evenly distributed throughout marine organic matter. Wolstenholme *et al.*, (1998) and Muir *et al.*, (2017) observed increased concentrations of anthropogenic ^{14}C in particulate organic carbon (POC) in the Irish sea compared to dissolved organic carbon (DOC). Megens *et al.*, (2002) measured ^{14}C in sediment organic matter particle size fractions and found ^{14}C concentration in the <20 μm size fraction around 80% higher than OM of larger particle size. Very little characterisation of organic matter fractions which are enriched in ^{14}C has been carried out to date, and therefore there is not a good understanding of whether incorporation into marine organic matter retards or enhances the mobility of radiocarbon. Investigating the composition of OM fractions containing ^{14}C to expand our understanding of their mobility is a subject addressed within this project.

1.8. Natural analogue sites: In situ studies of radionuclide mobility

The idea of studying natural systems to obtain information on processes relevant to radioactive waste disposal dates back to the late 1970s, and definitions of natural analogue sites were developed by a number of authors between 1984-1989. For example, Côme and Chapman (1985) defined them as "an occurrence of materials or processes which resemble those expected in a geological waste repository" while McKinley (Miller *et al.*, 1994) stated that "the essence of a natural analogue is the aspect of testing of models - whether conceptual or mathematical- and not a particular attribute of the system itself."

At the same time, a report by an IAEA review group stated that:

"Natural analogues are defined more by the methodology used to study and assess them than by any intrinsic properties they may possess" (IAEA, 1999).

Natural analogue sites have been used to study a wide variety of characteristics of radioactive waste repositories (Read *et al.*, 1993; Sasao *et al.*, 2006; Andrews, Samways and Shimmield, 2008; Hidaka and Kikuchi, 2010; Noseck *et al.*, 2012). In the modern context, natural analogue sites are those that can be used as model situations for predicting chemical and physical processes which may occur in or around a geological waste repository over the long timescales involved in safely storing nuclear waste. Important outcomes of the study of natural analogues are the generation of data to help set parameters in radionuclide mobility and to understand the geochemistry of radionuclides in the systems to in order to test radionuclide mobility models in a "blind prediction" (Miller *et al.*, 1994).

The natural analogue sites selected for the Lo-RISE project each have special chemical characteristics which make them suitable as analogues for geological disposal repositories.

1.8.1. Uranium

Many sites globally have been used as natural analogues for the study of U mobility from a geological repository. Two uranium deposits in Gabon, which are known as natural fission reactors, have been studied to assess the incorporation of U and other radionuclides into minerals and formation of secondary mineral precipitates (Hidaka and Kikuchi, 2010). U solubility and speciation have been analysed in U mineral deposits in Sweden and the Czech Republic (Noseck *et al.*, 2012). The leaching of U from a former U mine in the UK called South Terras has been studied (Miller *et al.*, 1994). Uranium was found to be dissolved in groundwater then immobilised in sediments. Broubster in Caithness has a site where a former quarry has exposed a U vein from which dissolved U leaches into a bog nearby (Read *et al.*, 1993). The bog has become enriched in U but oxic conditions have prevented the U(VI) from becoming reduced to U(IV). The mechanism of U immobilisation is binding to acidic functional groups in the highly organic soil. These diverse sites are each useful for analysis of specific characteristics in U mobility.

The site investigated in this study, the Needle's Eye natural analogue site, has been studied since the late 1980s and is discussed in detail in chapter 3.

1.8.2. Radiocarbon

1.8.2.1. Radiocarbon in the Irish sea

Studies into the geochemistry of anthropogenic ^{14}C discharged into the Irish Sea, NW England, from the Sellafield nuclear reprocessing facility reveal important information about the mechanisms controlling ^{14}C mobility and distribution among different environmental pools. In the 1990s it was found that the ^{14}C is discharged in an inorganic form and largely remains in the truly dissolved inorganic carbon (DIC) fraction of seawater, not becoming part of the particulate inorganic carbon fraction (PIC) (Begg *et al.,* 1992). Follow up studies have confirmed the importance of the DIC fraction and also shown a seasonal variation in the pools in which ^{14}C is found as there is an increase in activity of the DOC and POC fraction in summer months, indicative of the rapid uptake of DIC by phytoplankton (e.g. Cook *et al.*, 1995, 2004).

Enrichment of ^{14}C in biota in the vicinity of the discharge point is evident in organisms which occupy different ecological niches, for example plankton, seaweeds, fish, shellfish tissue and shells (Tierney *et al.,* 2015, 2017; Muir *et al*., 2017). This highlights the variety of biological processes involved in the transformation of the discharged ^{14}C and the potential risk to environmental and human health via transfer through the food web, and also leads to the understanding of the mechanisms involved in distribution of ^{14}C throughout the environmental pools examined. The ^{14}C is discharged in a DIC form which is rapidly metabolized and transferred to PIC and POC pools. It can also be incorporated into mollusc shells to become part of the PIC pool in a process which is slower than the incorporation into the organic pools due to the slow growth and mechanical breakdown

involved (Cook *et al.*, 2004). Particulate organic and inorganic forms of ^{14}C increase the activity in sediments as the particulate material precipitates. This elevated ^{14}C activity is seen in sediments collected from sites off-shore and on-shore in sediment deposits such as the saltmarshes around the Solway coast (MacKenzie *et al.*, 2004; Tierney *et al.*, 2015, 2017; Muir *et al.*, 2017). In off-shore sediment samples the organic carbon fraction is enriched in ^{14}C in samples collected close to Sellafield, however, samples from further away are depleted in ^{14}C relative to a background concentration of 250 Bq kg^{-1}. This depletion is likely to be due to mixing of "old" carbon from greater sediment depths with the younger deposits (Muir *et al.*, 2017; Tierney *et al.*, 2017).

In the Solway saltmarshes, South West Scotland, the organic component has been seen to be the dominant form of ^{14}C present, with activities around 10 times higher than in the inorganic component of the same samples (MacKenzie *et al.*, 2004). The fact that ^{14}C has been released into the Irish Sea from a point source for over 50 years means it is a useful tracer of the geochemical processes involved in C transport.

1.8.2.2. Dispersal of radionuclide discharges in the Irish Sea

The behaviour of radionuclides in the Irish Sea has been widely studied, with a focus on mobility, accumulation in sediments and bioaccumulation.

The movement of radionuclides in the Irish Sea has a very clear northerly trend, as is shown by the work of MacKenzie, Scott and Williams, (1987). They demonstrated that solution transport and particulate transport are important in the northerly movement of Sellafield waste. The authors showed that radionuclides from Sellafield are transported as far north as the Mull of Kintyre and the Firth of Clyde and that the sediments around the coast of Dumfries and Galloway have elevated radionuclide levels. The northerly trend has also been shown by Kershaw *et al.*, (1990) in a study examining the transit time of nuclides to

sediments in Maryport, around 40 km north of the Sellafield undersea discharge pipe. The transit time of the radionuclides 40 km northwards to Maryport was calculated by Aston and Stanners, (1982) as 1 – 1.5 years which can be compared with the movement 10 km southwards to Newbiggin which takes around around 2.5 years.

The northward dispersal trend highlights the importance of analysing radionuclide concentrations on the Solway sediments of Dumfries and Galloway as the coast is only around 30 miles from the Seallafield discharge point.

1.9. Chapter summary

Uranium and radiocarbon are important environmental contaminants from nuclear waste processing and potentially from long-term sequestration. They each pose a significant risk to the health of humans and ecosystems, can be widely dispersed and accumulate to potentially dangerous concentrations.

The incorporation of ^{14}C in the form of inorganic bicarbonate by marine plants is an important mechanism in its mobilisation as POC. The subsequent deposition into sediments leads to the accumulation of ^{14}C over time. Accumulation of anthropogenic ^{14}C has been identified in sediment organic matter of the Solway coast (MacKenzie *et al.*, 2004) but to date there has been no investigation into the organic matter components which incorporate ^{14}C. The results presented in chapter 5 are the first example of combined OM characterisation and ^{14}C analysis to identify those components of OM which incorporate anthropogenic ^{14}C in sediments.

Redox chemistry is important in U geochemistry due to the very different mobility of its two major environmental oxidation states. Uranium (VI) is soluble in solution and therefore highly mobile whereas U(IV) is sparingly soluble and tends to precipitate, which is seen as potentially important in limiting U mobility from anthropogenic sources. However, despite the redox chemistry of the two oxidation states being apparently relatively straight forward, in the environment U(IV) has been seen to be mobile when associated with porewater colloids and U(VI) has been seen to be immobile due to binding by soil surfaces, particularly Fe oxyhydroxides and humic substances. Uranium (VI) can form strong, inner sphere bonds with acidic functional groups on organic matter and Fe oxides, be associated to surfaces by weak adsorption or be incorporated into the organic or mineral matrix. The association of NOM and U can both promote and retard its mobility in both oxic and anoxic environments. The U mineralisation at the Needle's Eye and the accumulation of U in the

bog below the cliff has been subject to investigations since the discovery of the mineralisation in the 1960s (e.g. Miller and Taylor, 1966; Mackenzie *et al.*, 1989; Basham *et al.*, 1991; Jamet *et al.*, 1993; Braithwaite and Livens, 1997; Zhang *et al.*, 1997; Xu, 2013). However, the mechanism of U accumulation remains to be elucidated. The results presented in chapters 2 and 3 build on the findings of Xu, (2013) to verify the mechanism of U(VI) accumulation and investigate the importance of the properties of OM in binding U at the site. Greater understanding of the chemistry of U accumulation at the Needle's Eye will broaden our knowledge of U mobility in the environment and help to inform the selection of a geological repository site.

1.10. Project aims

As identified in the literature review (Chapter 1), the nature of interactions of NOM with U and anthropogenic ^{14}C and the effect interactions have on the mobility of these radionuclides remain ambiguous. The challenge within this project is to investigate interactions between these radionuclides and NOM by undertaking lab and field analyses while ensuring that conclusions drawn are relevant to an environmental setting. This is achieved by direct analysis of solid phase and extracted water samples to build on the results of past studies and develop a strong understanding of the geochemistry of the sample sites and, where possible, by limiting sample alteration and pre-treatment to ensure results are applicable to the natural setting.

The objectives of this study are outlined below:

i) Investigate geochemical characteristics of the Needle's Eye bog, determine geochemical influences on U accumulation and identify the oxidation state and speciation of U

The local geochemical environment plays a fundamental role in controlling the behaviour of U in soils. Key parameters such as pH, redox potential, organic matter content and concentration of other elements such as Fe and Ca influence the sorption, complexation, oxidation state and, ultimately, the mobility of U (e.g. Gu *et al.*, 1994; Lenhart and Honeyman, 1999; Liger, Charlet and Van Cappellen, 1999; Lenhart *et al.*, 2000; Brooks *et al.*, 2003; Newsome, Morris and Lloyd, 2014). The oxidation state of U is of particular importance due to the general solubility of U(VI) and insolubility of U(IV) in environmental settings (e.g. Pulford, 2010; Newsome, Morris and Lloyd, 2014). At the Needle's Eye, Jamet *et al.*, (1993) concluded, based on the results of modelling, that reduction of U(VI) to U(IV) is a reasonable mechanism of U immobilisation at the site while other investigations at the site have acknowledged that NOM may play a more

significant role in U binding (e.g. Mackenzie *et al.*, 1989; MacKenzie, Scott, *et al.*, 1991a). More recently Xu, (2013) demonstrated that U is found predominantly as U(VI) in the bog despite the prevailing reducing conditions. Direct analysis of bog samples using X-ray absorption spectroscopy (XAS) would confirm the oxidation state of U in the bog.

Furthermore, association of U with NOM and formation of colloids in porewaters have been implicated in both enhancing and decreasing the mobility of U in contaminated soils (e.g. Gu *et al.*, 2005; Ranville *et al.*, 2007; Graham *et al.*, 2011; Phrommavanh *et al.*, 2013; Wang *et al.*, 2013). At the Needle's Eye, identifying the fractionation and speciation of U in solution is an important step in unravelling the mechanism of immobilisation of U from porewaters to the solid phase.

ii) Investigate the composition of NOM in separated fractions and identify and characterise those which bind U

The importance of NOM in binding U has been acknowledged since the early investigations of U associations at the Needle's Eye site (e.g MacKenzie, Scott, *et al.*, 1991a; Xu, 2013) however, to date there have been no attempts to characterise NOM from the site and establish which fractions are involved on the binding of U. Identification of the types of NOM responsible for U binding would enhance understanding of U mobility in soils with particular NOM characteristics.

iii) Investigate the accumulation of anthropogenic ^{14}C in sediment NOM and identify and characterise the fractions of NOM which incorporate ^{14}C

MacKenzie *et al.*, (2004) identified the accumulation of Sellafield derived ^{14}C in sediments of the Solway coast. However, the characteristics of organic matter which incorporate ^{14}C have not been investigated. Understanding the composition of NOM which incorporates

^{14}C is fundamental to the understanding of the stability or potential for remobilisation of ^{14}C accumulated within coastal sediments.

These aims have been addressed and achieved by targeted sampling of two natural analogue sites, introduced in section 2.1. A suite of well-established and advanced analytical techniques have been applied in order to deconvolute and understand the complex interactions between NOM, U and ^{14}C in the natural environment.

2. Sampling, Materials and Methodologies

2.1. Sampling

2.1.1. Description of sampling sites

This section describes the two sampling sites, the Southwick Merse and the Needle's Eye bog, investigated in this study. Both are located in the south west of Scotland, near Dalbeattie, as shown in figures 2.1 and 2.2, below. Although in close proximity to each other, they have very different characteristics and receive inputs of radionuclides from different sources. The main focus of the analysis of the Southwick Merse samples was the investigation of the incorporation of Sellafield derived ^{14}C into saltmarsh organic matter while at the Needle's Eye bog the objective was to investigate was the effect of soil chemistry and organic matter characteristics on the binding and retention of uranium (U). In both cases the implications for radionuclide mobility were examined.

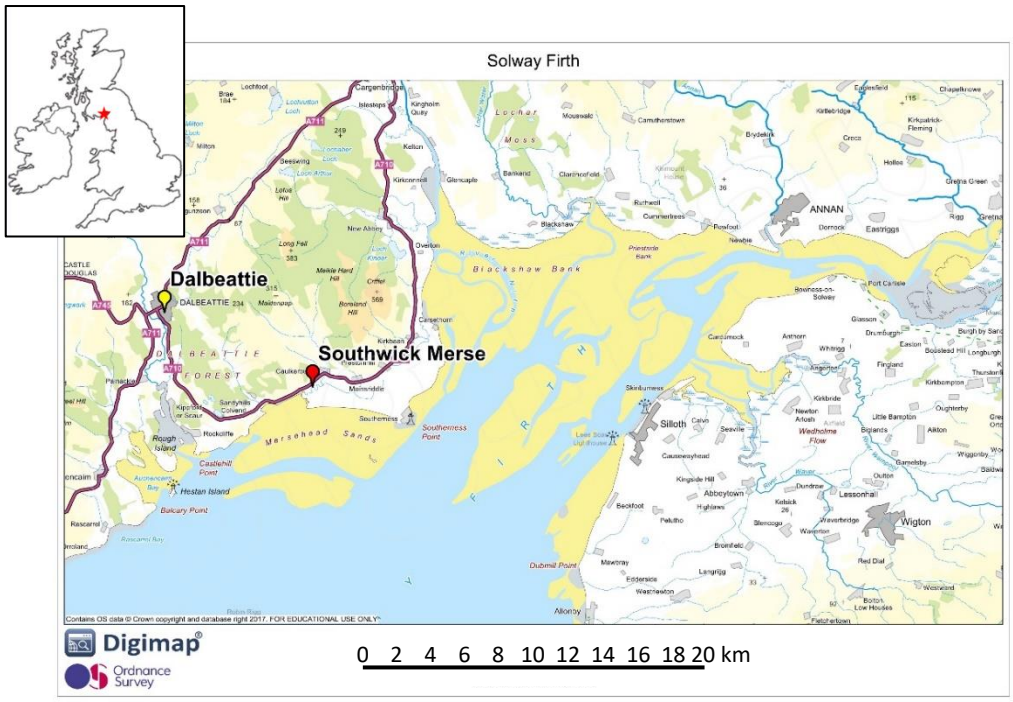

Figure 2.1. Map showing the sediments around the Solway Firth, the location of the Southwick Merse Saltmarsh and its proximity to the town of Dalbeattie. The red star on the inset map of the UK shows the location of the sampling sites in south west Scotland. The Sampling locations are shown in figure 2.2.

2.1.1.1. Southwick Merse Saltmarsh

The coastline of the Solway Firth in south west Scotland is made up of a large area of intertidal mud flats and sediments which start at the Nith and Eden estuaries and extends west along the north-west coast of England and south west coast of Scotland. The sediment comprises postglacial fluvial deposits of silt and sand which are protected from erosion by the rocky promontories around the coastline and also by sandbars and mud banks which dissipate the erosional energy of the incoming tide (Allan, 1993; Harvey and Allan, 1998; Hansom, 2007).

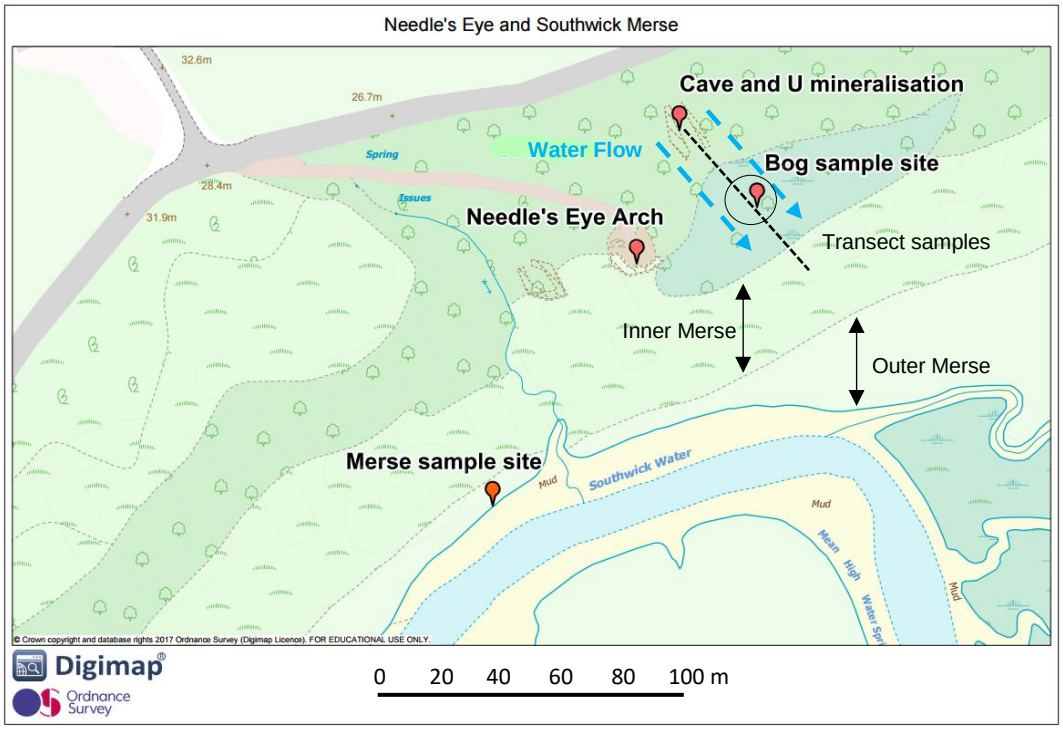

Figure 2.2. Map showing the Needle's Eye and Southwick Merse sampling locations, with the extent of the Inner and Outer Merse regions, the direction of water flow and the transect line of samples (described in section 2.1.3.2) indicated.

The transition from marine sediments to regularly inundated saltmarsh occurs where the sediments are raised and vegetated, mainly by *Puccinellia-Maritima* (common saltmarsh grass). The vegetation stabilizes the sediments, allowing them to accrete further, creating a unique and extensive saltmarsh ecosystem which is one of the largest areas of its type in

the U.K, covering an area of ~56 hectares (Burd, 1989; Scottish Natural Heritage, 2017). In recognition of its importance, the Southwick Merse has been designated as a site of special scientific interest (SSSI) due to its valuable habitat for rare plants, animals and migratory birds as well as being an excellent example of saltmarsh geomorphology (Scottish Natural Heritage, 2017).

The Southwick Water (figure 2.2) is a large channel through the marsh that has steep sides of around 1 – 1.5 m; these can be subject to undercutting and slumping. The sediments of the Southwick Merse have a depth of around 1.5 – 2.5 m sitting on top of the bedrock which is a carboniferous limestone, and fossil analysis has been used to date the sediments in the area to the early to mid Flandrian period, around 6000 - 7000 years ago (Hooker, 1991).

The area directly adjacent to the Southwick water is flat and is frequently tidally inundated. This zone, which is termed the outer Merse and is almost solely vegetated by *P. Maritima,* stretches from between 5 and 30 m inland to a step of around 10 - 20 cm high that marks the transition to a zone called the inner Merse which is vegetated with *Phragmites Australis.* Beyond the inner Merse zone is a band of native woodland which contains boggy ground leading up to a cliff and the Needle's Eye sea arch (figure 2.2).

Saltmarsh sediments have been shown to maintain profiles of anthropogenic radionuclides discharged by the Sellafield Nuclear processing facility (e.g. Mackenzie & Scott, 1993; MacKenzie *et al.*, 1994; Charlesworth *et al.*, 2006). One of the aims of this study was to investigate whether ^{14}C is incorporated into sediments in a way that can be related to its historic discharge from Sellafield, as has been shown for ^{137}Cs, ^{241}Am and other radionuclides.

2.1.1.2. Southwick Merse sampling strategy

Sediment cores were collected at the Southwick Merse to investigate the incorporation of Sellafield derived and natural radionuclides into the sediment profile. The sampling site

was an exposed and stable river cliff with a vegetated surface which was inundated twice daily. The exposed river cliff face made it possible to sample to depths of 1 m or more and also ensured that the samples collected were highly influenced by the deposition of sediment from the Irish Sea due to the proximity to the Southwick Water channel. Merse core A was collected (on 28/10/13) for analysis of anthropogenic radionuclides (^{14}C, ^{137}Cs, ^{241}Am), geochemical constituents like redox active elements Fe and Mn, and extraction and analysis of organic matter. Merse core B was collected on a later visit to the site (06/02/17), to a depth of 155 cm, in a second attempt to develop a chronology of the core using Sellafield derived ^{137}Cs and ^{241}Am.

Prior to collecting the cores, a spade was used to remove about 20 – 30 cm sediment away from the bank of the Southwick water to expose a vertical 1 m (Merse core A) or 1.6 m (Merse core B) depth section of sediment (figure 2.3). When preparing these exposed sections, a trowel was used in the horizontal direction to carefully remove the final outer layers of sediments to avoid downward smearing of the sediment layers. Merse core A was extracted by hammering a monolith tin of dimensions 100 cm length x 15 cm width x 7 cm depth straight into the exposed face using a mallet. The core was removed by carefully digging down the back of the coring tin with a spade until the core was free and could be tipped forward in the tin, taking care not to break the core. Excess sediment was then removed from the sample, again using a knife in a horizontal direction (across rather than down the core). The result was a long, rectangular core which was as uniform in size and shape as possible. This core was cut into 2 cm depth increments using a knife and was stored in plastic bags for transportation back to the lab. Forty-eight samples were taken from the core which had a final length of 96 cm. Merse core B was extracted from the same site by cutting 5 cm vertical length x 15 cm width x 7 cm depth blocks from a part of the

bank adjacent to the sampling site of the previous core. Thirty-one samples were collected in 5 cm depth increments to a depth of 155 cm.

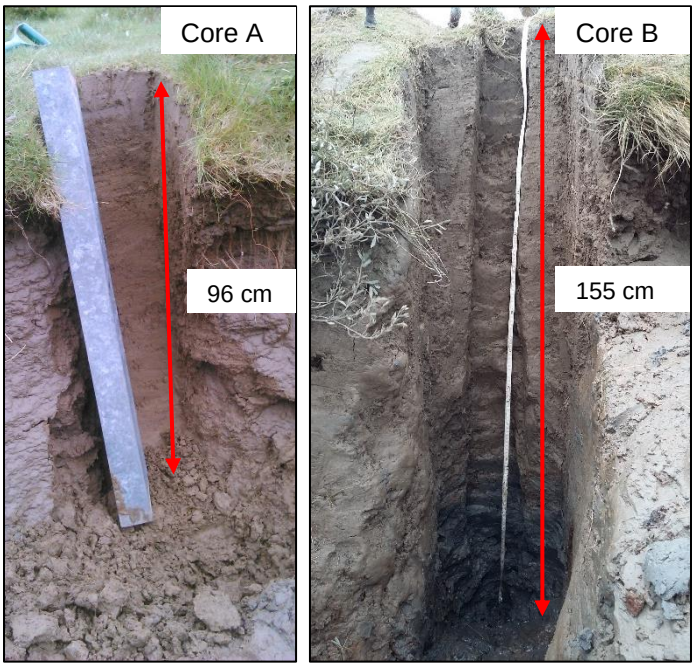

Figure 2.3. Photographs of the exposed faces excavated in the river cliff to collect sediment cores A and B from the Southwick Merse.

2.1.2. Needle's Eye natural analogue site

The study of the mobility of natural decay series radionuclides has been undertaken at the Needle's Eye since the discovery of a natural vein of U mineralization in the 1960s during a routine exploration by the British Geological Survey (Miller and Taylor, 1966). Directly below the cliff lies an area of highly organic bog which extends for around 25 m from the base of the cliff (figure 2.2). The Southwick Merse lies beyond the extent of the bog (section 2.1.1.1). The area from the cliff to the Southwick Merse makes an ideal "Natural Analogue" or "Natural Laboratory" site; one in which the natural conditions make the study of radionuclide behaviour possible in an environmental setting (section 1.8), as the natural mineralisation vein in the cliff leaches elevated levels of U, its daughter nuclides such as Ra and other potentially toxic elements (PTE) to the surrounding area. The bog beyond the cliff has been shown to have an organic matter content of up to 90% and retards and

accumulates U up to 2500 mg kg^{-1} (Mackenzie *et al.*, 1989, 1991a; b; Xu, 2013). The affinity of organic matter for binding metals, including U, is well documented, and the effect of organic matter on the mobility of uranium has been investigated in different settings (Read *et al.*, 1993; Zhang *et al.*, 1997; Graham *et al.*, 2008; Oliver *et al.*, 2008; Banning *et al.*, 2013; Tinnacher *et al.*, 2013; Li, Seaman, H.-S. Chang, *et al.*, 2014). The highly organic soil and the enhanced U concentrations at this site make it ideal for the study of U interactions with OM. Other environmental factors, such as pH, redox conditions and Fe and Mn concentration show considerable variation across the site (Mackenzie *et al.*, 1991a; Xu, 2013) which presents an opportunity to investigate the influence these variables have on the binding of U.

In the 1980s to 1990s the British Geological Survey (BGS) undertook an extensive study of the Needle's Eye natural analogue examining the geology, hydrology, mineralogy and geochemistry of the site. They found that the uranium was present in the vein in the form of uraninite, UO_2, which is subject to dissolution by oxidising and high pH (> 8) water which flows into the organic-rich soil below the cliff where the uranium accumulates. Results of mineral and solution analysis and associated geochemical modelling suggested that reduction of soluble U (VI) to insoluble U(IV) was an important mechanism of U removal from solution. However, experimental results also showed that around 90% of the U was intimately associated with organic phases of the soil and was locally enriched around plant roots. These findings suggested that a reduction mechanism was an overly simplistic view of the chemical processes taking place. At the time of the study it was acknowledged that the role of organic matter in binding uranium was not sufficiently understood to be well represented in the models used and that it was an area which warranted further investigation (Mackenzie *et al.*, 1989; Basham *et al.*, 1991; Hooker, 1991; MacKenzie, Whitton, *et al.*, 1991; Scott *et al.*, 1991; Jamet *et al.*, 1993). A schematic diagram of the

site, shown below in figure 2.4 shows the surface and underground water flow paths which transport U from the cliff into the bog.

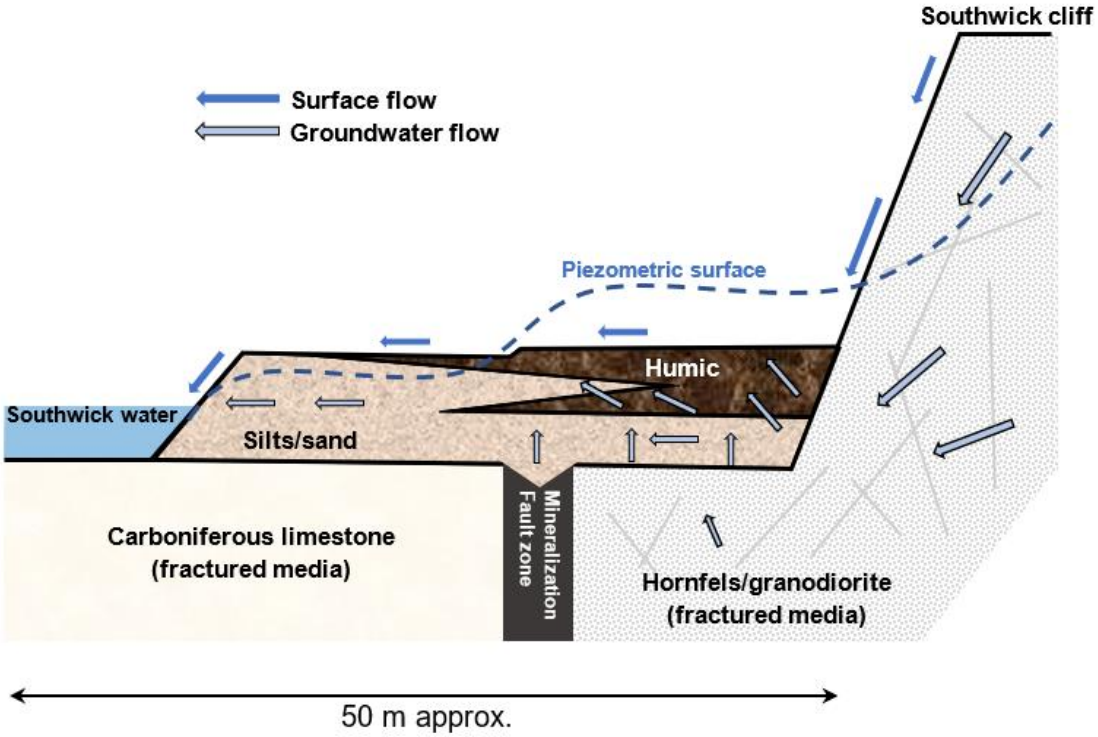

Figure 2.4. Schematic diagram of the Needle's Eye site, showing the above and below ground water flow paths and transition from bog to salt marsh (after Hooker, 1991).

2.1.3. Sampling of the Needle's Eye natural analogue site

Samples were collected from the Needle's Eye Natural Analogue site from 2013 - 2017. Solid phase peat samples and extracted pore waters were collected.

2.1.3.1. Core sampling

Soil cores were collected for analysis of U enriched peat in the surface layers of the bog. Five cores (NE cores A – E) were collected on separate sampling trips between 28/10/13 and 06/02/17. All cores were collected within an approximately 3 m^2 area in the centre of the bog. The cores were collected by excavating an approximately 30 cm x 30 cm pit to a depth of around 60 cm. One face of the pit was carefully cleaned and a monolith tin of

dimensions 50 cm length x 15 cm width by 7 cm depth was hammered into it using a mallet. A knife and a spade were used to cut around the sides of the tin to ensure it was free and the core was carefully laid back and lifted out of the pit. Bog core B was sampled in a different manner, by using a peat cutting spade to make a round cut and carefully levering out the intact core. The details of the cores collected from the bog are given in table 2.1.

Table 2.1. Cores collected from the Needle's Eye bog

Sample trip	Core identity	Date of collection	Depth of core	Sampling interval	Number of samples
1	NE core A	28/10/13	42 cm	2 cm	21
2	NE core B	08/05/14	39 cm	0 – 30 cm in 5 cm sections; 30 – 39 cm collected as a single section	7
3	NE core C	16/11/15	50 cm	2 cm	25
4	NE core D	04/02/16	44 cm	2 cm	22
5	NE core E	11/10/16	45 cm	5 cm	9

All cores collected were cut into sections on site and quickly sealed in polythene bags which were flushed with helium 2 – 3 times, sealed and stored in cool boxes for transport back to the laboratory for analysis. The analyses carried out on each core are summarised in figure 2.5.

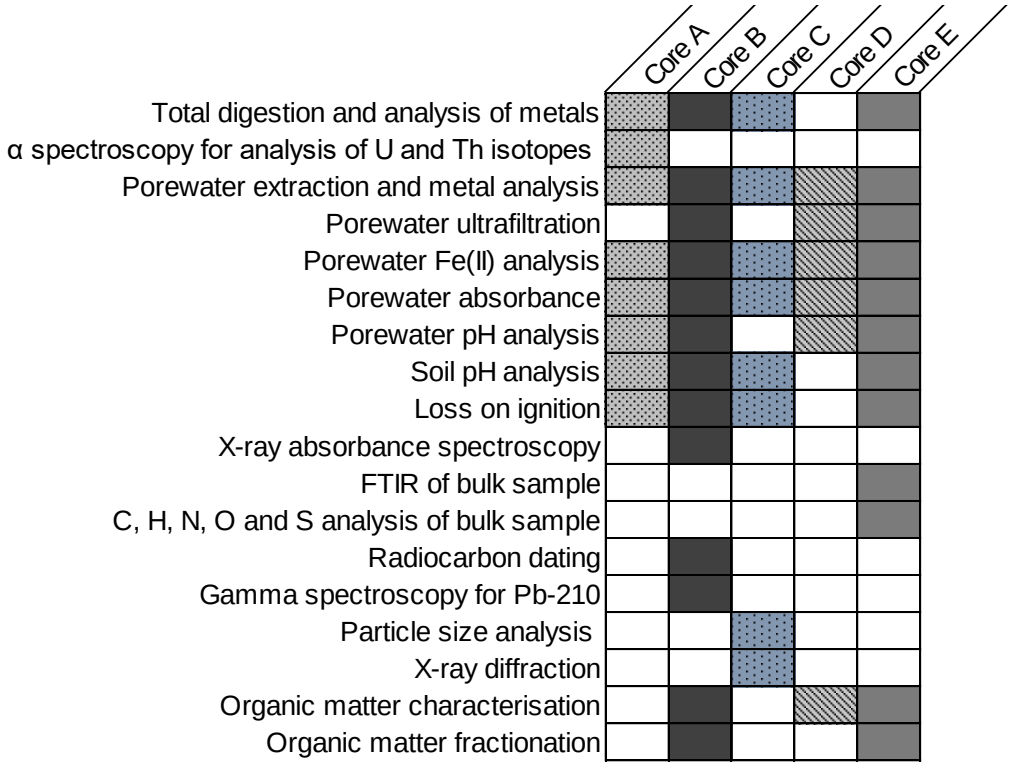

Figure 2.5. Analyses undertaken on collected cores. Filled boxes correspond to analyses carried out on each core.

2.1.3.2. Transect samples

Samples were collected along a transect from the cave towards the Merse in an approximately South Westerly direction (figure 2.2) on two occasions. On 08/05/14 a sample of 5 cm depth was collected from within the cave, bog core B was collected at 21 m from the cave and a sample was collected at 35 m from the cave to represent the furthest extent of the bog. On 06/02/17 transect samples were collected in 7 m intervals to a distance of 63 m from the cave. This transect covers the transition from the cave, through the bog and into the saltmarsh.

2.1.3.3. Collection of pore waters

2.1.3.3.1. On-site pore water extraction

Core and transect samples collected on site were immediately manually squeezed in a plastic bag and the drips collected in a petri dish. The extracted pore water was filtered into a clean sterilin tube using a 0.45 µm cellulose syringe filter. A pipette was used to transfer 1 ml of filtered sample into prepared 1.5 ml vials for Fe(II) analysis by the ferrozine method (see section 2.2.3) while the remaining pore water was stored in sterilin tubes (sample trips 2 and 3) or in pre-evacuated glass vacuum tubes (sampling trips 4 and 5) for transport back to the laboratory.

2.1.3.3.2. Laboratory pore-water extraction

On returning to the lab pore waters were extracted from transect and core samples by weighing soil samples into centrifuge tubes and centrifuging at ~8880 g for 30 minutes. Pore-water extracted was then decanted and filtered through a 0.45 µm cellulose syringe filter into Sterilin tubes or transferred by syringe into pre-evacuated glass vacuum tubes.

2.1.4. On-site analysis: redox measurement

Redox potential of the peat was measured using a handheld oxidation reduction potential (ORP) probe (HI-98121, Hanna Instruments). On two occasions transects were analysed across the surface of the bog. The measurements were made by digging a small hole, just big enough to insert the probe, around 5 cm deep into the surface of the bog. The redox potential of the surface water which filled the hole was measured by inserting the ORP probe and allowing it to stabilise for 30 – 60 seconds. On 04/02/16 samples were analysed from 10 m from the cave to 25 m from the cave at 1 m or 2 m intervals. On 11/10/16 a second transect was measured across the bog from 15 m from the cave to 35 m from the cave in 2 m intervals

2.1.5. Preparation and storage of collected samples

On returning to the laboratory after each sampling trip, the solid phase samples were organised into sub-samples which were stored and prepared in specific ways for different uses. The methods of sample storage used were air drying, freezing and refrigeration. The extraction of pore waters from samples was also carried out and is described in section (2.1.3.3). The details of sample preparation and storage are outlined below.

2.1.5.1. Air drying and moisture content analysis

Soil samples were gently disaggregated by hand and live plant material, sticks, stones and plastic contaminants were removed. The samples were then allowed to air dry at room temperature (~21°C) on pre-weighed paper plates or petri dishes until a constant mass was achieved. The mass of sample was measured before and after drying to obtain the moisture content of the original sample, calculated as follows:

Equation 2.1.

$$Moisture\ content\ (\%) = \frac{(Wet\ soil\ mass\ (g) - dry\ soil\ mass\ (g))}{Wet\ soil\ mass} \times 100$$

Once dry, the samples were coarsely ground with a ceramic pestle and mortar that was cleaned between samples by rinsing with DI water and drying under a stream of hot air. The coarsely ground samples were passed through a 2-mm sieve before being returned to the mortar and being finely homogenised by grinding. The homogenised samples were stored in plastic sample bags or plastic 50 ml tubes for use in experiments.

2.1.5.2. Preservation of Soil Samples by Freezing

The highly reducing conditions of the Needle's Eye bog means that once removed samples are very sensitive to exposure to air, with the potential of oxidation of species of interest, e.g. U(IV) to U(VI) or Fe(II) to Fe(III). For this reason, sample bags were flushed with He gas before sealing on site. On returning to the laboratory, a sub-sample was immediately removed and transferred to a second pre-labelled bag which was flushed with N_2 gas several times before being sealed with the N_2 atmosphere maintained. Since studies have shown that freezing is an effective way of maintaining soil redox conditions (Wilkin, 2006), the samples were then transferred to a freezer at -20°C for storage until analysis.

2.1.5.3. Storage of extracted pore waters

Pore waters from the Needle's Eye bog were filtered using a 0.45 μm syringe filter and were thereafter refrigerated in plastic sterilin tubes (sampling trips 1, 2, 3) or evacuated glass vacuum tubes (sampling trips 4,5). Ultrafiltration, (section 2.4.3.1) was carried out as soon as possible after returning to the laboratory and the fractions generated were refrigerated. Samples stored in evacuated vacuum tubes could be stored for longer as there was little risk of oxidation under vacuum. The results of a study by Peacock *et al.* (2014) show that samples which have been filtered have stable UV/Vis properties over a period of 12 weeks of refrigeration The collected pore water samples and ultrafiltration fractions were refrigerated for less than 48 hours before analysis by ICP-MS or UV/Vis.

2.2. Inorganic analytical methods

2.2.1. Inductively Coupled Plasma-Optical Emission Spectroscopy (ICP-OES)

2.2.1.1. Principles of ICP-OES

ICP-OES is an analytical method used for the analysis of trace elements in solution. The technique works by atomizing elements and promoting the atoms to a higher energy state within a high temperature plasma. The excited or ionised atoms return to a lower energy state by emission of photons which are diagnostic for specific elements (Boss and Fredeen, 2004).

In the instrument, torch ionization is initiated in a stream of argon flowing at a rate of 11 to 17 L min^{-1}. The argon ions interact with a magnetic field generated by applied RF (radio frequency) energy from an induction coil at the end of the torch and are accelerated causing them to collide with and ionise other argon atoms, forming a plasma. The continued application of RF power to the plasma causes a large increase in temperature to 6000 – 10000 K due to ohmic heating. The sample solution for analysis is taken up at a constant rate by a peristaltic pump and is then introduced into the plasma through a nebuliser which aspirates the solution into a fine mist. The high temperatures cause almost complete vaporisation and atomisation of the analyte and also promote electrons from the ground state to higher energy levels. As the electrons relax from a high energy state radiation, which can be detected by a charge coupled device (CCD) capable of monitoring multiple wavelengths at once, is emitted. Elements can be distinguished as the wavelength of emitted radiation (or photons) is related to the size of the gap between energy levels which is specific to each element (Boss and Fredeen, 2004; Skoog *et al.*, 2004). Elements often emit photons at a range of wavelengths which can lead to spectral overlap and interference between different elements. For this reason the wavelength monitored for a particular element must be chosen to have as little chance of interference as possible (Todorov, Wolf and Adams, 2014). ICP-OES analysis is fully quantitative as the intensity of photons at a

particular wavelength is directly proportional to the number of atoms in the sample emitting at that wavelength. Therefore, standards of known concentration can be used to calibrate the instrument and convert intensity measurements to concentration of a particular element in mg L^{-1}. ICP-OES instrumentation has excellent tolerance for high concentrations of dissolved solids in samples, up to 10 – 30 % depending on the instrument (Tyler, 2001), but is limited to element concentrations in the µg L^{-1} to mg L^{-1} range. Lower concentrations can be measured by ICP-MS (section 2.2.2).

2.2.1.2. ICP-OES method and instrumentation

All ICP-OES analysis was carried out using a Perkin-Elmer Optima 5300DV with an auto-sampler, peristaltic pump, Gem Tip crossflow nebuliser and Scott-type spray chamber. The instrument parameters are shown in table 2.2, below.

Table 2.2, ICP-OES instrument parameters

Parameter		Value
RF power		1400 W
Argon flow	Coolant	15 L min^{-1}
	Auxiliary	0.2 L min^{-1}
	Nebuliser	0.8 L min^{-1}
Pump flow rate		1.5 L min^{-1}

The elements analysed by ICP-OES were U, Fe, Mn, As, Pb, Cu, Al, and Ca. The elements for analysis were selected based on their known interaction with U or OM (Fe, Mn, Al, Ca) or their high concentration at the site and potential toxicity (As, Pb, Cu). The wavelengths used to measure each of these elements are shown in table 2.3. The wavelength selected for calculation of sample concentrations are shown in bold and these were chosen based on their relatively high intensity, good linear calibration and apparent lack of interference. The selected wavelengths were in agreement with those recommended by Todorov *et al.* (2014).

Table 2.3. Wavelengths used in ICP-OES analysis

Element	Spectral peak wavelengths (nm)
U	**409.014**, 385.958, 367.007, 393.203, 424.167
Fe	**239.562,** 238.204, 259.939, 234.349
Mn	**257.610**, 259.372, 294.920, 293.305
As	**193.696,** 188.979, 197.197, 228.812
Pb	**220.354**
Cu	**324.752,** 327.393, 224.700, 213.597, 222.778, 221.459
Al	**396.153**, 308.215, 394.401, 237.313, 309.271, 167.022
Ca	**317.933,** 315.887, 393.366, 422.673

Wavelengths shown in bold were those selected for calculation of measured concentrations.

2.2.1.3. ICP-OES calibration and quality control

Calibration standards for ICP-OES were prepared by serial dilution of single element standards (1000 ppm U, Th, Fe, Al in 2% HNO_3, Fisher Scientific) and multi-element standard MVI (multi-element standard solution VI, 2% HNO_3, Merck Millipore) with 2% HNO_3 (VWR International, Aristar 69% w/v). Nitric acid (2 %, Aristar) was used as the blank calibration standard. The concentrations used in the calibrations are shown in table 2.4.

Table 2.4. Calibration standards used for ICP-OES analysis

Element	Concentrations of calibration standards (ppm)
U	50, 25, 10, 5, 1, 0.5, 0.1, 0
Cu, Pb, Mn	10, 5, 1, 0.5, 0.1, 0
Fe, Al	500, 100, 50, 10, 5, 1, 0
Ca	1000, 500, 100, 50, 10, 0
As	100, 50, 10, 5, 1, 0

After every 6 samples a check solution of MVI diluted 10 times (prepared separately to the calibration standards) and rinse of 2% HNO_3 were analysed in order to ensure that the analysis was stable throughout the run and that the results were accurate. The independent check solutions were generally within 10 % of the solution concentration, e.g. U analysed along with the acid digested samples from NE core E: MVI independent check concentration = 1 mg L^{-1}, measured concentration = 1.08 ± 0.05 mg L^{-1} (n = 10).

2.2.2. Inductively Coupled Plasma-Mass Spectrometry (ICP-MS)

2.2.2.1. Principals of ICP-MS

ICP-MS is a versatile and high sensitivity instrumental technique which can be used to quantify metals in solution at concentrations as low as parts per trillion (ppt). The technique separates mixtures of ions by their m/z (mass to charge) ratio. The ICP torch works in much the same way as in ICP-OES (See section 2.2.1.1) and causes the complete atomisation of the sample by breaking all molecular bonds in the high temperature of the plasma.

The analyte solution is injected into the plasma as a very fine mist with a nebulizer. Once in the plasma the sample is vaporized and all molecules are atomized by the very high temperature (up to 10000 K). The atoms are then ionized during collisions with argon ions. This process forms a stream of ions directed towards sampler and skimmer cones which form the opening to the mass analyser and detector. The skimmer cones allow the ions to pass from the plasma torch, at atmospheric pressure, into the mass analyser and detector which are kept under a strong vacuum. The cones also serve to focus the stream of ions into the narrow beam necessary for separation within the mass analyser. The mass analyser consists of a quadrupole or octopole arrangement of cylindrical steel rods which have varying direct current (d.c.) and radiofrequency (RF) voltages applied in a manner which allows only ions of a specific m/z to make it all the way through the mass analyser to the detector. By scanning through a range of applied voltages multiple ions can be isolated in quick succession. The resolution of this type of mass analyser is approximately 1 atomic mass unit (amu), which allows for individual isotopes to be resolved. The isolated ions of a specific m/z that make it through the mass analyser reach the dynode electron multiplier transducer where ions impact a cathode and release electrons which in turn strike a dynode and release further electrons. An array of multiple dynodes can be used to amplify the strength of signal by a factor of up to 10^7. This creates a current which can be analysed by a computer and is proportional to the number of ions striking the cathode. Signal strength

is related to concentration by calibration using certified standards (Skoog *et al.*, 2004; Ammann, 2007).

ICP-MS is widely used in environmental science for direct analysis of trace elements in pore and surface waters but also in soil and plant samples which have undergone a digestion procedure to release the analytes of interest into the solution phase. It can also be used to analyse isotope ratios and coupled with chromatography systems to investigate elemental speciation (Jenner *et al.*, 1990; Farmer, Eades and Graham, 1999; Blair, 2013; MacGregor, 2016).

2.2.2.2. ICP-MS method and instrumentation

An Agilent 7500ce ICP-MS instrument was used for analysis of low concentrations of U, Fe, Mn, As, Pb, Cu, Th, Al, and Ca in solution. The instrument includes an auto-sampler, a micro-mist nebulizer, Scott-type glass spray chamber, nickel sample and skimmer cones and an octopole reaction system. The octopole reaction system eliminates the interference of polyatomic molecules which occur at the same mass as some elements of interest e.g. ^{57}Fe and $^{40}Ca^{16}OH$ (McCurdy, Potter and Woods, 2006).

The operating conditions of the instrument are shown in table 2.5.

Table 2.5. Operating conditions used in ICP-MS analysis

Instrument parameter	**Setting**
RF power	1540 W
Reflected power	1 W
Argon carrier gas flow	0.82 L min^{-1}
Argon make up gas flow	0.21 L min^{-1}
Nebuliser	Micro mist
Nebuliser up-take rate	0.02 mL min^{-1}
Analyser vacuum pressure	3×10^{-6} Pa
IF/BK vacuum pressure	8.5×10^{-1} Pa
Rinse speed	0.3 rps
Sample rinse time	40 seconds

The instrument was calibrated with standards prepared from Multielemental standard MVI (Merck Millipore). A serial dilution method was used to dilute the sample to the concentration range shown in table 2.6, below.

Table 2.6. Calibration range of elements analysed by ICP-MS

Element	**Concentrations of calibration standards (µg L^{-1})**
U, Cu, Pb, Mn, Al,	1000, 500, 100, 50, 10, 1, 0.5, 0.1, 0
Fe, As	10000, 5000, 1000, 500, 50, 10, 5, 1, 0
Ca	100000, 50000, 10000, 5000, 1000, 500, 100, 0

The calibration standards were diluted with appropriate solutions to match the sample matrix, e.g. DI water for pore-water samples, 0.01 M NaOH for eluted SEC fractions (section 2.4.3.3). The calibration standards were analysed from low to high concentration to minimise any carry over effect from analysis of high concentration solutions. Three rinse solutions were analysed after the calibration graph to ensure the high concentration standards were not carrying over into the sample analysis. Check solutions of MVI diluted 1000 times followed by a rinse were analysed after every six samples to account for any drift in seen in calibration throughout the analysis run. Independent certified reference material SRM 1640a, Trace Elements in Natural Water (National Institute of Standards and Technology) was analysed in every run to ensure the accuracy of the calibration.

2.2.3. Ferrozine method for measurement of reduced Fe(II)

The method of Viollier *et al.* (2000) was adopted for the measurement of Fe(II) in extracted pore waters. The method relies on the complexation of Fe(II) by "ferrozine" ($C_{20}H_{13}N_4NaO_6S_2 \cdot xH_2O$) forming a purple solution which can be analysed photometrically for absorbance at a wavelength of 562 nm.

Ferrozine solution was prepared at a concentration of 0.01 M in 0.1 M ammonium acetate. The solution was prepared in advance of field trips and 100 µl was measured by pipette into 1.5 ml plastic Eppendorf vials. At the field site, 1 ml of 0.45 µm filtered extracted pore water (see section 2.1.3.3) was pipetted into the vial, producing a final volume of 1.1 ml. On returning to the laboratory, the absorbance of the solution was measured at 562 nm with a Perkin Elmer Lambda 900 UV/Vis spectrophotometer using a matching pair of 1 cm quartz cuvettes.

The reference cell contained 1 ml DI water added to 0.1 ml ferrozine solution to account for solution matrix effects. The absorbance data was converted to concentration in µg L^{-1} by calibration with standards prepared from $FeCl_3$ in solution containing hydroxyl ammonium chloride in order to reduce Fe(III) to Fe(II). Due to the hygroscopic properties of $FeCl_3$ the concentration of the standards was confirmed by ICP-OES analysis and was determined to be accurate ($R^2 = 0.99$). The calibration curve used for calculation of Fe(II) concentration from absorbance data is shown below (figure 2.6).

The equation for the linear calibration is given below (equation 2.2):

$$Abs = 8.91\times10^{-4} + 3.47\times10^{-4}\,[Fe(II)] \qquad \text{Equation 2.2.}$$

The concentration of Fe(II) measured in samples was compared to total Fe analysed by ICP-MS to calculate the relative abundance of Fe(II) and Fe(III) species in water samples.

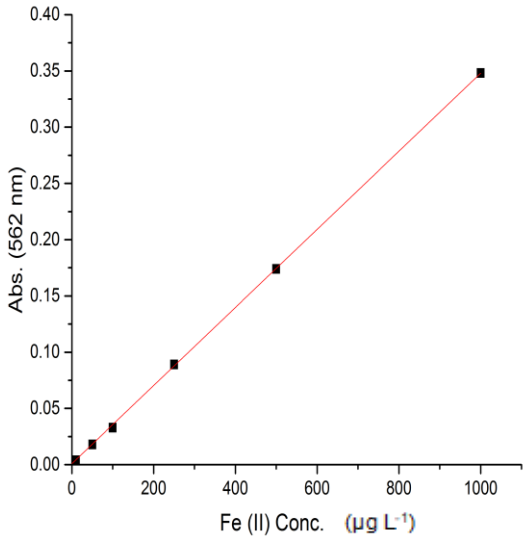

Figure 2.6 Calibration graph for Fe(II) analysis by the ferrozine method.

2.2.4. pH analysis of solid phase soils and soil pore waters

The pH of soils and soil pore water samples was measured using a Jenway model 3505 pH meter calibrated with buffer solutions of pH 7 and 4 (Fisher Scientific). The solid phase material was shaken with a mechanical shaker in a ratio of 1 g sample: 5 ml DI water for 15 minutes after which the pH of the soil solution was analysed. The measurement was made after the pH value had been stable for at least 10 seconds. The pH of extracted porewaters was analysed in the same way as the soil solutions.

2.2.5. Microwave-assisted acid digestion of soils

2.2.5.1. Background to microwave digestion techniques

The analysis of metal concentrations in solid phase soil samples by ICP-OES or ICP-MS requires total dissolution of the sample. Due to the resistant nature of some mineral phases,

e.g. silicates, present within soil, this is best achieved by application of concentrated strong acids at high temperatures. Traditionally dissolution was achieved using a single concentrated acid or mixture of acids, often nitric, hydrochloric or hydrofluoric, on a hot plate in Pyrex or Teflon beakers. A more modern approach involves using a specialised microwave system to heat samples, with the advantages including the use of considerably lower volumes of acids, better temperature monitoring, high temperature and pressures achievable, decreased analyte loss, better safety monitoring and more uniform and repeatable digestions. For these reasons microwave digestion techniques are widely used in soil analysis and standard methods have been developed to ensure good analyte recovery and comparability of results between studies. (Kuss, 1992) The method used in this study, outlined below, was a modified version of US EPA 3052 (1996), with the modification being the addition of a loss on ignition step by furnace ashing before digestion (Yafa *et al.*, 2004). This destroys the organic component of the soil and more consistently results in complete dissolution of the sample following microwave digestion.

2.2.5.2. Microwave-assisted acid digestion methodology

A sample of approximately 0.25 g air-dried and ground sample was accurately weighed into a beaker and oven dried at 105°C (Gallenkamp) for at least five hours in order to remove any remaining moisture. It was then re-weighed before being ashed at 450°C in a furnace for 4 hours in order to remove organic carbon (see section 2.4.1 and 2.2.5.1). The samples were then ready for digestion using a CEM Microwave Accelerated Reaction System 6 (MARS 6) with CEM HP 500 Teflon vessels and a reference vessel monitored for pressure and temperature with an ESP plus pressure sensor and MTS 300 fibre optic temperature probe (CEM). Ashed samples were weighed once more, so as to determine the LOI, before being carefully transferred into the Teflon microwave digestion vessel. A volume of 9 ml concentrated HNO_3 (69%, Aristar) was then added to the digestion vessel, some of which was used to rinse the sample beaker at least three times to ensure all the

sample had been transferred to the vessel. Then, 1 ml of concentrated HF (48%) was pipetted into each vessel after which the vessels were sealed with caps and transferred into the microwave. The microwave carousel holds a total of 14 vessels and in each run at least 2 reagent blanks and 2 certified reference materials (CRMs) were analysed. In accordance with US EPA 3052, the digestion was carried out at a temperature of 180°C with a maximum pressure of around 120 psi. The microwave was programmed to increase the temperature from around 20°C to 180°C over 5.5 minutes, hold for 9.5 minutes and then allow the vessels to cool. After digestion, the solution was transferred from each microwave vessel to a Teflon beaker. The microwave vessels were rinsed a few times with a small volume of 2% HNO_3 (Aristar) to ensure the complete transfer of the samples. The Teflon beakers were then heated on a hot plate to reduce the total sample volume to around 1 – 2 ml. The beakers were taken off the heat and allowed to cool to room temperature before being diluted to 25 ml in a volumetric flask with 2% v/v Aristar HNO_3. The diluted solutions were filtered through a Whatman No. 40 hardened ashless filter paper into sterilin tubes which were refrigerated until analysis.

2.2.5.3. Digestion of certified reference materials (CRMs)

Two CRMs and two blank solutions were digested along with each batch of samples. The digestion of CRMs was to ensure that the acid digestion method was effective in achieving total dissolution. The CRMs were analysed by ICP-MS due to their low concentrations of U compared to the samples analysed. Initially, the CRM used was IAEA 326 (Bojanowski *et al.*, 2001), a CRM developed specifically for radionuclide analysis. The concentration of U recovered from IAEA 326 was 1.56 ± 0.25 mg kg^{-1} (n = 38). This is higher than the certified HF extractable U content (1.45 mg kg^{-1}) but less than the certified total U content (2.38±0.11 mg kg^{-1}). This was considered to be due to the highly mineral and low organic matter matrix of the CRM making it hard to achieve total dissolution of the sample.

A second reference material, SRM 2710a; highly elevated trace element concentrations in soil (NIST, 2009), was acquired which was also digested with later samples. The results of analysis of NIST 2710a are shown in table 2.7.

Table 2.7. Measured concentration and calculated recovery of SRM 2710a (14 replicates)

	Units	Certified conc.	uncertainty	Measured conc.	Standard deviation	Recovery (%)	RSD (%)
U	mg kg^{-1}	9.11	0.3	8.59	0.64	94.27	7.50
Fe	%	4.32	0.08	3.9	0.50	90.46	12.74
Mn	%	0.214	0.006	0.21	0.02	96.61	9.47
As	%	0.154	0.01	0.16	0.02	102.14	14.89
Cu	%	0.342	0.005	0.34	0.02	99.42	4.69
Pb	%	0.552	0.003	0.55	0.06	98.88	10.93
Ca	%	0.964	0.045	0.53	0.26	55.13	48.13
Al	%	5.95	0.05	1.67	1.28	28.13	76.77

The results in table 2.7 show the overall good recoveries achieved by microwave assisted acid digestion and analysis by ICP-MS of SRM 2710a (>90%) except for Ca and Al. The low Al recovery is likely to be because of the formation of insoluble Al fluorides.

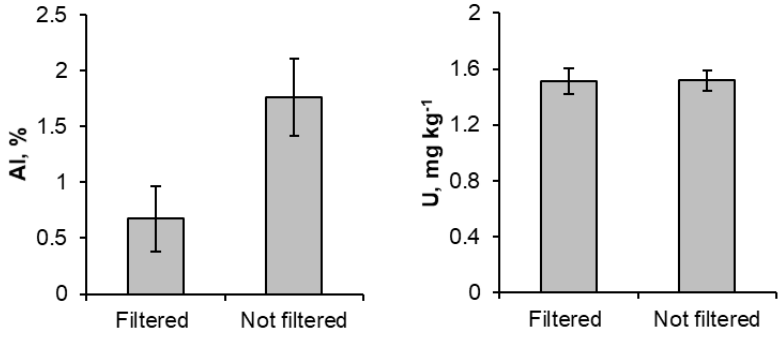

Figure 2.7, effect of filtration in the microwave assisted acid digestion of Al and U. Four replicates of each sample, error bars show standard deviation.

Figure 2.7 shows the comparison between analysis of Al and U in the CRM IAEA 326 with the filtration step included and omitted. The Al recovery is significantly lower in the filtered samples than those which were not filtered whereas the results of U and other metals were

unaffected, suggesting that precipitated Al is removed from the solution by filtration. The filtration step was maintained in the method despite the potential impact on the Al recovery to avoid causing a blockage in the nebuliser of the ICP-MS. The results of the analysis of U and other metals showed that they were unaffected by the filtration step. This is also evident from the good recoveries of SRM 2710a (table 2.7).

2.2.6. Developing sediment chronologies using ^{210}Pb dating and historic anthropogenic radionuclide discharges

Two methods of calculating sediment accumulation rates at the Southwick Merse were applied in this study: ^{210}Pb dating and comparison of anthropogenic radionuclide depth profiles with historic discharges.

Lead-210 dating is a method used to measure the depth chronology and accumulation rate of sediments and soils (e.g. MacKenzie *et al.*, 2011). The technique relies on the changing phase (solid, aqueous or gaseous) of members of the ^{238}U decay series. The decay of ^{226}Ra to ^{222}Rn severs the connection between the top of the decay chain and the isotopes below ^{222}Rn, as it causes a change of phase from solid or dissolved Ra to gaseous Rn which escapes through fine pores in rocks or soils to the atmosphere. Gaseous ^{222}Rn in the atmosphere decays by β emission to the short lived isotopes ^{218}Po, ^{214}Pb, ^{214}Bi and ^{214}Po which in turn decays to ^{210}Pb, with a $t_{1/2}$ of around 22 years (table 3.9, below). This results in constant deposition of ^{210}Pb from the atmosphere onto the surface of the Earth. Lead-210 becomes incorporated into sediments and soils as they accrete and are buried. As it decays at a constant rate to stable ^{206}Pb (via ^{210}Bi and ^{210}Po) the decline in ^{210}Pb concentration with depth can be measured to assess the age profile of the soil or sediment. This technique, ^{210}Pb dating, is useful in undisturbed soils and sediments, and has been applied in this project (Sections 3.6 and 5.2.4). However in areas with high levels of mixing

or contamination inputs of ^{210}Pb the profile can be affected so it is not possible to estimate the age accurately (McCartney, Kershaw and Allington, 1990; Thomson, Dyer and Croudace, 2002).

In some cases nuclides other than ^{210}Pb can be used to develop core chronologies. Anthropogenic radionuclides can be used to calculate sedimentation rates around the Solway Coast due to the well characterised inputs into the Irish Sea from the Sellafield nuclear reprocessing facility. The depth profiles of ^{137}Cs and ^{241}Am, amongst others, in coastal sediments around the Solway Coast have been shown to be linked to the historic discharge of these radionuclides into the Irish Sea from Sellafield (Jones, Roberts and Miller, 1988; Allan, 1993; MacKenzie *et al.*, 1994; Charlesworth, Service and Gibson, 2006).

2.2.6.1. Gamma spectroscopy

Gamma (γ) spectroscopy was used to investigate the distribution of natural and anthropogenic radionuclides in samples from the Southwick Merse and Needle's Eye bog in an attempt to establish chronologies using ^{210}Pb dating and the discharge profiles of anthropogenic radionuclides. The radionuclides measured by gamma spectroscopy were ^{237}Cs, ^{241}Am, ^{210}Pb, ^{234}Th, ^{214}Pb, ^{214}Bi, ^{212}Pb, ^{208}Tl and ^{228}Ac. High energy γ rays are often emitted when a radionuclide undergoes α or β decay but can also be a radionuclides sole decay mechanism. The highly penetrating nature of γ radiation means that it there is very little likelihood of self-absorption by the matrix in natural samples which means that the sample preparation is quite straight forward. However, the shape and geometry of samples can affect the efficiency of detection, so uniform geometries and must be used for samples to be comparable. This also applies to the standards chosen for calibration which should be as similar to the sample as possible. Detectors used in gamma spectroscopy have to be highly shielded with dense materials like lead to prevent natural background radiation from interfering with the detection of gamma emission by a sample. The energy of the radiation,

in keV, is characteristic of the nuclide from which it was emitted due to the differing magnitude of the gap between excited and ground states in each nuclide. This is exploited in gamma spectroscopy to identify an emitted nuclide by its characteristic energy. The concentration of a specific radionuclide in the sample is directly related to the intensity of the emission at a specific energy, and can be calculated if the half-life of the nuclide is known. The emission energy if the radionuclides analysed are shown in table 2.8, below.

Table 2.8. Energy used to identify radionuclides in gamma spectroscopy. Half-life data from (Rumble, 2017).

Radionuclide	Energy (keV)	Half-life
^{210}Pb	46	22.6 years
^{234}Th	63	24.1 days
^{214}Pb	295, 352	27.0 minutes
^{214}Bi	609	19.7 minutes
^{212}Pb	239	10.6 hours
^{208}Tl	584	3.05 minutes
^{228}Ac	911	6.15 hours
^{137}Cs	662	30.1 years
^{241}Am	60	432 years

In this study, γ spectroscopy analysis was carried out as follows:

Ten and 20 g samples of air-dried and ground peat and sediments respectively were pressed into pellets of uniform dimensions using cylindrical steel dies which had 10 tons of pressure applied using a hydraulic press. The samples were placed in petri dishes which were then sealed with glue to make them air-tight. The samples were left to stand for at least 30 days to allow radium and radon gas to reach secular equilibrium. Secular equilibrium is achieved due to the relatively long $t_{1/2}$ of ^{226}Ra (1599 years) compared to its daughters. The delay of 30 days (more than 7 half-lives of ^{222}Rn, 3.8 days) allows any radon trapped in the vessel when it was sealed to completely decay, so the only ^{222}Rn in the vessel is the direct decay

product of ^{226}Ra in the sample. At this point (within 1% or less of secular equilibrium) the activity of the daughter nuclide ^{222}Rn and the individual activities of both ^{214}Pb and ^{214}Bi are equal to the activity of ^{226}Ra (Mossini, Macerata and Giola, 2015). The samples were placed in a reproducible manner onto the γ detector. The instrument used was an n-type high purity germanium (HPGe) gamma photon detector housed in a 10 cm lead shield fitted with a Cd-Cu lining. Spectra were recorded using an Ortec ADCAM unit and peaks were assigned and quantified using the Ortec peak search analysis program GammaVision.

2.2.7. Alpha spectroscopy

The activity ratio of a radionuclide and its daughter, e.g. ^{234}U/^{238}U, can vary with local chemical conditions, as is described in section 1.1.3. In this project, alpha (α) spectroscopy was used to investigate the fractionation of ^{234}U/^{238}U, ^{230}Th/^{238}U and the concentration of ^{232}Th.

Alpha radiation emitted by certain radionuclides can be directly measured to determine the concentration of that nuclide in a sample. Alpha particles have the lowest penetration of the forms of ionizing radiation due to their relatively large size (4 amu). This means they can be stopped easily and α radiation emitted in soils is highly likely to be absorbed by the sample. For this reason, the detection of α radiation requires the sample to be thoroughly digested and deposited as a very fine layer of sample onto a flat stainless steel disc. In α spectroscopy the isotopes are distinguished by the energy of their α emission. For example, the decay of ^{238}U and ^{234}U release α particles at two distinct energies, 4.195 and 4.147 MeV for ^{238}U and 4.768 and 4.717 for ^{234}U (Edwards, 1968). As the half-lives of the radionuclides are known the amount of α radiation detected at a specific energy can be directly related to the concentration of the radionuclide from which it was emitted.

Alpha spectroscopy was used to analyse natural isotopes of U and Th in samples from the Needle's Eye Bog and from the Southwick Merse. The isotopes analysed were ^{238}U, ^{234}U, ^{232}Th and ^{230}Th. The method used is similar to that described in Oliver *et al.* (2007). Approximately 2 g of air dried, finely ground samples (section 2.1.5) were weighed into ceramic crucibles which were combusted at 600^{o}C in a furnace to remove organic matter. The ashed samples were transferred into Teflon beakers into which approximately 5 ml of 9 M HCl (Aristar, VWR) and 1 ml of a spike solution of ^{232}U (0.168 Bq ml^{-1}), to act as a yield tracer, were added. Samples were digested for 6 hours on a hotplate in a 1:1 mixture of concentrated HCl and HNO_3 (Aristar, VWR). After this first digestion stage the sample was evaporated to near dryness and hydrogen peroxide (H_2O_2) (Aristar, VWR) was added in order to remove any remaining organic material. The samples were evaporated to near dryness once more and around 5 ml of concentrated HF (48%, Aristar, VWR) was added and the samples were digested for 8 hours. The solution was completely evaporated and the HF digestion procedure was repeated for the samples from the Southwick Merse which had not fully dissolved. Once full dissolution of all samples was achieved, the samples were evaporated to dryness and the residue was re-dissolved in 4 M HNO_3. After digestion U and Th were isolated from solution to obtain a pure sample for electroplating. Addition of NH_4OH solution (35% v/v) caused the precipitation of $Fe(OH)_3$ and the co-precipitation of U and Th. The precipitate was isolated by decanting the supernatant solution after centrifugation and was washed with deionized water. The washed precipitate was dissolved in 9 M HCl, transferred to a clean beaker and boiled to dryness. The precipitate was re-dissolved in around 50 ml of 9 M HCl and a di-isopropyl ether (DIPE) solvent extraction was performed to remove Fe from the sample. The next stage was to separate the U and Th by passing the 9 M HCl sample solution through a chloride form anion exchange resin (Bio-Rad, AGl-x8, 100 – 200 mesh) preconditioned with around 20 ml of 1.2 M HCl followed by around 20 ml of 9 M HCl. Th was collected in two rinses of 25 ml 9 M HCl, after which the U fraction was eluted with 150 ml of 1.2 M HCl. The Th fraction was taken

to dryness, re-dissolved in around 50 ml of 4 M HNO_3 and had NH_4OH added to precipitate Al. The precipitate was washed, re-dissolved in a small volume of concentrated HNO_3 and transferred to a beaker wherein it was dried and re-dissolved in around 50 ml of 8 M HNO_3. This solution was eluted through a nitric form anion exchange column that had been pre-conditioned by washing with around 20 ml of 1.2 M HCl followed by the same volume of 8 M HNO_3. After the sample was introduced to the column it was washed twice with 25 ml of 8 M HNO_3 and finally the Th fraction was eluted with 100 ml of 9 M HCl. The separated U and Th fractions were taken to near dryness in a beaker and were re-dissolved in 3.75 % (w/v) NH_4Cl solution. The samples were then evenly coated onto stainless steel discs by electrodeposition. The discs were counted by alpha spectrometry using a silicon surface barrier detector (Octête plus, Ortec, USA).

2.2.8. X-ray diffraction and particle size analysis

2.2.8.1. Background

The mineral component of bog core C was analysed by XRD and particle size analysis to investigate the inorganic phases present in samples from the Needle's eye bog.

X-ray diffraction is a popular method for analyzing the mineral composition of soils and rock samples as it is non-destructive, widely available and can be used for quantitative as well as qualitative analysis. The method relies on Bragg's law which states that the angle at which an x-ray is diffracts off a crystal surface is dependent upon the spacing between units within the crystal lattice and the wavelength of incident light.

$$n\lambda = 2d \sin\theta$$ Equation 2.3 Bragg's law.

$n\lambda$ = whole number of wavelengths

d = spacing between crystal lattice layers

θ = glancing angle (angle at which the x-rays strike the sample surface)

During the analysis a monochromatic (single wavelength) beam of x-ray radiation is directed onto the surface of a sample and the glancing angle is varied, usually between around 2 and 70 degrees. The intensity of diffracted x-rays is measured across the range of glancing angles and the d – spacing value is calculated at the angle at which highest intensity is measured. The d – spacing can be used to determine the crystal analysed as the value is unique to each crystal lattice configuration. The technique is commonly applied to powder samples (powder diffraction) as at any given angle there are enough correctly orientated crystals to satisfy Bragg's law (Atkins, 2006). Minerals can be identified by comparison with databases of the characteristic diffraction patterns of individual minerals which have been compiled over many years. Soil and rock samples have a potentially large number of constituent minerals and any which have an abundance of greater than around 1% may be identified.

The samples for XRD and particle size analysis were prepared by ashing to remove organic matter. Approximately 50 g of fresh soil from each depth sample was oven-dried for 48 hours at 105 °C in dry pyrex beakers which had been pre-weighed. On removal from the oven the dry weight was recorded and the samples were then placed in a furnace at 450 °C for 12 hours. This destroyed the organic component of the samples leaving only the mineral phases. Moisture content and loss on ignition were calculated from the weight of samples before and after drying and ashing (as in section 2.1.5.1 and 2.4.1).

2.2.8.2. X-ray diffraction (XRD) analysis of mineral phases

For XRD analysis the ashed samples were ground to a fine powder using an agate mortar and pestle to achieve a particle size of less than 50 µm. Around 0.5 g of each were loaded onto circular sample plates as a loose powder, keeping the surface as level as possible. The analysis was carried out using a Bruker D8 Advance with Sol-X Energy Dispersive detector. Each sample taking around 1 hour. Any component present with an abundance of at least 1% can be identified.

Major minerals present were identified by comparing the resulting spectra with International Centre for Diffraction Data (ICDD) database. Quantitative results were obtained using TOPAS 3.0 Rietveld analysis software.

2.2.8.3. Particle size analysis

Approximately 1 g of ashed sample (unground) was suspended in 50 ml of 4% sodium hexametaphosphate solution in a 100 ml pyrex beaker. The beakers were transferred to an ultrasonic bath for around 2 hours to promote disaggregation of flocculated particles. The particle size distribution was ascertained using a Beckmann Coulter LS230 with photoionization detector and variable speed fluid module which measures grain sizes in suspension in the range 0.04 µm – 2000 µm.

2.3. X-ray absorption spectroscopy (XAS)

Understanding the oxidation state of U (and many other potentially toxic elements) is an important step in considering its potential mobility in the environment, due to the impact oxidation state has on U solubility.

X-ray absorption spectroscopy is a method of absorption spectroscopy whereby high energy X-rays, generated in a synchrotron, are used to excite electrons in the "core" electron shells of an atom, those closest to the nucleus, into higher energy orbitals, or to excite them so much that they escape the atom completely into the continuum (photoelectric effect) (Kelly, Hesterberg and Ravel, 2008). The term X-ray absorption refers to the situation when all the energy applied as an X-ray is absorbed by an atom, either by the nucleus or the electrons. Electrons in core orbitals absorb energy from X-rays and are promoted into higher energy states within the atom, or escape the pull of the nucleus completely. The promotion of an electron to a higher energy state leaves a "hole" in the core orbital it was excited from. This is a very unstable state, and an electron in a higher energy level immediately undergoes relaxation to transition into the core hole. The relaxation occurs by a rapid release of energy, for example by X-ray fluorescence. The energy required to promote a core electron is specific to each element, and to the arrangement of orbitals within the atom. With increasing distance from the nucleus, the binding energies of the electrons in each orbital decrease. The energy required to overcome the binding of the nucleus and promote a core electron to a higher energy level therefore also decreases with distance from the nucleus. The energy absorbed by the promotion of an electron from a different shell is called the absorption edge. Elements have specific absorption edges at the binding energies of their electrons. By scanning a sample with a range of X-rays from low to high energy a profile can be obtained showing where absorption edges (total energy transfer from an X-ray to an atom) occur.

The information derived from analysis by XAS is divided into two distinct experiments focusing on different regions of the XAS specrum. X-ray Absorption Near Edge Structure (XANES) is based on the analysis of the first absorbance edge while the Extended X-ray Absorption Fine Structure (EXAFS) uses the following part of the spectrum. The absorption edge in the XANES can be used to gain information about the oxidation state and electronic configuration of the atom investigated, while EXAFS provides information about the local binding environment of the atom, such as the bond distances to adjacent atoms. In XANES, the absorption edge shows variation caused by the oxidation state of the atom, so comparison of unknown samples with standards of known oxidation state makes it possible to assess the dominant oxidation state present in an environmental sample.

In EXAFS the absorption edges are influenced by the binding environment of the atom analysed. The spectrum of a measured sample is modelled with different conditions. Different elements in the local environment surrounding the atom of interest are nearby and their bond distance can be modelled, until a good fit is achieved (Kelly, 2010).

2.3.1. Preparation of samples for XAS analysis

XAS was applied to measure the oxidation state of U in samples from the NE core B. Uranium in its reduced state, U(IV), is highly sensitive to exposure to air which can trigger oxidation. For this reason, great care was required in the preparation of samples. Two depth samples of NE core B, 0 – 5 cm and 10 – 15 cm, were selected for analysis. As is described in section 2.1.3 the samples were stored frozen under an atmosphere of N_2 in order to preserve their oxidation state. For preparation for XAS analysis the frozen samples were removed from the freezer and placed in a glove bag which was purged with N_2 several times. The samples were left to slowly defrost and after around 1 hour, still within the glove bag, the samples were broken up and a small amount (~2 – 5 g) was extracted from the

middle of each sample and transferred to small plastic test tubes. The tubes were sealed and labelled and placed into an air tight container which was flushed with N_2 and sealed, still within the glove bag underan atmosphere of N_2. The samples were transported to Manchester where they were opened in an air free glove box, mounted and sealed into samples holders for XAS analysis. The analysis was undertaken at the Diamond Light Source synchrotron, Didcot, on beamline I18.

This work was carried out in collaboration with consortium partners within the Lo-RISE project from Manchester University and Diamond Light Source.

2.4. Organic analysis methods

2.4.1. Soil organic matter content by loss on ignition (LOI)

The total amount of organic matter in the solid phase samples was measured by loss on ignition (LOI). Duplicate aliquots of 0.25 g air dried sample were accurately weighed into pre-weighed, dry beakers. Clean watch glasses were placed on the top of each beaker to prevent loss of material during the drying and ashing processes and to keep out contaminants. The sample beakers were then oven-dried at 105°C for at least 5 hours (Gallenkamp). After oven drying the beakers were allowed to cool in a desiccator for around 30 minutes before being re-weighed to ascertain the dry weight of the sample. Finally, the beakers were placed into a furnace (Carbolite) at 450°C for four hours. On removal from the furnace the beakers were again allowed to cool in a desiccator before being weighed for a final time to obtain the ashed weight of the sample. The LOI was calculated as a percentage using the following calculation (equation 2.4):

Equation 2.4

$$LOI\ (\%) = \frac{(Dry\ mass\ (g) - Ashed\ mass\ (g))}{Dry\ mass\ (g)} \times 100$$

2.4.2. Organic matter extraction

Various techniques have been employed in the extraction of organic matter, using both aqueous and organic solvents. Extractions under basic conditions are known to be very efficient and concentrations of NaOH of 0.1 M or greater are able to dissolve up to 80% of soil organic matter (Stevenson, 1982). Increasing the pH causes the de-protonation of functional groups and leaves them negatively charged, allowing the organic molecule to dissolve as water molecules interact with the polarized functional groups (Hayes, 2006). The traditional definition of humic substances, organic molecules which can be extracted from soils and do not belong to specific classes of bio-molecules (Stevenson, 1982) has

been updated by the improvement of analysis techniques, like NMR, which show that extractable soil organic matter is actually a very complex mixture of recognisable compound classes including peptides, alcohols, aromatic and aliphatic acids and carbohydrates (Simpson *et al.*, 2002; Hertkorn, 2006; Leenheer, 2009). The description of humic substances is therefore purely operational, based on the extraction method and solvent used.

Sodium hydroxide can dissolve organic matter, biologically derived organic compounds and can cause the lysis of cells leading to the release of biological components within (Simpson *et al.*, 2007). Using higher concentrations and longer extraction times allows for a more complete recovery of extractable organic matter; however these conditions also create some problems, as described in Stevenson (1982), such as the dissolution of mineral components. These conditions also lead to an increased risk of oxidation of the organic matter. However extraction under an inert atmosphere, such as N_2 gas, has been shown to limit this oxidation (Hayes, 2006). The mechanism of organic matter dissolution at high pH is due to the presence of H-bonding between acidic functional groups of organic molecules, which limits their solubility in water.

2.4.2.1. Organic matter extraction and preparation: Southwick Merse Sediment samples

The sediments of the Southwick Merse are known to have a low organic matter content of around 5% or less (Harvey, Hansom and MacKenzie, 2007). A ratio of 1:5 sediment to 0.1 M NaOH (w/v) was used to maximise the amount of OM dissolved into solution. Initially extractions were done on a small scale to investigate the extractability of organic matter from the samples. The extractions were then scaled up to generate enough humic substances for ^{14}C analysis, NMR and fractionation by SEC (Chapter 5).

The presence of oxygen can lead to an increase in oxidation of organic matter during extraction. For this reason the 0.1 M NaOH used had to be de-gassed as thoroughly as possible to avoid the addition of dissolved O_2 gas to the sample.

De-gassed 0.1 M NaOH was prepared by addition of approximately 3.99 g of solid NaOH to a 1 L volumetric flask that contained just under 1000 cm^3 of deionized water which had been purged with N_2 gas for around 30 - 60 minutes using a glass Pasteur pipette connected to a stream of N_2. On addition of the solid NaOH the purging continued until it was thoroughly dissolved. The volumetric flask was made up to the mark with a small volume of DI water and the 0.1 M NaOH solution was carefully transferred to a bottle attached to an aspirator vacuum pump. The NaOH solution was stored under vacuum in an ultrasonic bath until being added to samples, causing any dissolved O_2 to be liberated.

Approximately 4 g of air-dried, ground sample was weighed accurately into a 50 ml centrifuge tube. Twenty ml of degassed 0.1 M NaOH solution was pipetted into each centrifuge tube and the time noted. The sample solutions were bubbled with N_2 for around 5 minutes, using a clean Pasteur pipette for each sample, in order to release air trapped within the ground soil. The lids were carefully placed on the centrifuge tubes to avoid air intrusion and sealed with gas impermeable tape. The samples were put onto bench top wrist-action shakers and left to extract overnight for an extraction time of around 17 hours. On removal from the shakers, the samples were centrifuged for 5 minutes at 8873 g and the supernatant liquid was carefully decanted and filtered using a 0.45 μm syringe filtration system.

The extracted solution was analysed by UV/Vis spectroscopy. The samples required either a five or ten times dilution with 0.1 M NaOH so the absorbance at 254 nm was not higher than two, as sensitivity decreases at higher absorbance values and the absorbance becomes non-linear with concentration. The concentration of dissolved organic matter was

calculated by calibration of the absorbance at 254 nm with standards prepared from dried extracted humic substances. After the initial investigation of extracted soil solution by UV/Vis spectroscopy and ICP-MS (section 2.2.2.1 and 2.4.6) the extractions were scaled up to generate enough humic substances for ^{14}C analysis, NMR and fractionation. In these larger scale extractions 80 g of dry sediment was extracted with 500 ml 0.1 M NaOH. These extractions were carried out in 500 ml conical flasks or round bottom flasks with Quickfit connections for bubbling with gas. This can be seen in the diagram below (figure 2.8). 400 ml of DI water was added to the conical flask which was then degassed for 20 – 30 minutes by bubbling with N_2. 1.6 g of NaOH was then added to the water and it was bubbled for a further 10 minutes until it dissolved to make a 0.1 M NaOH solution. About 80 g of dried and ground sediment sample was accurately weighed into the conical flask which was flushed with N_2 for a further 10 minutes to remove all oxygen. Finally, the tubing clamps were closed in order to maintain an N_2 gas atmosphere in the flask and the joints were given an extra seal of gas non-permeable tape. The sample bottles were then left to shake gently on a bench top wrist action shaker overnight for around 17 hours.

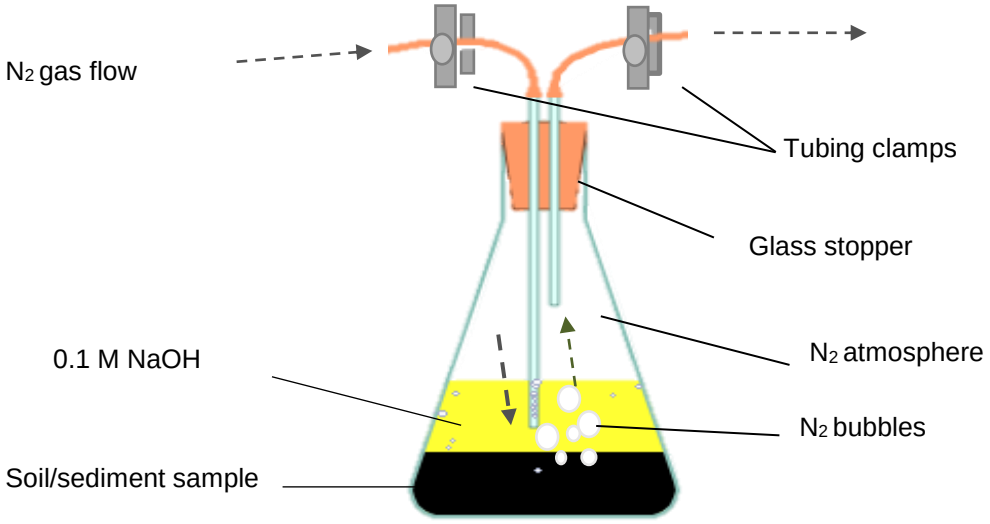

Figure 2.8, Apparatus used for degassing of NaOH for organic matter extraction.

Once extracted, the samples were allowed to settle for 20 – 30 minutes and the supernatant was carefully decanted onto a Buchner apparatus for filtration under vacuum using Whatman glass microfiber filters (GF/C, 1.2 µm pore size). After filtration the extracted organic matter solution was transferred to dialysis tubing with a 3.5 kDa MWCO (SnakeSkin, 35 mm internal diameter) and was dialysed against deionized water for at least 5 days, with the dialysis water changed twice a day. The final pH of the solutions was between 4 and 5.5. Dialysis was used to desalt the samples because the high concentrations of NaCl in the samples from the Merse caused HCl to form in the cation exchange column as the Na^+ was exchanged for H^+. This caused a sharp drop in pH which in turn caused humic acids in the extracted NOM to precipitate and block the column. After dialysis samples were transferred from the dialysis tubing to a glass bottle which was then degassed under vacuum for around 30 minutes, sealed under a nitrogen atmosphere and placed in a freezer at -20°C. This final degassing stage was to release carbonate dissolved in the

samples as CO_2 so to minimize interference from carbonate in ^{14}C analysis (section 2.4.5 and Chapter 5). The samples were not acidified further to purge CO_2 as this can lead to concentration of the acid on freeze drying which can degrade the organic matter by oxidation, potentially interfering with its accurate characterization. The frozen samples were freeze-dried and stored in a desiccator prior to analysis.

2.4.2.2. Organic matter extraction and preparation: Needle's Eye bog samples

Extraction of organic matter from samples from the Needle's Eye bog was carried out in the same manner as is shown in figure 2.8 and described in section 2.4.2.1, above, with the minor modification of using a 1:10 ratio of dry, ground sample to 0.1 M NaOH and a shaking time of 4 hours. After filtering through Whatman GF/C glass microfiber filters the very dark organic matter solution was de-salted by passing over a cation exchange resin (Amberlite IR120 hydrogen form). Cation exchange resin was packed into plastic columns and to create a resin bed of 5 cm length and around 1 cm internal diameter. The cation exchange resin was prepared by rinsing well with a large volume of DI water, followed by 0.1 M HCl and then more DI water until the eluent had a pH ~7. Before the first use the resin was rinsed with 0.1 M NaOH, DI water, 0.1 HCl and more DI water. This procedure was repeated 7 times to ensure the resin was clean and to minimize leaching of organic contaminants from the resin beads. The extracted organic matter solution in NaOH was passed over the cation exchange resin and the pH was monitored with pH indicator paper. The initial solution pH was around 11 – 12, while the pH of the eluting organic matter solution was around 3.0 – 4.0. This is due to the Na^+ ions in solution exchanging for H^+ from the resin which neutralizes the excess OH^-. The naturally acidic properties of the organic matter in solution cause the low pH. When the pH of the eluent began to rise, indicating sodium ions were getting through the column without being scavenged, the cation exchange resin was re-generated by rinsing with DI water, 0.1 M HCl and more DI

water after which more sample could be applied. The methods used in de-salting the OM are discussed detail in chapter 4.

2.4.3. Organic matter fractionation methods

2.4.3.1. Centrifugal ultra-filtration

Ultra-filtration is a method employed to separate material into operationally defined size fractions by use of filtration membranes with defined molecular weight cut off (MWCO). It is widely applied in the analysis of natural water samples to investigate the partitioning of potentially toxic elements (PTE's) between "colloidal" and "truly dissolved" fractions and to investigate compositional differences between the organic matter found in these pools. (Graham *et al.*, 2008; Landry and Tremblay, 2012; Wang *et al.*, 2013; Xu, 2013) The terms "colloidal" and "truly dissolved" are operationally defined by the MWCO of the ultrafiltration units used and no standardised definition exists, leading to different values being adopted by different investigators. The filtrate from ultra-filtration with a membrane of 3 kDa MWCO or less can be described as the "truly dissolved" fraction, while the "colloidal" fraction is the material in the range of 0.45 or 0.22 µm to 3 kDa MWCO. The material of a size greater than 0.45 µm is designated the term "particulate" fraction.

2.4.3.2. Ultra-filtration methodology

Filtered pore waters were fractionated using Vivaspin® 20 ml poyethersulfone filtration units (Vivaproducts) by two ultra-filtration approaches:

i) Separation with a single ultra-filtration unit of 3 kDa MWCO

ii) Sequential ultra-filtration with three units of 100 kDa, 30 kDa and 3 kDa MWCO

The first approach was used to separate samples into two fractions, "colloidal" and "truly dissolved," while the second was used to achieve greater resolution by further separating

colloids into “large,” “medium,” and “small” colloid fractions (Graham *et al.*, 2008; Xu, 2013). The size ranges of the colloid fractions from each approach are shown in table 2.9.

Table 2.9. Ultrafiltration size fractions

Ultra-filtration approach	Fraction	Size range
i)	Colloid	0.45 µm - 3 kDa
	Truly dissolved	< 3 kDa
ii)	Large colloid	0.45 µm - 100 kDa
	Medium colloid	100 kDa - 30 kDa
	Small colloid	30 kDa - 3 kDa
	Truly dissolved	< 3 kDa

In procedure i), where samples were separated into “colloid” and “truly dissolved” fractions, a 3 kDa ultra-filtration unit was accurately weighed to four decimal places on an analytical balance and the weight recorded. An aliquot of 0.45 µm filtered pore water was added to the top of the ultra-filtration unit and the new weight recorded so the accurate volume was known. The ultra-filtration unit containing the sample was then centrifuged at 6000 x g for 10 minutes after which the retentate was removed by Pasteur pipette and transferred to a pre-weighed Sterilin tube. The filter was carefully and thoroughly rinsed with three or four small aliquots of DI water and the washings added to the Sterilin tube which was again weighed to ascertain the final solution volume. The final filtrate was transferred to a pre-weighed sterilin tube and the mass re-weighed to obtain an accurate volume.

In the sequential method, ii), an aliquot of 0.45 µm filtered pore water was first added to the top of a pre-weighed 100 kDa ultra-filtration unit and the accurate weight recorded. This was centrifuged at 6000 x g for 10 minutes and the retentate was carefully removed by Pasteur pipette and stored in a pre-weighed Sterilin tube. The procedure was repeated using a 30 kDa ultra-filtration unit, with the filtrate from the 100 kDa filter added onto the

filtration membrane. It was again centrifuged at 6000 g for 10 minutes, the retentate collected in the same manner and the filtrate transferred to a 3 kDa ultra-filtration unit which was centrifuged at 6000 g for 60 minutes. The final retentates and filtrate were collected and transferred to pre-weighed Sterilin tubes.

The fractions from ultra-filtration were analysed by ICP-MS (section 2.2.2.2) to investigate the distribution of metals between the fractions and by UV/Vis (section 2.4.6) for qualitative assessment of the DOM character and to measure its concentration.

Sequential ultra-filtration was also used as a fractionation technique of extracted soil organic matter. A 5 ml volume of an approximately 500 mg l^{-1} OM solution was fractionated in the same manner as the procedure described above. The collected fractions were de-salted by cation exchange, freeze dried and had elution profiles measured by SEC to compare the methods and to give an approximate molecular weight value to molecules fractionated by SEC.

2.4.3.3. Size exclusion chromatography (SEC)

Size exclusion chromatography separates molecules in solution according to their apparent size. The technique involves carefully packing a column with gel which has swollen in the solvent used for the separation. The gel beads are porous and so the column has range of pore sizes of pore: large pores in between the gel beads and small pores within the gel beads. As the solvent carrying the sample flows through the column large molecules can't fit into the microstructure of the porous beads and travel around the outside of them. The smaller molecules take a longer path as they flow through the small pore structure within the gel beads and so they are retained within the gel for a longer time. The gel has pores of varying size, so some molecules are excluded from the smallest pores but travel through the medium and large pores whereas the smallest molecules have access to all the internal porosity and so take the longest path and therefore the longest to elute (Lewis, 2007). In a

complex mixture of varying sized molecules, like natural organic matter, this leads to a peak of the largest molecules or aggregates which elute first followed by a shoulder of molecules which range from medium to small size. The size range of molecules in organic matter means that the elution profile tends to be broad and poorly resolved; however molecules of known size can be used to calibrate the approximate size of sample molecules eluting from the column. These can be prepared by use of a different method, for example ultra-filtration, where the fixed pore sizes of the filters can be used to separate organic matter into operationally defined size fractions.

SEC is a common method to separate OM into "size" fractions (Trubetskoj *et al.*, 1997; Zhang *et al.*, 1997; Graham *et al.*, 2000; Oliver *et al.*, 2007; Trubetskoj, Hatcher and Trubetskaya, 2010; Trubetskaya, Trubetskoi, *et al.*, 2011; Peel, Martin and Bednar, 2017). The traditional description of humic substances, as very large macro-molecules with molecular weights of up to 100,000 Da, has largely been superseded by the updated definition of supra-molecular clusters of lower mass molecules (200 – 5,000 Da) held together by intermolecular forces, such as hydrogen bonds, electrostatic forces and hydrophobic interactions (Vindedahl *et al.*, 2016). Therefore, size fractionation does not necessarily separate large and small molecules, but separates those with properties which cause them to aggregate or disperse based on local chemical conditions (section 4.7). This is an important distinction to bear in mind when interpreting the results of size fractionation experiments.

The most common methods of SEC fractionation used in recent years are HPLC-based systems. While the fractionation achieved using HPLC has been claimed to be of superior resolution to that achieved by gel chromatography there are still some benefits of using the column chromatography method. These include larger sample size (important for characterisation of isolated fractions), good chemical resistance, ease of monitoring of gel

quality (e.g. precipitation of humic substances can be observed when it occurs), and low cost (approx. £20 per column as opposed to £800+ per column).

2.4.3.4 Separation of humic and fulvic acids

To separate humic and fulvicacid fractions around 30 mg of freeze dried NOM was dissolved in a centrifuge tube with approximately 5 ml of DI water. The solution had a pH ~3 due to the acidity of the OM. The solution was shaken on a bench top shaker for 15 minutes to promote dissolution, however not all the OM dissolved due to the relatively low pH. The pH was adjusted to between 1 and 2 with 20 µL aliquots of 0.1 M HCl (VWR scientific, Aristar, 69%). The solution was shaken by hand before being centrifuged at 8000 x g for 30 minutes. The solution containing the fulvic acid was carefully removed with a glass Pasteur pipette and the humic fraction, which was stuck to the bottom of the centrifuge tube, was carefully rinsed once with DI water to remove remaining fulvic acid before being suspended in 5 ml DI water. Both fractions had their pH adjusted to around 7 by the addition of 0.05 M NaOH in 10 µL aliquots. The samples, which were now in dilute NaCl solution, were frozen at -20°C before freeze drying and further analysis.

2.4.3.5 Measurement of percentage fulvic acid composition of NOM

Fulvic acids have considerably different properties and structure to humic acid, so the % fulvic composition of a sample is an interesting and straightforward parameter to investigate in order to learn more about its composition. The % fulvic acid in extracted samples and column fractions was analysed by comparing the absorbance at 254 nm of total NOM samples to those which had the humic fraction removed by precipitating with acid. The samples in solution were acidified with small volumes of HCl to a pH of 1 – 2. The solutions which contained suspended humic acids were centrifuged for 15 minutes at 8000 x g after which the solution was filtered with a 0.45 µm syringe filter. The absorbance at 254 nm by UV/vis spectrophotometry was used to analyse the sample before and after precipitation with acid and the % fulvic acid was calculated using equation 2.5 below.

$$\%\ fulvic\ acid = \frac{abs_{254}\ fulvic\ fraction}{abs_{254}\ total\ NOM} \times 100 \qquad \text{Equation 2.5.}$$

A solution containing no added OM which matched the sample matrix was used as the baseline for the total NOM and acidified sample to avoid any potential background effects of using solutions of different pH or ionic strength.

2.4.3.6 Total organic carbon (TOC) analysis

Pore-water samples from bog core E (centrifuge sampled) were analysed by TOC analysis to generate a calibration graph to relate TOC and absorbance at 254 nm. Blank solutions from SEC, ultrafiltration, cation exchange and syringe filtration were also analysed. The instrument used was a Rosemount Dohrmann DC 80 TOC Analyser with UV promoted chemical oxidation and IR detection. A 400 mg L^{-1} solution of potassium hydrogen phthalate was used for calibration and drift checks throughout the analysis. A volume of 5 ml of each sample was acidified with 100 µL of 85% phosphoric acid and bubbled with nitrogen for 10 minutes to promote evolution of CO_2 gas from dissolved carbonate before measurement.

2.4.4 Elemental C, H, N, S analysis

Elemental analysis of total peat samples and extracted organic matter samples was undertaken to investigate the composition of extracted and fractionated organic matter. The analysis was performed using a Carlo Erba NA 2500 Elemental analyser. Two mg samples were accurately weighed into to 4 decimal places into tin combustion containers. One by one the samples were flash combusted at 900^{o}C, converting all organic matter into combustion products. The combustion products flowed over a copper filter to remove excess oxygen and reduce nitrogen dioxides to N_2. The combustion products then passed into a chromatography column as CO_2, H_2O, SO_2 and N_2, which eluted separately and were

detected by a Thermal Conductivity Detection system. The detection system was calibrated with a cystine calibration standard of known composition. This was also used throughout the analysis to ensure instrumental stability. Table 2.10 shows the comparison of the certified values of the cystine reference material with the measured concentration.

Table 2.10. Comparison of certified concentration of the cystine standard with the results of analysis of check samples analysed with each sample run. Number of samples = 22.

Element	Certified concentration (%)	Uncertainty	Measured concentration (%)	Recovery (%)	Standard deviation
N	11.59	0.21	11.13841	99.7	0.400059
C	29.95	0.18	29.85739	96.1	0.207401
H	5.09	0.28	4.81455	94.6	0.049381
S	26.67	0.26	22.25609	83.7	5.050529

The results of analysis of the certified cystine standard throughout the analysis runs showed excellent agreement with the certified values of C, H and N (table 2.10). The measured C, H and N concentrations fall within the error of the certified values, while the S concentration falls only slightly outside.

2.4.5 Measurement of ^{14}C and $\partial^{13}C$

Organic matter samples extracted from Merse core A and peat samples from NE core B were analysed by Accelerator Mass Spectrometry (AMS) (National Electrostatics Corporation, 5MV tandem AMS) at the NERC radiocarbon facility located at the Scottish Universities Environmental Research Centre (SUERC)in East Kilbride. The goal was to investigate the distribution and characteristics of organic matter which has incorporated anthropogenic ^{14}C and been deposited in on-shore sediments. The results obtained were compared to records of ^{14}C discharged into the Irish Sea from the Sellafield nuclear fuel reprocessing facility to see if a link could be made between the historic, and ongoing,

discharges into the Irish Sea and the accumulation profile of ^{14}C in the sediment. Organic matter fractionated by SEC was also analysed in order to identify fractions of OM which are enriched in anthropogenic ^{14}C. The stable carbon isotope ratio, $\partial^{13}C$ was analysed to provide information on the origin of organic matter samples as marine or terrigenous (MacKenzie *et al.*, 2004). The results are explained in detail in chapter 6. Samples from the NE bog were also analysed for ^{14}C in order to establish a depth chronology of the bog profile by carbon dating.

2.4.5.4 Methodology used for the analysis of ^{14}C and $\partial^{13}C$

The methodology of Dunbar *et al.*, (2016) was used for sample preparation and analysis. Approximately 12 mg of freeze-dried OM samples or dried, ground and sieved soil samples were weighed into small quartz test tubes, which had previously been combusted in a furnace at 850^{o}C to remove any carbon contamination. The samples in quartz test tubes were transferred into larger quartz combustion vessels containing a small amount of copper oxide, and a piece of silver foil was added. The copper oxide provides oxygen for the silver to remove gaseous impurities. The quartz vials were evacuated on a vacuum line to remove all air from the combustion vessel and sealed using a blow torch to melt the top of the combustion tube and seal in the sample and the vacuum. The combustion tube was then combusted at 850^{o}C overnight to ensure complete conversion of the sample to CO_2. After combustion the combustion tube was returned to the vacuum line and carefully opened by cracking the quartz glass to release the CO_2 into the vacuum line. Cold traps of liquid nitrogen were used to hold the CO_2 before transferring it through the vacuum line to be converted into graphite by high temperature reduction with zinc used as a catalyst. The graphite formed was pressed into an aluminium cathode which was later loaded into the AMS for ^{14}C analysis.

A separate sample of graphitized carbon was taken for $\partial^{13}C$ analysis by continuous flow isotope ratio mass spectrometry coupled to an elemental analyser (Costech ECS 4010). International reference materials are analysed throughout the sample run to ensure stability. The results $\partial^{13}C$ analysis are reported as per-mil (‰) relative to the international standard VPDB (Dunbar *et al.*, 2016).

2.4.6 Ultraviolet/visible (UV/vis) spectroscopy

2.4.6.4 Background and applications

UV/visible spectroscopy is a simple, non-destructive and widely available technique which can be used to gather information on the quantity and quality of natural organic matter in solution.

UV/vis spectra of natural organic matter samples are largely featureless and lack distinctive peaks due to the overlapping absorbance of many chromophores, which are the components responsible for absorbance of light. Examples of light-absorbing components important in natural organic matter include unsaturated double bonds, as are found in alkenes and aromatic rings, and non-bonding electrons on oxygen atoms, such as on carbonyl or carboxyl functionalities. The majority of the absorbance in the UV range of the spectrum (200 to 400 nm) is attributed to aromatic chromophores such as mono and poly-substituted phenols and aromatic acids. (Stevenson, 1982; Hart *et al.*, 2007)

2.4.6.5 UV/Vis as a proxy for dissolved organic matter concentration

The absorbance of the solution at 254 nm can be used as a proxy for dissolved organic matter (DOM) content due to the linear relationship between solution concentration and absorbance, as explained by the Beer Lambert Law.

$$A = \epsilon c l \qquad \text{Equation 2.6}$$

A = absorbance

ϵ = molar absorptivity constant ($mol^{-1}\ L^{-1}\ cm^{-1}$)

c = concentration ($mol\ L^{-1}$)

l = cell path length (cm)

The absorbance of samples at 254 nm can be directly compared or calibrated using a linear calibration graph prepared from a known concentration standard in order to calculate the

DOM concentration in mg L^{-1}. In either case it is important to ensure the comparisons are made between samples of similar origin or that an appropriate calibration solution is used as compositional variations between samples or samples and standards can lead to different absorption behaviour and therefore inaccurate estimates of organic matter quantity. (Dobbs, Wise and Dean, 1972; Stevenson, 1982; Edzwald, Becker and Wattier, 1985; Graham *et al.*, 2008; Xu, 2013; Peacock *et al.*, 2014) In this study the absorbance values of OM are stated, with measurement at 254 nm being used as a proxy for concentration. In cases where the total OM extracted was calculated (e.g. section 4.8) calibration graphs were prepared from dried OM from the same depth in the bog profile as the sample of interest. Samples of freeze dried OM were accurately weighed to 1 mg and dissolved in 10 ml of 0.01 M NaOH. Serial dilution with 0.01 M NaOH was used to prepare standards of 0, 33, 50 and 100 mg L^{-1} which were analysed at 254 nm.

2.4.6.6 UV/Vis qualitative ratios and SUVA 254

UV/vis spectroscopy is widely used in organic matter analysis to examine the properties of OM. Two common methods of interpreting data are the use of ratios between the sample absorbance at particular wavelengths and the analysis of spectral slope properties. Commonly evaluated ratios are the E2:E3 ratio (the ratio between absorbance at 250 nm:365 nm) and the E4:E6 ratio (465 nm:665 nm). The E2:E3 ratio has been shown to have an inverse relationship with molecular size and aromaticity (Peuravuori and Pihlaja, 1997; Dalzell, Minor and Mopper, 2009). The E4:E6 ratio, known as the "index of humification" also has an inverse relationship with molecular size and aromaticity but can sometimes be impacted by low absorbance at 665 nm when samples have low DOM concentrations (Chen, Senesi and Schnitzer, 1977; Fan, Song and Peng, 2012; Kiss *et al.*, 2014; Minor *et al.*, 2014; Peacock *et al.*, 2014, 2015).

The Single UV Absorbance at 254 nm (SUVA 254) has also been measured. The SUVA 254 is calculated by dividing the absorbance at 254 nm by the DOC concentration of the

sample. The SUVA 254 has been shown to be correlated with aromaticity (Peacock *et al.*, 2014; Fernández-Romero *et al.*, 2016).

2.4.6.7 UV/Vis spectral slope and slope ratios

The spectral slope (S_{total}) of a UV/Vis spectrum can be calculated by modelling a section of the absorption spectrum (e.g. 300 – 700 nm) using a single exponential decay function (equation 2.7):

$$a_\lambda = a_{\lambda_{ref}} e^{-S(\lambda - \lambda_{ref})} \qquad \text{equation 2.7}$$

a = Napierian absorption coefficient (m^{-1})
λ = wavelength (nm)
λ_{ref} = reference wavelength
S = spectral slope (nm^{-1})

The absorbance at each wavelength is converted to Napierian absorption coefficient by equation 3.8:

$$a = 2.303A / l \qquad \text{Equation 3.8}$$

a = Napierian absorption coefficient (m^{-1})
A = absorbance
l = path length (m)

The spectral slope values calculated using equation 3.7 are influenced by organic matter composition such as molecular weight, origin (e.g. terrestrial or aquatic) and humic and fulvic acid content (Twardowski *et al.*, 2004; Helms *et al.*, 2008; Sulzberger and Durisch-Kaiser, 2009; Fichot and Benner, 2012). An enhancement of the method is to calculate the

S value of two narrower regions of the spectrum or look at the "slope ratio" (S_R) between two regions of the spectrum. This approach was first put forward by Helms et al. (2008) who calculated the slope value of two regions in different parts of the spectrum ($S_{275-295\ nm}$ and $S_{350-400\ nm}$) which were chosen as the greatest variation in S_{total} (300-700 nm) values were seen to occur within these narrow regions. The $S_{275-295}$ has greater sensitivity and reproducibility for identifying variation between samples compared to the other slope measurements and it was therefore recommended as a useful parameter to employ in spectroscopic investigations of organic matter (Helms *et al.*, 2008; Minor *et al.*, 2014; Rodriguez, Schlenger and Garcia-Valverde, 2016). In this study, the E2:E3 and E4:E6 ratios, $S_{(275-295)}$, $S_{(350-400)}$ and SR values have been analysed in various samples and the differences between them discussed in relation to the results of other spectroscopic analysis methods.

2.4.7 Fourier transform infrared spectroscopy (FTIR)

FTIR spectroscopy is an analytical technique which can be used to investigate the presence of reactive and structural organic components in natural organic matter and soil. It is a quantitative method which can be used to examine oxygen containing functional groups such as carbonyl and carboxyl moieties, as well as carbon to carbon double bonds and alkyl groups. Functional groups can be discriminated by their absorbance at diagnostic frequencies across the infrared spectrum, usually between 400 and 4000 cm^{-1} in environmental analysis. A series of sharp or broad peaks are seen on the FTIR spectrum which correspond to the absorbance by different functionalities within the sample. Absorption of radiation occurs as bonds vibrate by bending or stretching with different absorption peaks appearing on the spectrum for different types of absorbance exhibited by each functional group. Stretching, which can be symmetric or asymmetric, is used to describe the change in distance between two atoms with no side to side movement, whereas bending vibrations are described as scissoring, rocking, wagging or twisting depending on

the movement of bonded atoms relative to each other. The number of different types of vibration means that a single functional group can exhibit peaks in more than one region of the spectrum, which can aid the identification of a specific functional group by cross referencing with other peaks, but in a complex mixture like natural organic matter it also leads to many overlapping peaks which makes accurate assignment more challenging. Each of the molecular vibrations described above are caused by absorbance of a distinct amount of energy, therefore the intensity of energy absorbed by a sample at a given point in the spectrum is influenced by the type of vibration as well as the concentration of the absorbing moiety (Stevenson, 1982; Hart *et al.*, 2007; Minor *et al.*, 2014).

Two of the most common methods of FTIR analysis of environmental samples are transmission spectroscopy (T-FTIR) and the more modern attenuated total reflectance spectroscopy (FTIR-ATR). In T-FTIR samples are finely ground with potassium bromide and pressed into a uniform disc around 1 – 2 mm thick. Infrared light is passed through the disc and the energy of the transmitted radiation is measured with 100% transmission at a particular wavelength indicating that no energy has been absorbed. In FTIR-ATR analysis the powdered sample is placed directly onto the surface of a crystal and pressure is applied to ensure good covering is achieved. A beam of IR radiation is shone into the crystal. The IR light reflects due to total internal reflectance off of the underside of the crystal which has the sample pressed onto it. As it reflects an evanescent wave is created which can extend above the surface of the crystal and interact with the sample. Components within the sample then absorb the radiation, as is described above, and the attenuated (decreased intensity) beam is then reflected back out of the crystal to a detector where the intensity of reflected light is measured. In both T-FTIR and FTIR-ATR the difference between the applied and reflected IR radiation is used to gain insight about the composition of the sample (Herres and Gronholz, 1989; Perkin Elmer Life and Analytical Sciences, 2005; Tinti *et al.*, 2015).

FTIR instruments can produce a spectrum quickly as several frequencies of IR radiation are applied to the sample at once so it is therefore not necessary to scan a whole spectrum from high to low frequency as in older instrumental methods. The process is repeated over several iterations by altering the combination of irradiating frequencies until the whole spectrum has been covered. The complex data generated by this method of analysis is deconvoluted by applying a Fourier Transform mathematical function which makes it possible to plot the intensity of transmitted radiation against the irradiating frequency as a spectrum. In FTIR-ATR the finely ground sample can be applied directly onto a crystal and pressure applied to ensure a good contact is made. This has the advantage over T-FTIR of being faster, requiring little preparation and being very simple, however it also has a slight drawback of lower sensitivity and deformations in the spectra from the crystal used.

2.4.7.1 FTIR methodology

Two methods of FTIR analysis were used in this study, T-FTIR and FTIR-ATR. For the analysis of organic matter by T-FTIR approximately 1 mg of freeze-dried organic matter was weighed and transferred to an agate mortar. Then, 400 mg of dry KBr (spectroscopy grade, Fisher Scientific) was added to the mortar and the mixture was ground to a very fine powder with an agate pestle. Blank KBr disks were prepared in the same manner but with no organic matter added. The KBr and organic matter mixture was carefully transferred to a polished steel dies and 10 tons pressure was applied for 10 minutes to achieve a uniform round disc with a thickness of approximately 1 mm. If the disc was not clear on removal from the press it was re-ground and pressed again. Once prepared, the disc was transferred to a benchtop FTIR instrument (Perkin Elmer). 32 scans were collected with an applied wavenumber range of 400 – 4000 cm^{-1}, and a resolution of 4 cm^{-1}. A blank KBr disc was run before any samples to set the instrument background level and take account of atmospheric moisture and CO_2.

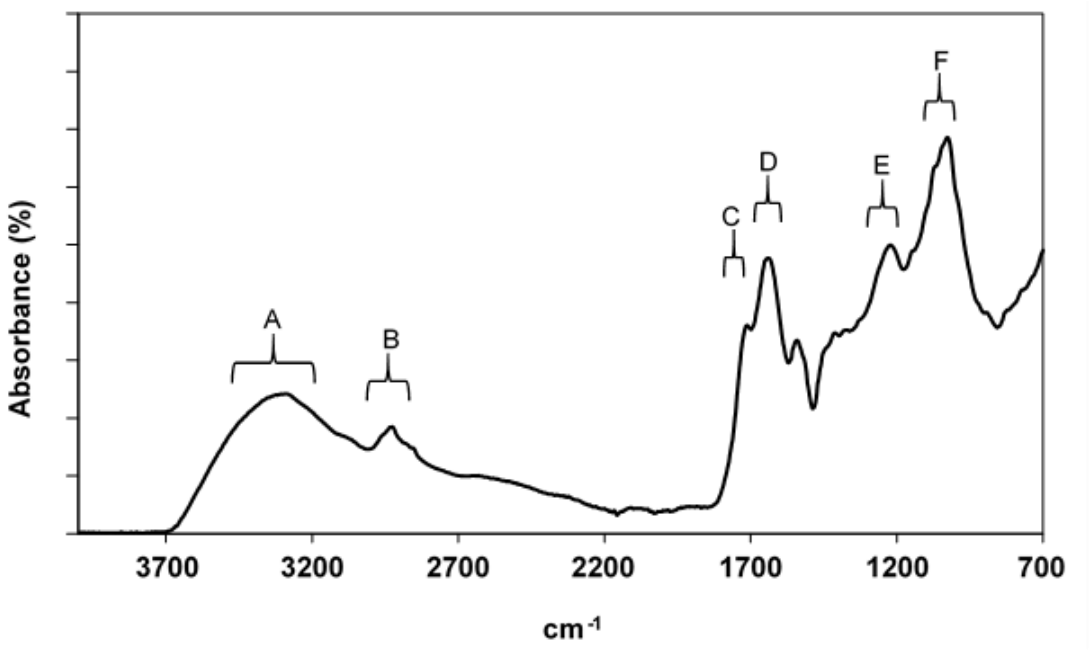

Figure 2.9, Example FTIR spectrum showing regions indicative of different organic functional groups. The regions A – F are described in table 2.11.

Table 2.11 Functional group assignment of peaks in different wavelength regions of FTIR spectra (Dick, Santos and Ferranti, 2003; Gondar *et al.*, 2005; Artz *et al.*, 2008; Abdulla *et al.*, 2010; Giovanela *et al.*, 2010; Matilainen *et al.*, 2011; Biester *et al.*, 2014; Busetti *et al.*, 2014; Enev *et al.*, 2014; Dhillon *et al.*, 2017). The letters A – F correspond to the spectral regions indicated in figure (2.9)

Region of spectrum (figure 2.9)	Range (cm^{-1})	Assignment
A	3400 – 3200	O-H stretch of alcohols, phenols and carboxylic acids
B	2980 – 2870	Asymmetric and symmetric C-H stretch of aliphatic methyl and methylene groups
C	1700 – 1720	C=O stretch of carboxylic acid and carbonyl groups
D	1600 – 1650	Structural vibration of aromatic C=C and antisymmetric C=O stretch of COO^-
E	1200 – 1240	C-O stretch of carboxylic groups, phenols and aromatic/unsaturated ethers
F	1010 – 1060	C-O stretch of alcohols, aliphatic esters, polysaccharide components

Before samples were analysed by FTIR-ATR a background spectrum was first run to take account of instrumental background and atmospheric CO_2 and H_2O. Samples were analysed by applying a few mg of finely ground peat or organic matter directly onto the crystal surface of the ATR detector. Pressure was applied to ensure good contact was achieved between the sample and the crystal surface. 32 scans were collected with an applied wavenumber range of 700 – 4000 cm^{-1}, and a resolution of 4 cm^{-1}. Duplicate measurements were made if enough material was available. The spectra collected were converted from transmission to absorbance and normalised by subtraction of the lowest value and dividing by the average absorbance of the whole spectrum (Artz *et al.*, 2008). Peaks at particular wavenumbers were assigned by comparison to published studies. These are shown in table 2.11 and figure 2.9.

2.4.8 Nuclear magnetic resonance (NMR) spectroscopy

2.4.8.1 Background and theory

NMR is powerful technique for structural analysis of organic molecules and is widely used in organic chemistry. The basis of the technique relies on the spin quantum number of the nucleus, a property determined by the protons and neutrons that form the nucleus, each with their own spin value. Two protons or two neutrons with opposing spin can form a pair with an overall spin of zero as the opposing spins cancel out. A nucleus with an even total number of protons and neutrons will have a spin of zero, whereas a nucleus with an odd number of protons or neutrons in its nucleus will have a spin which is non-zero. The spin number is directly related to the magnetic moment of the nucleus. A nucleus with a spin number of zero will also have zero magnetic moment and a nucleus with a non-zero spin number will have a magnetic moment which is also non-zero. The magnetic moment is a property which causes the nucleus to behave like a magnet, so a nucleus with a non-zero magnetic moment can interact with an external magnetic field. When an external magnetic field is applied around the nuclei which exhibit a magnetic moment it causes their magnetic field to become aligned with the applied external magnetic field. This is a stable configuration for a nucleus called the α-spin state, a low energy state. Application of electromagnetic radiation, usually radio frequency (RF), can promote the nucleus to a higher energy state in which the magnetic field of the nucleus runs opposite, but parallel to the external magnetic field. This is known as the β-spin state, an excited energy state that is still stable, but is a higher energy state than the α-spin state. When all nuclei have been promoted to the same energy state this is known as being in resonance.

In the situation where an atom which exhibits a magnetic moment is part of a molecule then the environment that surrounds it can influence its behaviour in a magnetic field. Electrons surrounding the atom can shield the nucleus from the effect of an external magnetic field. This means the nucleus magnetic field does not to align itself with the

applied magnetic field and the nucleus remains in an energy state above the α-spin state. On application energy in the form of RF radiation the nucleus is promoted to the β-spin state, but because the nucleus was never in the low energy α-spin state it takes a smaller amount of applied RF energy to promote it to the β-spin state.

2.4.8.2 NMR analysis of natural organic matter

Different techniques have been applied to the analysis of NOM by NMR. The most useful NMR-active isotopes in NOM are ^{13}C and ^{1}H. `These isotopes both have advantages and disadvantages in NMR analysis. Since ^{13}C has a natural abundance of only around 1% (Maberly, Raven and Johnston, 1992) NMR experiments to analyse the environment of ^{13}C within natural molecules require the accumulation of thousands of scans over many hours in order to achieve a good signal to noise ratio. On the other hand, the NMR active ^{1}H is the dominant isotope of hydrogen with an abundance of over 99%, so a proton spectrum NMR of a NOM sample can be collected in a matter of minutes. Drawbacks of ^{1}H NMR analysis of NOM are the relatively low peak resolution achievable due to the large numbers of overlapping peaks present and the potential for signal to be reduced by hydrogen from water present in the sample. The first issue can be overcome by use of multi-dimensional NMR experiments which have been used to separate overlapping peaks and assign regions of the ^{1}H spectrum with more accuracy (see section 2.4.8.3). The issue relating to interference from ^{1}H introduced into the sample can be overcome by the use of deuterated solvents, where ^{1}H has been substituted for the NMR-inactive, but chemically similar isotope, deuterium (^{2}H). Even with the use of deuterated solvents, such as D_2O, the signal from water in the sample or DOH formed within the sample solution can cause a large peak in the NMR spectrum. Fortunately, the development of instrumental techniques to suppress the signal of water in NMR analysis has led to an increase of popularity in aqueous phase analysis of NOM. The background and methodology of NMR analysis techniques used in this project are outlined below.

2.4.8.3 ^{1}H NMR

Solution state ^{1}H NMR, or proton NMR, has been applied in analysis of natural organic matter to assess the relative contribution of specific functional moieties in isolated humic substances. A spectrum from the analysis of humic substances by ^{1}H NMR can be divided into regions to identify the relative abundance of different functional moieties. Common regions used to identify different organic compound classes are: aromatic (around 10.0 – 6.0 ppm), carbohydrate (around 4.5 – 3.2 ppm), carboxylic rich alicyclic molecules (CRAM, around 3.2 – 1.6 ppm), and aliphatic molecules (around 1.6 – 0.0 ppm) (Hertkorn, 2006; Woods *et al.*, 2010; Simpson, McNally and Simpson, 2011). These regions are shown in the figure 2.10, below.

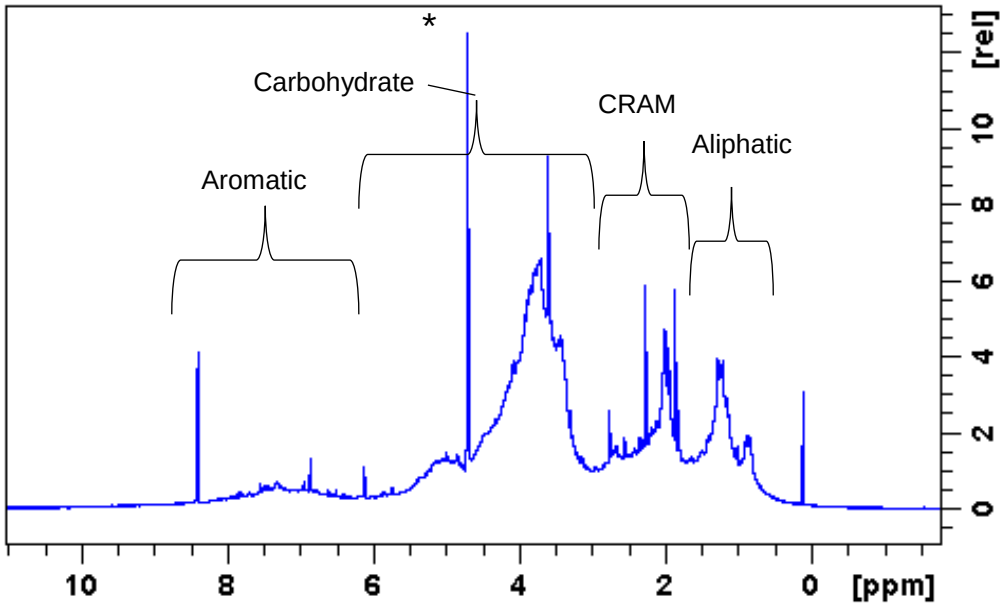

Figure 2.10, ^{1}H NMR spectrum of Needle's Eye dissolved organic matter, dissolved in D_2O. Regions representing different types of organic molecule are shown using the brackets. The asterisk (*) denotes the residual DOH peak from water. CRAM are Carboxylic Rich Alicyclic Molecules (Simpson et al., 2011).

The 1-dimensional proton NMR spectrum of NOM contains many overlapping and indistinct peaks which allow regions to be defined, as is shown in the figure above (figure 3.9). However, application of multidimensional NMR techniques has made it possible to achieve a more detailed analysis of the spectrum and assignment of different structures. Figure 2.11 shows a ^{1}H spectrum of extracted soil organic matter with more specific functional assignments (Simpson, McNally and Simpson, 2011).

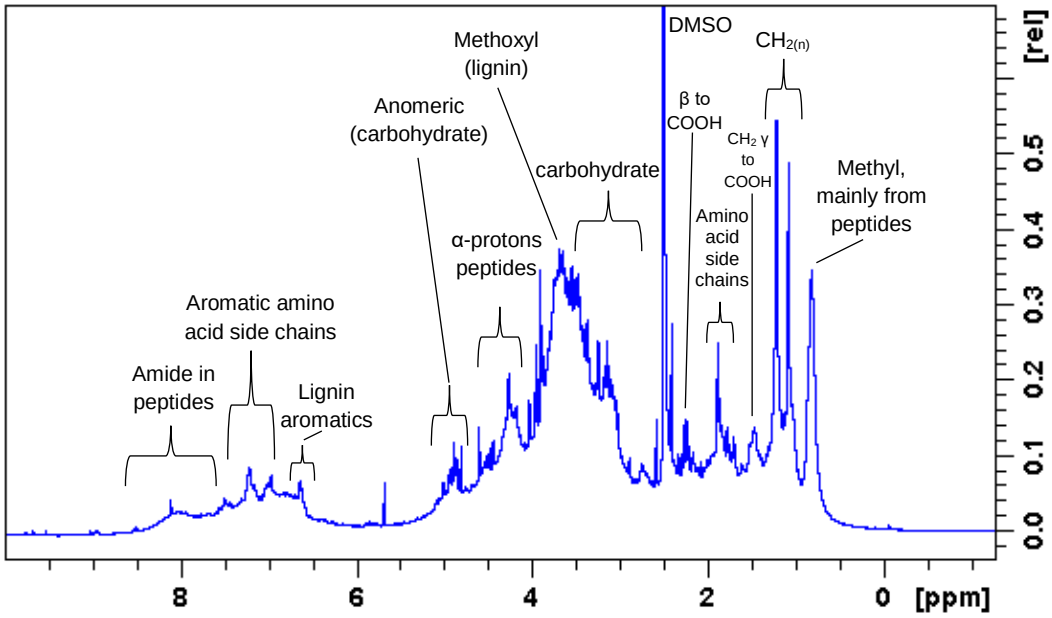

Figure 2.11, ^{1}H NMR spectrum of organic matter extracted from Needle's Eye core D, 5 – 10 cm depth with 0.1 M NaOH. The sample was dissolved in deuterated DMSO for NMR analysis. The major structural components are identified by comparison of 1-D and 2-D NMR experiments (after Simpson et al., 2011).

By the use of 2-D NMR experiments it is possible to identify individual molecules and minor components of natural organic matter. This information has been used to assign components of a 1-D proton spectra, as is shown in figure 2.11, in order to achieve a more detailed analysis of spectral features. This allows the identification of the major structural components in a sample from a proton spectrum. Individual molecules and minor contributors to the mixture of organic matter cannot be resolved due to the overlap of peaks in 1-D experiments but these can be identified by the use of multidimensional NMR experiments, some of which are described below.

2.4.8.4 Multi-dimensional NMR methods

In multi-dimensional NMR experiments homo or heteronuclear correlations are made between atoms in different molecular environments. Examples of homonuclear correlations are COSY (correlation spectroscopy) and TOCSY (total correlated spectroscopy) experiments. In these experiments two protons interact through bonds via *J* coupling, an interaction where the magnetic field of one nucleus influences that of another. The number of bonds in between the nuclei involved, the binding angle and the magnetogyric ratio of both nuclei involved (ratio between the magnetic moment and angular momentum of the nucleus) all influence the magnitude of the coupling constant, *J*, which is measured in Hz (Hertz). A COSY spectrum shows the *J* coupling interactions between nuclei within a distance of 3 – 4 bonds, while a TOCSY spectrum shows the interaction over a greater number of bonds. In a COSY spectrum, like the example shown below (figure 2.12), the central diagonal line is the same as the 1-D proton spectrum while points which do not sit on the line (cross peaks) represent the coupling of two protons in different bonding environments, indicated by their chemical shifts on the x and y axes.

The separation achieved by applying this simple 2-dimensional technique adds to the assignment from the 1-D proton spectrum, as overlapping peaks are resolved. This allows a single group from the 1-D spectrum to be separated into distinct fractions. For example in figure 2.12, below, the "carbohydrate" region of the 1-D spectrum has been resolved into desoxy sugars, ethers and esters (figure 2.12, group B), functionalized aliphatic with one N or O heteroatom (group E) and carbohydrate with and without anomeric centres (D and F respectively).

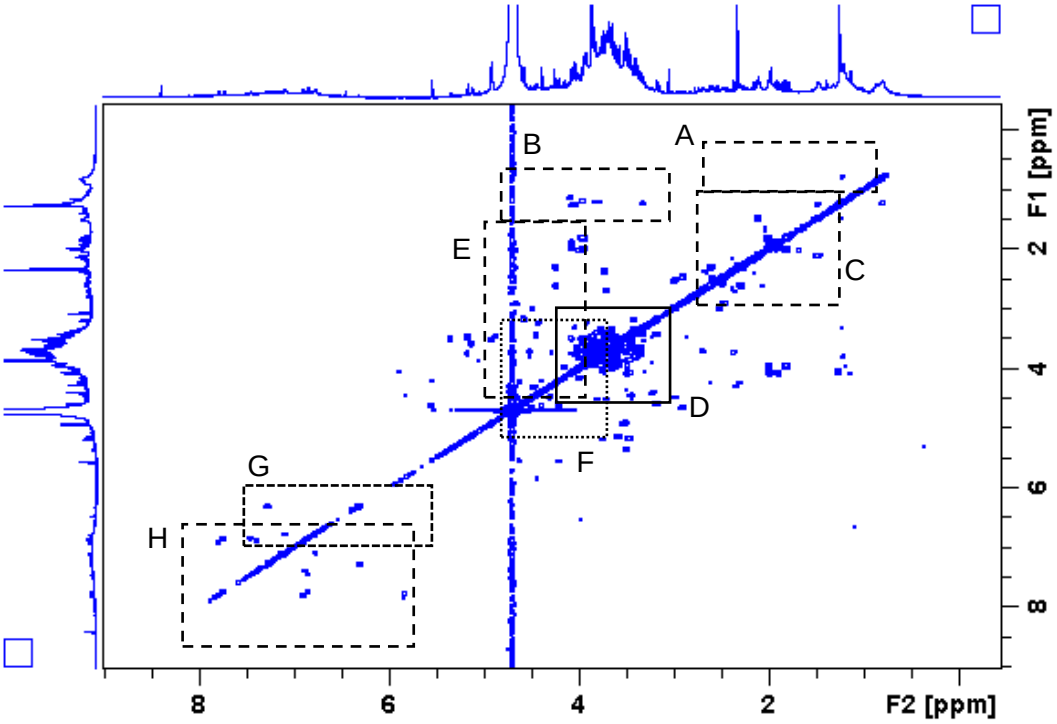

Figure 2.12. COSY spectrum of OM extracted from bog core B 10 – 15 cm, dissolved in deuterated 0.05 M NaOD in D_2O. The region assignments (A to H) are explained in table 2.12 (after Hertkorn, 2006).

Table 2.12. The region assignments (A to H) of the COSY spectrum in figure 2.12 (Hertkorn, 2006).

Region	Assignment	Humic constituent
A	-C-CH-CH_3	Methyl groups bound to purely aliphatic carbon
B	-C-CH-CH-O-	Desoxy sugars, ethers, esters
C	-C_f-CH-C_fH-C-	Intra functionalised aliphatic, β to heteroatoms
D	-CH(O)-CH(O)-	Intra carbohydrate, without anomerics
E	-CH(x)-CH-C_f	Functionalised aliphatic unit with one heteroatom (x = O, N)
F	-O-CH(O)H-CH	intra carbohydrate, with anomerics
G	-CH=CH-	double bonds, five membered heterocycles
H	-C_{ar}H-C_{ar}H-	ortho protons in aromatic rings

Peaks on a COSY spectrum arise due to the coupling of two ^{1}H nuclei in different regions of the 1-dimensional ^{1}H spectrum. The same ^{1}H spectrum is shown on both the x and y axes of the COSY plot. The diagonal line across the plot are the same peaks as the 1-dimesnsional ^{1}H spectrum while cross peaks (those which are not on the diagonal line) arise due to the coupling of protons in two different regions of the ^{1}H spectrum. The cross peaks

represent a proton in a specific binding environment, with the intensity of the peaks related to the concentration of that functional group.

Another commonly used 2D-NMR method is heteronuclear single quantum correlation (HSQC). In this experiment the proton NMR signal is correlated with the ^{13}C NMR signal which allows for good peak separation, due to the relatively long axis of the ^{13}C spectrum. The peaks in an HSQC spectrum show where a proton is directly bonded to a ^{13}C atom. The position of the peak on each 1-D spectrum is combined to provide detailed information on binding environment of the two nuclei in question.

2.4.8.5 NMR Methodology used in this investigation

2.4.8.5.1 Solvents

Solvents in solution phase NMR analysis have to be selected to achieve as close to 100% dissolution of humic substances as possible while having as small an impact as possible on the NMR spectrum. The spectrum effects of the solvent can be minimized by using deuterated solvents where the ^{1}H is replaced with NMR-inactive ^{2}H. In this investigation the solvents tested were DMSO- D_6, DMSO-D_6 acidified with CF_3COOD (final concentration 2%), D_2O and D_2O with NaOD (final concentration 0.05 M).

Increasing the concentration of soluble salts in an NMR sample can cause broadening of the spectrum peaks and decreased signal to noise ratio (s/n). Initially DMSO and acidified DMSO were used; however, although successful in dissolving samples of total extracted NOM, these solvents could not completely dissolve all samples after fractionation by SEC (section 4.3.1). D_2O was able to successfully dissolve samples with a more fulvic acid like character, but samples which were more like humic acids remained un-dissolved. Addition of 1M NaOD to a sample in D_2O to make a final concentration of 0.05 M NaOD was the most successful solvent for dissolving organic matter fractions. This low concentration of NaOD appeared not to have too much negative impact on the quality of NMR spectra and

so it was adopted for all further analyses. The method for NMR sample preparation is detailed below.

Approximately 12 mg of freeze-dried humic substances was accurately weighed into a 1.5 ml eppendorf vial. Then, 570 µL of D_2O was added by pipette and the sample was left to absorb the D_2O for 10 – 20 minutes. After this time 30 µL of 1 M NaOD was added by pipette and the vials were shaken on a bench top wrist action shaker for around 10 minutes. After shaking, the vials were removed and centrifuged at 6322 g (MSE micro centrifuge) for 5 minutes. The supernatant was carefully removed with a glass Pasteur pipette and transferred to a Pyrex NMR tube with a 5 mm diameter (Norell inc.).

2.4.8.5.2 NMR experimental parameters and instrumentation

The NMR experiments were carried out on a Bruker Avance™ 600 MHz with a triple resonance cryoprobe (TXI) optimized for ^{1}H analysis and with the ability to analyse ^{13}C and ^{15}N. Water suppression was achieved by using a presaturation pulse program. Receiver gain was fixed at 64 to aid comparison between samples. The temperature the analysis was carried out at was 300 K. 64 scans were collected for each sample.

2.4.9 Statistical analysis of results

Correlation statistical analysis has been applied to compare the similarity of trends between organic matter analysis parameters in chapters 5 and 6. The Spearman's Rank, also known as Spearman's Rho, correlation is a non-parametric test of the linear relationship between two variables. As it is non-parametric, the populations analysed do not need to be normally distributed (Gauthier, 2001). Spearman's rank correlations were carried out using Minitab 18 statistical software. In analysis of trends in OM characterisation of bog profiles (Section 3.4) Pearson's linear regression was used in Excel 2013.

Where the significant difference between two or more groups has been investigated the one-way ANOVA has been used, also in Minitab 18. Tukey's Honest Significant Difference test was applied to analyse which groups showed statistical similarity or differences. Where replicates have been analysed the means and standard deviation have been calculated.

3. Geochemistry of the Needle's Eye Natural Analogue site

The Needle's Eye Natural Analogue Site offers a unique opportunity to study geochemical processes involving uranium over long timescales in the natural setting of a highly organic peat soil (section 2.1.2). In this chapter, the results of analysis of the inorganic and organic constituents of the soils and pore waters of the site are presented. The system is complex, with significant variations in hydrology and geochemistry occurring over small distances (metres) and depths (centimetres). Previous investigations involving transects of the site and vertical depth profiles have shown areas of uranium accumulation with solid phase soil concentrations of up to 2500 mg kg^{-1} (e.g. Xu, 2013). The mechanism of accumulation suggested from studies of the site in the late 1980s and early 1990s (Hooker, 1991; Jamet *et al.*, 1993) was the reduction of U(VI) to U(IV) as oxic, U-bearing water flows into the highly reducing conditions in the waterlogged, organic zone prompting the formation of stable U(IV) minerals. The dominant role of organic matter in the accumulation of U was suggested in sequential extraction procedures which showed that over 85% of U was extracted with tetra sodium pyrophosphate, a reagent used to dissolve organic matter, with less than 5% of the total U extracted in the "readily available" or "ion-exchangeable" fractions (MacKenzie, Whitton, *et al.*, 1991). More recently the results of targeted extraction experiments lead to the hypothesis that the accumulated uranium is actually present in the form of U(VI) and is associated with both organic matter and with iron minerals which were intimately associated with the organic matter (Xu, 2013). These previous studies highlight the potential importance of the characteristics of organic matter at the site but until now a study of the properties and structure of the OM has not been undertaken. The results presented in this chapter build upon the earlier work, summarised above, to provide a detailed description of the geochemical conditions at the site, particularly in relation to the mobility of U. Organic matter characterisation methods have

then been applied to the site for the first time in order to understand the structure and properties of extractable humic substances, porewater dissolved organic matter (DOM) and peats. Inorganic analysis methods have been used to determine the distribution of U, trace elements and minerals with depth in the bog and X-ray absorbance spectroscopy has been used to investigate the speciation and local binding environment of U at the atomic scale.

3.1. Variation in geochemical characteristics across the sample site: transects

3.1.1. Inorganic analysis of the solid phase

Soil samples were collected along a transect from the cave in the cliff containing the uranium mineralisation towards the saltmarsh (Figure 2.2) to characterise the variations in soil conditions across the site. The first sample of the transect, from within the cave, was collected on 08/05/14 and all others were collected on 06/02/17. In each case, soil from a depth of 0 – 5 cm was ground and digested as is described in section 2.2.5.2. Figure 3.1 shows the variation in pH, organic matter content (by loss on ignition), moisture content and selected elemental concentrations across the site. The results shown are the average of duplicate analyses.

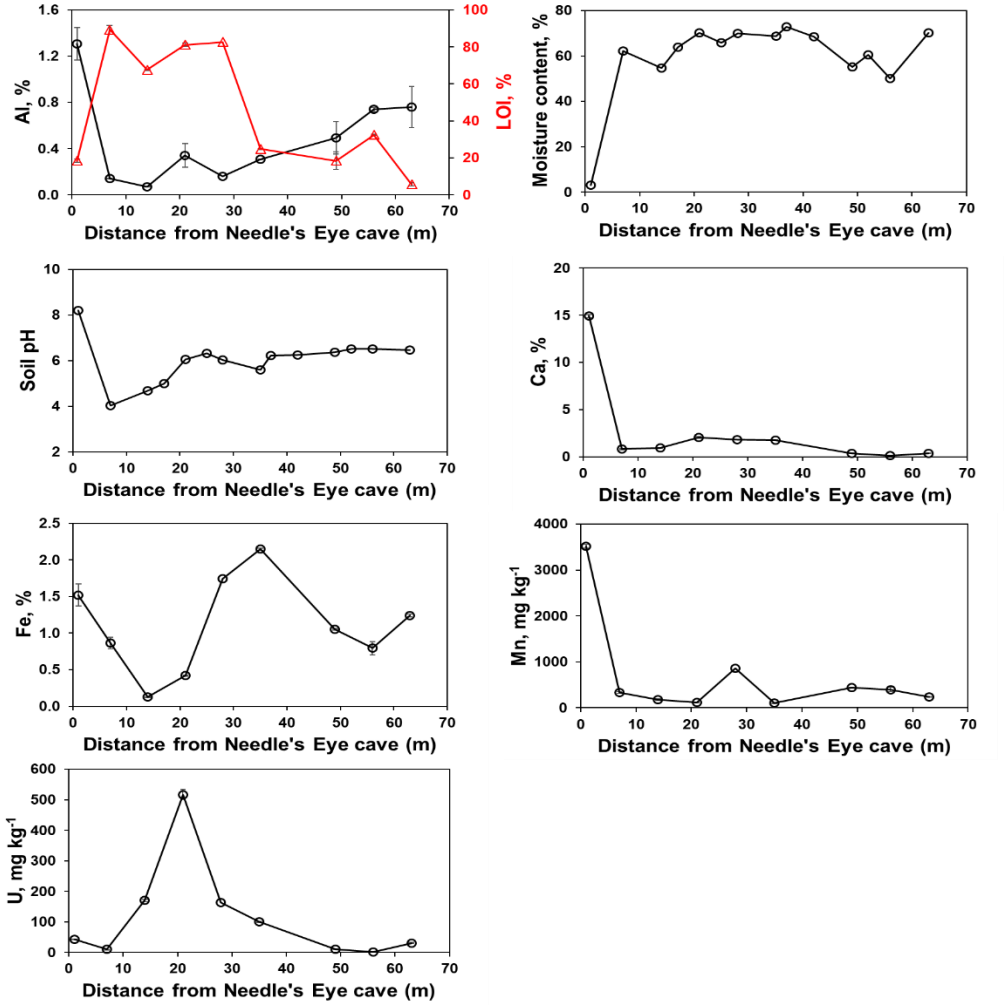

Figure 3.1. Elemental concentrations and geochemical characteristics of soils (0 - 5 cm) across a transect from the cave to the saltmarsh. Error bars (which in some cases are smaller than the figure symbols) show the standard deviation between duplicates.

The LOI and concentration of Al showed the relative contribution of organic and mineral phases to the soil composition and were negatively correlated ($\rho = -0.9$, $p < 0.001$). The soil within the cave had a relatively low concentration of organic matter and correspondingly high concentration of Al. The cave soil was also very dry, with a moisture content of only ~3%, despite the near-continuous flow of water down the back wall of the cave. This was possibly due to the low OM content leading to low water retention. The water flow rate within fissures near the U mineralization has previously been measured as 0.1 – 0.2 l hr^{-1} (MacKenzie, Whitton, *et al.*, 1991) and, although the flow rate was not measured in this study, water was observed flowing down the cave wall on every visit to the site. The soil within the cave contained a high concentration of Ca, likely to originate from the dissolution of calcium carbonates within the cliff. This consequently caused a soil pH in the cave of over 8. The U concentration in the cave soil of 43 mg kg^{-1}, although more than four times higher than the background natural level in soils of < 10 mg kg^{-1} (Pulford, 2010; Rawlins *et al.*, 2012a), was relatively low compared to other parts of the sampling site, and might seem unusual when considering the proximity to the uraninite mineralization which acts as the source of U to the site. The low concentration of U in the cave soil was likely to be due to the relatively high pH (compared to the rest of the site) and Eh, as U (VI) forms various highly soluble complexes in solution at pH values above 7.5 such as uranyl carbonates or uranyl hydroxides. This is discussed in more detail in section 3.1.2. The presence of the ternary complex calcium uranyl carbonate further increases U solubility in a pH range of around 7 – 9.5 (Gorman-Lewis, Burns and Fein, 2007). The pH, relatively high concentration of Ca and aerated soil are favourable conditions for the U remain complexed and in solution.

The concentration of Fe is ~1.5% in the soil of the cave and decreases to ~0.15% before increasing to its maximum concentration of ~2.1% within the bog. The concentration of Mn is over ten times higher in the sample from the cave compared to the surface samples

collected along the transect. The soil of the cave is dry and loosely grained so it is likely that the Fe and Mn are present as oxides.

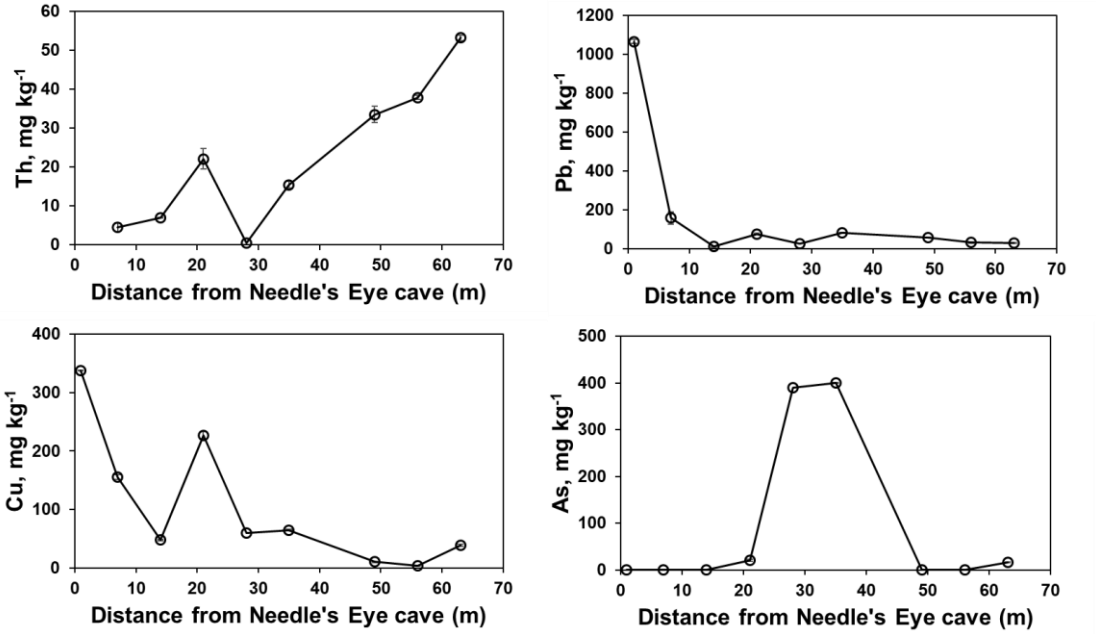

Figure 3.2. Elemental concentrations of potentially toxic elements (PTEs) Th, Pb, Cu and As in soils (0 - 5 cm) across a transect from the cave to the saltmarsh. Error bars (which in some cases are smaller than the figure symbols) show the standard deviation between duplicate.

Uranium is not the only potentially toxic element (PTE) that is found at elevated concentrations at the site. Lead, As, Th and Cu also have concentrations greater than the UK soil average (Pb = 81, As = 20, Th = 7.9 and Cu = 24 mg kg^{-1}) (Environment Agency, 2007; Rawlins *et al.*, 2012b). The transect profiles of As, Cu, Th and Pb, in figure 3.2, indicate the significantly different chemistry exhibited by these elements in a complex environmental system. In the cave soil, As was undetectable while Pb and Cu were at their highest concentration. Like U, As is highly soluble at pH >7 (Masscheleyn, 1991; Drever, 1997) so As is likely to remain in solution rather than accumulate in the cave soil. Copper and Pb minerals have been identified at the mineralisation site within the cliff (Braithwaite and Knight, 1990; Basham *et al.*, 1991) and, like U, they can be leached out from the rock by weathering and distributed into the organic soils below. The concentrations of Pb and Cu were highest in the cave, possibly due to their ability their association with Fe and Mn

oxides, which have a high affinity for binding Pb and Cu, with increasing pH over a range of 5 - 8 leading to increased adsorption and stronger binding (Gadde and Laitinen, 1974; Ponthieu *et al.*, 2006). The concentration of Th has a strong correlation with Al, (ρ=0.91, $p < 0.002$) showing its strong association with the soil mineral phases. The associations of Th are discussed in more detail in section 3.2.7.

Beyond the entrance of the cave the conditions change significantly as the land slopes to the bog, at distances of 7 – 18 m from the cave entrance. The soil surface is covered with a dense layer of leaf litter from the surrounding trees. In this area the soil organic matter increases to over 85% with a corresponding increase in soil moisture content to ~62%. The soil pH also drops here to ~4.0, a change which can be attributed to the large decrease in Ca carbonate concentration and increase of organic matter. The concentrations of Fe and Mn are lower here than within the cave, most likely due to the lower mineral content and increased OM content of the soil beyond the cave entrance, exemplified by the low Al concentration. The soil U concentration was also very low for this site, at ~9.6 mg kg^{-1}.

At 21 m from the cave entrance the soil was again highly organic (LOI ~68%) and wet (moisture content ~70.2), with a solid phase pH of ~6.1. This sample was collected from the bottom of the slope and within the bog. The bog, which extends from ~17 m to ~35 m from the cave, is sparsely vegetated with plants tolerant of the waterlogged conditions such as *Iris pseudacorus* and *Chrysosplenium oppositifolium.* In the first sample within the bog (21 m sample) Fe and Mn concentrations were low. It is at this point that the highest concentration of U was observed, with over 500 mg kg^{-1} in the surface samples. Beyond 21 m the U concentration decreased, accompanied by an increase in Fe, Mn and As. A distance of 35 – 50 m marks the transition from the peat bog to the irregularly inundated saltmarsh zone, evident in the change of vegetation as the trees give way to plants of the upper saltmarsh such as *Juncus gerardii*, *Festuca rubra* and *Puccinellia maritima.* The transition

was also seen in the sharp decrease in organic content as the LOI falls from ~80 % to ~20 %, marking the extent of regular marine sediment deposition.

The peak in the concentration of U along the transect at 21 m occurs at the leading edge of the bog and does not coincide with the maximum concentration of any other elements analysed, although Cu also has an elevated concentration at the same distance.

In these results it is evident that there are zones with different characteristics across the site:

i) Relatively low organic and high pH soil within the cave

ii) Drier, highly organic area with low pH sloping down towards the bog (7 – 17 m)

iii) Waterlogged, sparsely vegetated and highly organic bog zone (17 – 35 m)

iv) Transition zone between bog and saltmarsh (35 – 49 m)

v) Saltmarsh (49 m onwards)

The zonation across the site is discussed further in section 3.1.5.

3.1.2.Organic analysis of extracted OM

UV/vis, FTIR-ATR and NMR spectroscopy were used to characterize the 0.1 M NaOH extractable OM in samples along the site transect from 7 m to 63 m from the cliff. The results from the different techniques were compared in order to draw conclusions about the properties and structure of OM across the site. The results are presented below.

3.1.2.1. UV/vis analysis of extracted OM

Samples prepared for NMR analysis (approximately 12 mg OM in 600 µL 0.05 M NaOD) were analysed by UV/vis spectroscopy. The samples were pH adjusted to pH 7 using 0.1 M HCl and diluted to 50 mg L^{-1} OM using DI water.

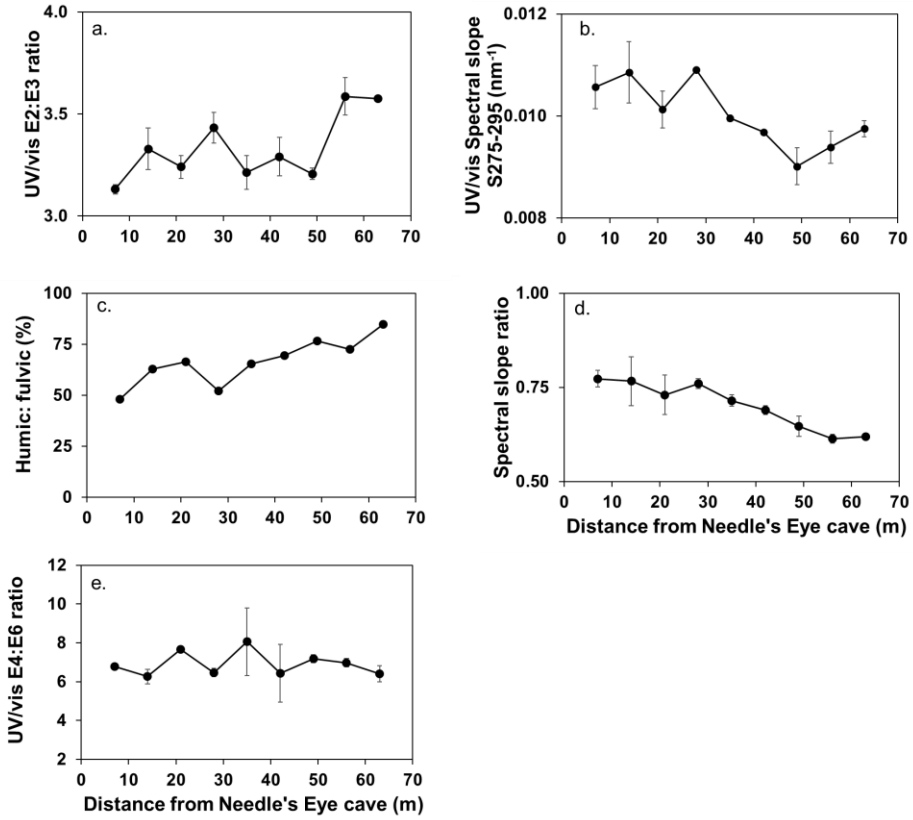

Figure 3.3. Variation in UV/Vis parameters with distance from the cliff. Results presented are the average of duplicate measurements with error bars showing the standard deviation of the two replicates. The relative percent difference (RPD) between the duplicates was also calculated and was < 1 % for every parameter.

The UV/Vis spectra were collected from 800 to 200 nm at a resolution of 0.001 absorbance units. The results of the analysis of extracted organic matter from the transect samples at distances of 7 – 63 m are presented in figure 3.3.

The E2:E3 ratio is the ratio of the absorbance at 250:365 nm and is considered to be inversely proportional to molecular size (Minor *et al.*, 2014). The increase of the ratio in the samples at 56 and 63 m (figure 3.3, a.) was therefore suggestive of a decrease in molecular size from the bog to the saltmarsh. The E2:E3 ratio has also been reported to be inversely related to aromaticity (Peuravuori and Pihlaja, 1997; Minor *et al.*, 2014), which would suggest a decrease in aromaticity with the transition from the bog to saltmarsh.

The spectral slope $S_{275–295}$ (figure 3.3, b.) showed a decrease between 28 – 49 m, then a slight increase for the last two samples at 56 and 63 m. The $S_{275–295}$ has been shown to be negatively correlated to aromaticity and molecular weight (Helms *et al.*, 2008; Fichot and Benner, 2012; Rodriguez, Schlenger and Garcia-Valverde, 2016), therefore the results of the E2:E3 and $S_{275-295}$ contradict each other in this case. Comparison with the humic: fulvic ratio and the results of FTIR and NMR analysis help in the interpretation of the UV/Vis results . The spectral slope ratio (SR, figure 3.3 d.) is the ratio between the slope of two regions of the spectrum, $S_{275-295}$ and $S_{350-400}$.The SR showed an overall decrease from 28 to 63 m. The analysis of spectral slope characteristics has been shown to be related to molecular size and dissolved organic matter origin, with the SR having lower values for larger molecular weight fractions (Helms *et al.*, 2008) and peat and soil samples having lower values than fresh water and marine DOM samples (Chen *et al.*, 2011). The decrease in SR seen along the transect is again indicative of increasing humification and molecular weight in the transition from the bog to the saltmarsh.

The ratio of humic:fulvic acids (figure 3.3, c.) in the samples shows a general increase with distance from the cave. The sample at 28 m, in the peat bog area of the site, has a slightly

more fulvic acid character than the samples around it. There is a strong negative correlation ($\rho = 0.92$, $p < 0.001$) between SR and increasing humic character of the NOM. As humic acid tends to be larger and more aromatic than fulvic acid (Stevenson, 1982), this is in agreement with the results of Helms *et al.* (2008).

The E4:E6 ratio (figure 3.3, e.) is the ratio of the absorbance values at 465:665 nm. It tends to be negatively correlated with humifaction indicators such as aromaticity and size. Fulvic acids tend to have E4:E6 ratios of > 6 while humic acids, which are generally considered to have higher molecular weight, tend to have E4:E6 ratios of around 4 – 6 (Stevenson, 1982). Along the transect the E4:E6 ratio doesn't show a trend and is in the "fulvic" range of between 6 and 9. The interpretation of the different UV/Vis parameters are discussed more fully in Chapter 5.

3.1.2.2. FTIR-ATR analysis of extracted OM

As explained in section 2.4.7, the relative intensity of peaks in FTIR analysis is directly proportional to the concentration of the functional group responsible for the absorbance at a particular wavelength. However, the interpretation of the spectra is complicated by the overlapping peaks arising from the absorbance of different structures. Figure 3.4 shows the spectra for three samples along the transect, highlighting the peaks used to identify different organic functionalities.

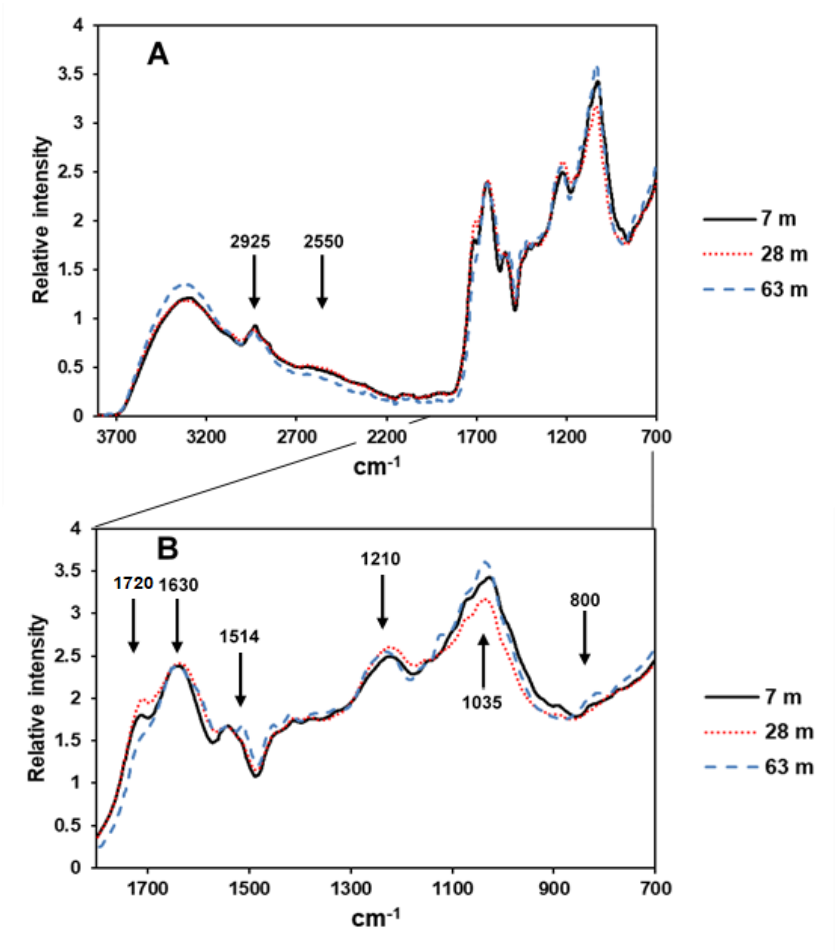

Figure 3.4. Examples of full FTIR spectra (A) and an expanded section to show the fingerprint region in more detail (B) of OM samples at three distances from the cave.
Functional group assignments are as follows: 2925: CH_2, 2550: COOH, 1709: COOH, 1630: Aromatic C=C and aliphatic C=O, 1514: aromatic C=C, 1210: phenolic OH, 1035: carbohydrate C-O, 800: aromatic CH.

The peak at 2925 cm^{-1} arises from aliphatic C-H stretch. The broad region from 2400 – 2650 cm^{-1} is caused by the OH stretch of H-bonded carboxylic groups. The peak at 1705 – 1720 cm^{-1} arises from the C=O stretch of COOH (Gondar *et al.*, 2005; Artz *et al.*, 2008). The peak at 1630 cm^{-1} has input from the stretching of aromatic C=C and the stretching and deformation of C=O of aliphatic carbonyl groups. The small peak at 1514 cm^{-1} is attributed to the vibration of aromatic rings. The region 1205 – 1225 cm^{-1} arises from the C-O stretch and OH deformation within carboxylic acids, phenols and alcohols (Niemeyer, Chen and Bollag, 1992; Abdulla *et al.*, 2010; Pospíšilová *et al.*, 2015). The prominent peak at 1035

cm^{-1} is due to the C-O stretch and OH deformation of carbohydrates. The small peak at 800 cm^{-1} is assigned to the out of plane deformation of aromatic C-H. The variation in some peaks is relatively small, such as aromatic C-H at 800 cm^{-1}, while some variations are more prominent like the peak at 1720 cm^{-1}, indicative of carboxylate functional groups.

The variations in regions of the FTIR spectra between samples along the transect are shown in Figure 3.5.

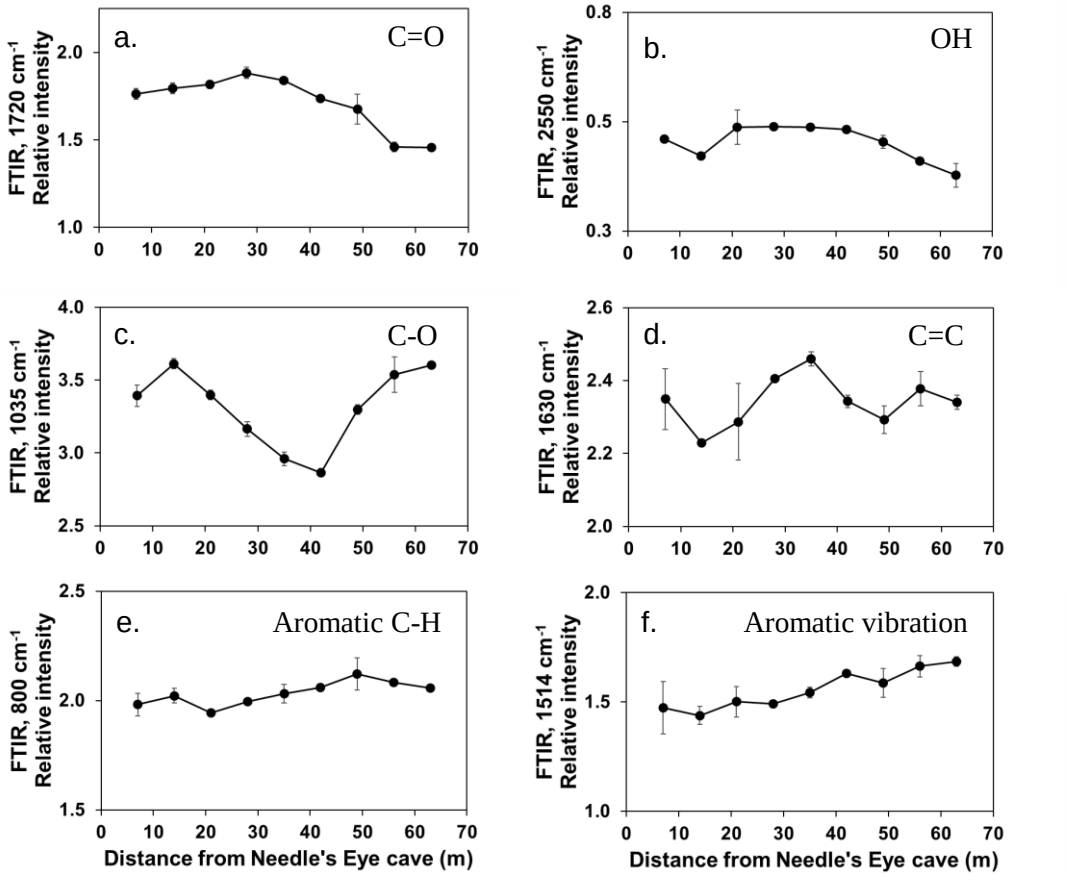

Figure 3.5. Variation in intensity of regions of FTIR spectra between samples along the transect. Error bars show the standard deviation of duplicate analyses. The relative percent difference (RPD %) between the duplicates was also calculated and was < 1 % for every sample.

The results of FTIR analysis show that the carboxylic functional groups (figure 3.5, a. and b., 1720 and 2550 cm^{-1}) are at their highest concentration within the bog and show a decrease from 28 to 63 m from the cave. The intensity of the peak at 1035 cm^{-1} (figure 3.5, d.), indicative of carbohydrate structures, shows an initial small increase from 7 to 14 m before a decrease to the minimum intensity at 42 m. The intensity then rises increases to the furthest extent of the transect at 63 m. Of the intensities representative of aromatic molecules, the wavelengths of 800 and 1514 cm^{-1} (figure 3.5, e. and f.) show a gradual increase over the full transect while the region at 1630 cm^{-1} (figure 3.5, c.) is quite variable along the transect, with a peak in the maximum intensity at 35 m. The variation seen in this peak could be due to the overlap of signals contributed by aromatic structures and carbonyl groups, making the peak hard to interpret.

The results of FTIR analysis indicate changes in OM composition across the site with a decrease in carboxyl functional groups and increase in aromaticity from 7 – 63 m. Although only semi-quantitative, the relative changes seen in these functional groups compare favourably with the results of UV/vis analysis (section 3.1.2.1). Results of all organic analysis techniques applied to the transect samples are compared and discussed at the end of this section (section 3.1.2.2).

3.1.2.3. NMR analysis of extracted OM

An exemplar NMR spectrum is presented in figure 3.6, below. This spectrum was obtained for the organic matter extract obtained from the soil sample collected at 21 m from the cave, within the bog.

The NMR spectrum in figure 3.6. is typical of extracted soil organic matter, with broad and overlapping peaks making identification of the individual molecules responsible for each signal impossible. The integration regions highlighted are proportional to the amount of ^{1}H in those particular chemical environments within the sample.

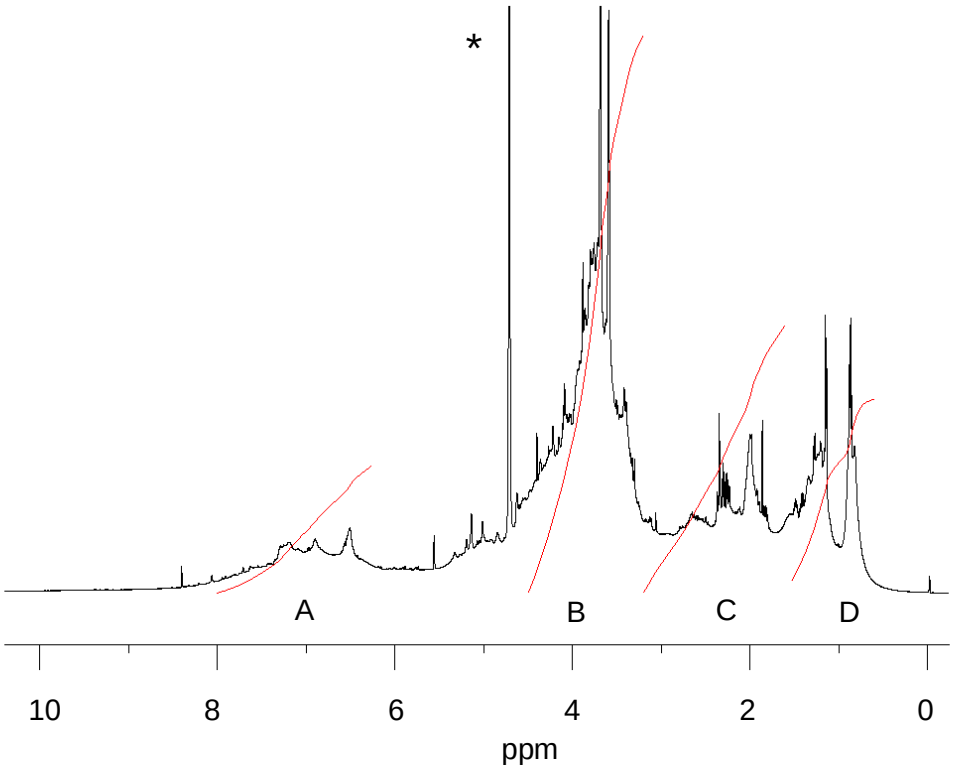

Figure 3.6. ^{1}H NMR spectrum of OM extracted from a sample collected at 21 m from the cave. Approximately 12 mg of OM sample was dissolved in 0.05 M NaOD for analysis. The red lines show the integrated regions used to quantify the proportion of ^{1}H in different organic environments within the sample. A = aromatic molecules, B = carbohydrate, C = functionalised aliphatic and D = unfunctionalised aliphatic chains. The peak highlighted by the asterisk (*) is the residual DOH peak from H^{+} within the sample combining with the D_2O used as a solvent. This peak has been suppressed using the PRESAT pulse sequence to have minimal effect on the spectrum (section 3.4.8.5).

The variation between the integrals of these regions along a transect is presented in figure 3.7 below. As can be seen in figure 3.7, the samples collected at 7 m and 14 m from the cave have a relatively low contribution of aromatic structures and higher amount of carbohydrate and unfunctionalized aliphatic structures. Within the bog (21-42 m) there is an increase in oxygen rich aliphatic moieties of around 6 % to a peak of around 25 % of the total protons present being found in this fraction at 21 – 42 m, while the carbohydrate structures are relatively low at this point. At the 42 and 49 m sample points aromatic structures are found at high concentration.

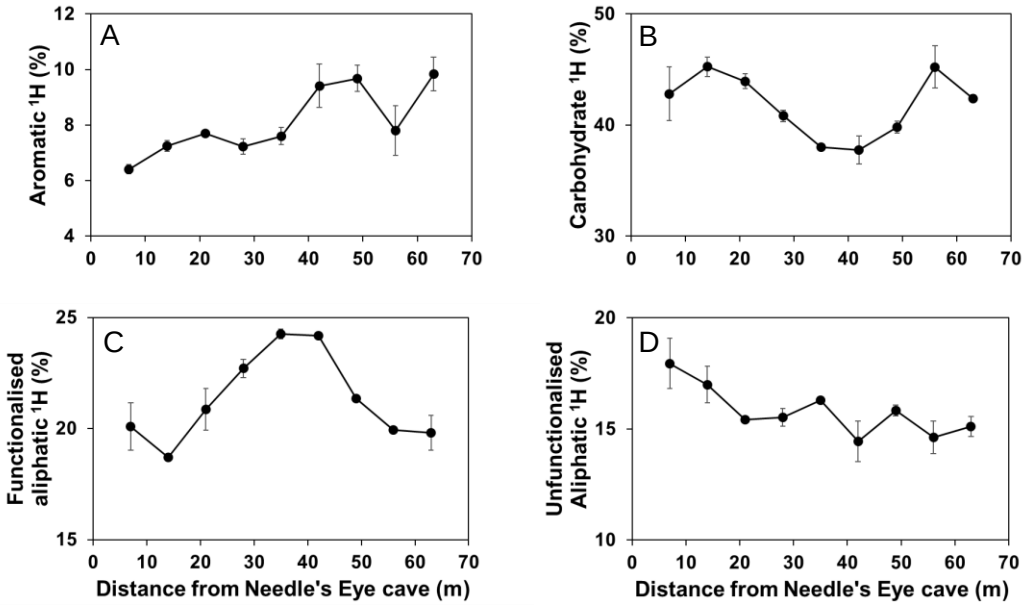

Figure 3.7. Relative intensity of different organic regions from ^{1}H NMR analysis of extracted soil organic matter from transect samples.
The graphs show the percentage of ^{1}H within each organic environment in each sample. Error bars show the standard deviation of duplicate measurements. The relative percent difference (RPD %) was <5 % for each of the duplicates. The regions a.-d. are the same as those described in figure 3.6. A = aromatic molecules, B = carbohydrate, C = functionalised aliphatic and D = unfunctionalized aliphatic chains.

The 42 and 49 m points of the transect are in the region of transition from bog to saltmarsh where the transect passes under some thick tree cover and then becomes more densely vegetated with grasses. Although it is likely that the different local vegetation has a significant effect on the properties of the organic matter, it is not possible to make a direct link from the results of 1-dimensional NMR experiments. This can be achieved through application of multidimensional experiments (Bell, Graham and Uhrín, 2016) but was not within the scope of the current project. There is a slight decrease of aliphatic structures along the whole transect, of around 3.5% which is inversely proportional to aromaticity (ρ= -0.67, $p < 0.05$). Analysis of the aliphatic NMR results by ANOVA and Tukey's HSD test showed that the samples from 42, 56 and 63 m have significantly different aliphatic ^{1}H content to the sample from 7 m. Despite there being only two replicates for each sample this result suggests that the change in aliphatic content across the site is significant.

3.1.2.4. Conclusions from OM characterisation of transect samples

The increase in aromaticity seen in ^{1}H NMR and analysis of samples along the transect strongly correlates with the increase in humic:fulvic acid with distance from the cave (ρ = 0.983, $p < 0.001$) and is negatively correlated with $S_{275\text{-}295}$ (ρ = -0.82, $p < 0.01$) and SR (ρ = -0.87, $p < 0.005$). The content of aromatic ^{1}H is also correlated with the aromatic regions of the FTIR spectra at 1514 cm^{-1} (ρ = -0.87, $p < 0.002$) and 800 cm^{-1} (ρ = -0.72, $p < 0.05$). The agreement of results from different analysis supports the conclusion that OM aromaticity increases with distance from the cave and that the OM from samples beyond 42 m is more humified. This change in OM composition occurs at the transition from bog to saltmarsh, suggesting that the composition of organic matter is related to the soil type (Mahieu, Powlson and Randall, 1999). Furthermore, the correlation between the aromatic content from analysis by ^{1}H NMR, the humic:fulvic content and the UV/Vis parameters $S_{275\text{-}295}$ and SR suggests that $S_{275\text{-}295}$ and SR are linked to sample aromaticity and humification and not only molecular size.

3.1.3. Transect pore waters

3.1.3.1. Inorganic analysis of cave drips and soil porewaters

The concentration of U in water emerging from the mineralization in the water dripping within the cave, collected on several occasions, were typical of the concentrations seen in previous studies (e.g. Xu, 2013), with a concentration of over 200 µg $L^{-`}$ measured in 5 samples collected over three sampling trips (225.10 ± 11.36 µg l^{-1}, n = 5) and a lower concentration of 69.85 ± 5.78 µg l^{-1} (n=2) on a further sampling trip. The concentration of Ca in the cave drip waters, also measured on several occasions, had a concentration of 70.6 ± 12.9 mg l^{-1} (n = 7).

The results of analysis of soil porewaters in a transect from the cave to the Merse are shown in figure 3.8. The results for the first sample in the transect is from drip water collected from the cave on the day of sampling, not extracted pore water, as the soil in the cave was too dry to collect pore water.

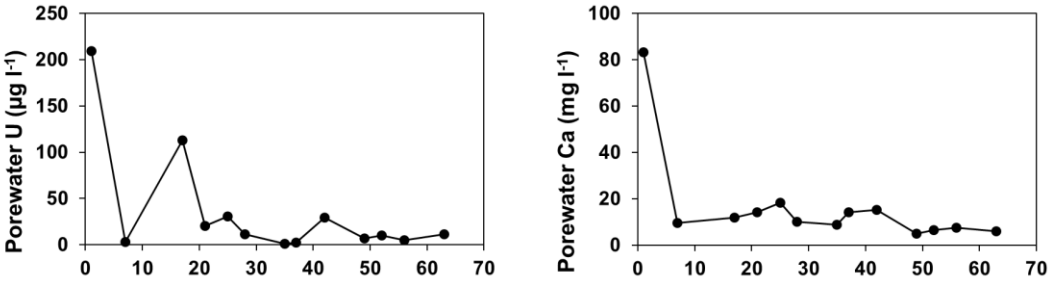

Figure 3.8. Uranium and Ca concentrations in porewaters extracted from transect samples on 06/02/17.

Beyond the entrance of the cave the porewater U concentration mirrored the solid phase and had a relatively low concentration of ~3 µg L^{-1}. This is likely to be due to the deep flow of the U bearing water from the cliff which re-emerges in the bog (Hooker, 1991). At the foot of the slope, 17 m from the cave, the porewater U concentration was at its highest level, of ~113 µg L^{-1}. Beyond this point the concentration decreased to around 30 µg l^{-1}

from 17 – 28 m from the cave and then further decreased to <1 µg L^{-1} at 35 m from the cave. The relatively low concentration of <12 µg L^{-1} was maintained beyond 42 m. This concentration is below the recommended concentration of U in drinking water of 15 µg L^{-1} (WHO, 2012) but greater than the majority of UK groundwaters which tend to have concentrations of less than 1 µg L^{-1} (Smedley *et al.*, 2006). The transect profiles of U and Ca were significantly correlated ($\rho = 0.59$, $p < 0.05$) supporting the results of Xu, (2013) who observed that the solubility of U in porewaters at the site is related to the formation of soluble calcium uranyl carbonate species. There is no statistically significant relationship between the concentration of U in porewater and U in soil, as might be expected. This is likely to be because the porewater U concentration is continually influenced by the changing flow of water emanating from the cliff, creating variability in the porewater U concentration compared to the solid phase.

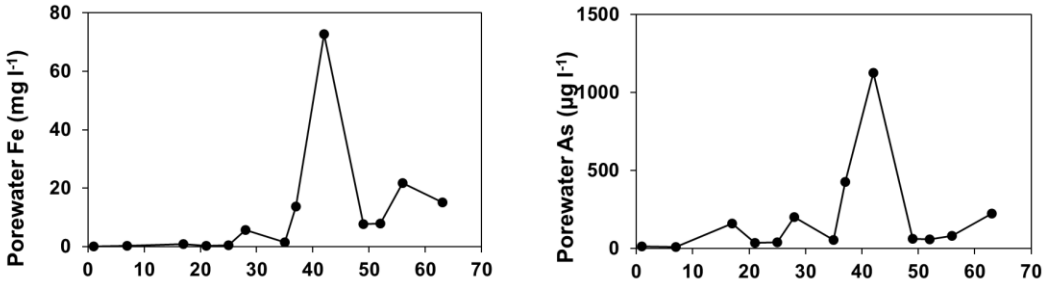

Figure 3.9. Iron and As concentrations in porewaters extracted from transect samples on 06/02/17.

The increase in U concentration at 42 m coincided with the maximum concentration of Fe and As in porewater of ~72 mg l^{-1} and ~1125 µg l^{-1} respectively (figure 3.9). There was a significant correlation between the concentrations of Fe and As in the transect porewaters ($\rho = 0.83$, $p < 0.001$) suggesting that the solubility of Fe and As is similar, as is often seen with these two elements as they are both soluble under reducing conditions and can co-precipitate under aerobic conditions (Arai, 2010).

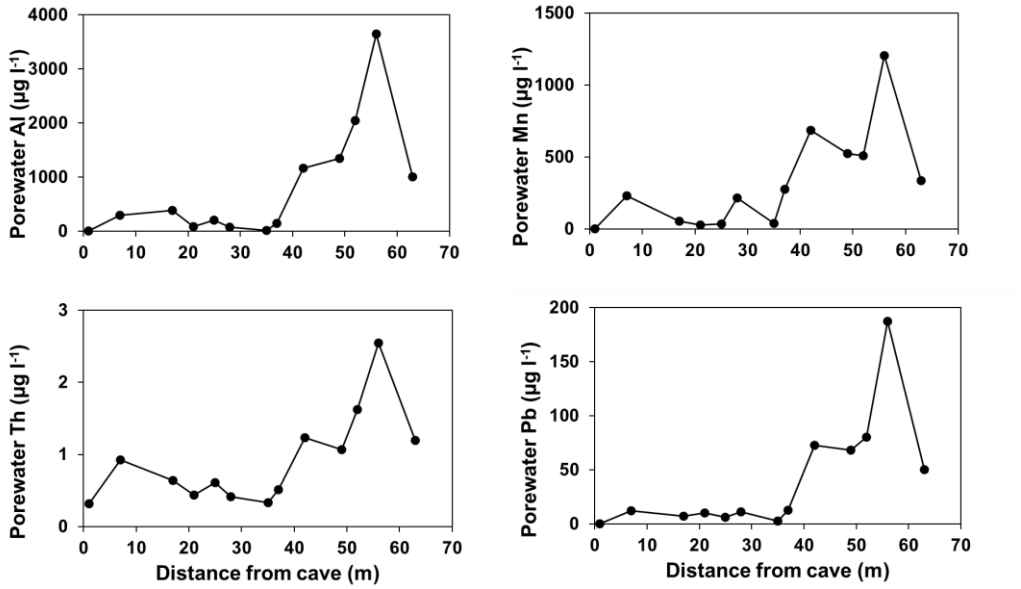

Figure 3.10. Aluminium, Mn, Th and Pb concentrations in porewaters extracted from transect samples on 06/02/17.

The maximum concentrations of Mn, Th and Pb and Al in porewaters (figure 3.10) all occurred at the same point in the transect at 56 m from the cave. Manganese, Th and Pb were correlated with Al and had Spearman's ρ values of 0.86, 0.98 and 0.87, respectively ($p < 0.001$). The Fe concentration had a secondary maximum at this point of 21 mg l^{-1} and Fe also had a correlation with Al ($\rho = 067$, $p < 0.01$) and with Mn ($\rho = 0.89$, $p < 0.001$). The similarity of the profiles of Pb, Th, Mn, Fe and Al suggests that their increase in the latter part of the transect is related to the increasing mineral content of the soil and suggests that the increase of their porewater concentrations beyond 35 m could be related to colloid formation. The porewater absorbance at 254 nm (figure 3.11), as a proxy for DOM concentration, showed a similar trend, with an increase beyond 35 m.

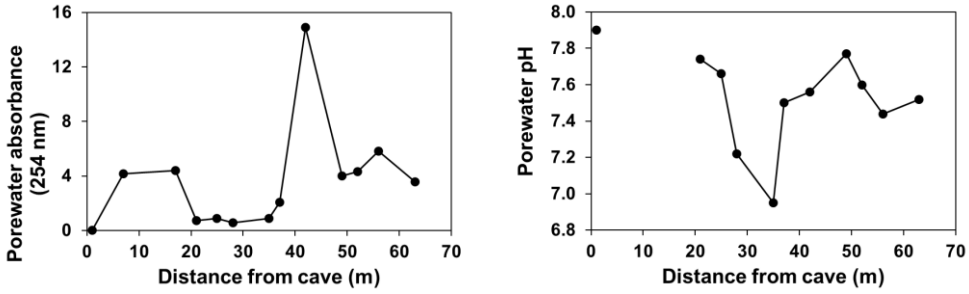

Figure 3.11. pH and absorbance at 254 nm of porewaters extracted from transect samples on 06/02/17.

The transect profile of porewater absorbance at 254 nm was also correlated with the porewater concentrations of Al, Mn, Th, Pb (ρ = 0.84, 0.86, 0.86 and 0.82 respectively, $p<0.001$) and Fe (ρ = 0.66, $p<0.05$). The increase in porewater concentration of DOM, Fe and Mn along with the sparingly soluble elements Pb, Th and Al again indicates that the increase in the concentration of these analytes beyond 35 m was likely to be due to colloid formation. The absorbance at 254 nm also had a negative correlation with soil moisture content. This suggests that the high moisture content points of the transect had a diluting effect on the porewater DOM concentration. It is also possible that the lower moisture content areas of the transect do not experience such high water flow, allowing more contact time for organic soil components to dissolve into the porewater.

The cave drip water had a pH of 7.9. Along the transect, the 0 – 5 cm porewater samples had a pH of ~7.5 but showed a minimum of 6.95 in the middle of the peat bog at 35 m from the cave. This point, at which the pH is lowest, is also where the lowest U concentration in solution is found. The low U concentration at this point is likely to be due to the sorption of U onto solid phase organic or mineral surfaces (Echevarria, Sheppard and Morel, 2001) possibly due to the change of pH from ~7.5 to ~ 6.95 favouring the formation of the neutral $UO_2CO_3^o$ ion from the negatively charged $UO_2(CO_3)_2^{2-}$ in solution (1.7).

The cave drip water showed a UV/vis absorbance at 254 nm close to the limit of detection as it does not contain a significant concentration of organic material when it exits the cliff. There were two elevated regions of relatively high dissolved OM concentration in the transect (shown by the absorbance at 254 nm). The first occurred in the samples at 7 and 17 m from the cave, which had an absorbance of ~4 absorbance units. This slight peak of OM coincided with the highest concentrations of U and Cu, suggesting a possible interaction of these elements with OM. From 21 to 35 m the absorbance of the pore waters in the bog had values of less than one. There was a large spike in absorbance at 42 m, which

coincides with the highest concentration of Fe in the transect which could suggest an interaction between OM and Fe or influence of Fe compounds on the UV/Vis absorbance.

3.1.4. Redox chemistry across the bog

The variation in redox chemistry across the site was measured by analysis of surface porewater samples. Two methods were used on three occasions. On 16/11/15 a portable redox probe was used to make 14 measurements along a transect from 12 – 26 m from the cave entrance. It was not possible to take measurements nearer the cave due to the low soil moisture content. On 04/02/16 nine redox probe measurements were also taken at distances between 16 and 32 m from the cave. On the same occasion 7 porewater samples were collected from 0-5 cm depth samples and the ratio of Fe(II) to Fe(III) was measured by the ferrozine method (Viollier *et al.*, 2000). Duplicate samples were analysed between 16 and 28 m from the cliff. On 16/02/17 collected porewater samples (as above in section 3.1.2) were also analysed by the ferrozine method to calculate the percentage of Fe(II) present by comparison with the total Fe concentration measured by ICP-MS. The results are presented in the figures below (figures 3.12 - 3.14).

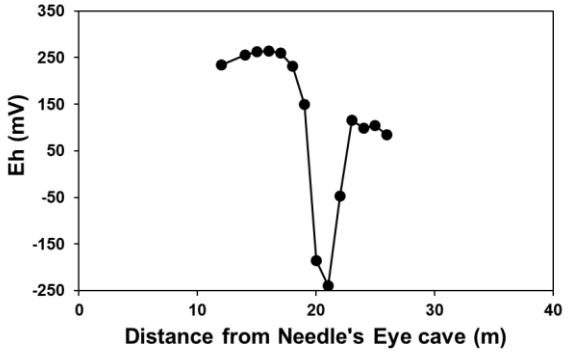

Figure 3.12. Redox potential across the site measured in situ with a portable redox probe on 16/11/15.

The redox potential measured on 16/11/15 showed a steep transition from oxidizing to reducing conditions at a distance of 17 m from the cave with a sharp minimum of -240 mV at 21 m from the cave. The surface reducing conditions did not prevail for a great distance and by 23 m oxidizing conditions were encountered again until the final point measured at 26 m. The redox potential measured on 04/02/16 (figure 3.13, a.) showed a similar profile to that shown in figure 3.12.

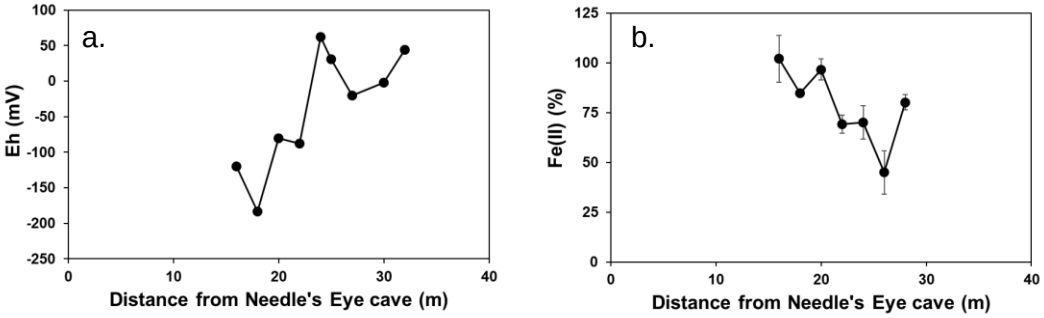

Figure 3.13. Redox potential measured in situ across the site with a portable redox probe (a.) and the percentage of total Fe in porewaters present as Fe(II) (b.) on 04/02/16. The error bars represent the standard deviation of duplicates analysed by the ferrozine method.

There were highly reducing conditions between 16 and 22 m from the cave, with a minimum of -183 mV at 18 m. Beyond 22 m the redox potential was higher, between -20 and 60 mV out to a distance of 32 m. The percentage of porewater Fe present as Fe(II), shown in figure 3.13 (b.), was in good agreement with the redox probe results with up to ~100 % of Fe found as Fe(II) at a distance of 16 – 20 m from the cave. Beyond 20 m the value decreased to a minimum of 45 % at 26 m before increasing again to 80 % at 28 m. The two methods of assessing the surface redox conditions proved consistent, with a highly reducing zone present at around 21 or 22 m from the cave transitioning to more oxic conditions beyond. This pattern was also observed in the Fe(II) analysis transect measured on 16/02/17, shown below in figure 3.14.

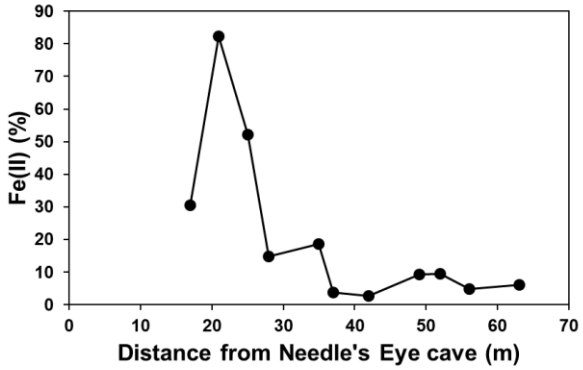

Figure 3.14. Percentage of total Fe in porewaters present as Fe(II) on 16/02/17.

The percentage of Fe as Fe(II) in porewaters collected on 16/02/17 had a peak of 82 % at 21 m distance from the cave. Beyond this point there was a rapid decrease of Fe(II) to 15 and 19 % at 25 and 28 m respectively, and <10 % for the remainder of the transect to 63 m.

The results presented show the variability in redox conditions over the space of a few metres within the bog.

3.1.4.1. Organic analysis of transect porewaters

3.1.4.1.1. Porewater analysis by ^{1}H NMR

Porewater samples were taken at four sites along the transect for analysis by ^{1}H NMR. Four samples were collected by digging a small hole to a depth of around 30 cm which rapidly filled with water. The water was sampled, stored in sealed containers and on returning to the laboratory around 50 ml from each sample site was de-salted by cation exchange and freeze dried. The small amount of dried organic matter obtained was then re-dissolved in 0.05 M NaOD for analysis. The spectrum of the sample collected at a distance of 25 m from the cave is shown below (figure 3.15)

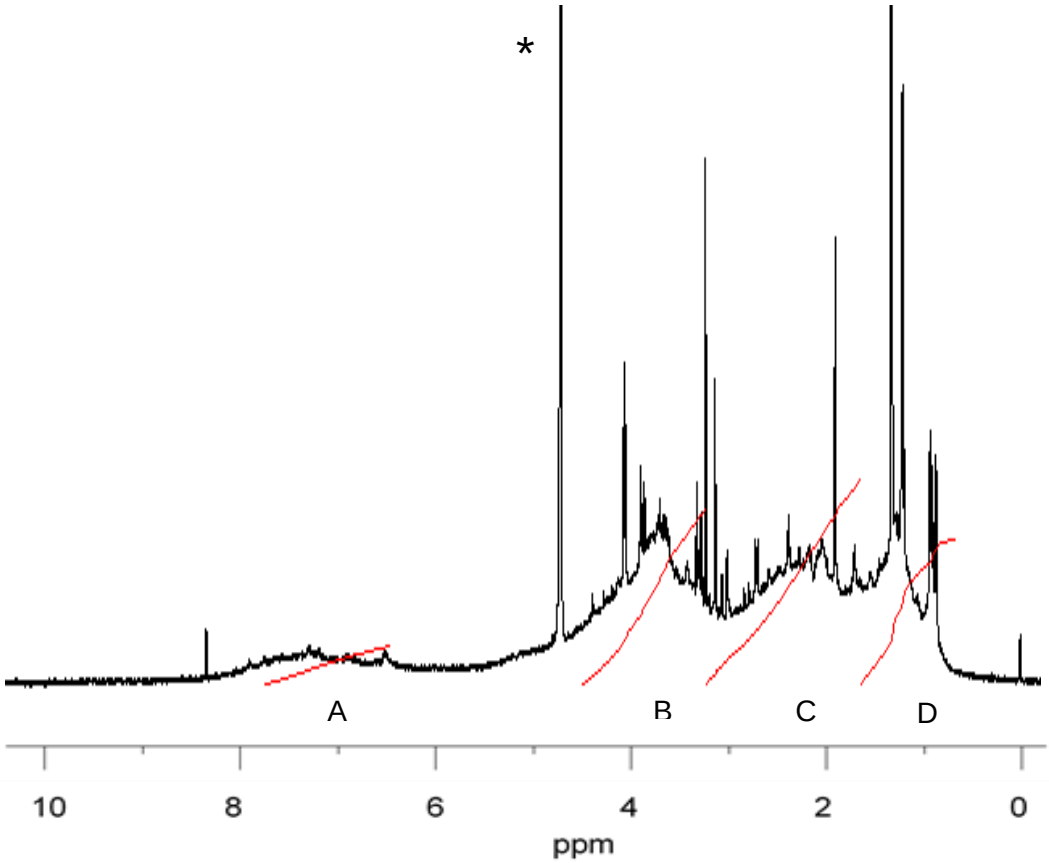

Figure 3.15. ^{1}H NMR spectrum of porewater organic matter from a sample collected at 25 m from the cave in the peat bog. The red lines show the integrated regions used to quantify the proportion of ^{1}H in different organic environments within the sample. A = aromatic molecules, B = carbohydrate, C = functionalised aliphatic and D = unfunctionalized aliphatic chains. The peak highlighted by the asterisk (*) is the residual DOH peak from H^{+} within the sample combining with the D_2O used as a solvent. This peak has been suppressed using the PRESAT pulse sequence to have minimal effect on the spectrum (section 3.4.8.3).

The ^{1}H NMR spectrum of the porewater organic matter has many overlapping sharp peaks, indicative of discrete chemical environments that are found in smaller organic molecules. The four regions (A, B, C and D) identified in the soil organic matter spectrum (figure 3.3) are easily identifiable in the pore water samples, but their relative abundance is significantly different. Apart from the greater abundance of small molecule signals, the major differences between the porewater OM and the OM extracted from soil are a decreased aromatic region (A) and a greatly increased signal in the functionalized aliphatic region (C).

The variations in composition between the four samples is shown below (figure 3.16).

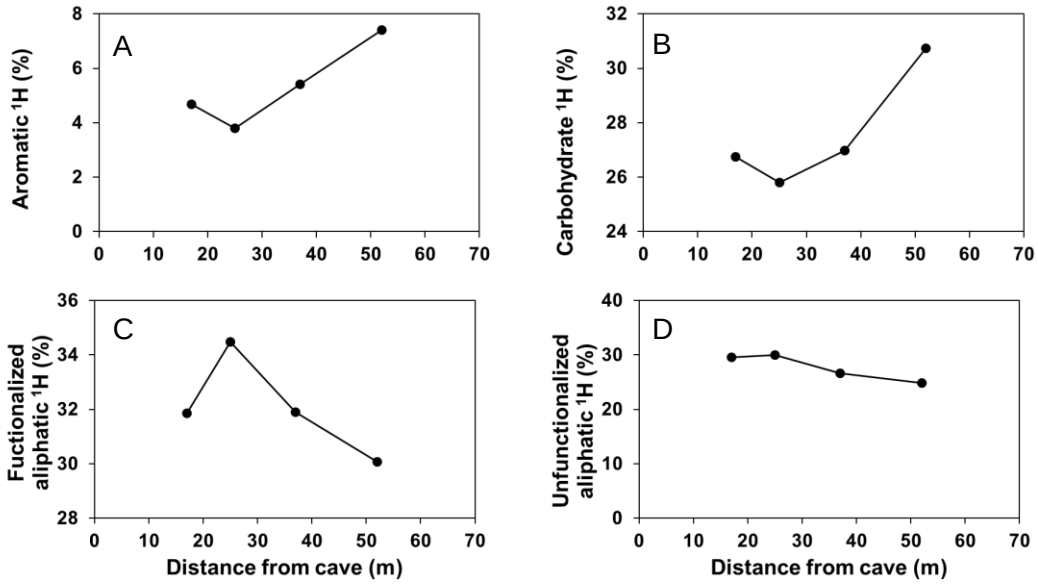

Figure 3.16. Integrated regions of 1H NMR spectra of pore water organic matter with distance from the cave. The regions A, B, C and D are the same are as shown in figure 3.15. A = aromatic molecules, B = carbohydrate, C = functionalized aliphatic and D = unfunctionalized aliphatic.

Comparison of the results for porewater OM with those of extracted soil OM (Figure 3.6) show that there are similar trends in composition with distance from the cave. The porewater organic matter shows an increase of aromatic character (figure 3.16, A) with distance from the cave after a slight decrease on entering the middle of the peat bog. The carbohydrate region (figure 3.16, B) is at its lowest concentration within the peat bog and

highest at the furthest extent into the saltmarsh, a distance of 52 m from the cave. The functionalized aliphatic component is highest in the bog sample at 25 m from the cliff (figure 3.16, C). As was seen for soil OM there is a general decrease in the relative intensity of aliphatic chain ^{1}H with distance from the cave (figure 3.16, D).

3.1.4.1.2. UV/Vis analysis of porewaters

The results of spectral slope calculations and E2:E3 ratio from the analysis of porewaters by UV/Vis are presented in figure 3.17. The porewaters were analysed after extraction by centrifugation in the lab and filtration through 0.45 µm syringe filters.

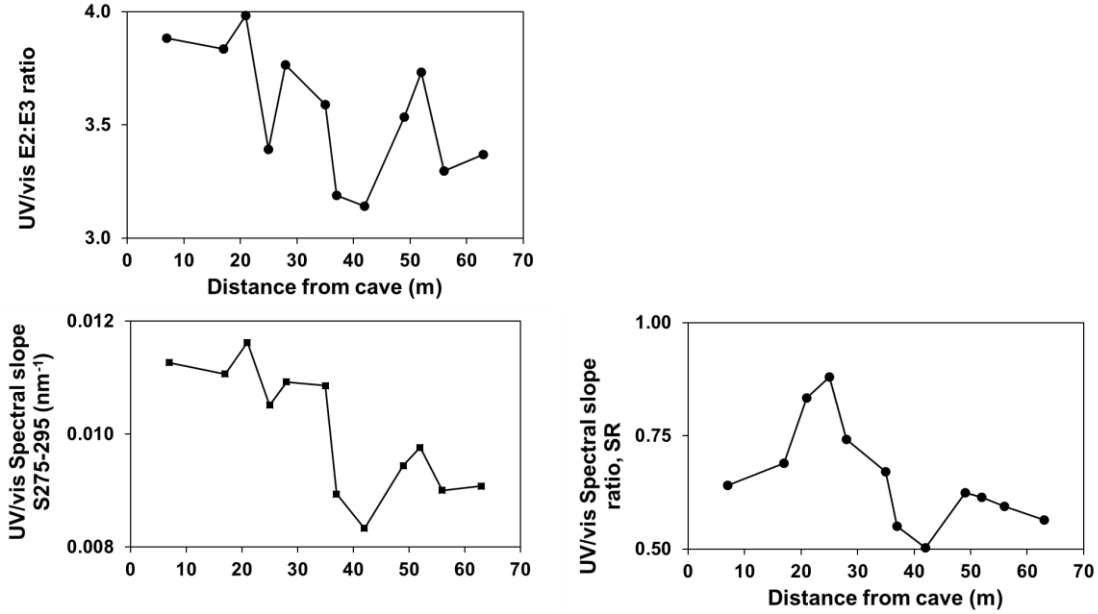

Figure 3.17. Results of analysis of porewater OM by UV/Vis

The spectral slope, $S_{275\text{-}295}$, showed little variation from 7 – 35 m but then decreased to 42 m, before recovering to an intermediate level for the rest of the transect. The SR increased to a maximum at 28 m but then showed a decrease between the bog and the saltmarsh. These trends were similar to those seen in the extracted OM (figure 3.2) but with greater difference between the maxima and minima in the porewater organic matter.

The peak in the SR occurred in the middle of bog, indicating an increased fulvic acid character, while the decrease towards the end of the transect indicated a more humic acid-like character (higher molecular weight, more aromatic). This is in agreement with the results of analysis of porewater OM by ^{1}H NMR, which showed increased aromaticity with distance from the cave (Figure 3.16).

The E2:E3 ratio was very variable in the porewater transect but showed similarities to the $S_{275\text{-}295}$ spectral slope and the two are positively correlated with a Spearman's ρ of 0.97 ($p < 0.001$). This is the opposite trend to that seen in the extracted OM and suggests that these UV/vis parameters are sensitive to the type of OM being analysed.

The results of analysis of porewater OM by UV/Vis are quite variable, but trends similar to those seen in the analysis of extracted solid phase OM are discernible, such as the decrease in $S_{275\text{-}295}$ and SR, indicating OM of more humic character and larger size with distance from the cave. The results of analysis of porewater OM indicate that the composition of porewater OM is related to the composition of the 0.1 M NaOH extracted OM, and show variation across the different areas of the site, particularly in the transition between the bog and the saltmarsh, with an increase in aromaticity and decrease in aliphatic components.

3.1.5. Summary of analysis of transect samples

Analysis of inorganic and organic components of soil and porewater samples across the site highlights the spatial variability of important geochemical characteristics across a small area. The organic matter analysis shows a relatively high abundance of oxygen-rich aliphatic organic matter in the bog with increasing humic acid character, aromaticity and molecular size through the transition from the bog to the saltmarsh.

The peak in soil U concentration coincides with the reducing conditions encountered at the leading edge of the bog. The coincidence of the sharp onset of reducing conditions with the

U accumulation was also noted by (Jamet *et al.*, 1993) who modelled the redox and other geochemical conditions at the site and concluded that the reduction of U(VI) to U(IV) was a feasible mechanism of U retention in the bog. However, the authors note the limitations of their model approach as they did not have access to sufficient data on the interaction between U and OM to include the possibility of U adsorption onto OM in their model as a mechanism of U immobilisation.

The highest concentration of U in porewater at 17 m from the cave coincided with an increase in OM in solution, shown by the absorbance at 254 nm. Copper also had its highest porewater concentration at this point, and is known to bind strongly to OM (e.g. Hering and Morel, 1988; Christl and Kretzschmar, 2001; Gondar *et al.*, 2006). These results suggest an interaction between U and Cu with OM in the porewater samples at this site. Copper and U also both had a peak in their soil concentration at the same point, 21 m from the cave, and appear to have similar behaviour at this site.

The interactions between U and OM are assessed further in cores collected from the zone of U accumulation, discussed below (section 3.2) and in OM fractionation experiments (Chapter 4).

The redox chemistry at the bog surface also influences the behaviour of other trace elements. At a distance of ~25-30 m the bog becomes increasingly aerobic. This coincides with the maximum porewater concentrations of Fe and As (figure 3.11), suggesting a link between As and Fe due to the changing redox chemistry. Reduced Fe dissolved in the porewater emerges at the surface of the bog where it oxidises and precipitates causing a high concentration of Fe to be found in the soil (figure 3.1), which has its peak at 35 m from the cave. The maximum solid phase concentration of As occurs at the same point, showing the association of As with Fe oxide minerals, an association which is well known (e.g Arai, 2010).

The combined results of analysis of soil, porewater and organic matter samples reveals zonation across the site from, cave to saltmarsh, summarised in figure (3.18).

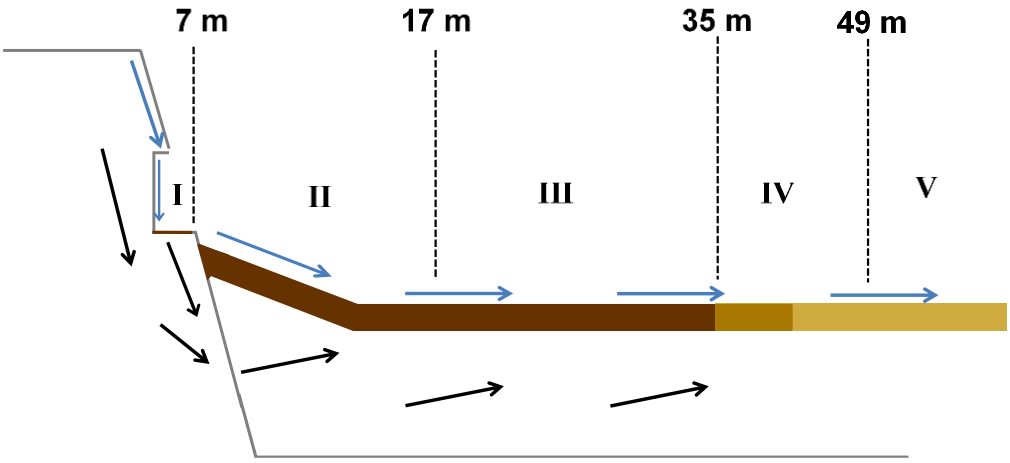

Figure 3.18. Schematic diagram of zonation across the Needle's Eye site (not to scale). The zones identified, I – V, are described in the text below. Blue and black arrows indicate surface and sub-surface water flows respectively, as reported by Hooker, (1991).

I. Within the cave. Soil had relatively low LOI and moisture content, high pH and high Fe, Mn and Ca concentration. The water flowing through fissures in the cave also had a high Ca concentration of ~70 mg L^{-1} and the highest measured U concentration, over 200 µg L^{-1}, while U had a relatively low soil concentration of 43 mg kg^{-1}.

II. 7 – 17 m from cliff. Highly organic area sloping down towards the bog with lowest measured pH. Organic matter had relatively low aromatic content and humic: fulvic acid content. Soil U concentration was found at its lowest concentration while a relatively high U porewater concentration of 113 µg L^{-1} coincided with a peak in the absorbance at 254 nm, as a proxy for DOM concentration.

III. 17 -35 m from cliff. Waterlogged, sparsely vegetated and highly organic bog. The soil in zone III had the highest U concentration of over 500 mg kg^{-1} which coincided with a relatively low soil Fe concentration. Up to 80 % of Fe in

porewater was present as Fe(II), indicating the highly reducing conditions present.

IV. 35 – 49 m from cliff. Transition zone between bog and saltmarsh, characterised by a decrease in LOI and increase of the aromatic and humic acid components of OM. Porewater had high absorbance at 254 nm, Fe and As concentrations.

V. 49 m onwards. Saltmarsh, with increasingly mineral soil and low LOI. Porewater concentrations of Mn, Al, Pb and Th had their maxima in this zone, while U had a low porewater and soil concentration.

The zones identified have particular characteristics that affect the accumulation and mobility of U, as is evident from the large variation in U concentration with distance from the source mineral vein.

3.2. Geochemical depth profiles in the Needles' Eye peat: solid phase and pore waters

The results of analysis of core samples collected from within the U enriched bog are presented. The cores were collected within the region of U accumulation, shown in section 3.1.1, between 20 and 25 m from the cliff. The description of the cores and the dates that they were sampled are shown in table 2.1 in section 2.1.3. The results shown are from the inorganic and organic analysis of solid phase and porewater depth profiles.

3.2.1. Uranium depth profiles in cores from the Needle's Eye bog

The U depth profiles of cores collected on four occasions are presented below (figure 3.19).

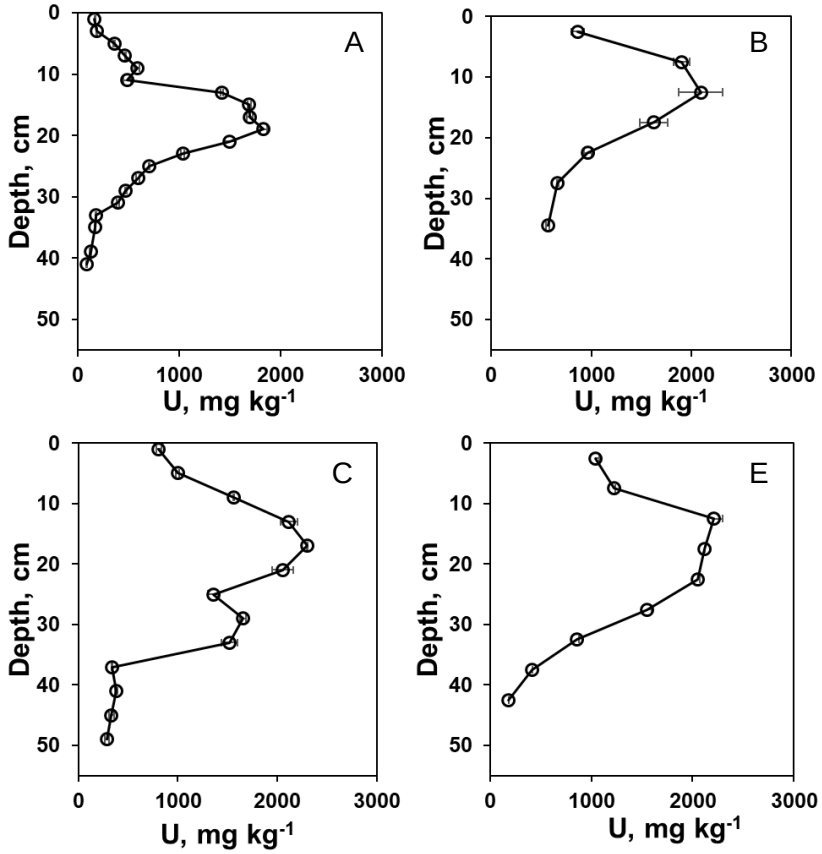

Figure 3.19. Total U concentration (mg kg $^{-1}$) with depth. The results shown are from cores A, B, C and E. The results are the average of duplicate analyses, error bars, which are mostly smaller than the symbols, show standard deviation.

The cores collected show a similar U profile, with a relatively low concentration at the surface increasing to a maximum at a depth of 10 – 20 cm, with some variation between the maxima in each core. Below the peak of U accumulation, the profiles show a decrease with depth, with the exception of bog core C which shows a slight decrease at 25 cm followed by an increase in concentration before a sharp decrease between 32 and 38cm. The maximum concentrations measured are uniformly high on each occasion, ranging from ~1830 – 2300 mg kg^{-1}.

3.2.1.1. Analysis of ^{234}U, ^{238}U, ^{230}Th and ^{232}Th by α spectroscopy

Five samples from bog core A were analysed by α spectroscopy and the $^{234}U/^{238}U$ and $^{230}Th/^{238}U$ activity ratios calculated (Table 3.1).

Table 3.1. $^{234}U/^{238}U$ and $^{230}Th/^{238}U$ activity ratios and ^{232}Th concentration in samples from bog core A

Depth (cm)	$^{234}U/^{238}U$	$^{230}Th/^{238}U$	^{232}Th, mg kg^{-1}
0 – 2	1.022 ± 0.007	0.015 ± 0.0007	0.71 ± 0.073
8 – 10	1.05 ± 0.007	0.009 ± 0.0003	0.67 ± 0.057
8 – 10 (repeated)	0.982 ± 0.036	0.01 ± 0.0008	0.67 ± 0.057
20 – 22	0.968 ± 0.006	0.009 ± 0.0003	1.86 ± 0.111
20 – 22 (repeated)	1.014 ± 0.015	0.008 ± 0.0005	1.86 ± 0.111
28 – 30	1.021 ± 0.005	0.017 ± 0.0004	2.64 ± 0.106
38 – 40	1.021 ± 0.008	0.049 ± 0.0024	4.52 ± 0.362

MacKenzie *et al.*, (1991) showed that the vein mineral at Needle's Eye had a $^{234}U/^{238}U$ activity ratio of unity, as did the ground water flowing from the cliff and samples from the bog. The study concluded that bulk dissolution of minerals in the vein and transport in the groundwater was the main mechanism by which U entered the bog. The $^{234}U/^{238}U$ activity ratios in Table 4.1 are very close to unity throughout the depth profile, in agreement with the findings of MacKenzie *et al.*, (1991), confirming that U arrives in the bog as a result of the rapid bulk dissolution of U bearing minerals in the cliff. If slow leaching processes were occurring in the vein the recoil effect would cause a $^{234}U/^{238}U$ ratio of greater than unity to be seen in the bog samples, as ^{234}U would be preferentially leached from the vein and accumulate. A $^{234}U/^{238}U$ activity ratio of less than unity would suggest a loss of U from the bog. The very low values of the $^{230}Th/^{238}U$ ratio confirms the high mobility of U from the mineralisation vein in contrast to the immobility of ^{230}Th, and shows that the high U concentration in the bog is not due to the distribution of rock material from the cliff on the bog surface, as this would result in a $^{230}Th/^{238}U$ activity ratio of near unity. There is an increase in ^{232}Th with depth from ~0.7 to ~4.5 mg kg^{-1}. This increase in concentration with

depth is related to the increasingly mineral character of the profile (section 3.2.2). The Th in the vein has negligible solubility (MacKenzie *et al.*, 1991) and therefore is found in the bog as fragments of bulk vein mineral material.

3.2.1.2. X-ray absorption spectroscopy: Investigation of U oxidation state and binding environment

In this section, the results of XAS analysis of two samples from core B are presented. The samples were analysed at the Diamond Light Source synchrotron on beamline I18 with the involvement of collaborators within the RATE LoRISE consortium from The University of Edinburgh, Diamond Light Source and The University of Manchester. Samples were selected from the surface (0-5cm) and U enriched region (10-15 cm) of NE core B. The samples were carefully collected, stored and prepared for analysis to ensure no alteration to redox conditions occurred in the samples (section 2.3.1). X-ray Absorption Near Edge Structure (XANES) spectroscopy was used to determine the oxidation state of U in the sample as U(IV) or U(VI), and Extended X-ray Absorption Fine Structure (EXAFS) spectroscopy was used to determine the local binding environment of U. The results are presented below.

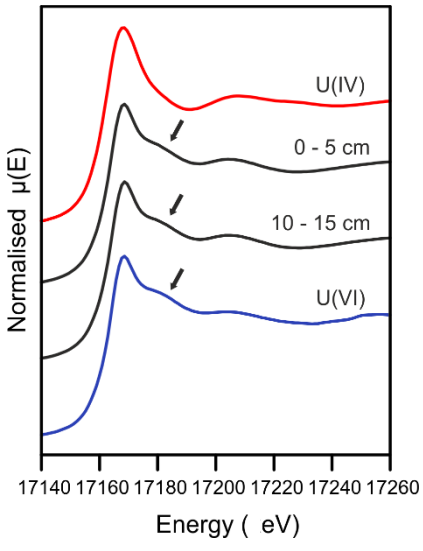

Figure 3.20. Results of XANES analysis showing the two samples analysed (NE core B, 0-5 cm and 10-15 cm) compared with the spectra of a U(IV) and a U(VI) standard (top and bottom lines, respectively).

Figure 3.20 shows the results of XANES analysis of the two samples and a U(IV) and U(VI) standard. The arrows indicate the shoulder, just after the main absorption edge, which arises due to the different arrangement of O atoms around the central U atom in the two oxidation states. Uranium in the U(VI) oxidation state has greater absorption in the region around 17,171 eV than U(IV), allowing the two oxidation states to be distinguished (Kelly, 2010). It is evident that the shoulder is present in both the samples, showing that the main oxidation state of U present is U(VI).

More detailed information about the U binding environment can be derived by examining the results of EXAFS analysis (Figure 3.21).

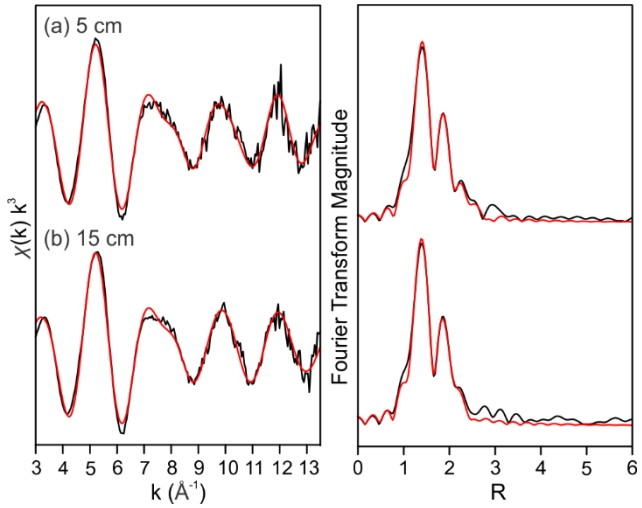

Figure 3.21. Results of EXAFS analysis, showing the two samples analysed (NE core B, 0-5 cm and 10-15 cm) showing the modelled data (red) and the spectral data (black). The Fourier transform of the normalised spectra are shown on the right, and the Fourier transform magnitude on the left.

The Fourier transform of the normalized data are shown on the left-hand side of figure 3.21, while the right-hand side shows the Fourier transform magnitude. In each case the black line shows the EXAFS spectra and the red lines show the fitted models. Peaks in the Fourier transform magnitude spectrum arise from the contributions of coordinating atoms which are at the same distance from the central atom. The large peaks arise from the axial and equatorial atoms of the first coordination shell. The spectra are modelled with different

variables and the fit tested to find the model with best agreement. The parameters for the model shown in the figure are given in table 3.2.

Table 3.2 EXAFS model parameters used to give a good fit with the collected spectra. N = number, R = bond distance in Å, σ2 = disorder in neighbour distance, χ^2= reduced chi squared fit test, R-factor = goodness of fit

Sample	Atom	N	R (Å)	σ^2	χ^2	R-factor
5 cm	O_{ax}	2	1.82 ± 0.01	0.003 ± 0.001		
	O_{eq}	3	2.34 ± 0.02	0.005 ± 0.003		
	O_{eq}	2.5	2.49 ± 0.03	0.005 ± 0.004		
	C	1.5	2.89 ± 0.04	0.004 ± 0.005	204.07	0.012
15 cm	O_{ax}	2	1.79 ± 0.01	0.003 ± 0.001		
	O_{eq}	3	2.33 ± 0.03	0.006 ± 0.004		
	O_{eq}	2.5	2.47 ± 0.03	0.006 ± 0.005		
	C	2	2.90 ± 0.05	0.008 ± 0.007	544.58	0.014

The model parameters shown in table 3.1 gave a good fit to the measured data with R-factor of <0.02. The axial and equatorial bond distances of around 1.78 Å and 2.39 Å, respectively, arise from complexation with carboxyl O (Schmeide *et al.*, 2003). The modelled data show that the U exists as U(VI) organic complexes with C in the second coordination shell. The bond distance of 2.90 Å between U and C arises due to carbonyl C, indicating bidentate complexation of U by carboxylic acid functional groups (Schmeide *et al.*, 2003). Importantly, models including Fe and Mn did not produce such a good fit of the data. The results from analysis by EXAFS are indicative of U complexed by organic bidentate or monodentate ligands.

The results of XANES analysis show definitively, for the first time at this site, that the U is found in the U(VI) oxidation state, despite the highly reducing conditions which are prevalent. This, therefore, shows that the mechanism of immobilisation of U in the bog is not due to the direct reduction of U(VI) to U(IV), despite being shown to be feasible at the

site by Jamet *et al.*, (1993). The results of EXAFS analysis show that U is coordinated with carbon via oxygen, suggesting the importance of oxygen functional groups, such as carboxylic acids, in binding U. This confirms the importance of organic matter in the retardation of U in the bog at the Needle's Eye. The results also suggest that the coordination with OM stabilises U in its oxidised form and protects it from reduction, despite the prevailing reducing conditions in the bog.

3.2.2. Organic content and moisture content profiles of collected cores

Figures 3.22 and 3.23 show the total OM content and moisture content of the cores.

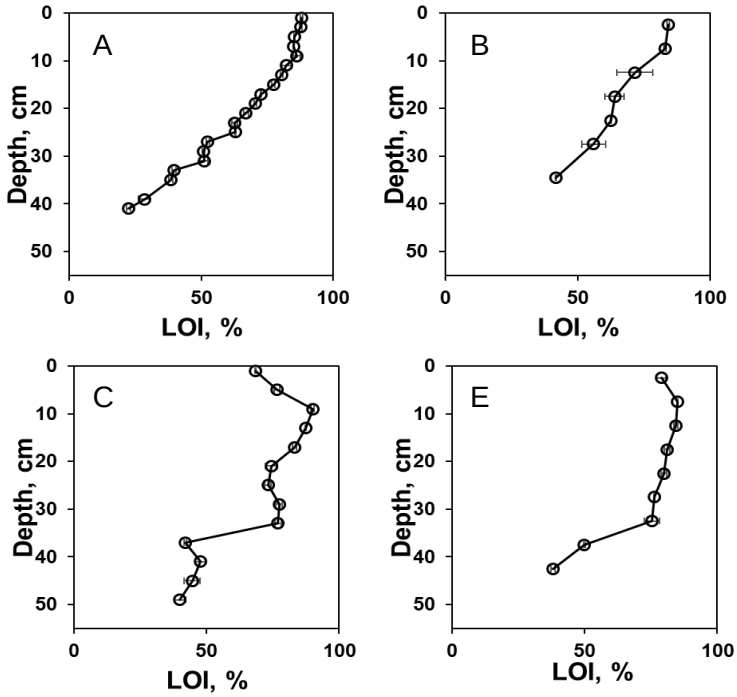

Figure 3.22 Organic matter content by LOI (%) with depth. The results shown are from cores A, B, C and E. The results are the average of duplicate analyses, error bars, which are mostly smaller than the symbols, show standard deviation.

The organic content decreases smoothly with depth in cores A and B from 87 and 84 % to 23 and 45 % respectively. Cores C and E show a slight increase in LOI at the surface and then a sharp decline at around 34 cm.

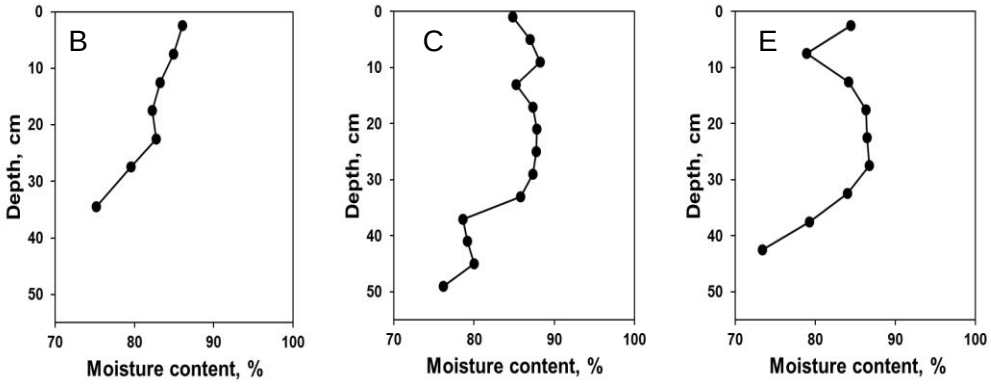

Figure 3.23. Moisture content (w/w %) with depth. The results shown are from cores B, C and E (left to right).

The moisture content is related to the organic matter content, and, for all cores, water accounts for over 80 % of the total weight of the peat from the surface to a depth of around 35 cm. At greater depth, the moisture content decreases as the mineral content increases. As demonstrated in section 3.2.1, the zone of U accumulation is between 10 and 25 cm, in the highly organic, waterlogged region of the depth profile. The importance of the relationship between U and organic matter is further suggested by the positive correlation between the U and OM in cores C and E, which have Spearman's ρ values of 0.88 and 0.80, respectively ($p<0.01$). However, a linear correlation is not seen in cores A or B.

3.2.3. Aluminium in bog core depth profiles

The Al profiles are presented in figure 3.24.

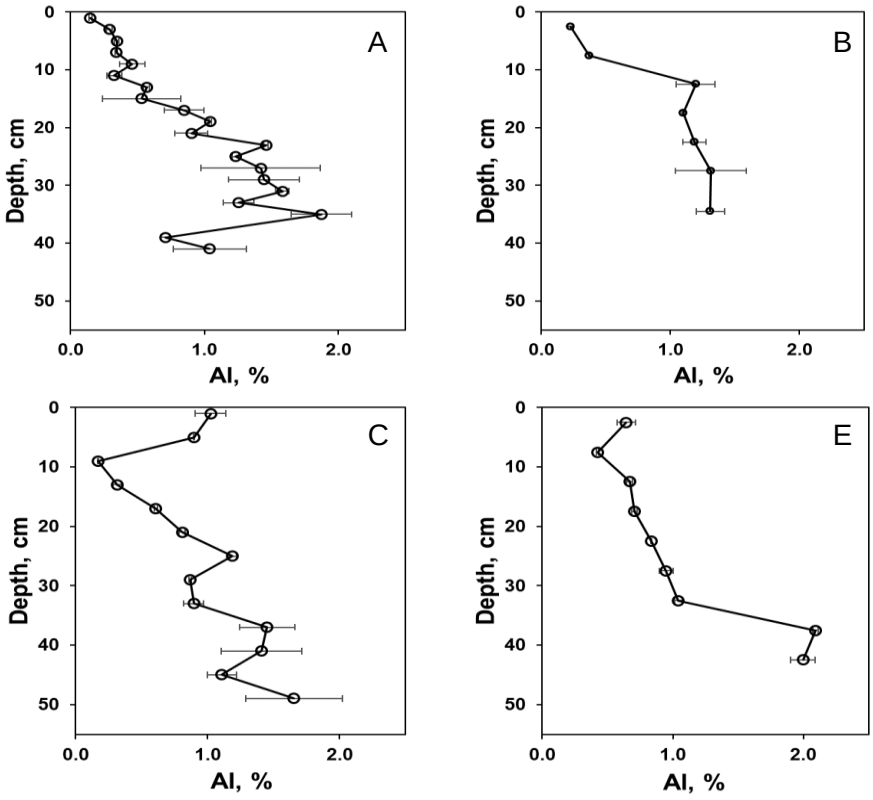

Figure 3.24. Total Al concentration (%) with depth. The results shown are from cores A, B, C and E (left to right). The results are the average of duplicate analyses, with error bars showing the standard deviation.

In all cases there is an increasing trend of Al with depth which is the opposite of the trend in organic matter content. In cores C and E there is a decrease from a slightly elevated concentration at the surface which is not seen in cores A and B. The LOI analysis (figure 3.22) shows that the inorganic component of the profile is up to 75 % of the total soil at depths below 35 cm, so it appears that Al is not a major constituent of the mineral phase. This is confirmed by the analysis of the mineral fraction of core C by XRD (section 3.3), which shows that Al minerals, like clays, are only a minor component throughout the profile.

3.2.4. Iron and Manganese in bog core depth profiles

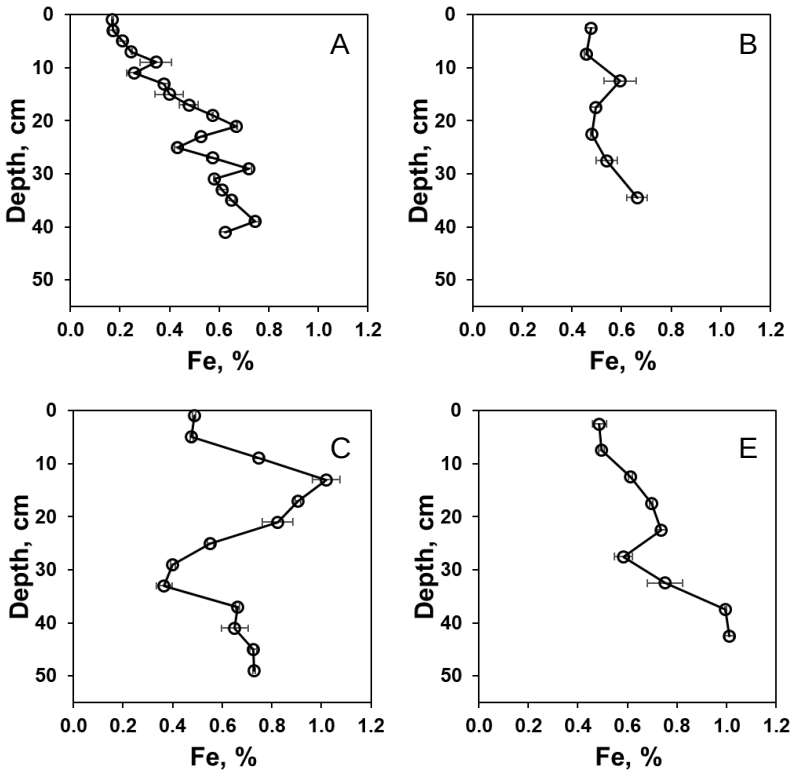

Figure 3.25 Total Fe concentration (%) with depth. The results shown are from cores A, B, C and E (left to right). The results are the average of duplicate analyses, error bars show standard deviation.

The concentration of Fe (Figure 3.25) shows a trend of increasing concentration with depth in three of the four cores analysed. The exception is core C which has a large peak in Fe concentration between 12 and 22 cm, which coincides with the peak of U concentration (figure 3.19). A less significant peak is also seen at a similar depth in core B. The variation in Fe concentration, like Al, is likely to be due to the increasing mineral content of the core with depth. It is also likely that the strongly reducing conditions increase the concentration of Fe sulphide minerals. This has been seen previously at the site (Xu, 2013). The changes in redox conditions with depth are further exemplified in the Mn profiles (Figure 3.26).

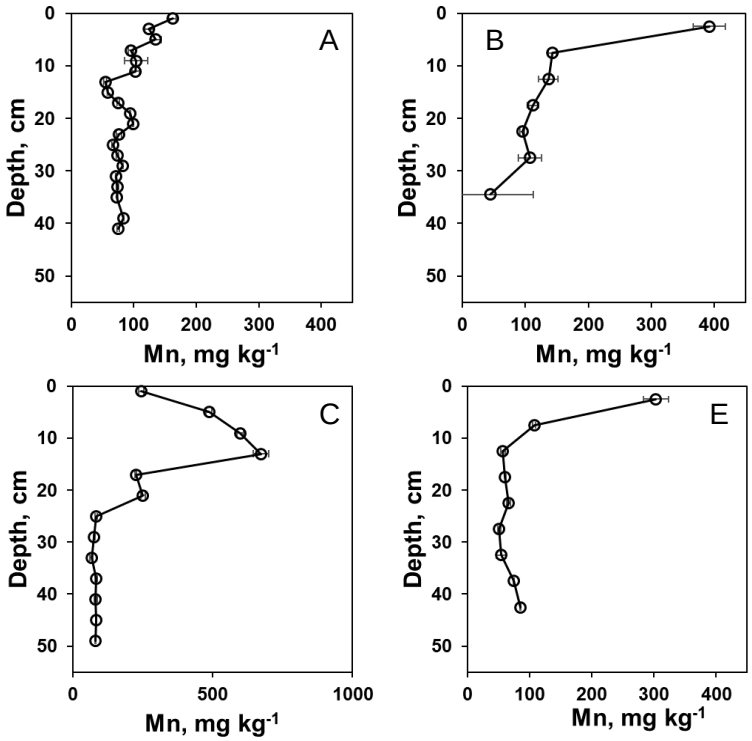

Figure 3.26. Total Mn concentration (mg kg $^{-1}$) with depth. The results shown are from cores A, B, C and E (left to right). The results are the average of duplicate analyses, error bars show standard deviation.
n.b. The x axis scale of core C is twice that of the others.

The highest concentration of Mn is seen in the surface 0 – 5 cm in cores A, B and E, indicative of the shallow aerobic region of the peatbog profile. Manganese accumulates as an insoluble oxyhydroxide in the Mn(VI) or Mn(III) oxidation states at the surface with the

sharp decline indicative of the transition to the soluble Mn(II) oxidation state as the Mn is leached from the soil. The maximum concentration is found at 10 – 12 cm in core C which is indicative of a change of depth of the redox zones on this occasion compared to the others, highlighting the temporal variation in redox active elements like Fe and Mn. The Fe and Mn profiles are suggestive of redox zones with the peak in Mn concentration at 4 – 12 cm abruptly giving way to the Fe peak from 12 – 22 cm as the microbial reduction of Mn occurs before the reduction of Fe(III) (Vepraskas and Lindbo, 2012; Osman, 2013; Vodyanitskii and Shoba, 2015). The redox chemistry of the bog profile is discussed further in section 3.5.3.

3.2.5. Calcium in bog core depth profiles

The features of the Ca profiles are very consistent between the four cores analysed (figure 3.27).

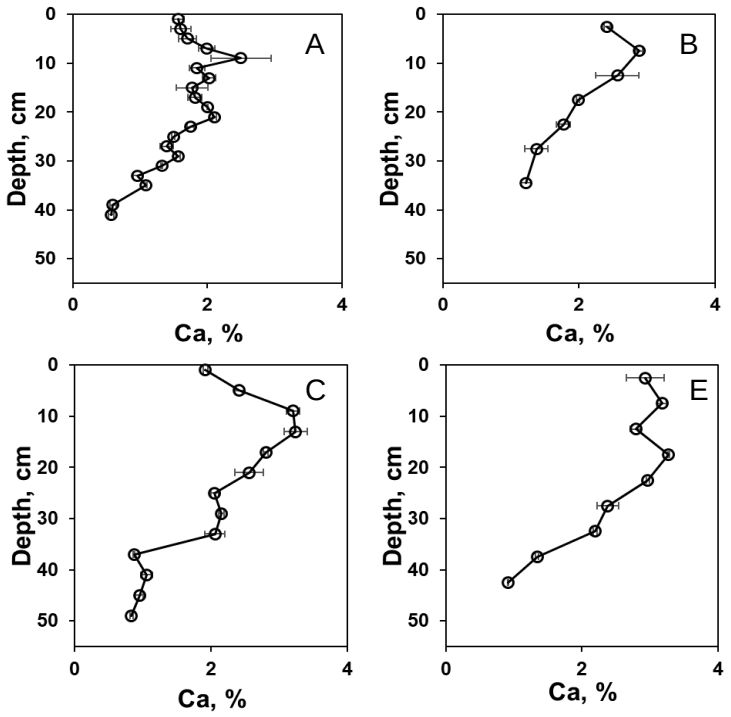

Figure 3.27. Total Ca concentration (%) with depth. The results shown are from cores A, B, C and E (left to right). The results are the average of duplicate analyses, error bars show standard deviation.

In each of the four profiles Ca showed an initial increase with a broad peak at a depth between ~5 and 20 cm. The concentration was consistently above 2% of the total soil in

this zone, and gradually decreased to less than 1% below 35 cm. The Ca, like the U, is considered to originate from calcium-bearing minerals in the cliff which are dissolved and transported into the bog zone of the site (MacKenzie, Scott, *et al.*, 1991a). The Ca concentration in all 4 cores correlated with the U concentration (ρ = 0.71, 0.86, 0.91 and 0.72 for cores A, B, C and E respectively, $p<0.05$). This indicates an association between U and Ca which is likely to be due to the fact that both U and Ca become associated with the soil from the water flowing from the cliff. Calcium, like U, can bind directly to organic matter and competes for binding sites on humic substances (Li, Victor and Chakrabarti, 1980; Hering and Morel, 1988; Ouatmane, Hafidi and Gharous, 1999). The Ca profiles for all cores positively correlated with LOI, which suggests a link between OM and Ca in the soils which could be due to direct binding of Ca to OM. Calcium precipitation as carbonate minerals can also occur where there are high concentrations of Ca in solution and the pH conditions are favourable (Stumm and Morgan, 1970; Levy, 1980). The form of Ca present in bog is discussed in more detail in section 3.3.

3.2.6. Soil pH profiles of bog core samples

The pH of the soil exhibited some similar trends with depth in the four cores (figure 3.28)

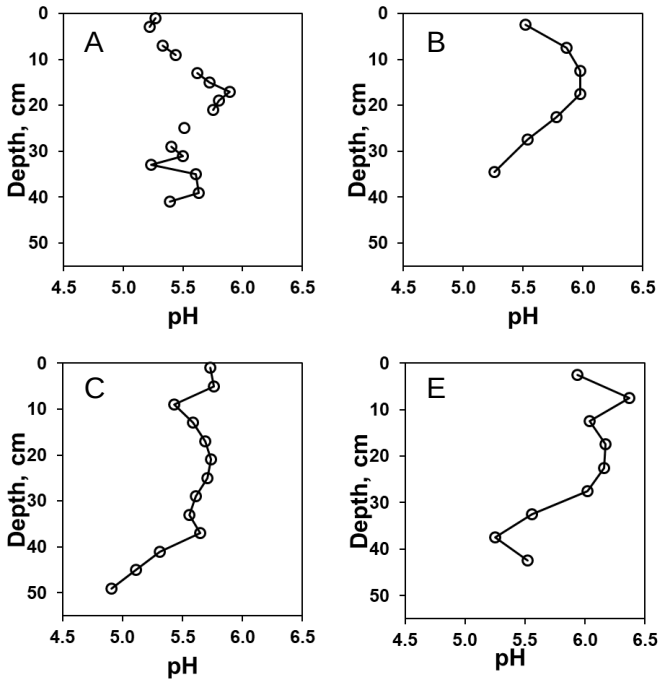

Figure 3.28. Soil pH, measured after a 10 minute shake with deionised water in a 1:5 ratio (soil: water). The results shown are from cores A, B, C and E.

The soil pH was consistently below 6.5 and decreased to less than 5.5 below a depth of ~30 cm. Cores A and B showed an initial increase in pH to a maximum between 10 and 20 cm while there was little variation in cores C and E 0 and 30 cm, except for a localised minimum at ~8 – 15 cm. The pH was consistently nearest neutral in the upper section of the profiles, in the zone of U accumulation. The upper section (0 - ~30 cm) of core E had a pH of ~ 6, the highest seen at the bog surface compared to the other cores. The pH of surface (0 – 5 cm) soil samples collected in a transect on the same sampling trip as core E showed similar pH values adjacent to the area the core was collected (figure 3.1). The pH profile was very similar to the Ca profile shown in figure 3.27, suggesting the presence of Ca carbonates could be causing an increase in pH in the 5 – 20 cm depth zone. The decrease in pH occurs in the zone of decrease in organic content and decrease in U accumulation

and is likely to be related to the decrease in Ca and the highly reducing conditions with depth. The pH profiles of cores A, B and E positively correlate with the U concentration (ρ = 0.66, 0.90 and 0.72 respectively, $p<0.02$). The binding of U to organic matter is related to pH, with U being released form OM at a pH of < 4 (Li, Victor and Chakrabarti, 1980) . Uranium binds onto mineral surfaces in the presence of humic substances in a pH range of 4 – 9 (Lenhart and Honeyman, 1999; Murphy, Lenhart and Honeyman, 1999). The pH between 6 and 7 and the high concentration of organic matter in the upper section of the profile create the optimal conditions for U binding by organic functional groups.

3.2.7. Arsenic, lead and copper

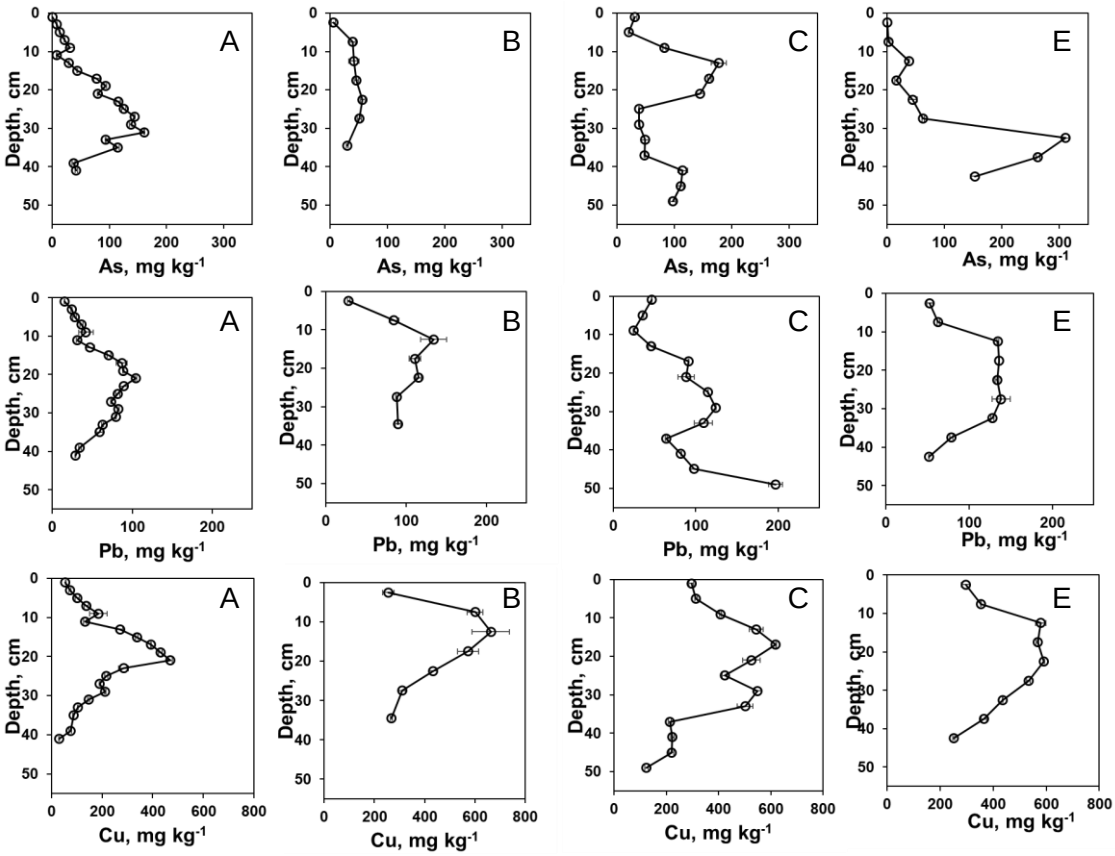

Figure 3.29. Profiles of As, Pb and Cu (mg kg $^{-1}$) with depth in soil cores. The results shown are from cores A, B, C and E (left to right). The results are the average of duplicate analyses, error bars show the standard deviation.

The As (Figure 3.29) profiles showed considerable variation between the cores with A and E showing maximum values at a depth of around 30 cm while core C had two peaks, one at the surface and one at depth.

Core B had a considerably lower concentration than the other three, with a profile which is featureless other than a small increase in the surface 0-5 cm. The differences between the profiles is likely to be due to temporal variations in redox, pH and hydrological conditions at the site on different occasions.

The Pb and Cu profiles are much more consistent than As. Pb has an increase in concentration from the surface to a mid-depth and then a decrease from around 25 – 30 cm. The Pb in core C shows a second increase in concentration below 40 cm. The profiles of Cu are very similar to U, suggesting a similarity in the behaviour of the two elements at this site.

3.3. Analysis of the mineral phase: Particle size analysis and XRD

Analysis of the mineral phase of the soil was undertaken by particle size analysis and XRD. Particle size analysis was carried out to investigate if water flow paths through the bog might be influenced by layers of mineral deposits in the bog acting as a barrier to water flow, while XRD was carried out to identify the mineral phases present and consider their effect on U mobility. Figure 3.30 shows the particle size distribution with depth, with the particle size definitions shown in table 3.3 (FAO, 2006).

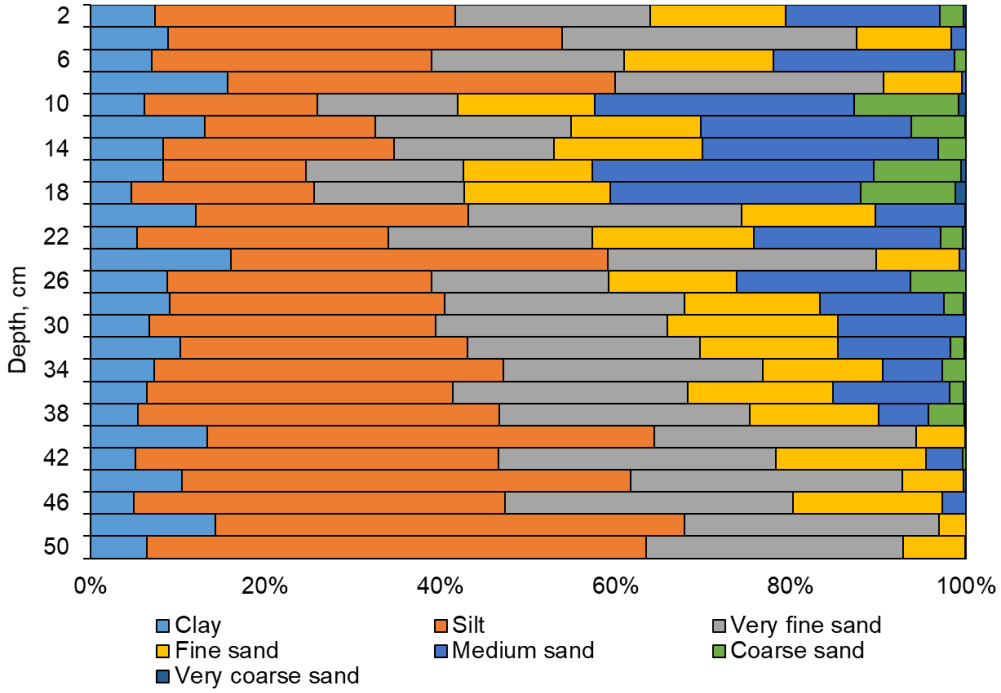

Figure 3.30, particle size analysis of the mineral fraction of depth samples from bog core C

Table 3.3 Particle size analysis size range (FAO, 2006)

Particle size (µm)	Texture
2000	Very coarse sand
1250	Coarse sand
630	Medium sand
200	Fine sand
125	Very fine sand
63	Silt
8	Clay

Initially there was an overall increase in particle size from the surface to a depth of around 10 – 20 cm with the silt size fraction decreasing and the medium sand and coarse sand fractions increasing. Below 20 cm the particle size became smaller with the silt fraction increasing to over 50 % of the total mineral content and the medium and coarse sand fractions decreasing and becoming undetectable by the bottom of the core at 46 – 50 cm. The decrease in particle size followed the decrease of total organic content, with the maximum LOI of 90 % at 8 – 10 cm decreasing to 40 % at 48 – 50 cm (figure 3.22). The

increasing inorganic material with depth was predominantly in the silt size and very fine sand fractions.

The results of XRD analysis (figure 3.31) give further insight into the composition of the mineral phases in the bog.

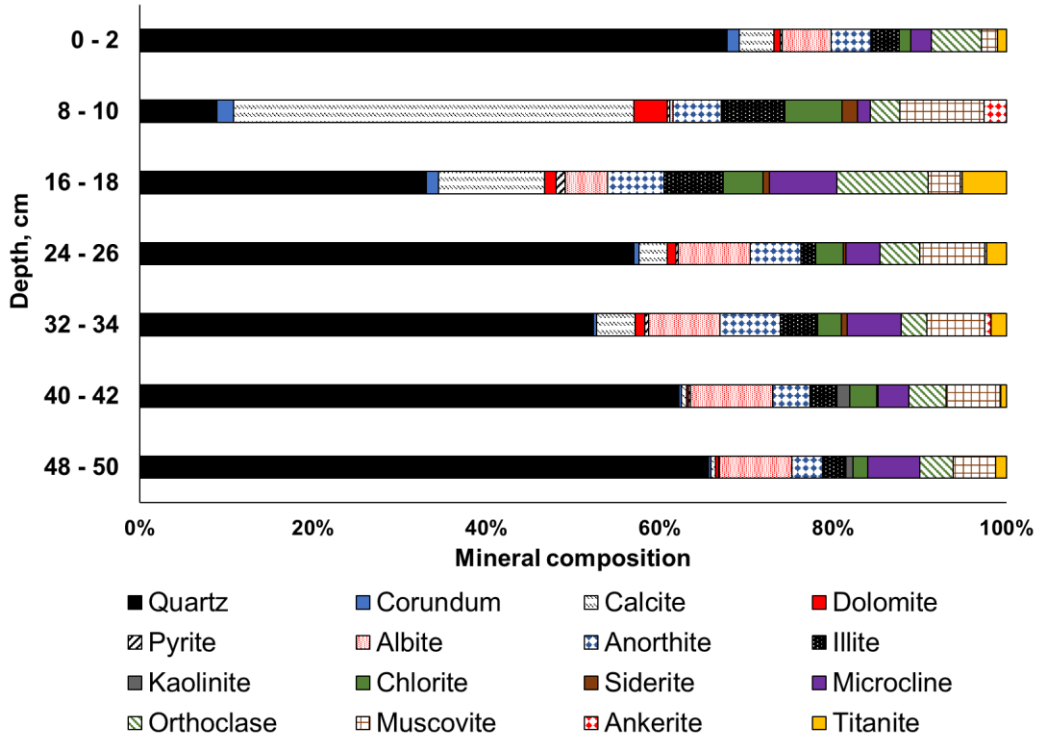

Figure 3.31, results of XRD analysis of the mineral fraction of depth samples from bog core C.

The XRD analysis of bog core C (figure 3.31) showed that the change in particle size distribution is mirrored by the change in mineral composition of the soil inorganic fraction with depth. The small particles seen at the surface and at depths below around 20 cm were dominantly comprised of quartz, with a lesser contribution from feldspar and mica minerals. The peak of larger particle size at 10 – 20 cm was characterised by a large increase in the proportion of calcite present.

The contribution of quartz is relatively low at 8 – 18 cm depth where calcite and clay minerals have their highest abundance throughout the core. Siderite, an Fe carbonate mineral, was also found at its highest concentration at a depth of 8 – 10 cm, highlighting the importance of carbonates at this depth compared to the rest of the core.

Carbonate is likely to have been brought into the bog by the flow of water from the cliff which has very high calcium concentration and pH where the water emerges (MacKenzie, Whitton, *et al.*, 1991)(Section 3.1.1).

The presence of calcite at high concentration coincided with the largest particle size range in the core. However, it is possible that the calcite has been formed from other calcium minerals by the ashing process involved in the sample preparation. The samples were ashed at 450^{O}C for 8 hours prior to analysis and the transformation of aragonite, a common calcium carbonate mineral, to calcite has been reported to occur from 200 ^{O}C (Yoshioka and Kitano, 1985) therefore it is possible that the heating has had some effect on the calcium minerals present. However, the large increase in calcite at this point with the relatively low quartz concentration is still significant as it indicates a major change in the mineral composition between 10 and 20 cm compared to the rest of the core. This was also the zone of highest organic matter concentration so, although the change appears large, it is important to note that the mineral component only accounts for 10 – 25 % of the total composition at this point.

The concentration of pyrite in the samples was ≤ 1.0 %, however, as is the case with calcite, it is possible that pyrite could have decomposed as it has been shown to oxidise in air at temperatures above 400 ^{O}C (Schwab and Philinis, 1947). The lack of oxidation products magnetite and hematite (not detected, < 1.0 % of total mineral content) suggests that the oxidation did not occur. The total Fe concentration of the mineral fraction of the soil is 1.5 – 8.1 %. The fact that pyrite was detectable by XRD (at a concentration of ≤ 1.0) suggests

it is likely to be an important Fe mineral at the site with amorphous minerals like ferrihydrite also likely to be present. A previous study of the site showed by sequential extraction that the majority of Fe was extracted by sodium dithionite, buffered to pH 4.8, which targets Fe oxide minerals goethite, akageneite and hematite (Xu, 2013). However, as in this study, Fe oxide minerals were not identified by XRD.

The particle size and XRD analysis of the ashed samples from core C show evidence of changes in the mineral component of the peat with depth. Two zones of differing characteristics are evident, with the transition occurring between 20 - 30 cm. The increase of silt size particles with depth could be a factor influencing water flow and encouraging a sub-surface flow path above ~30 cm through the highly organic section of the profile. The region of the profile from the surface to 30 cm is where the U enrichment in the solid phase is seen and is a zone of variable redox chemistry (section 3.7.3). This could be indicative of a preferential flow path of water bearing U from the mineralisation into the bog.

3.4. Analysis of OM extracted from soil cores

Organic analysis of total peat samples and humic substances extracted with 0.1 M NaOH was undertaken by UV/Vis, FTIR, ^{1}H NMR and elemental analysis in order to investigate the changes in OM properties and structure with depth in the profile. The results are presented below.

3.4.1.1. FTIR analysis of total peat samples and extracted OM

The FTIR analysis of the dried and ground peat samples from core E (figure 3.32) shows that the spectra are dominated by the prominent peak at around 1035 cm^{-1}.

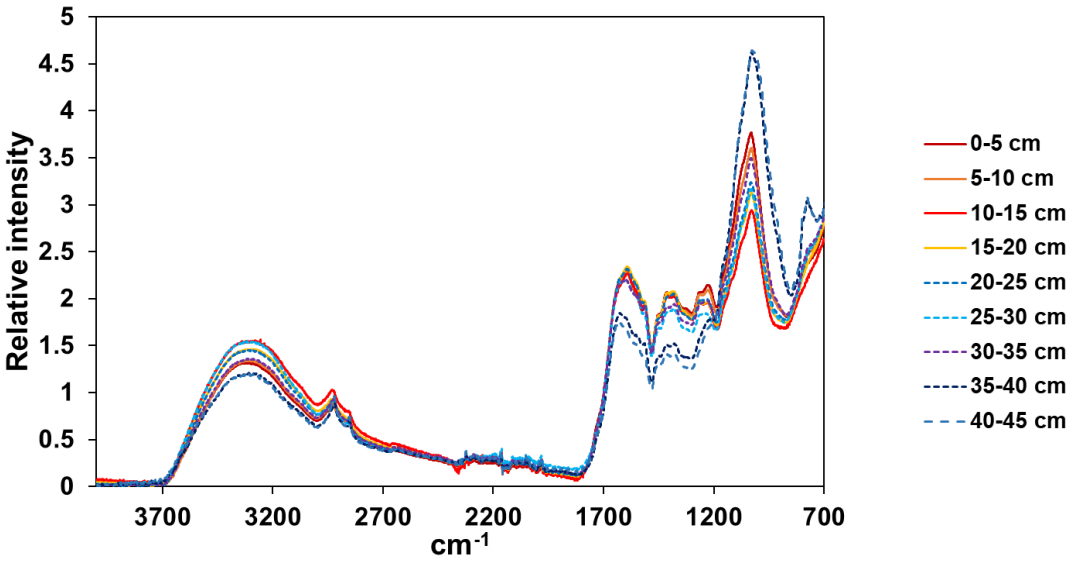

Figure 3.32, results of FTIR analysis of total peat samples from bog core E.

This peak has a much higher intensity in the two deepest samples, 35 – 40 and 40 – 45 cm than all samples from 0 – 40 cm. The dominance of this peak is likely to be indicative of the increasing mineral content with depth in the profile. The two deepest samples also have a peak at around 775 cm^{-1}, which could be indicative of aromatic structures, however minerals are also have absorbance in the region below 900 cm^{-1}, so the peak could be due to inorganic soil components. Oxygen-containing functional groups, such as the

carboxylate peak at 1370 - 1420 cm^{-1}, also show a decrease in relative intensity below 30 cm. The peak at 2925 cm^{-1}, due to the C-H stretch of CH_2 and CH_3 groups, shows little variation between the depth samples. The changes in relative intensity of specific regions with depth are shown more clearly in figure 3.33.

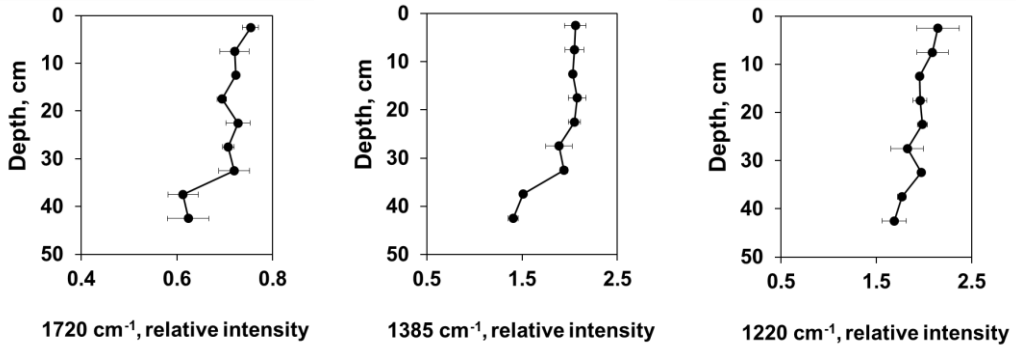

Figure 3.33, Changes in FTIR regions with depth in the analysis of total peat samples from bog core E. The regions arise due to the absorption by carboxylate functionalities.

A main feature of these spectra is that the peaks related to carboxylic functional groups (1720, 1385 and 1220 cm^{-1}) decrease with depth.

Peaks which are associated with aromatic C=C bonds show two different trends (figure 3.34). The peaks at 1514 and 1630 cm^{-1} are featureless to a depth of 35 cm, below which they decrease. This decrease appears to be related to the increase in the peak at 1035 cm^{-1} as the whole region from 1800 – 1200 cm^{-1} is lower in the deepest two samples which also have the relatively high peaks at 1035 cm^{-1}. There are also many overlapping peaks in this region, so it is likely that oxygen containing functional groups are influencing the peaks

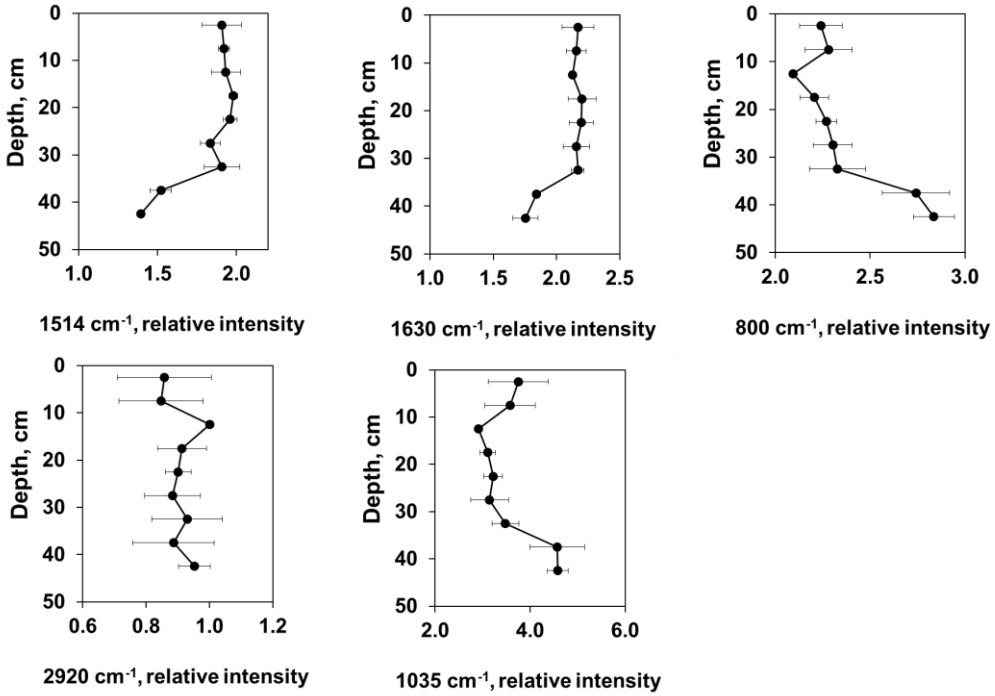

Figure 3.34, Changes in FTIR regions with depth in the analysis of total peat samples from bog core E. The regions arise due to the absorption by aromatic C=C (1514 and 800 cm^{-1}), aromatic C=C and aliphatic carbonyl (1630 cm^{-1}), methyl (2920 cm^{-1}) and carbohydrate (1035 cm^{-1}) structures.

assigned as C=C, for example, carbonyl C=O bonds are known to absorb at around 1630 cm^{-1} as well as aromatic C=C. The region at 800 cm^{-1} (figure 3.34), due to aromatic skeletal vibrations, shows an overall increase with depth, however this region is also influenced by soil minerals, so it is not possible to conclusively assign the increase in intensity to aromatic structures alone.

The peak at 2920 cm^{-1} (figure 3.34), due to C-H stretch of methyl groups, shows no trend with depth and has relatively high variation between the three replicates.

The peak at 1035 cm^{-1} (figure 3.34) has a small initial between 0 and 10 cm before increasing from 10 – 45 cm, with the sharpest increase occurring in the deepest section of the core between 35 and 45 cm.

The main conclusion to be drawn from the analysis of the total peat sample by FTIR is the overall relative decrease in oxygen containing functional groups with depth, and particularly COOH.

The spectra from the FTIR analysis of extracted organic matter samples are not dominated by the large peak at 1035 cm^{-1}, as the spectra of the total peat samples are, and clear trends with depth can be seen in several peaks in different regions of the spectra.

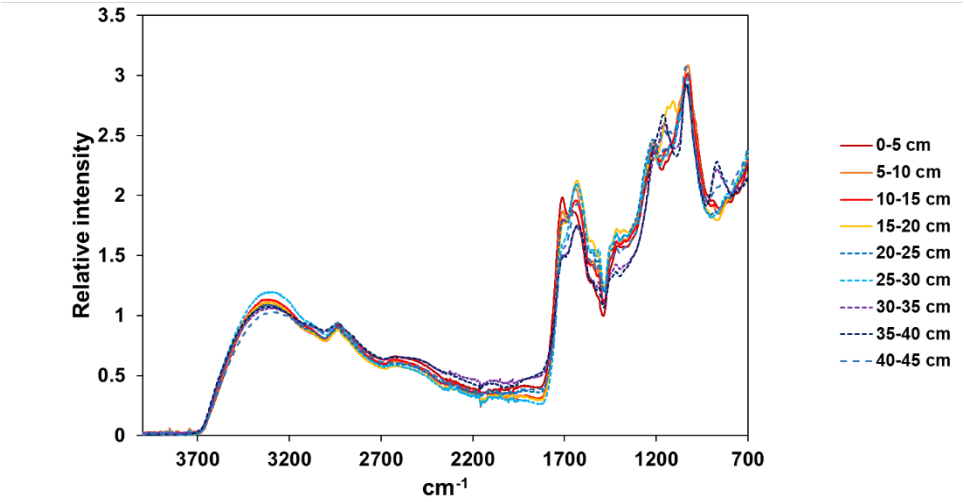

Figure 3.35, FTIR spectra of extracted OM from bog core E with depth.

The FTIR spectra of extracted organic (figure 3.35) matter show that the peak at 1035 cm^{-1} is very consistent between all samples with depth, and has a lower relative intensity than the results of the analysis of peat samples. This suggests that this peak is influenced by the increasing mineral character of the soil with depth in the total peat spectra.

The peak at around 1720 cm^{-1} corresponds to C=O of carboxylic acids and decreases linearly with depth (R^2 = 0.90), as can be seen in figure 3.36.

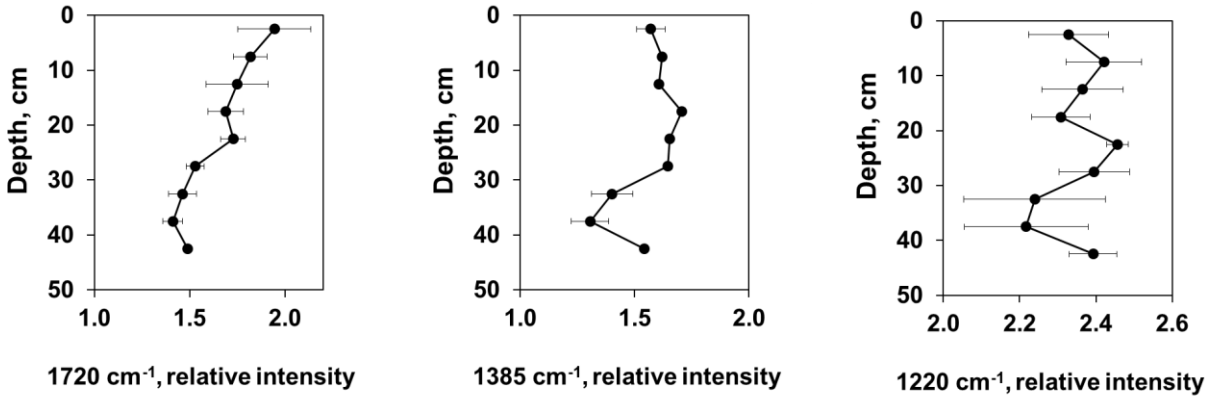

Figure 3.36, Depth profiles of carboxylate bands from FTIR analysis of extracted OM from bog core E.

The peak at 1385 cm^{-1} increases to a maximum at 15 – 20 cm before decreasing to 35 – 40 cm and increasing again to the final point at 40 – 45 cm. The region at 1220 cm^{-1} has no trend with depth and shows considerable variation between the replicates, as can be seen by the large error bars (representing standard deviation).

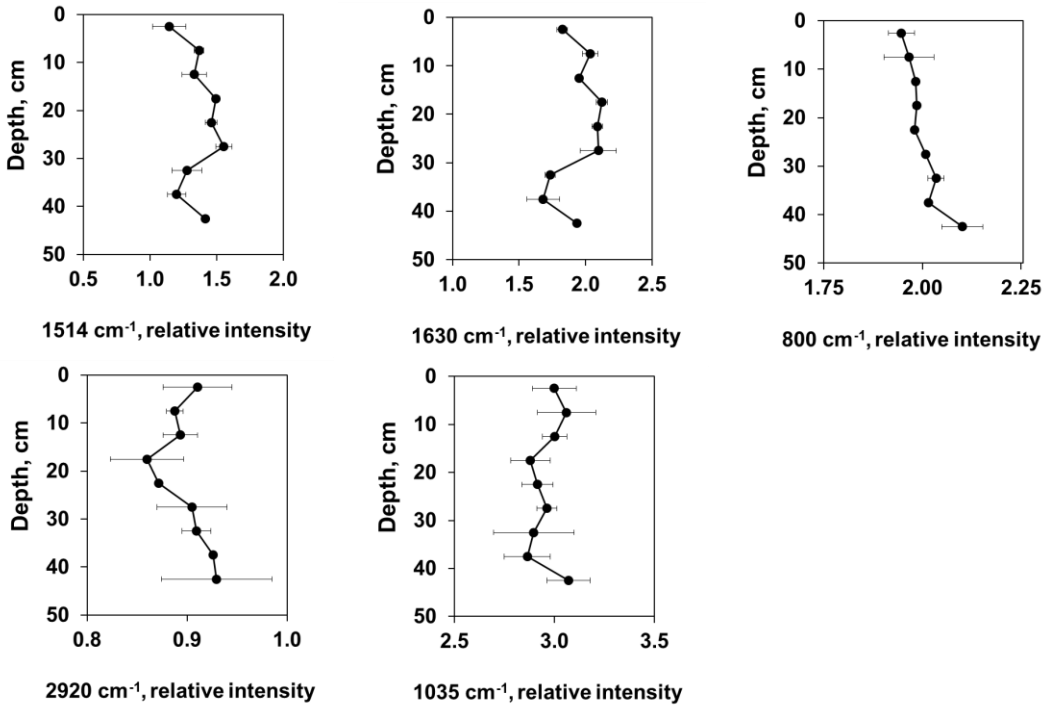

Figure 3.37, Changes in FTIR regions with depth in the analysis of extracted OM samples from bog core E. The regions arise due to the absorption by aromatic C=C (1514 and 800 cm^{-1}), aromatic C=C and aliphatic carbonyl (1630 cm^{-1}), methyl (2920 cm^{-1}) and carbohydrate (1035 cm^{-1}) structures.

The profiles of the peaks which arise due to aromatic C=C bonds (Figure 3.37) are similar to those seen in the analysis of the total peat samples, with 1514 and 1630 cm^{-1} being similar to each other, with an initial increase, a decrease from 30-40 cm and an increase in relative intensity in the final sample. The peak at 800 cm^{-1}, on the other hand, shows a steady increase with depth (R^2 = 0.80). The sharp peak at around 800 cm^{-1} seen in the FTIR analysis of the total peat sample (Figure 3.32) which appears in the deepest three samples is also seen in the spectra of extracted organic matter, suggesting that this has an organic rather than inorganic origin.

The intensity of the peak at 2920 cm^{-1} (C-H stretch of methyl groups) decreases to a depth of 20 cm and then increases again to the final sample at 40 – 45 cm. The strong peak at 1035 cm^{-1} (carbohydrate C-O) shows little variation with depth in the extracted organic matter samples.

Overall, the clearest trend from FTIR analysis is the decrease in carboxyl functional groups with depth, evident in the NaOH extracted NOM. This trend has been seen in other studies (e.g. Tfaily *et al.*, 2014) and can be understood in the context of microbially driven decomposition of organic matter over time, as deoxygenation of the organic matter occurs (Stevenson, 1982).

3.4.1.2. UV/Vis analysis of soil organic matter

The UV/Vis analysis of extracted organic matter from cores B, D and E shows some consistent trends between samples collected on different occasions.

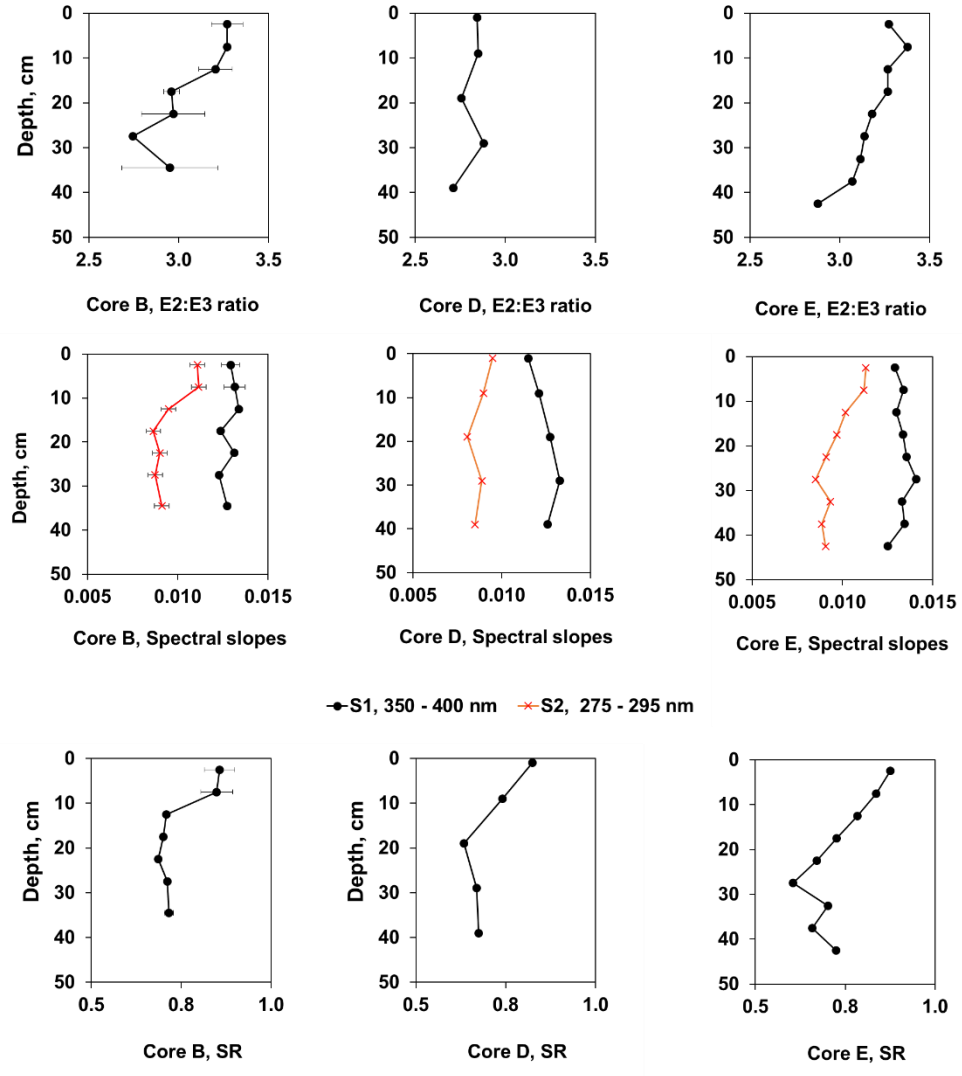

Figure 3.38, Profiles of UV/Vis analysis parameters of OM extracted from bog cores B, D and E.

The E2:E3 ratio (Figure 3.38) shows a clear decrease in cores B and E, but is relatively featureless in core D. As mentioned in section 3.1.2, the E2:E3 ratio is inversely related to the size of humic molecules and has also been shown to be inversely proportional to aromaticity of organic matter (Minor *et al.*, 2014). The decrease in the ratio is therefore consistent with an increase in molecular size and aromaticity with depth.

The spectral slope S1 shows an increase with depth in cores D and E to around 30 cm, below which a slight decrease is seen. The profile of core B is rather featureless in comparison.

The spectral slope $S_{275-295}$ has a decreasing trend with depth to a point at around 20 cm in cores B and D and 30 cm in core E where the value shows little variation for the remaining depth of the core. The slope ratio, SR, is strongly correlated to $S_{275-295}$, with R^2 values of 0.93, 0.83 and 0.94 for cores B, D and E respectively. There is no correlation between S1 and the SR for cores B and E, and in core D there is a negative correlation ($R^2 = 0.78$). This shows that $S_{275-295}$ is the dominant contributor to the SR parameter in the extracted organic matter. The SR appears to be a robust method of analysis of the raw UV/Vis spectra data as the results for the three cores show the same trend of an initial decrease from a value of around 0.8 – 0.9 to a value of around 0.6 – 0.75 at 10 – 30 cm which remains stable for the remainder of the core, below a depth of 30 cm.

The overall decrease in $S_{275-295}$ and SR is, like the E2:E3 ratio, indicative of an increase in molecular weight, humification and aromaticity with depth. This is confirmed by the results of analysis of the humic:fulvic acid ratio, in figure 3.39.

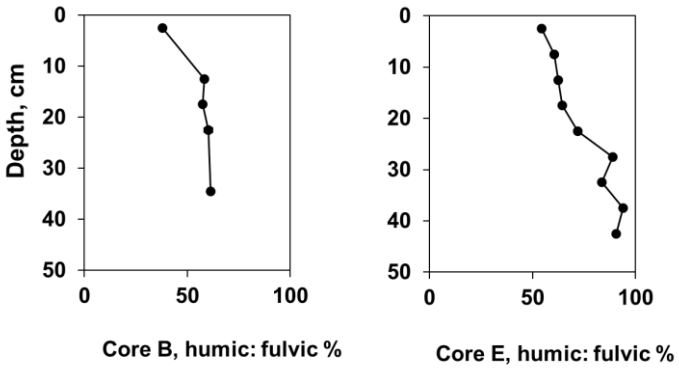

Figure 3.39, Humic:fulvic acid ratios of extracted OM in depth samples from bog cores B and E.

The ratio of humic to fulvic acids in the extracted organic matter of cores B and E show that there is an increase of humic acids with depth. This is most pronounced in core E, which shows an increase from 54 % at the surface to 93 % humic acid at a depth of 40 cm.

3.4.1.3. ^{1}H NMR analysis of extracted soil organic matter from depth samples

The analysis of extracted organic matter from cores B, D and E by liquid state ^{1}H NMR makes it possible to identify the relative abundance of major components of the samples.

Cores D and E show an increase of aromatic character with depth, while core B shows an initial increase and a slight decrease to the final sample (figure 3.40). This is a good indication of humification processes occurring with the ageing of organic matter (Zech, Haumaier and Kogel-Knaber, 1989).

The carbohydrate region of the spectra show variation between the cores with the relative abundance of carbohydrate ^{1}H remaining relatively high in core B, between 45 and 50 %, while cores D and E show a slight decrease from around 45 % to around 35 – 40 %. The decrease seen in the latter two cores with depth could also be an indication of humification processes as carbohydrates are degraded through use as the substrate for microbial respiration.

Cores B and D show a decrease in functionalised aliphatic ^{1}H with depth while the profile of core E is relatively featureless with depth. The decrease seen in cores B and D is again likely to be due to the degradation of labile, oxygen rich organic matter with depth as it is used as a substrate for microbial degradation.

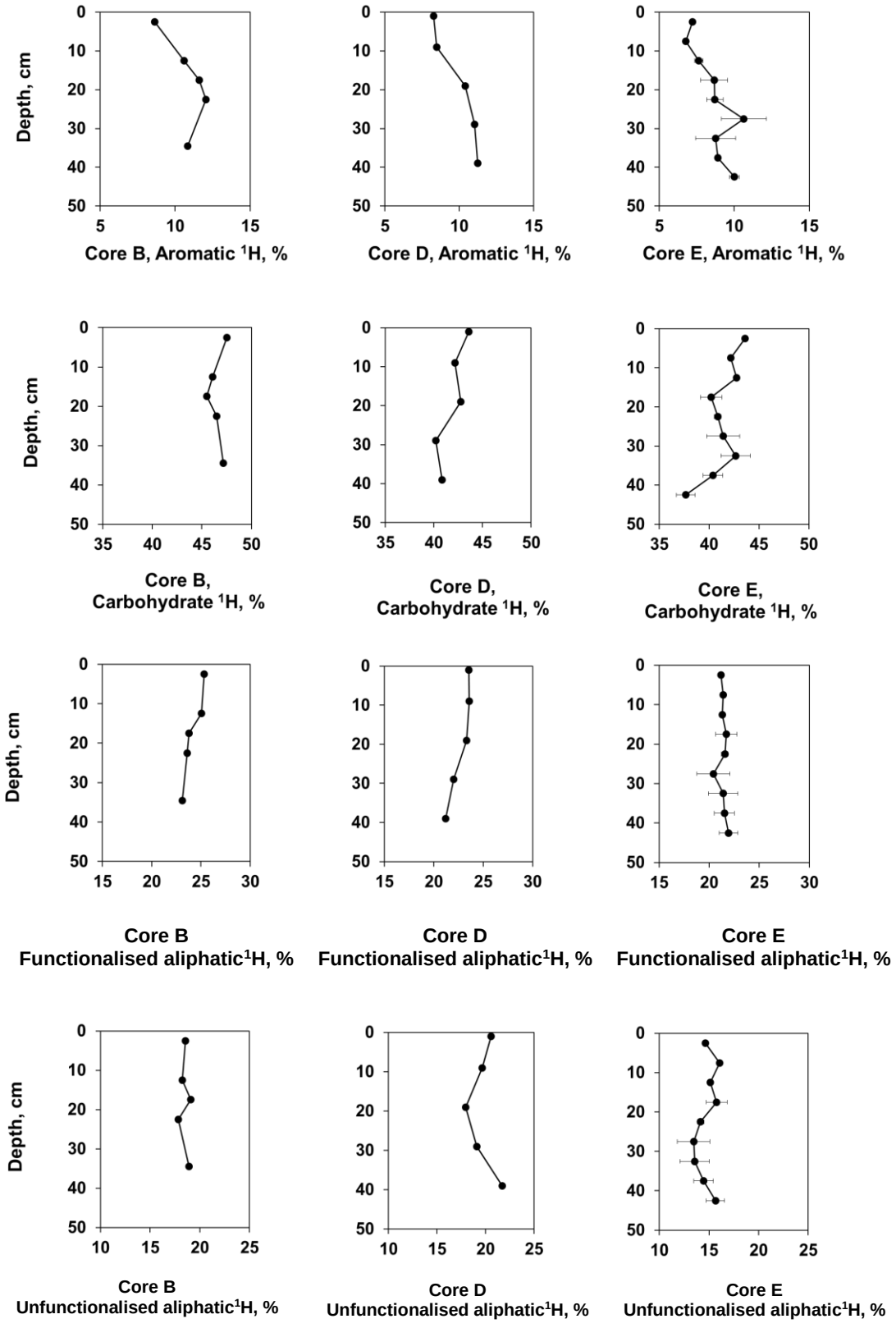

Figure 3.40, Depth profiles of the components identified by ^{1}H NMR analysis in extracted OM samples from cores B, D and E

Finally, the variation in unfunctionalized aliphatic ^{1}H with depth has a similar trend in cores B and D with an initial decrease to a depth of around 20 cm and around 30 cm respectively, below which an increase is seen to the final samples of the cores. On the other hand, the profile of core B is relatively featureless, with little variation with depth.

The clearest trend in the analysis by ^{1}H NMR is the increase of aromaticity with depth, with the decrease of functionalised organic matter also evident. These results are in agreement with the results of analysis of organic matter from Core E by FTIR which also showed an overall decrease of oxygen containing organic matter and increase of aromaticity with depth. These changes can be explained by the microbially driven humification of organic matter as it is degraded over time and becomes less reactive and more stable (Zech, Haumaier and Kogel-Knaber, 1989). This is confirmed by the analysis of the humic acid:fulvic acid ratio which shows the organic matter has increasing humic acid character with depth. More information on the changes with depth, derived from the analysis of fulvic and humic acid fractions, is shown in section 4.4. The results of UV/Vis analysis also follow the same trend, with the E2:E3 ratio and SR indicating an increase in molecular size and aromaticity with depth.

3.4.1.4. C, H, N, O and S elemental analysis of peat and extracted OM

The results of C, H, N, S analysis of bog core B total peat and extracted organic matter are shown below. The percentage composition of the extracted NOM and the total peat are shown in figure 3.41. The results are presented as percent by weight on a dry, ash-free basis. C, H and N were directly measured while O was calculated by adding the percentage of C, H, N, S and, in the case of the peat, ash and subtracting from 100.

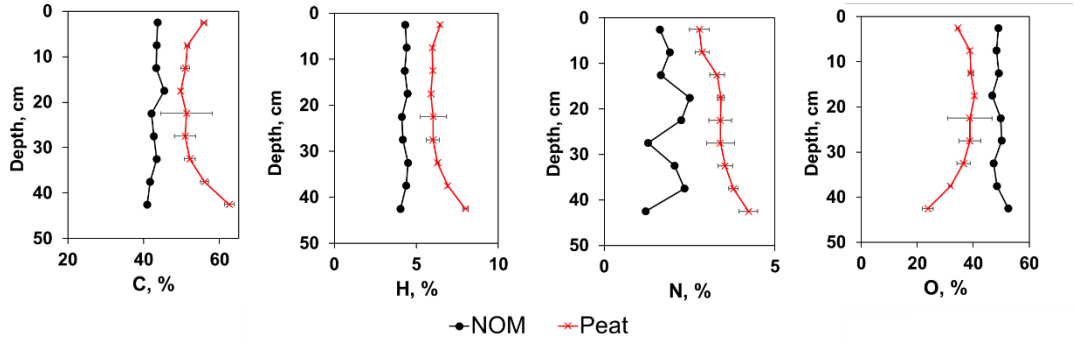

Figure 3.41, C, H, N and O composition with depth in the total peat sample and extracted organic matter from bog core E

The total peat samples have higher C, H and N concentrations than the extracted NOM but lower oxygen content. The oxygen concentration of the total peat samples decreases below 30 cm by around 15 %. There is an increase of N in the peat samples from around 2 to 4 % with increasing depth. In the extracted NOM, the N profile is more variable but with no distinct trend. The percentage of these elements is within the range that would be expected of similar samples (Rice and MacCarthy, 1991; Fujitake *et al.*, 1999).

The profiles of element ratios (figure 3.42) can be used to determine changes in the characteristics of samples with depth.

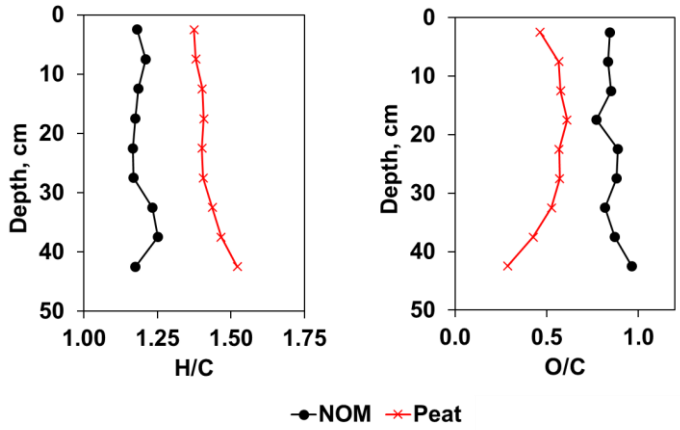

Figure 3.42, Elemental ratios H/C and O/C for the total peat samples and extracted organic matter from bog core E.

The H/C ratio can be used as an estimate of aromaticity, with a low H/C of <1 indicative of higher levels of condensation and aromaticity. Figure 3.42 shows that the total peat has a higher H/C ratio than the extracted NOM, with a slight increase with depth. This suggests the peat contains a fraction of aliphatic organic matter which is resistant to extraction by 0.1 M NaOH.

The O/C ratio of the peat sample is typical of that seen in the analysis of humic substances and peats (Rice and MacCarthy, 1991; Fujitake *et al.*, 1999; Zaccone *et al.*, 2017) and is indicative of a fraction of non-extractable humin material on the peat which has a low oxygen content. The U depth profile from the same samples strongly correlates with the O/C ratio of the total peat, ($\rho = 0.95$, $p<0.001$). This is in agreement with the results of XAS analysis of U binding in the peat which showed that U was directly bound to the oxygen functional groups of OM (section 3.2.1.2). The O/C ratio of the NOM shows little variation with depth and is nearly double that of the peat and higher than would be expected for such a sample (Rice and MacCarthy, 1991). This is likely to be because the ash content

of the extracted OM was not measured, which would lead to an overestimate of O in the extracted OM.

The profile of S in peat and NOM is shown in figure 3.43. The % S is given on the basis of total sample (rather than ashless basis) because S is often a significant component of inorganic minerals.

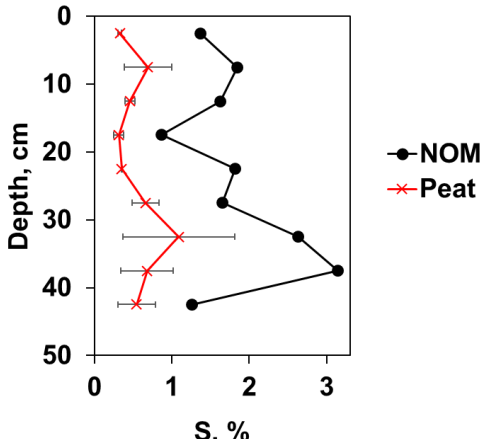

Figure 3.43, Concentration of S in total peat samples and extracted organic matter from bog core E.

Both profiles show two peaks of S with depth. The concentration of S in the extracted NOM is around three times higher than the concentration in the peat, suggesting the S present is readily extracted by 0.1 M NaOH. The profile of the total peat samples shows a decrease in S concentration between 10 and 30 cm. This is the region of U accumulation (figure 3.19) and is also the region of variable redox conditions, as shown by the Fe speciation in porewaters (section 3.7.3). The decrease of S between 10 and 30 cm is therefore possibly due to the more aerobic conditions which occur at that depth in the profile. The profile of S in NOM shows a similar trend to the analysis of the peat samples, but with a more erratic profile shape. Unfortunately, due to lack of material, it was not possible to analyse replicates of the extracted NOM material.

3.5. ^{14}C analysis of Needle's Eye peat

The ^{14}C concentration was measured in dried and ground peat samples from core B in order to estimate the age of the peat with depth. Figure (3.43) shows the ^{14}C "age" of the samples in years BP (years before 1950). The samples from the surface to a depth of 20 cm have a negative "age," with a prominent spike at 5 – 10 cm. Zero is indicated in the figure by the dotted red line. The negative spike is likely to be due to the large input of ^{14}C from the atmospheric testing of nuclear weapons which had its peak in the mid 1960's. Radiocarbon from the weapons tests became incorporated in biota and accumulated in soils and sediments (e.g. Goodsite *et al.*, 2001).

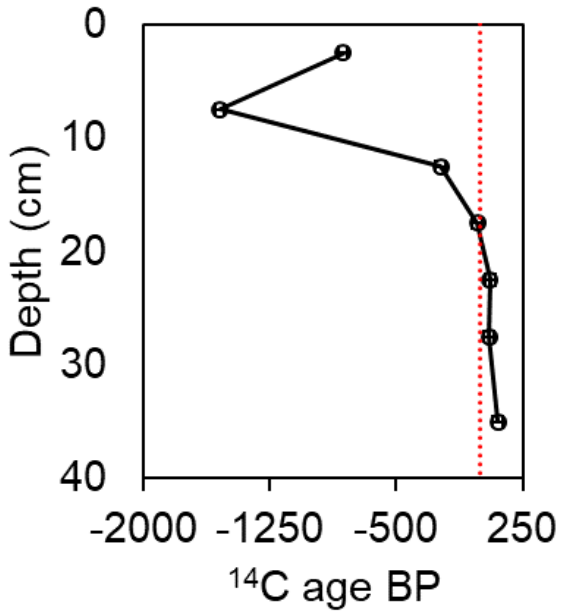

Figure 3.43. ^{14}C "age" of samples from the Needle's Eye bog core B, showing the incorporation of "Bomb pulse" radiocarbon at a depth of 5 – 10 to cm. "BP" stands for before present, defined as the year 1950. The red dotted line highlights zero years BP.

^{14}C from the bomb peak overwhelms the natural background ^{14}C in samples formed from material which was alive since the 1950s and therefore complicates the calculation of the age of recent materials. However, thanks to the detailed records of global atmospheric ^{14}C concentrations before and since the 1950s the spike has proved to be useful age marker of ^{14}C incorporated into material. "Bomb pulse dating" has been used in geological, biological and forensic studies to accurately date samples originating since 1950 by calibration with the historical atmospheric or marine ^{14}C record (Zoppi *et al.*, 2004; Hodge *et al.*, 2011; Falso and Buchholz, 2013). The bomb pulse ^{14}C peak has been seen in peats and used to accurately date peat profiles (Jungner *et al.*, 1995; Goodsite *et al.*, 2001; Goslar *et al.*, 2005; Piotrowska *et al.*, 2011).

In this study, the online open-access ^{14}C bomb pulse calibration software OxCal (Version 4.3, available at https://c14.arch.ox.ac.uk/oxcal.html) (Ramsey, 1994, 2009) has been used to calibrate measured ^{14}C concentrations in the peat cores using the IntCal13 atmospheric ^{14}C historical record for the northern hemisphere (Hua, Barbetti and Rakowski, 2013). A deposition model was used (Ramsey, 2008) to generate the peat core chronology with depth shown in figure 3.42.

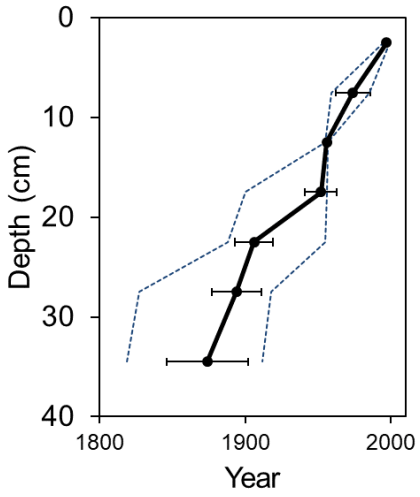

Figure 3.42, Peat core chronology calculated based on the incorporation of "bomb pulse" ^{14}C. Dates calculated using OxCal software (Ramsey, 1994, 2009). The error bars show 1 σ and the blue dotted lines show the 95 % confidence interval.

The ^{14}C chronology profile shows the aging of the peat with depth with the deepest sample of 30 – 39 cm dating from around 1874 ± 28. The black line is the mean of the modelled age range, with the error bars as 1 standard deviation and the blue dashed lines as the 95 % confidence interval. Based on this chronology the accumulation rate of the peat is calculated as 0.28 ± 0.09 cm $year^{-1}$. This rate compares favourably with the rate of accumulation of four Scottish bogs which had an average accumulation rate of 0.22 ± 0.1 cm $year^{-1}$ (Cloy *et al.*, 2009).

3.6. ^{210}Pb and ^{226}Ra in the Needle's Eye bog

Lead-210 dating is often used to calculate the accumulation rate and approximate age profile of peatbogs. It is a useful technique for generating chronologies of around 100 – 200 years, but can be subject to many site-specific sources of variation (Le Roux and Marshall, 2011). The technique relies on measuring the difference between supported ^{210}Pb, that which is in equilibrium with its parent nuclide ^{226}Ra in the peat, and unsupported ^{210}Pb which is deposited on the surface of the peat from the decay of atmospheric ^{222}Rn. The moderate radioactive half-life of ^{210}Pb of 22.2 years allows the calculation of the peat accumulation rate as the concentration of unsupported ^{210}Pb decreases with depth as it decays.

In this study, the results of analysis of core B by gamma spectroscopy have been used to calculate the concentration of supported and unsupported ^{210}Pb.

The concentration of ^{226}Ra is indirectly measured by calculating the average activity of ^{214}Pb at measured by gamma spectrometry at 295 and 352 keV and ^{214}Bi measured at 609 keV. The activities of ^{226}Ra and total and unsupported ^{210}Pb are shown in figure 3.43.

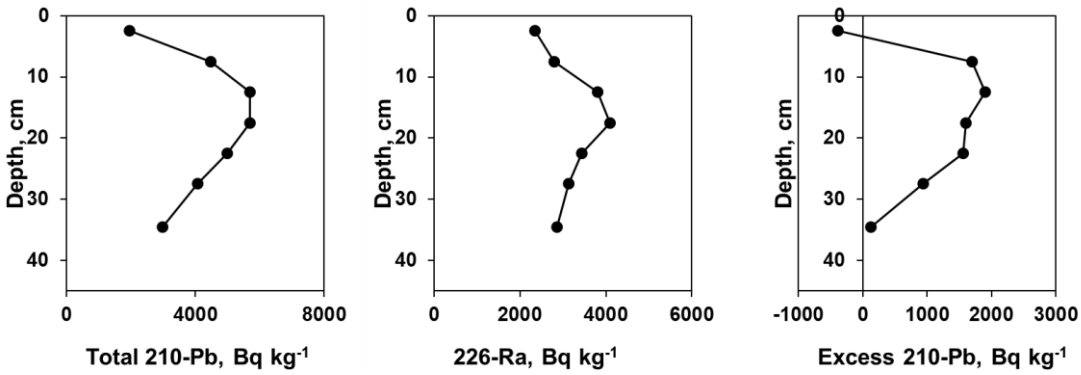

Figure 3.43, ^{210}Pb, ^{226}Ra and excess ^{210}Pb in the profile of Needle's Eye core B.

The total ^{210}Pb is closely related to the total lead concentration (figure 3.29) with $R^2 = 0.81$. The ^{226}Ra profile has a peak at 15 – 20 cm, just below the maximum U concentration in this core (Figure 3.19). The unsupported ^{210}Pb does not have a profile which can be used to calculate peat accumulation as the 0 – 5 cm sample is depleted in ^{210}Pb when compared to the equilibrium activity with its parent nuclide. ^{210}Pb dating relies on assumptions that the peat accumulates at a constant rate, the unsupported ^{210}Pb accumulates at the surface and decreases with depth as it is incorporated in the peat and decays, and the ^{210}Pb is largely unaffected by geochemical processes in the peat. The low concentration of unsupported ^{210}Pb at the surface is indicative of rapid removal of ^{210}Pb from the surface layers of the bog. The unsupported ^{210}Pb is correlated with the total soil Pb concentration with an R^2 value of 0.69. These results indicate that there may be geochemical processes controlling the mobility of Pb within the peat bog which are affecting the unsupported ^{210}Pb and therefore the stable accumulation required for calculation of a chronology is not present. Given the highly dynamic nature of the site, with high and variable water flow, large variations in redox conditions (section 3.1.3) and varying geochemical conditions with depth, it is not surprising that the unsupported ^{210}Pb does not show a profile consistent with constant accumulation.

3.7. Depth profiles of metals in pore waters in the Needle's Eye Bog

The profiles of total metal concentration in the soil porewaters and in ultrafiltration fractions of the porewaters are presented. The porewaters from cores A, B and C were extracted by centrifugation in the lab within 5 hours of sample collection, while the porewaters from cores D and E were extracted within 30 minutes of core sampling and stored under vacuum in evacuated tubes for transportation back to the lab. The ultrafiltration of porewaters from core B was carried out around 20 hours after sample collection, while the ultrafiltration of porewaters from cores D and E was carried out within 5 hours of sample collection.

3.7.1. Uranium depth profiles in bog core porewaters

The depth profiles of total U concentration in soil porewaters show variation between cores, but also some common features, as can be seen in figure 3.44.

All profiles of the analysis of U in porewater show a peak in concentration at around 10 – 20 cm. In all cores, except core B, the highest U concentration is found in this region, the same depth as the solid phase U accumulation (figure 3.19). In core B the deepest sample, 30 – 39 cm, has an increase in concentration at depth, also evident in core D and to a lesser extent, in core A. The U concentration was quite stable on the five occasions, with all values

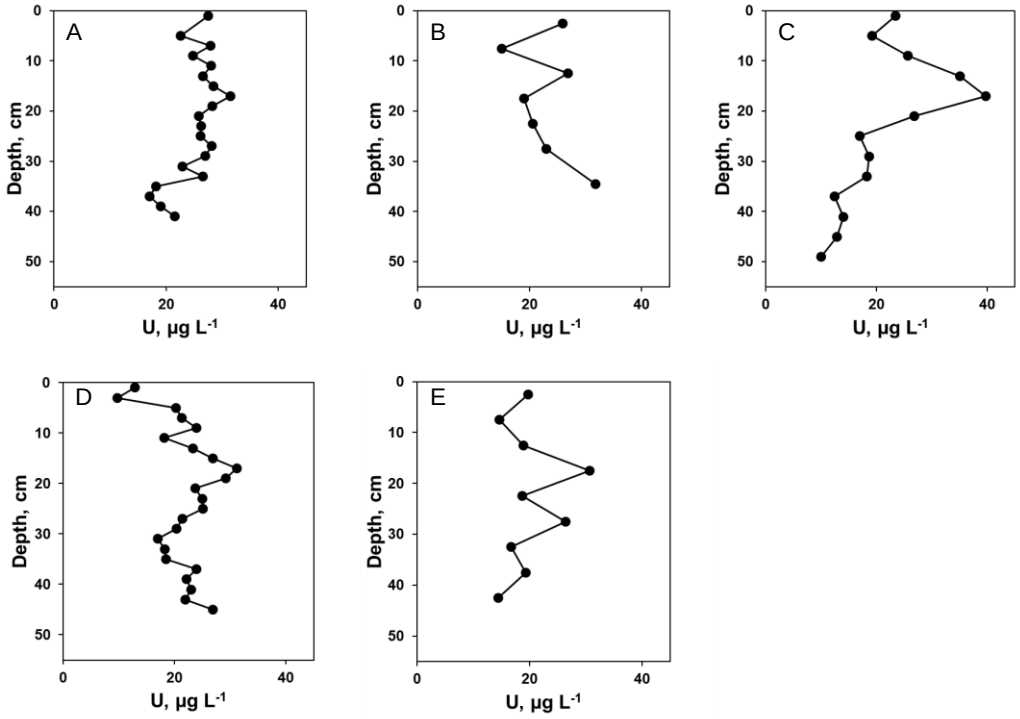

Figure 3.44. Profiles of U in porewater with depth. Top row left to right are cores A, B and C and bottom row left to right are cores D and E.

falling between 9 and 40 µg L^{-1}. These profiles are suggestive of two zones of U enriched porewater, a consistently elevated concentration between 0 and 30 cm and a secondary zone of variable U concentration below 30 cm. The U porewater profiles of cores A and C were significantly correlated with the soil U concentration of the same cores ($\rho = 0.62$ and 0.89 respectively, $p < 0.005$) while cores B and E showed no correlation. This is likely to be due

to the porewater U concentration showing variability due to the different water flow conditions on different occasions.

The results of the analysis of U in porewater ultrafiltration fractions are shown in figure 3.45. The operationally defined "truly dissolved" fraction (< 3 kDa) and colloidal fractions (> 3 kDa) are shown, with the colloidal fractions further separated into large (> 100 kDa), medium (100 – 30 kDa) and small (30 – 3 kDa) colloids at all depths from core B and selected depths from cores D and E.

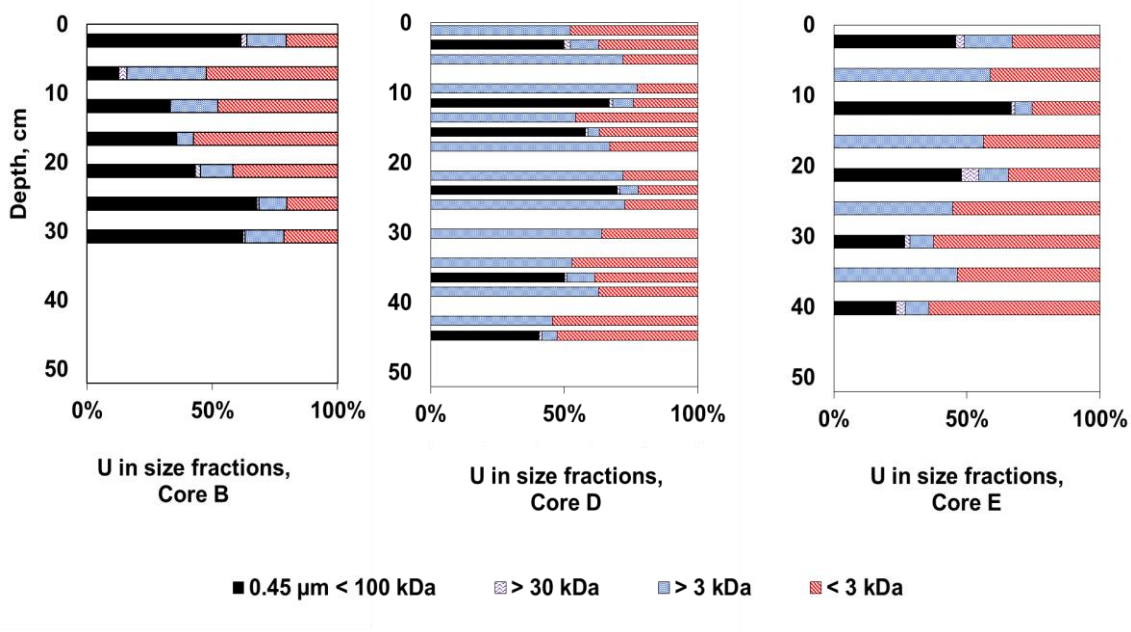

Figure 3.45. Profiles of U in ultrafiltration porewater fractions (%) with depth. The results shown are from cores B, D and E (left to right).

The "large" fraction dominates the colloidal forms of U in all three cores, with a lesser contribution from the "small" colloid fraction. The ratio of colloidal to dissolved U is different in core B compared to cores D and E, which are very similar. In core B there is a decrease in colloidal U from the surface to a minimum of ~40% at a depth of 20 cm, below which the colloidal U increases to ~80% of the total. The U in the small colloid fraction is greater than that in the large colloid fraction in core B at 5 – 10 cm, the only point in the

data set where this is seen, although the truly dissolved U is the most significant contributor to the total porewater U at this depth. Cores D and E have a different pattern of colloidal: truly dissolved U, with the colloidal form dominant in both cores from the surface to around 25 cm (52 – 80 %). Below 25 cm there is an increase of truly dissolved U, most prominent in core E where 53 – 65 % of U is in the truly dissolved fraction below 25 cm.

The change in U fractionation with depth seen in cores D and E are very similar to the results seen in a previous study of the site, which showed a peak in colloid associated U at a depth of around 5 – 20 cm and a subsequent decrease in colloid associated U with depth in 3 cores (Xu, 2013). This peak in colloidal U concentration occurs in the zone of the depth profile where the maximum U soil concentration is found (3.19), indicating that colloid formation is an important step in the removal of U from the porewater to the solid phase. The different results from the ultrafiltration of core B porewaters could be due to variation in conditions evident at the site on different occasions, particularly the highly variable water flow conditions.

3.7.2. Depth profiles of absorbance and dissolved organic carbon in bog porewaters

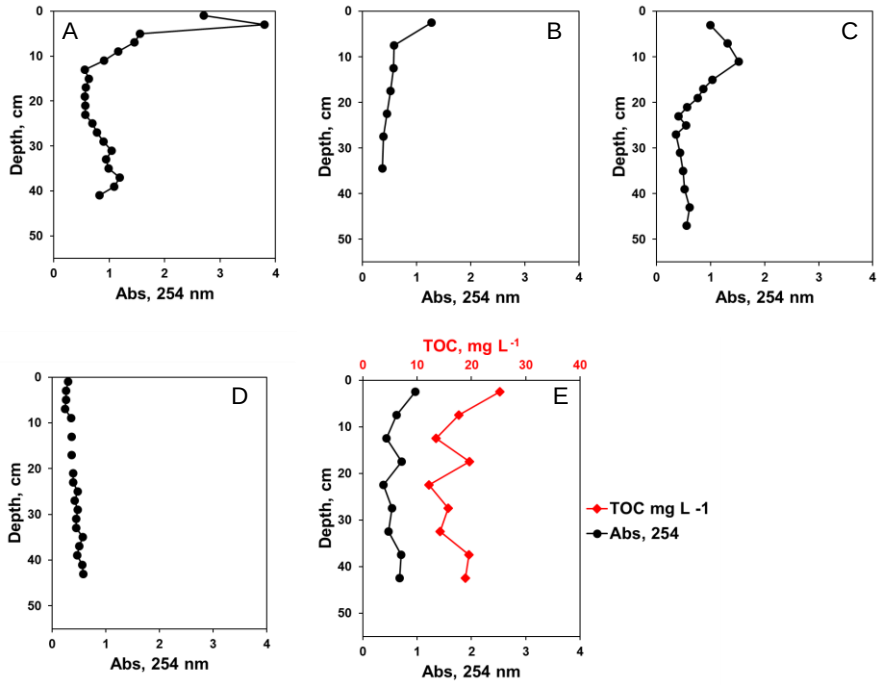

Figure 3.46. Profiles of porewater absorbance at 254 nm, as a proxy for organic matter concentration, and total organic carbon (TOC) concentration of core E porewaters with depth. Top row left to right are cores A, B and C and bottom row left to right are cores D and E.

The absorbance of porewater measured at 254 nm is used as a proxy for dissolved organic matter concentration. The TOC concentration of porewater samples from core E was directly measured and had a strong correlation with the absorbance at 254 nm ($R^2 = 0.986$). Although it is known that Fe can influence the porewater absorbance (Weishaar *et al.*, 2003), based on this result, it is clear that TOC is the major contributor to absorbance at this site. The TOC concentration in porewaters from core E is shown as an example (Figure 3.46). The porewaters from cores A, B and E have an elevated absorbance in the top 0 – 5 cm. Core C has a peak in concentration at 10 – 12 cm and core D has a featureless profile with a slight increase in absorbance with depth. Cores A, C and E also show a slight

increase in absorbance from ~30 cm and below. Characterisation of the porewater organic matter is discussed in section 3.8.

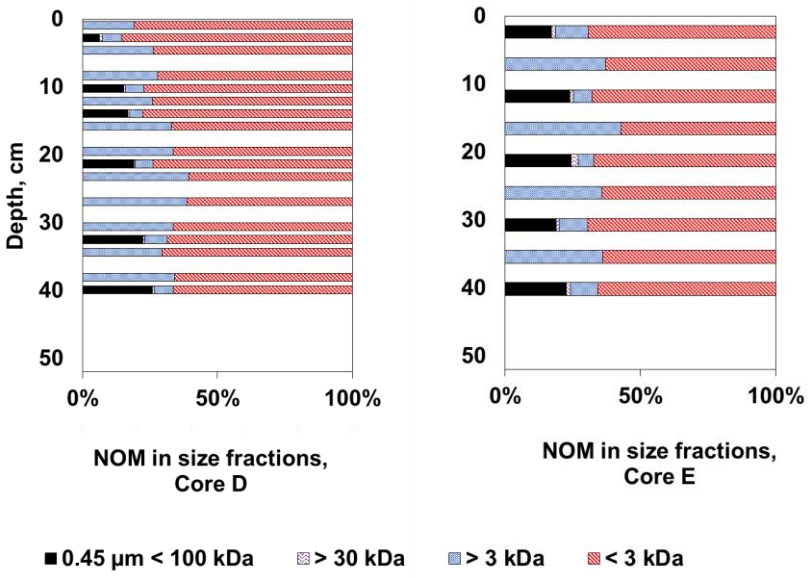

Figure 3.47. Profiles of porewater absorbance at 254 nm, as a proxy for organic matter concentration, in ultrafiltration fractions from cores D and E.

The absorbance of organic matter in ultrafiltered size fractions is shown in figure 3.47. The "truly dissolved" fraction is dominant throughout the core, accounting for 57 to 85% of the total absorbance, with very little variation in the concentration profile with depth.

3.7.3. Iron and manganese depth profiles in bog porewaters

Total Fe, Fe(II) and Mn in soil porewaters indicate changes in redox chemistry with depth and temporal variation between the cores collected on different occasions. Figure 3.48 shows the concentrations of total Fe and Fe(II) in porewaters from each core.

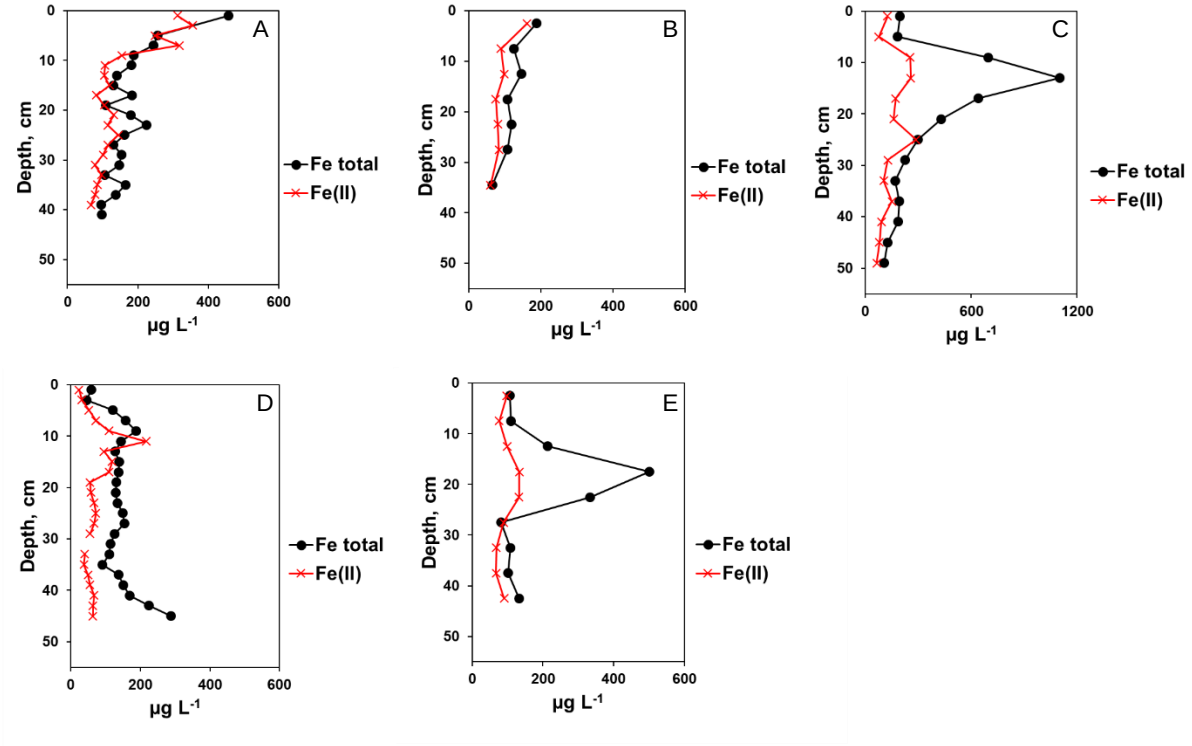

Figure 3.48. Profiles of Fe total and Fe(II) (µg L^{-1}) in porewater with depth. The x axes of core C is a larger scale than the others due to the high concentration of Fe on that occasion. Top row left to right are cores A, B and C and bottom row left to right are cores D and E.

In core A the maximum total concentration of ~460 µg L^{-1} occurred at the surface with a decrease to a fairly constant concentration of 100 – 150 µg L^{-1} between 10 – 42 cm depth. In this core Fe(II) is the dominant oxidation state throughout the profile, with over 90 % of Fe present as Fe(II) (93 ± 24%). The porewater Fe profile of core A is negatively correlated with the soil Fe concentration of the same core (ρ = -0.57, $p<0.01$). The soil Fe profile shows low accumulation in the upper half of the core increasing with depth below ~ 20 cm (figure 3.25) while the porewater Fe shows the opposite trend. This trend, along with the

predominantly reduced Fe in porewater, is indicative of reduction and dissolution of solid phase Fe(III) minerals from 0 – 20 cm and accumulation of Fe below 20 cm in the highly reducing conditions, perhaps as iron sulphides or pyrite. The profile of porewater Fe from core B has a similar shape to that of core A, with an initial decrease from the highest total concentration at the surface of 183 µg L^{-1} to a concentration of 100 – 150 µg L^{-1} to a depth of 30 cm and a decrease to ~67 µg L^{-1} in the final point of the profile at 30 – 39 cm. As in core A, Fe(II) is the dominant oxidation state with 77 ± 9% of the total Fe as Fe(II). Core D has a different profile with an initial increase of total Fe concentration to 188 µg L^{-1} at 8 – 10 cm followed by consistent concentration of 90 – 140 µg L^{-1} from 12 – 36 cm. Below 36 cm there is an increase to 288 µg L^{-1} at 46 cm. Unlike the other cores, the relative concentration of reduced iron decreases below 20 cm, with the peak below 30 cm being due to an increase in Fe(II) in the porewater.

Cores C and E show a different profile to cores A, B and E, with a large peak in Fe concentration between 10 and 20 cm with maximum concentrations of ~1100 and ~500 µg L^{-1}, respectively. These concentrations are much higher than are seen at the same depth in the cores collected on other occasions. Below the peaks, the Fe concentration stabilizes to 100 – 200 µg L^{-1} in core C and around 100 µg L^{-1} in core E. The peaks of total Fe concentration in cores C and E have a much higher concentration of Fe(III) compared to the other samples from the same cores and the same depth of the other cores. The porewater Fe profile is positively correlated with the soil Fe profile (figure 3.25) of the same core ($\rho = 0.58$, $p < 0.05$). The soil profile has a peak of Fe concentration at the same point as the peak of Fe(III) in porewater, between 12 and 22 cm. This suggests that Fe(III) is precipitating from porewater and becoming associated with the solid phase. This is the opposite process to that occurring in core A which shows the reduction and dissolution of Fe minerals to a depth of around 20 cm. These results highlight the variability of redox processes occurring at the site, with changes in oxygenated water flow through the bog at

a depth of ~0 – 25 cm and microbial activity likely to be responsible. This depth is also the region of elevated solid phase U concentration (figure 3.19) which suggests that U co-precipitates to the solid phase as part of mixed aggregate colloids containing Fe which form under the variable redox conditions . Further evidence for colloid formation in the upper section of the bog profile was found in the results of porewater ultrafiltration.

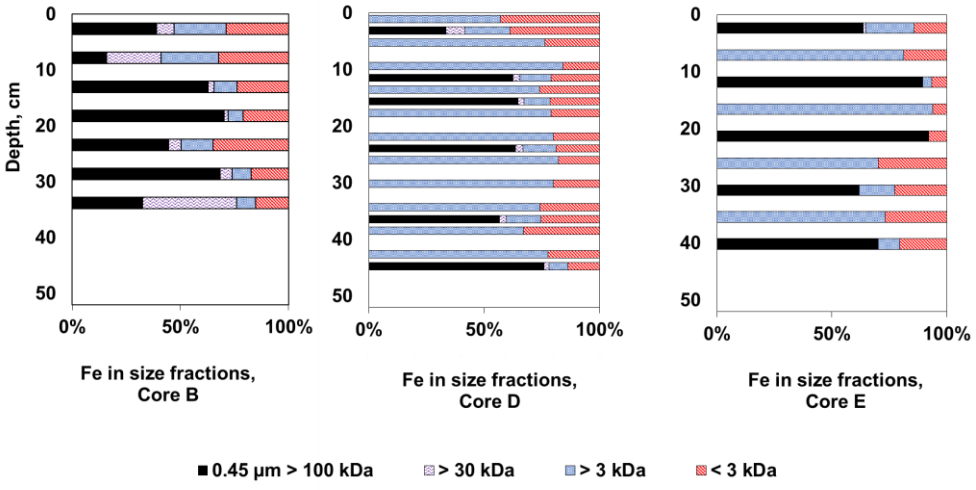

Figure 3.49. Profiles of Fe (%) in porewater ultrafiltration fractions from bog cores B, D and E.

The analysis of Fe in porewater ultrafiltration fractions (Figure 3.49) shows that more than 57% of Fe is present in a colloidal form with the "large colloid" fraction being dominant. However, the "small colloid" and "medium colloid" fractions are also important, particularly in core B. In core D there is an initial increase in colloidal Fe from 57 – 84 % between 0 and 12 cm and an increase in truly dissolved Fe of 15.2 % from 26 – 40 cm. Below 40 cm the colloidal Fe increases again to 86 % in the final sample at a depth of 44 cm. In core E there is an increase in truly dissolved Fe from ~11 ± 6% between 0 and 25 cm to ~25 ± 4 % below 25 cm. This increase in truly dissolved Fe is similar to that seen in core D at a similar depth. The same trend is also seen in the fractionation of U in porewaters

from cores D and E (Figure 3.45), which show a similar increase in truly dissolved U below 25 cm. As in the analysis of U porewater fractions, the distribution of Fe between ultrafiltration fractions in core B is different to that seen in cores D and E and does not show the increase in truly dissolved Fe with depth.

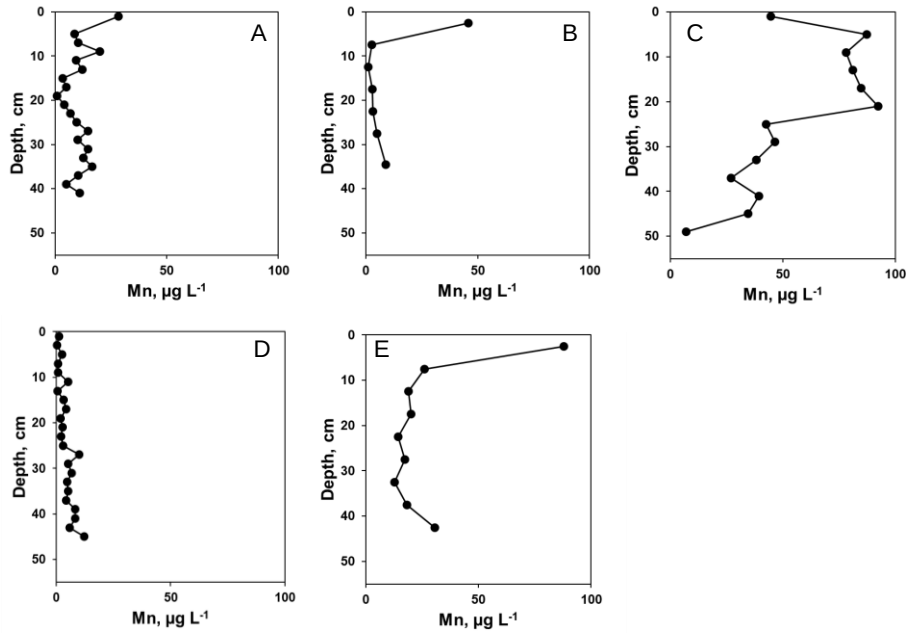

Figure 3.50. Profiles of Mn in porewater with depth (µg L^{-1}). Top row left to right are cores A, B and C and bottom row left to right are cores D and E.

The profiles of Mn in porewaters (figure 3.50) had two different shapes with depth which are closely related to the solid phase profiles. Cores A and D had comparatively featureless profiles with a relatively low Mn concentration throughout of <30 µg L^{-1}. Cores B and E had a highly elevated concentration in the surface sample of 0 – 5 cm, while core C had a broader peak of Mn in porewater between 2 and 22 cm. Cores B, C and E showed a sharp decline in Mn concentration below the peak.

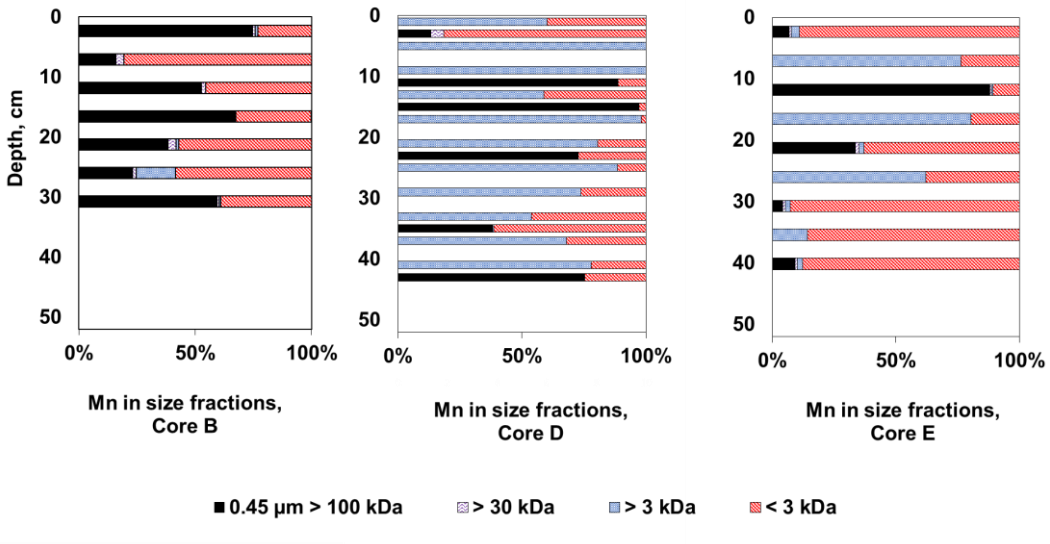

Figure 3.51. Profiles of Mn (%) in porewater ultrafiltration fractions from bog cores B, D and E.

The ultrafiltered profiles of Mn in porewaters (figure 3.51) show clear transitions between colloidal and truly dissolved Mn. In cores D and E there is an initial increase of colloidal Mn from the surface to a peak between 10 and 15 cm. In core E this is followed by a decrease in colloidal Mn below 25 cm to less than 15 %, while colloidal Mn in core D also decreases from 18 – 36 cm but increases again to a depth of 44 cm. The Mn in ultrafiltration fractions in both cores has a very similar pattern to the distribution of Fe in porewater size fractions. These elements are known to be very sensitive to changes in redox chemistry and the decrease of colloidal Fe and Mn with depth is indicative of the change from poorly soluble oxidized Fe(III) and Mn(IV) to readily soluble Fe(II) and Mn(II) below around 25 cm. This is consistent with the results of Fe speciation (Figure 3.48) which show that up to 76 % of total Fe is present as Fe(III) between 5 and 25 cm on two occasions. The porewater Mn profile of core C was positively correlated with the soil Mn concentration ($\rho = 0.68$, $p < 0.01$) as was also seen for the soil and porewater Fe concentration of the same core. The maximum porewater Mn concentration of core C occurs slightly above the soil Mn concentration (4 – 14 cm) and above the peaks of soil and porewater Fe concentration which occur at around 8 – 18 cm indicating the sequential reduction of Mn before Fe. The

peak of soil Mn concentration of core E was found at the surface of the core at the same point as the truly dissolved Mn was prevalent and there is a positive correlation between the porewater and soil concnetrations ($\rho = 0.77$, $p<0.02$). This is indicative of redox cycling of Mn with a peak of truly dissolved Mn in the reduced form and precipitation below. It is likely that the high concentration of soil Mn at the surface of core E is due to precipitation of oxidised Mn, similar to that seen in core C, however the sampling resolution of 5 cm is not fine enough to confirm this.

3.7.4. Aluminium depth profiles in bog porewaters

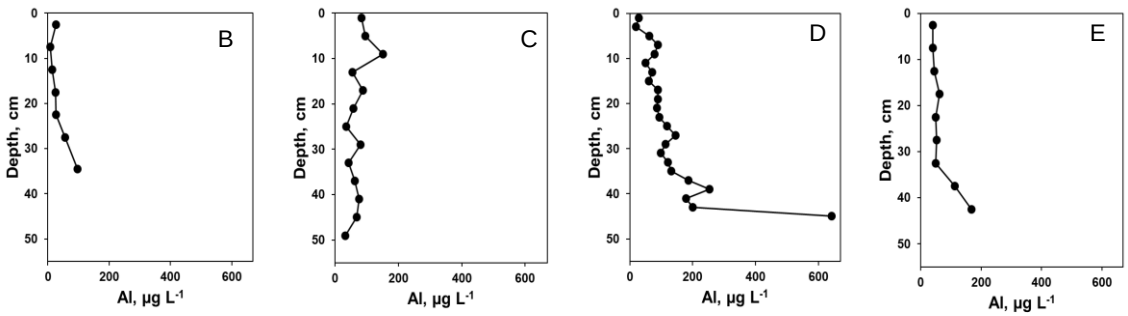

Figure 3.52. Profiles of Al (µg L^{-1}) in porewater with depth. The results are from cores B, C, D and E (left to right).

In cores B, D and E the concentration of Al increases with depth (Figure 3.52), with the increase most prominent below a depth of around 25 – 30 cm. Contrary to the other profiles, core C has a featureless profile which shows a slight decrease in concentration with depth. The increase of Al concentration in cores B, D and E is similar to the increase in Al in the solid phase samples, shown in figure 3.24, showing the increasing importance of Al with depth as the profile becomes more mineral and less organic.

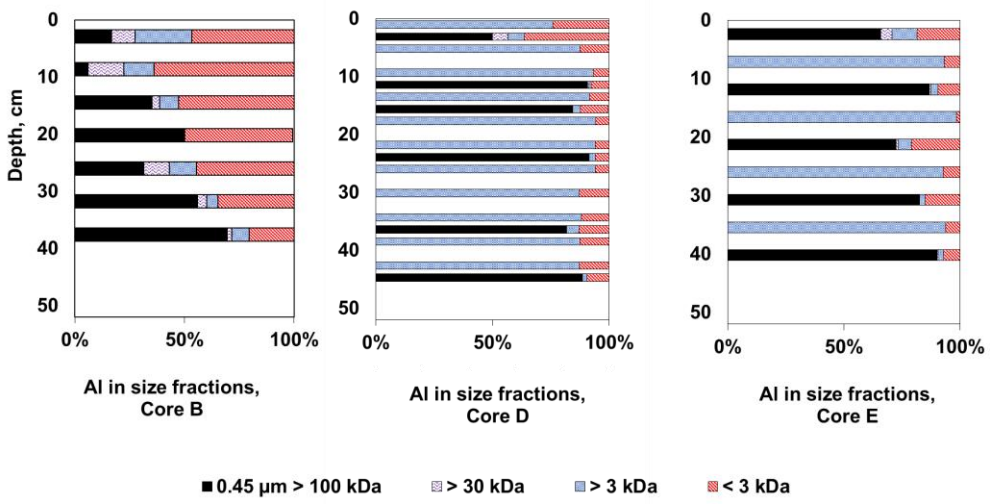

Figure 3.53. Profiles of Al (%) in porewater ultrafiltration fractions form bog cores B, D and E.

The results of ultrafiltration show that Al is predominantly in the colloidal fraction in cores D and E with the large colloid fraction dominant (figure 3.53). A different pattern is evident in core B, which shows an overall increase in colloidal Al with depth. The predominantly colloidal Al size fraction has implications for the mobility of trace metals such as Pb which can associate with aluminosilicate clays. The importance of Al colloids in controlling potentially toxic elements may become of increasing importance with depth in the bog as the composition becomes increasingly mineral.

3.7.5. Depth profiles of calcium in bog porewaters

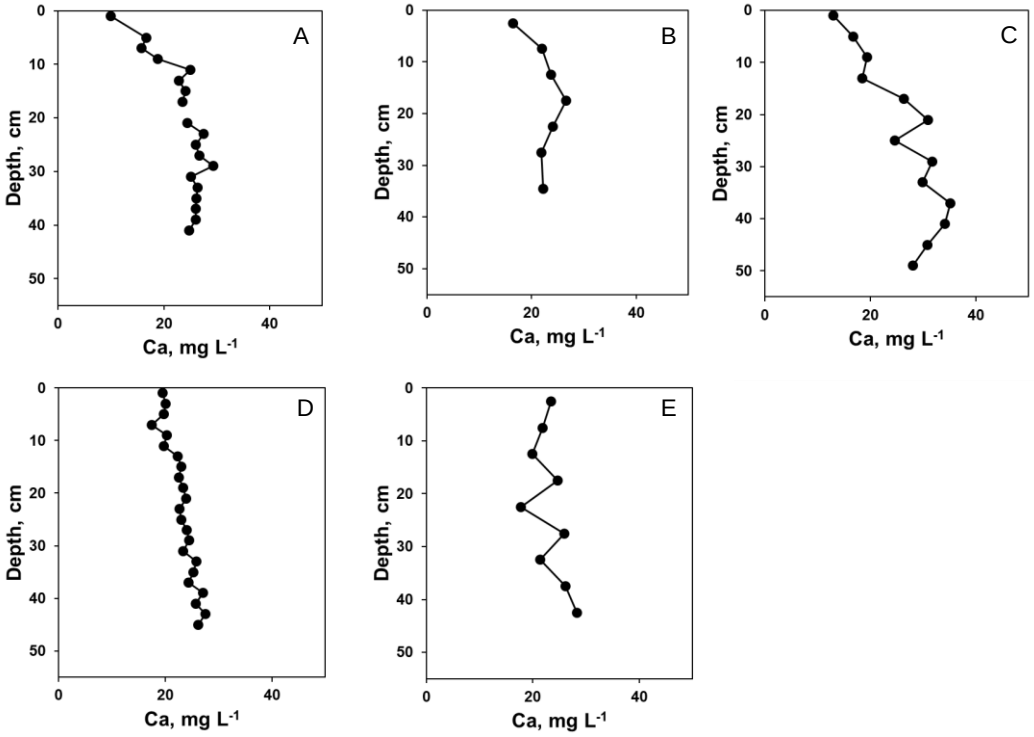

Figure 3.54. Profiles of Ca in porewater with depth (mg L^{-1}). Top row left to right are cores A, B and C and bottom row left to right are cores D and E.

The profile of Ca in porewaters (figure 3.54) shows a general increase with depth, with two different profile shapes. Cores A – C increase in concentration from the surface to a depth of around 30 cm. Below this depth, the Ca concentration profiles for cores A and B remain fairly constant while core C shows a decrease between 35 and 50 cm. Cores D has a featureless Ca concentration profile with a slight increase in concentration with depth, while core E has a variable porewater Ca concentration between 15 and 30 cm and an increase below 30 cm. The concentration of Ca between the different cores is quite consistent, with all samples having concentrations between 9 and 40 mg L^{-1}. The Ca concentration in porewater appears to be independent of the Ca soil concentration as no correlation is seen between the two parameters in any of the four cores.

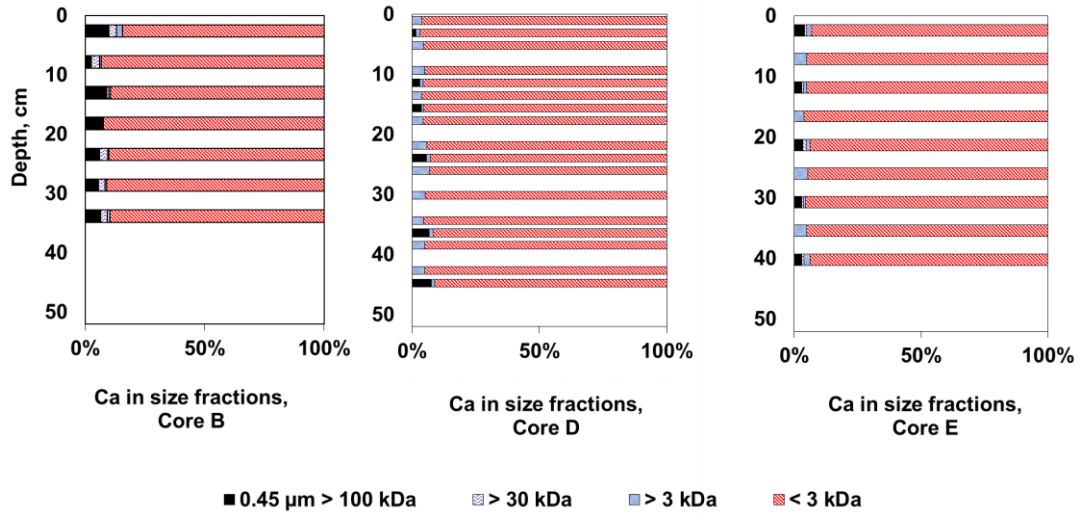

Figure 3.55 Profiles of Ca (%) in porewater ultrafiltration fractions form bog cores B, D and E.

The ultrafiltration profiles of Ca in porewaters are very consistent (figure 3.55) with over 85 % found in the "truly dissolved" fraction, in all samples. This is consistent with the dissolution of calcium carbonate material in the cave being dissolved by oxic water flow conditions and flowing into the bog. The fact that the majority of Ca is in the truly dissolved fraction shows it has little association with OM or Fe colloids. Uranium flows into the bog in the oxic and high Ca concentration waters, most likely in a U(VI) uranyl carbonate or calcium uranyl carbonate form (Xu, 2013). Within the upper sections of the bog U is largely found in a colloidal form, showing a change in association from truly dissolved U as calcium uranyl carbonate to colloidal U no longer associated with Ca. The change from truly dissolved to colloidal U could be an instrumental step in the immobilisation of U within the bog.

3.7.6. Depth profiles of pH in bog porewaters

The pH depth profiles of porewaters (figure 3.56) show some variability between the cores sampled.

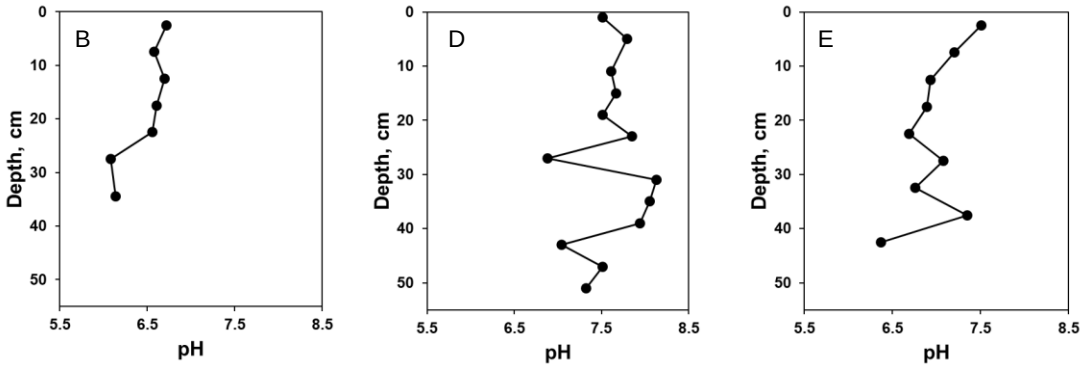

Figure 3.56. pH profiles of porewaters from cores B, D and E (left to right)

The pH profiles of porewaters from cores B and E show a similar shape with an overall decrease in pH from the surface to below 20 cm. The porewaters of cores D and E below a depth of 20 cm appear to have quite variable pH, although the reasons for this are not clear. The pH of all the porewaters measured is higher than the corresponding solid phase pH, shown in figure 3.28. The pH of cores B and D is between 6.08 and 7.51, while the pH range of core D is from 6.88 to 8.13. The reasons for the considerably higher pH of core D are not clear from these results as factors which could influence pH such as Ca concentration and DOM concentration (Figures 3.54 and 3.46) are both in the same range as the other cores.

3.7.7. Depth profiles of arsenic, lead and copper in bog porewaters

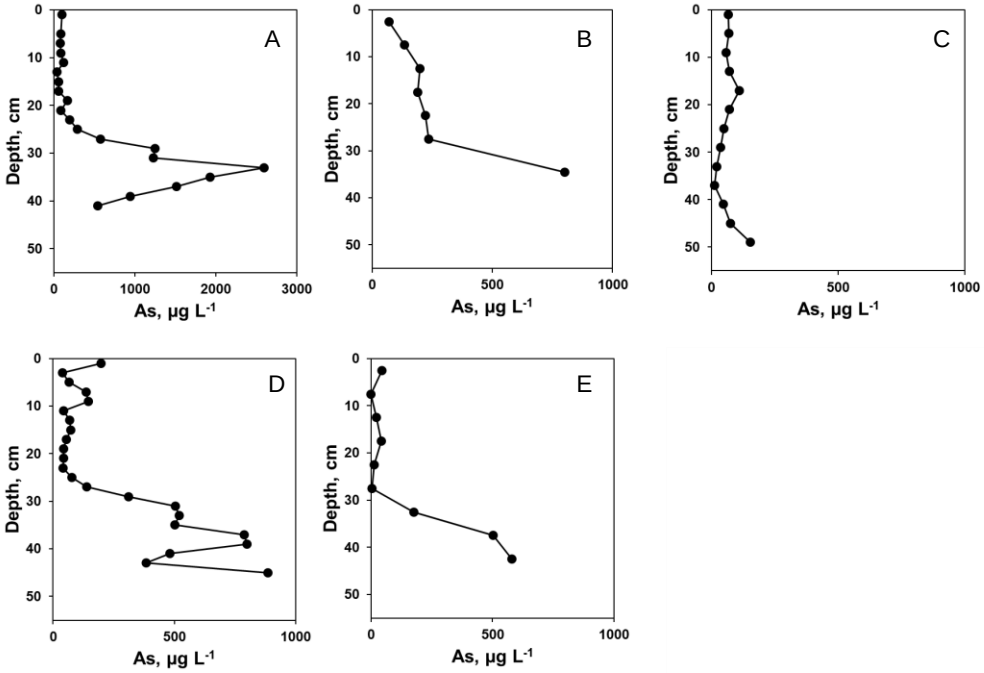

Figure 3.57. Profiles of As in porewater with depth (µg L^{-1}). The x axis of core A is on a larger scale than the other cores due to the high As concentration found on this occasion. Top row left to right are cores A, B and C and bottom row left to right are cores D and E.

The porewater profiles of As (figure 3.57) have a featureless profile with depth until around 25 cm, below which a sharp peak is seen in cores A, B D and E. Core C also shows an increase in concentration at depth but does not reach the high concentrations seen in the other profiles. The profiles indicate a change in the redox conditions of the bog below around 25 cm where the sharp increase in As concentration is seen. Arsenic readily co-precipitates with Fe and Mn oxides and hydroxides, so the relatively low concentration in solution between 0 and 25 cm could be due to the precipitation of insoluble oxidized Mn and Fe species in this region, as shown in the Fe(II): Fe(III) ratio of the porewaters of cores C and E and the ultrafiltration profiles of Fe and Mn which show the dominance of colloids to a depth of around 25 cm. However, this is not supported by the ultrafiltration results (figure 3.58) which show that over 85% As is found in the "truly dissolved" fraction

throughout the cores, and not in the colloid fractions associated with Fe and Mn. This suggests that As is likely to be present in its reduced form, As(III), which is highly soluble.

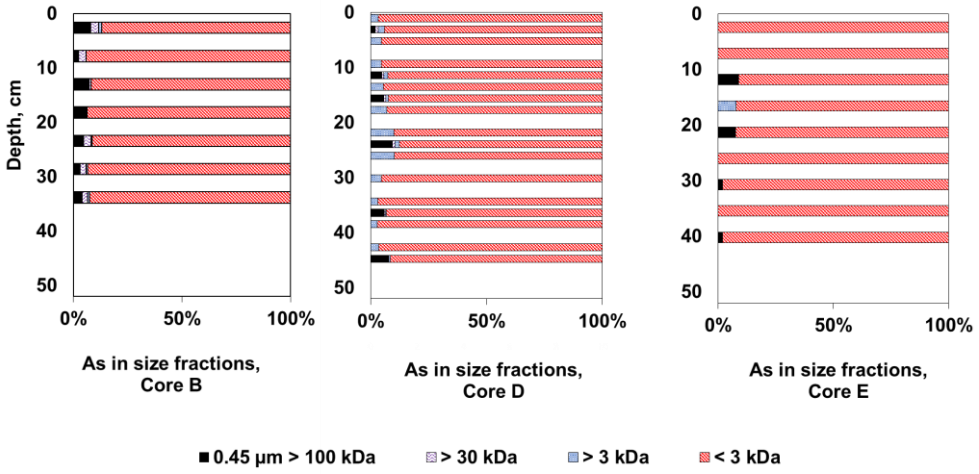

Figure 3.58. Arsenic (%) in ultrafiltration fractions of bog porewaters from cores B, D and E.

The concentration of Pb in the bog core porewaters is less than 20 µg L^{-1} in each of the 5 cores (figure 3.59).

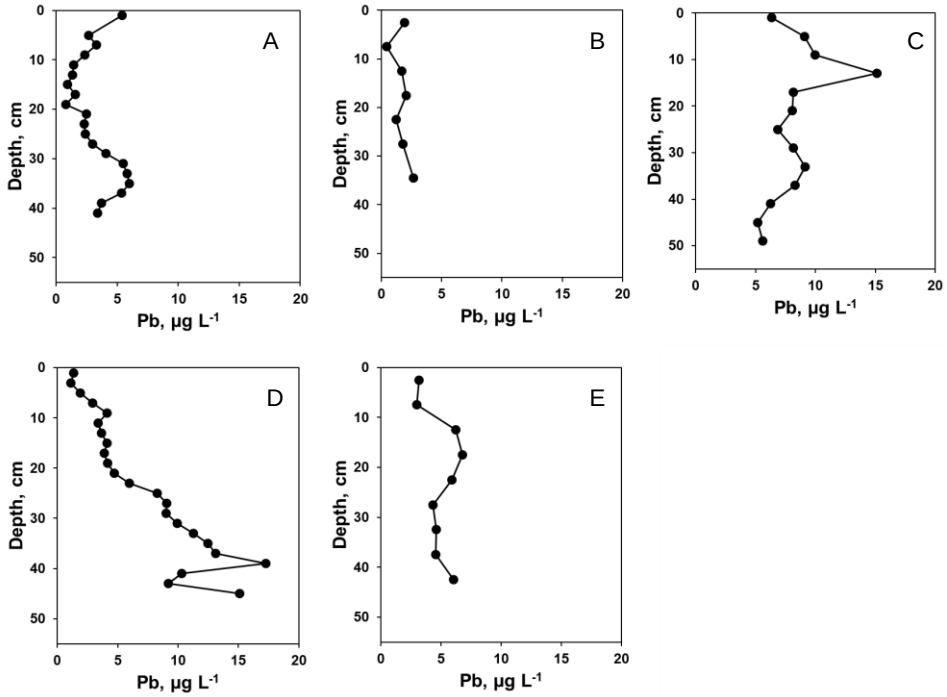

Figure 3.59. Profiles of Pb in porewater with depth (µg L^{-1}). Top row left to right are cores A, B and C and bottom row left to right are cores D and E.

Cores A, B and D show an overall increase in Pb with depth while cores C and E have their maximum concentration between 10 and 20 cm.

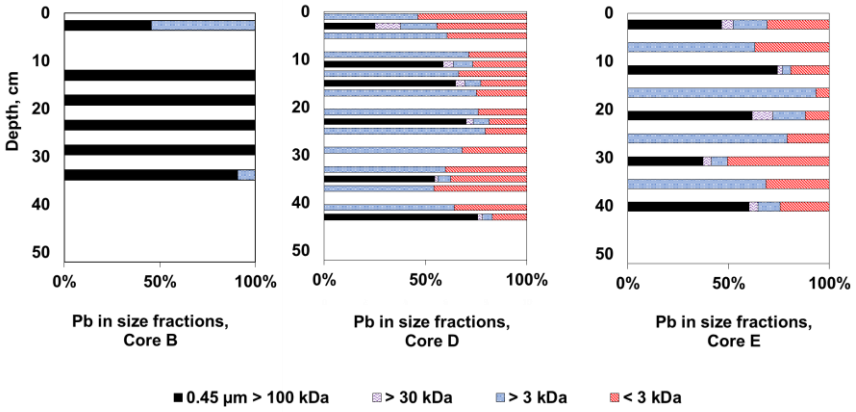

Figure 3.60. Lead (%) in ultrafiltration fractions of bog porewaters from cores B, D and E.

The profiles of Pb in ultrafiltration fractions in cores D and E are very consistent, with an increase in colloidal Pb from the surface to a depth of around 15 – 25 cm, followed by a decrease to a depth of 30 – 35 cm and subsequent increase in colloidal Pb to 40 cm and below. The increases in colloidal Pb in the porewaters occur in the same regions as the higher solid phase Pb concentrations (figure 3.29). Lead in porewaters appears to be affected by the redox cycling of Fe and Mn and is incorporated into colloids between 15 and 20 cm. This is similar to the U fractionation in ultra-filtered porewaters which are also found in a colloidal form in the upper region of the bog profile.

As is seen in the analysis of solid phase material, the Cu profiles of the porewaters (Figure 3.61) are very similar to the U profiles, suggesting similarities in their chemical behaviour at this site. Cores C, D and E have a peak at around 20 cm. Core C also has an increase in Cu concentration below 35 cm. Core B also features an increase in Cu concentration with depth.

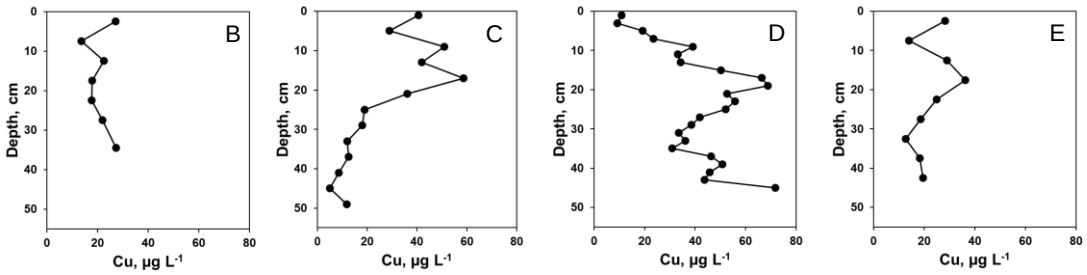

Figure 3.61. Profiles of Cu in porewater with depth (µg L^{-1}). The results are from cores B, C, D and E (left to right)

The similarity with U is not seen in the ultrafiltration profiles of Cu, however, which show a general increase of Cu in the colloidal fraction with depth (figure3.62). Unlike for Pb and U, the depths of increased colloidal Cu character are not the same as where the peaks in solid phase Cu concentration are seen.

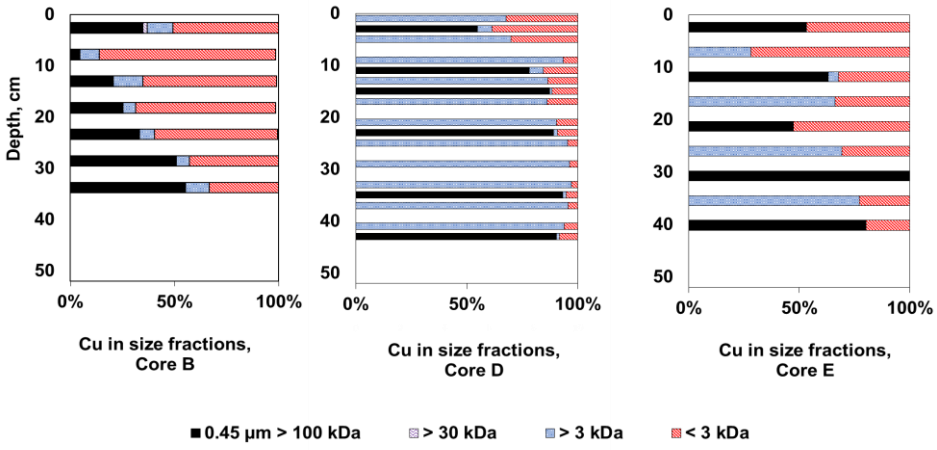

Figure 3.62. Copper (%) in ultrafiltration fractions of bog porewaters from cores B, D and E.

3.8. Porewater organic matter characterisation

Porewater organic matter was analysed by UV/vis, FTIR, fluorescence and NMR spectroscopy. The results provide information about the variation in organic matter characteristics with depth, and allow comparison of the results from different analysis techniques.

3.8.1. Porewater organic matter characterisation depth profiles

The E2: E3 ratio (figure 3.63) of the five cores show very little variation with depth, with all the ratio values being around 5. Core E is the most variable with depth and has the highest ratio values of up to 7.7, however there is no overall trend.

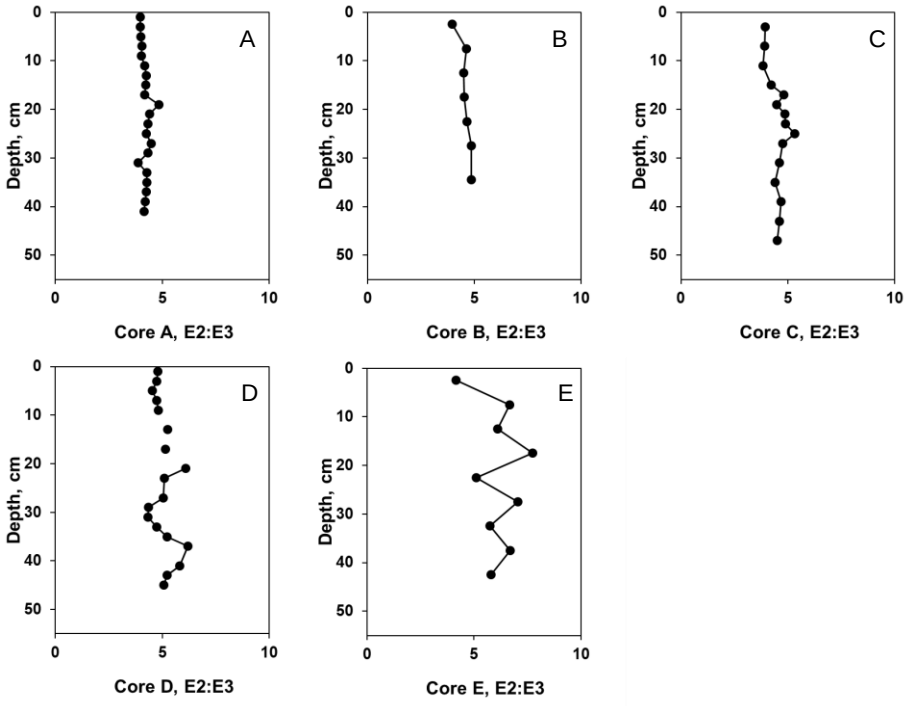

Figure 3.63. E2:E3 ratios of porewater depth profiles.

The slope ratio (SR) calculated from the same spectra show more variation than the E2: E3 ratio, as can be seen in figure 3.64. Cores A, D and E show a general decrease with depth while cores B and C have featureless profiles. The SR is inversely correlated with aromaticity and molecular size, suggesting an increase in DOM aromaticity and molecular weight with depth. However, the analysis of ultrafiltration fractions by UV/vis (3.47) did not show an increase in organic matter in the larger colloid fractions with depth.

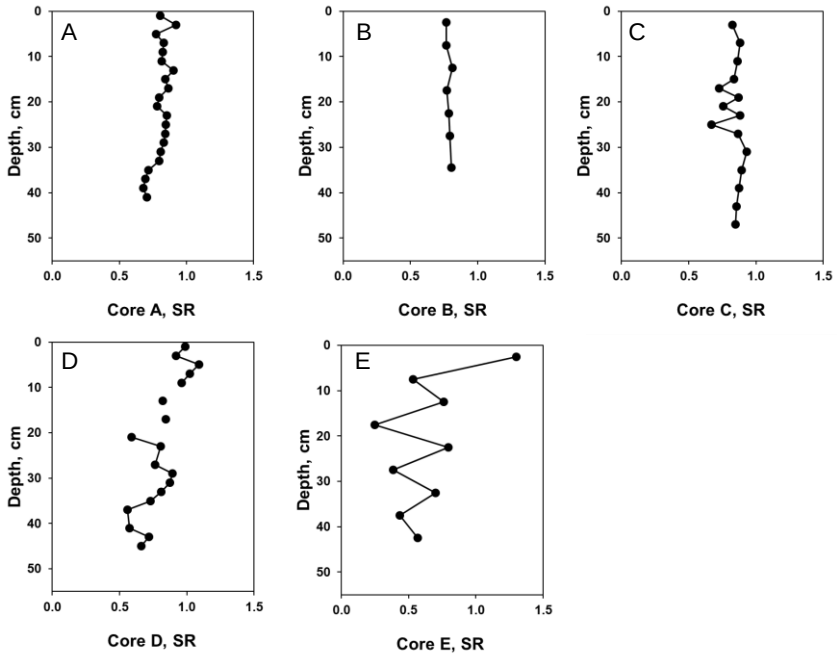

Figure3.64. Spectral slope ratios (SR) of porewater depth profiles.

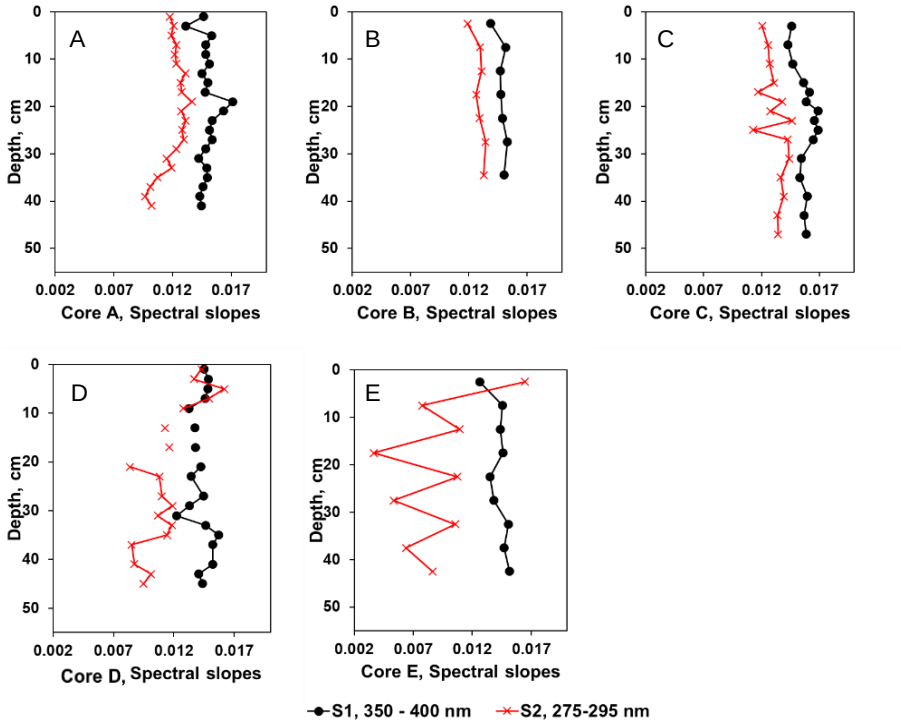

Figure 3.65. UV/vis spectral slope paramaters $S_{275\text{-}295}$ and $S_{350\text{-}400}$ of porewater depth profiles.

The results of spectral slope analysis in figure 3.65 show that $S_{275\text{-}295}$ has a greater influence on the value of SR than $S_{350\text{-}400}$. The values of $S_{350\text{-}400}$ show little variation with depth, while the profiles of $S_{275\text{-}295}$ have a decreasing trend in cores A, D and E similar to the SR. $S_{275\text{-}295}$ has been shown to have an inverse correlation with molecular size and humification (Chen *et al.*, 2002; Helms *et al.*, 2008; Fichot and Benner, 2012) indicating larger and more humified OM with depth in cores A, D and E. Again, this is not in agreement with the results of ultrafiltration, which showed very little variation in the amount of colloidal:truly dissolved OM with depth.

3.8.1.1. FTIR and ^{1}H NMR analysis of core E porewater organic matter

Porewater organic matter from core E was freeze dried and analysed by FTIR-ATR. It proved to be difficult to desalt and recover the small amounts of OM in the low sample volumes available, so a comparison was made between the results of analysis of samples with and without cation exchange. The cation exchanged samples were around pH 4.5 while the samples which were not cation exchanged and were directly freeze dried were around pH 7. The pH influences the FTIR profiles, as can be seen in figure 3.66.

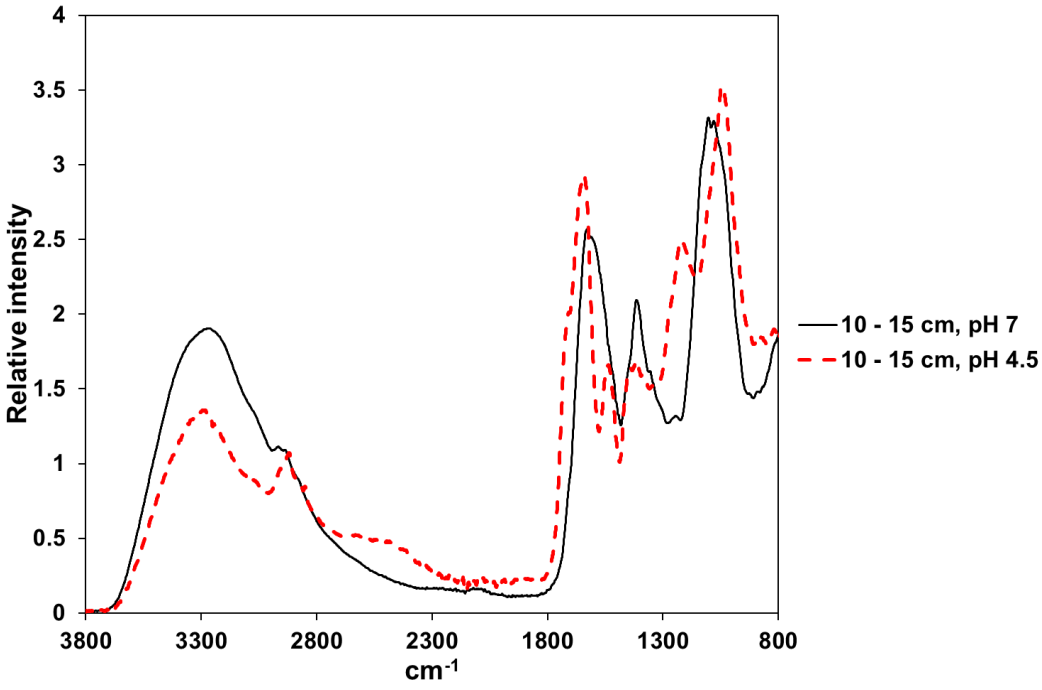

Figure 3.66. FTIR analysis of freeze dried porewater OM with (red dashed line) and without (black line) de-salting by cation exchange prior to freeze drying.

The differences between the spectra collected at pH 7 and pH 4.5 (figure 3.66) are due to the protonation of functional groups with the decrease in pH. The broad band at 3000 – 3500 cm^{-1} decreases with pH. This band arises from the OH stretch of phenols, alcohols and carboxylic acids, but also is influenced by water. The peak at 1410 cm^{-1} is due to the asymmetric stretch of COO^{-} and decreases with pH as COO^{-} groups are protonated to form

COOH. The peaks at 2250 – 2700 cm^{-1}, 1720 cm^{-1}, and 1220 cm^{-1} increase as pH decreases and can be attributed to the formation of COOH. The variation with pH highlights the carboxylic peaks in the spectrum. Similar changes with pH are shown in the study of Gondar *et al.*, (2005) in a pH range from 4 – 9.5.

Although significantly different to the spectra of the cation exchanged OM, the results of FTIR analysis of freeze dried porewater OM which had not been cation exchanged still showed differences between samples, and so this method was used to analyse samples of porewater OM from core E with depth in the bog. The changes between the spectra of porewater organic matter, measured at pH 7, can be seen in figure 3.67 below.

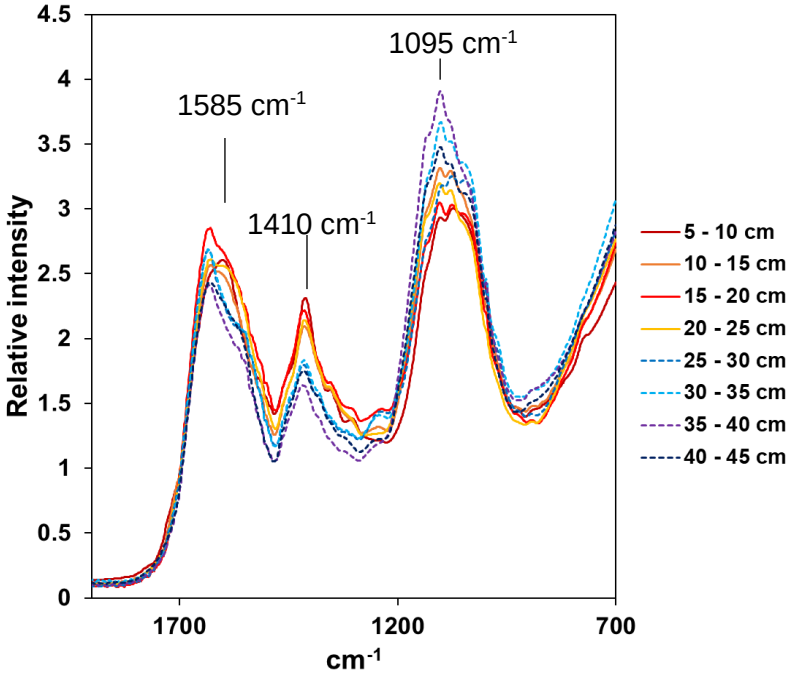

Figure 3.67. Spectra of porewater OM from different depths of core E analysed by FTIR without prior cation exchange. The expanded region of the spectra from 700 – 1700 cm^{-1} is shown.

The regions at 1585 and 1410 cm^{-1} (carboxylic acids) show a general decrease with depth (figure 3.68). The profiles of these two different regions are strongly correlated ($R^2 = 0.93$) lending confidence to the assignment of these two bands as due to carboxylic acids. The large peak at 1095 cm^{-1} (alcohols, esters and carbohydrates) shows a general increase with depth.

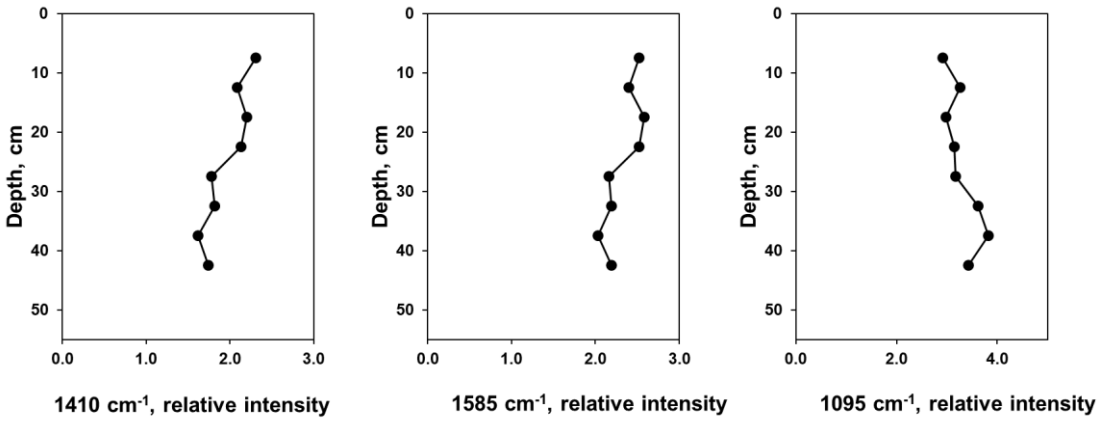

Figure 3.68. Spectra of porewater OM from different depths of core E analysed by FTIR without prior cation exchange. The expanded region of the spectra from 700 – 1700 cm^{-1} is shown.

The results of analysis of porewater organic matter by ^1H NMR (figure 3.69) show the variation in different regions of the NMR spectra with depth.

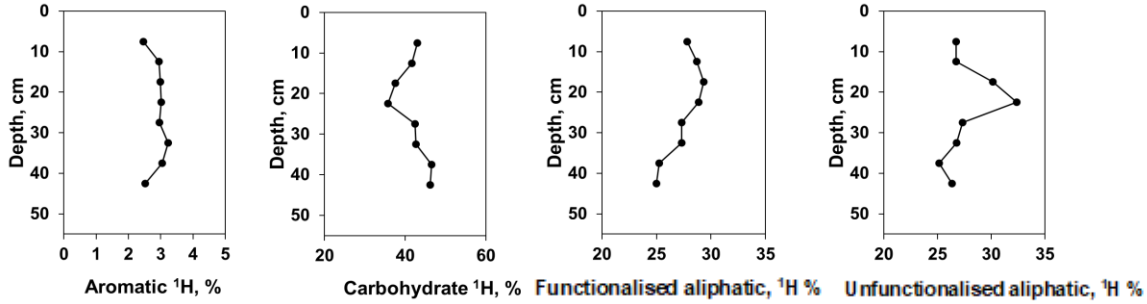

Figure 3.69. Changes in regions of the ^1H NMR spectra of analysed porewater organic matter with depth

The percentage of total ^1H in aromatic molecules is 4.3 – 7.5 % lower in the porewater organic matter than in the extracted soil organic matter (figure 3.40) while there is 3.1 – 7.6 % more of the total ^1H in oxygen rich organic aliphatic organic matter the porewater

organic matter compared to the extracted soil organic matter. The percentage of carbohydrate ^{1}H is very similar in the porewater and soil organic matter samples and is the largest component in both, on the other hand there is around 10 - 15 % more of the total ^{1}H in aliphatic methyl organic structures in the porewater organic matter compared to soil organic matter.

The results of characterisation of porewater OM with depth show a decrease in functionalised organic matter (^{1}H NMR) and carboxylate functionality (FTIR) with depth. There is a positive correlation is between functionalised aliphatic results from NMR analysis and the carboxylic acid peak at 1410 cm^{-1} from FTIR analysis, with an R^2 value of 0.67. This gives more confidence to the result showing the decreasing oxygen content with depth in the porewater OM. The upper region of the core profile, where the porewater OM has a relatively high oxygen content, is also where the U is found in the colloidal form. It is possible that the more oxygen rich OM preferentially forms colloids with Fe with which U is associated.

3.9. Depth profile zonation: Redox and ageing effects

Results presented from the analysis of cores and porewaters from the Needle's Eye peat bog highlight the complex and dynamic geochemical processes occurring at the site. The profiles indicated zonation with depth influenced by redox chemistry and water flow patterns. The changes with depth can be described by sections, each with different characteristics, as is shown in the schematic diagram below (figure 3.70).

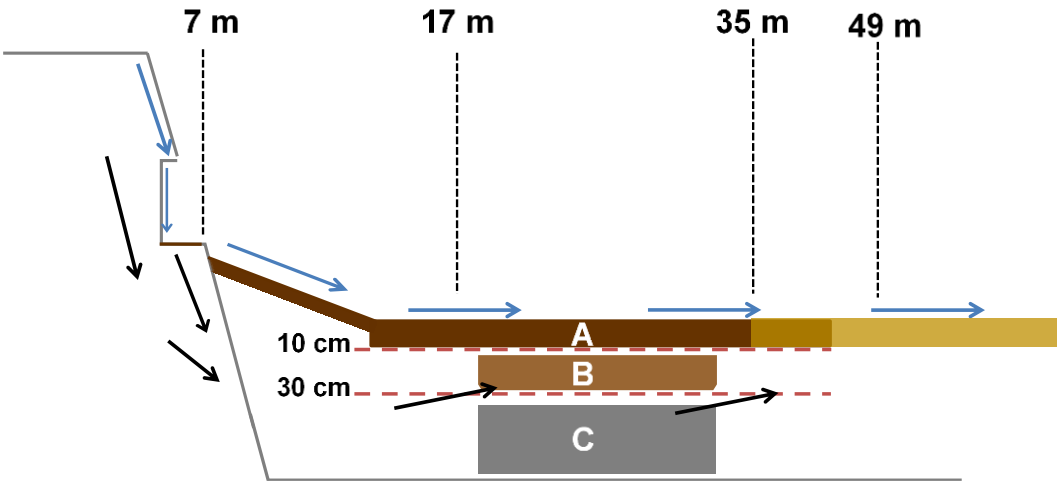

Figure 3.70. Schematic diagram of zonation with depth in the highly organic Needle's Eye bog (not to scale). The depth zones identified, A – C, are described in the text below. Blue and black arrows indicate surface and sub-surface water flows respectively, as reported by Hooker, (1991).

Zone A extends from the surface to between 5 and 10 cm depth and is a region of very organic, wet and relatively young peat (c. 20 yrs, ^{14}C analysis). The high Mn concentration in soils in this section indicates an aerobic zone near the surface where precipitated Mn oxides accumulate. However, analysis of Fe in porewaters shows that almost 100 % of the total Fe is present as Fe(II), which indicates that there are reducing conditions in the porewater at this point. The sample depth resolution (minimum 2 cm depth) means it is not possible to distinguish the limit of the Mn deposition zone, which could be occurring at the very surface of the bog and not penetrate more than a few mm. The first of two peaks of soil sulphur concentration is present in this region which is also indicative of reducing

conditions. The results of XAS analysis of U in this zone show that it is predominantly in the U(VI) oxidation state, which would not be expected in reducing conditions as U is susceptible to microbial reduction.

Zone B, from around 10 to around 25 cm, is characterised by elevated concentrations of U, Cu and Pb in the soils. The results of Fe analysis in porewater in this zone show that it is a region of highly variable redox chemistry, with up to 74 % of Fe present as Fe(III) on two out of five sampling occasions. This zone also has high colloidal Fe and Mn in porewaters, with a clear peak in the colloidal Mn compared to above and below in the profile. This suggests that oxidation followed by precipitation is leading to the formation of colloids at this depth. Uranium and Pb also have their maximum colloid concentrations in this region, which is possibly due to co-precipitation with Fe and Mn oxyhydroxides, making this a potential mechanism of U removal from porewater to the solid phase. As in zone A, the XAS analysis of the sample from this zone shows that the U is present as U(VI) and is complexed by organic molecules via oxygen atoms. The porewater and solid phase organic matter in this zone are rich in oxygen containing functional groups such as carboxylic acids which are likely to be involved in the binding of U. The solid phase pH is at its maximum in this zone at around 5.5 – 6.5, despite the Ca concentration being highest in zone A. The particle size analysis of the mineral phase shows a decrease of particle size at the bottom of zone B, which could act as a barrier to water flow. This could encourage oxic, U and Ca rich water from the cave to flow through zone B bringing oxic water into the otherwise reducing conditions of the bog and trigger the variability in redox conditions seen in the analysis of Fe(II) and Fe(III). Oxidation and reduction of Fe in this zone causes the formation of Fe-OM colloids, seen in the ultrafiltration of porewaters. The colloids are able to bind U, in zone B of the bog, and act as a mechanism of U transfer to the solid phase as has been shown previously at the Needle's Eye (Xu, 2013) and in other soils (Graham *et al.*, 2011).

Zone C, from around 25 - 30 cm and below has much lower organic matter content and another change in redox chemistry back to highly reducing conditions, as is shown by Fe(II) being the dominant oxidation state in the porewaters and the peak of S. The U, Pb and Cu solid phase concentrations show a general decrease from the peak in zone B, as does the pH to become more acidic at around 4.5 – 5.5. There is a large increase in the porewater As concentration in this region, present in the truly dissolved fraction, which could be due to the lack of oxidised Fe minerals which can bind As strongly, particularly at low pH. There is a continued decrease in the organic oxygen functional groups throughout this zone, and a particular decrease in the total O content of the organic fraction of the peat.

Organic characterisation analysis showed that there were changes in OM composition with depth in the profile. The decrease in carboxylic acids seen in the FTIR analysis of porewater and solid phase organic matter, the increase in aromaticity seen in the ^{1}H analysis of solid phase organic matter, the increase in the humic: fulvic acid ratio, the decrease of the extracted organic matter E2:E3 ratio and the decrease of the $S_{275\text{-}295}$ slope ratio all follow constant trends with depth. These changes with depth are indicative of the humification process of natural organic matter as it ages (Stevenson, 1982; Zech, Haumaier and Kogel-Knaber, 1989). This is confirmed by the ^{14}C age analysis which shows that core B covers a range of around 137 years over 39 cm of depth. The O/C ratio of the soil of core B has a strong correlation with the U concentration in the same samples ($\rho = 0.95$, $p<0.001$). This is a further demonstration of the importance of organic oxygen content in binding U at the site, as was proven in the results of EXAFS analysis. The statistical analysis of the associations of U in soil samples from core E are summarised in figure 3.71.

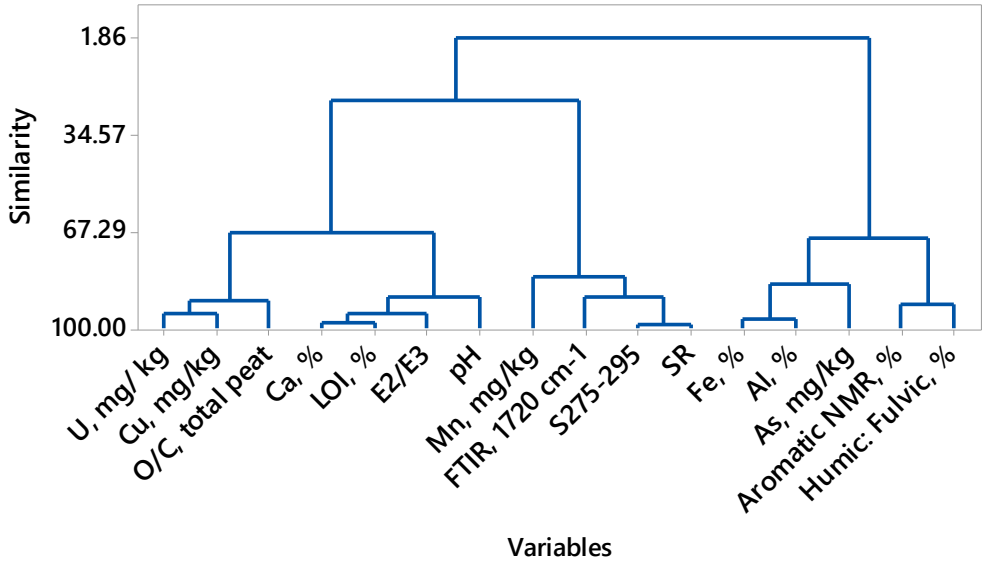

Figure 3.71. Dendrogram showing the soil organic and inorganic associations of samples from core E. Strong correlation is indicated by close proximity on the x axis and short height of connecting bars.

The dendrogram in figure 3.71 clearly shows the parameters which were correlated with U concentration in core E soil samples. Soil O/C ratio and Cu concentration had the strongest correlation with U indicating the similarity of behaviour of U and Cu in the core. Studies of copper binding to OM have found that Cu^{2+} directly binds to the oxygen functional groups of OM (Xia, Bleam and Helmke, 1997; Frenkel and Korshin, 2001), and that binding of Cu to OM can be a mechanism for its retention (Mao, Young and Bailey, 2015), therefore the correlation of Cu with O/C ratio indicates that Cu, like U, is likely to be found directly bound to the OM. The correlations found between U and pH, LOI and Ca highlight the importance of these parameters on the accumulation of U in the bog. The group on the far right of the dendrogram Fe, As, Al, aromaticity of OM and humic: fulvic acid ratio show the humification of OM and increasingly mineral content of the profile with depth. There were no correlations seen between these parameters and U concentration, demonstrating the controlling influence of LOI, pH and O/C ratio on U accumulation.

4. Organic characterisation and investigation of U binding in Needle's Eye OM fractions

4.1. Introduction

Organic matter extracted from Needle's Eye bog samples and dissolved organic matter (DOM) recovered from porewaters was fractionated by size exclusion chromatography (SEC), ultrafiltration and pH-based humic/fulvic acid separation. Spectroscopic analysis techniques were then applied to characterise the isolated fractions and their ability to bind U and other metals was then assessed following analysis by ICP-MS. The influence of pH and redox conditions on U binding to organic matter was also investigated.

4.2. Preparation of OM for characterisation: Extraction and de-salting

4.2.1. Choice of solvents for extraction an analysis

The choice of solvents used for organic matter extraction and analysis can influence the results obtained as OM has varying solubility in different solvents. The aim of extracting OM for characterisation analysis is to obtain a sample which is representative of the OM in its natural state, free from salts and organic solvents, dry and reproduceable.

The procedure adopted in this study for preparation of organic matter samples suitable for characterisation is outlined below.

4.2.1.1. Extraction of natural OM using dilute aqueous solutions containing NaOH.

Various organic and inorganic extractants have been successfully employed in the extraction of humic substances from soils. All extractants are selective to some degree, with organic matter recoveries varying from around 1% with H_2O or alcohol, to 80% with

dilute solutions of strong bases such as NaOH (Hayes *et al.*, 1975; Stevenson, 1982), which have proven to be the most effective extractants (Stevenson, 1982). There are some drawbacks associated with such high extraction efficiency, with two of the most significant being: (i) the potential to oxidise OM by contact with a high pH solution and; (ii) the addition of high concentrations of inorganic salts which must be removed before matrix-sensitive analytical techniques can be used. The first of these potential issues can be mitigated by extraction under an inert gas atmosphere (e.g. N_2, Ar or He) using carefully de-gassed solutions to remove oxygen from the extraction solution (Schnitzer, 1982; Pansu and Gautheyrou, 2006). The second can be resolved by the removal of added inorganic matrix components by de-salting. In this study, dried, ground and sieved peat samples were suspended in alkaline aqueous solution for four hours under an atmosphere of N_2 (section 2.4.2). Organic matter was extracted with 0.1 M NaOH for fractionation and characterisation. Selective solubility of OM constituents was also tested by extraction with solutions of 0 – 1 M NaOH.

The alkaline extracts were filtered through glass fibre filter papers (Whatman GF/C glass microfiber filters) before de-salting and drying, as is described below.

4.2.2. De-salting to remove inorganic salts.

Various approaches are used to remove background matrix components, each with positive and negative aspects. In this study, two methods of removing NaOH from the OM solution were tested: dialysis against deionised water (molecular weight cut off (MWCO) = 3500 Da) and cation exchange chromatography. The UV absorbance profiles for Size Exclusion Chromatography (SEC) fractionated OM resulting from the two desalting methods are compared below (figure 4.1).

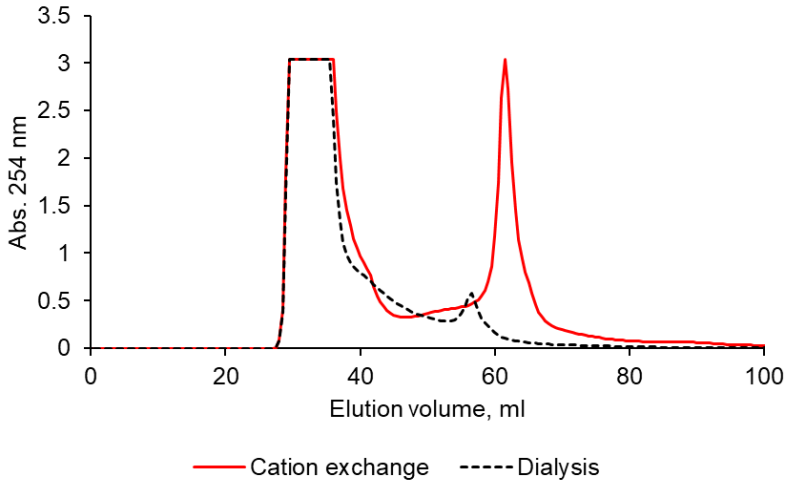

Figure 4.1. The elution profiles of OM extracted from NE core B, 10 – 15 cm sample and de-salted by dialysis (black dashed) or cation exchange (red). (Sephadex G25, 30 cm length, flow rate 2 ml min^{-1}, eluted with DI water)

Following de-salting and freeze drying, around 20 mg of OM sample (extracted from bog core B, 10 – 15 cm depth) was dissolved in 2 ml 0.1 M NaOH and the pH was adjusted to around 7 with small volumes of 0.01 – 0.5 M HCl (final volume of sample solution < 2.5 ml). Samples were eluted through an SEC column (G25, 30 cm length, flow rate 2 ml min^{-1}, eluted with DI water). The elution profiles show that both samples predominantly contain OM which is excluded from the gel internal porosity and elutes as a broad peak at around 30 – 40 ml (the peak has a flat summit as the detector reached its maximum absorbance). A second sharp peak is seen at around 60 – 62 ml in the samples prepared by cation exchange and a much smaller peak at around 56 – 58 ml in the samples prepared by dialysis.

This shows that almost all the OM eluting beyond the 56 ml point has been lost from the sample de-salted by dialysis. It can therefore be concluded that de-salting the samples by cation exchange generates samples which are a better representation of the extractable organic matter fraction compared to dialysis, as the smallest material is not lost. Based on this result cation exchange was chosen as the preferred method of sample de-salting.

The OM isolation and clean-up procedure adopted in this study is as follows:

i) Extraction with 0.1 M NaOH under N_2 atmosphere for 4 hours (ratio of 1:10 sample, g: NaOH, ml). Solution thoroughly de-gassed under vacuum)

ii) Centrifugation and filtration through Whatman GF/C glass fibre filter papers using Buchner apparatus

iii) De-salting by cation exchange to remove Na^+

iv) Freeze drying

This procedure maximises the solubility of soil OM, was found to be manageable with volumes of up to 500 ml per sample, is straight-forward and reproducible and generates a homogenous, dry, low-density powder product. This OM product is suitable for analysis in its solid state by FTIR and, with re-dissolution in selected solvents, by solution state NMR.

The same procedure was adopted to investigate the solubility of OM in DI water, 0.01 M, 0.1M and 1.0 M NaOH. In this experiment the filtration was carried out with 0.45 µm syringe filters. The results are shown in Section 4.6.

4.3. Fractionation of OM

In this study, two types of fractionation methods have been applied based on the chemical and physical properties of OM:

i) Fractionation by extraction with different concentrations of NaOH solutions

ii) Fractionation of extracted, de-salted and freeze-dried OM

The first method of fractionation relies on the variation of the extractability of OM from soil in NaOH solution of varying concentration. Organic matter extracted in increasingly high concentrations of NaOH has differences in character due to pH and ionic strength effects, as is shown in section 4.6. The concentrations used were 0, 0.01, 0.1 and 1.0 M NaOH. The ionic strength was not controlled because adding salt solutions to the matrix, such as NaCl, renders it impossible to desalt the extracted OM by cation exchange.

Fractionation techniques used in this study which fit into the second group are size exclusion chromatography (SEC), ultrafiltration, and separation into humic and fulvic acids by precipitation of humic acid at low pH. In these cases fractionation occurs based on physical and chemical properties of extracted and freeze dried OM, such as molecular size or solubility. These properties can be influenced by the chemical environment applied, e.g changing the pH alters the surface charge of OM and its solubility.

4.3.1. Size exclusion chromatography

4.3.1.1. Factors influencing the choice of SEC mobile phase

The mobile phase used for OM separation by SEC has to fulfil certain requirements to be suitable for metal analysis by ICP-MS and characterisation of OM. The requirements limit the choice of mobile phase, as outlined in table 4.1. In order to maintain solubility of NOM derived from soil in SEC fractionation it is necessary to maintain a high pH. For example,

at a pH of 5 or below there is a risk of precipitation of humic acid components. In other work this has been achieved by use of high pH buffer solutions or alkali mobile phase (Zhang *et al.*, 1997; Graham *et al.*, 2000; Sadi *et al.*, 2002; Trubetskaya *et al.*, 2011). Studies of OM fractionation often focus on dissolved organic matter (DOM) or fulvic acid fractions to avoid issues of insolubility. Organic matter characterisation techniques are sensitive to the presence of inorganic components in samples for analysis. It is therefore desirable, and often necessary, to have purified organic substances for analysis. The characterisation techniques employed in this study (FTIR, NMR, UV/vis) are all affected by the inorganic matrix of a sample being analysed. Analysis by ^{1}H NMR is further complicated by the resolution of sample spectra being decreased by any addition of protons. This limits the use of any solvents which are not deuterated in NMR analysis. For these reasons, it is necessary to de-salt and freeze dry OM before direct analysis (e.g. by FTIR) or re-dissolution in a suitable solvent.

Table 4.1. Factors influencing choice of SEC mobile phase

Requirements	Reasoning	Outcome
i) Mobile phase must keep as much OM as possible in solution	If OM does not remain in solution it may precipitate and block the column	High pH aqueous solutions or some organic solvents should ensure all extracted OM remains in solution
ii) Mobile phase must be suitable for inorganic analysis by ICP-MS and for OM characterisation	ICP-MS is used to identify fractions where U and other metals accumulate and organic matter characterisation techniques are applied to investigate the properties of OM in these fractions	ICP-MS analysis requires a matrix with low concentration of dissolved solids. Analysis of organic matrices requires specialist hardware in order to be resistant to the organic chemicals and to tolerate the high levels of soot that can build up. Organic characterisation requires samples to have low inorganic concentration and low additions of organic contaminants. This is best achieved by removing the sample from the matrix.
iii) It must be possible to remove the sample from the solvent	Characterisation requires a pure, dry OM sample	This is best achieved by removing the solvent by freeze drying. Aqueous inorganic solvents must be de-salted before freeze drying. Organic solvents, like DMSO, which keep as much OM as possible in solution tend to be harder to remove by freeze drying.
iv) It must be possible to de-salt the sample with minimal sample alteration	De-salting an aqueous sample renders it suitable for freeze drying to obtain a pure OM sample.	As is shown in figure 4.1, dialysis causes the loss of small organic components. Cation exchange does not have the same associated issue, therefore it is the preferable method of desalting collected fractions
v) Must be suitable for de-salting by cation exchange	Cation exchange is an effective and simple method of de-salting with minimal sample alteration	Buffer solutions or salt solutions containing anions other than OH^- are not suitable for cation exchange as there is a large decrease in pH on removal of cations from solution to < 2. This causes OM to precipitate around the cation exchange resin.
vi) Must not affect the behaviour of metal analytes of interest in solution.		Extreme pH or ionic strength conditions affect the behaviour of U and other analytes, making it difficult to compare experiments to environmental conditions.

The use of 0.1 M NaOH as the SEC mobile phase fulfils the requirements i) – v) in table 4.1, however, high pH is known to impact the speciation and mobility of metals in solution (e.g. Waite *et al.*, 1994) (section 4.7). With the use of solutions below pH 5 there is the risk and that OM will precipitate in the column. This highlights one of the fundamental challenges involved in combined OM and metal analysis: maintaining samples in a form which can be fractionated and analysed while also maintaining experimental conditions relevant to the environment.

4.3.1.2. Finalised SEC methodology for analysis of OM and metals

The type of gel and mobile phase used, column dimensions, flow rate, analyte concentration and other variables can have large effects on the sample elution profile. In this study Sephadax gel G75 was used, with 0.1 M NaOH as the mobile phase. A column length of 35 cm was used as this resulted in good separation. Columns of shorter length (25 cm) did not achieve good separation, while using a longer column length (50 cm) did not significantly improve separation and significantly increased elution time and dilution of the eluting sample. Elution from the column and addition of mobile phase to the top of the column was controlled with a peristaltic pump (Minipuls 2, Gilson) which maintained a constant flow rate of 2 ml min^{-1}. A glass column with internal diameter 2.5 cm was carefully stoppered with glass wool and the gel was added and allowed to settle for 24 hours. The elution profile of the sample was measured at 254 nm using a UV/Vis spectrophotometer (Spectraseries UV100, Thermo Separation Products) before being retained by a fraction collector (FC 204, Gilson) which collected 5 ml fractions in acid-washed glass test tubes. The elution profile of the system was highly reproducible. Figure 4.2 shows 22 runs of an OM solution (approx. 1000 mg L^{-1}) extracted from the NE core B 0 – 5 cm sample.

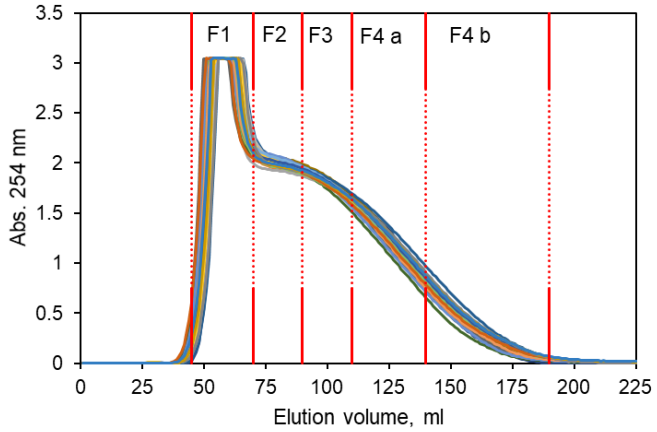

Figure 4.2. Twenty-two SEC elution profiles (measured by absorbance at 254 nm) of OM extracted from the NE core B 0 – 5cm sample (2.5 ml, 100 mg l^{-1} in 0.1 M NaOH). The red lines indicate the 5 fractions (F1 – F4b) which were used in OM characterisation experiments.
(Sephadex G75, 35 cm length, 2 ml min^{-1} 0.1 M NaOH)

The reproducibility achieved in this study was very good and results of fractionation, including elution profiles of OM and metals, are comparable to those obtained in other studies using both column gel chromatography (Trubetskoj *et al.*, 1997; Trubetskoj, Hatcher and Trubetskaya, 2010; Trubetskaya, Shaloiko, *et al.*, 2011) and HPLC-SEC techniques (Conte and Piccolo, 1999; Sadi *et al.*, 2002; Laborda *et al.*, 2008). The large peak eluting at around 40 – 70 ml is the largest OM which is followed by a tail of OM decreasing in size with increasing elution volume. For OM characterisation experiments the OM was initially divided into four fractions F1, F2, F3 and F4. In later experiments, the smallest fraction was divided further into two fractions F4 a and F4 b, as can be seen figure 4.2. The fractions were chosen based on the elution profile and early results of UV/vis analysis.

Size exclusion chromatography can be calibrated by use of model compounds of known molecular weight to define the mass range of components eluting at a particular elution volume. However, the complexity of OM means it is difficult to choose appropriate model compounds for comparison. In this study, the separation of the OM by SEC was compared to ultrafiltration in order to ensure that good separation was achieved and to give an approximate molecular mass range for different stages of elution. Ultrafiltration of the same sample shown in figure 4.2 was carried out as described in section 2.4.3.2 to generate four fractions of decreasing size. This is shown in figure 4.3. The fractions separated by SEC

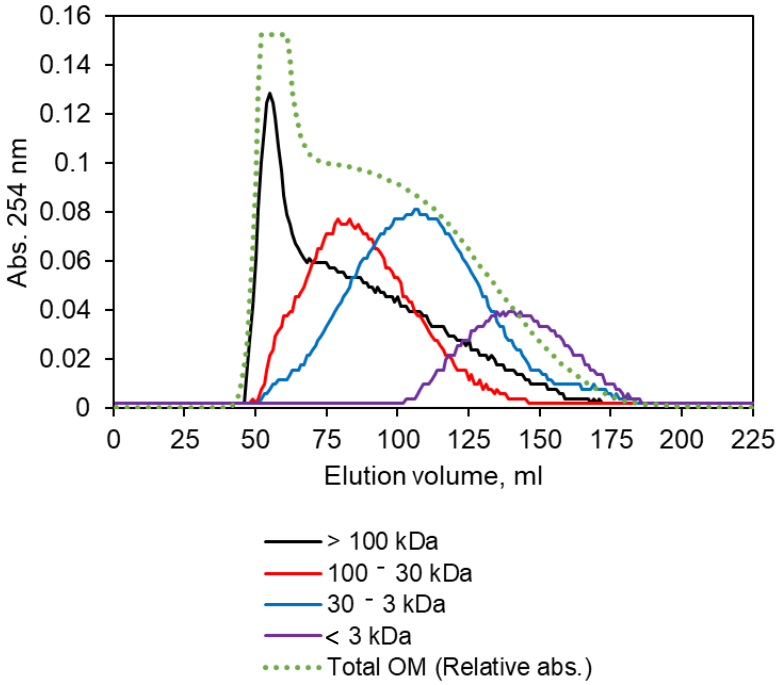

Figure 4.3. The SEC elution profiles of ultrafiltration fractions of NE core B 0 – 5 cm sample compared to the elution profile of total extracted OM of the same sample.
(Sephadex G75, 35 cm length, 2 ml min^{-1} 0.1 M NaOH)

(F1 – F4, figure 4.2) approximately correspond with the peaks of the elution profiles of the ultrafiltration fractions. It is therefore possible to use the ultrafiltration fractions to give an approximate size range to the SEC fractions (table 4.2).

Table 4.2. Approximate molecular size of SEC fractions by comparison with ultrafiltration

SEC fraction	Approx. molecular size by ultrafiltration
F1	> 100 kDa
F2	100 – 30 kDa
F3	30 – 3 kDa
F4 (a + b)	< 3 kDa

The elution profiles of the ultrafiltration fractions verify that the two methods of separating OM into size fractions are highly comparable.

4.4. Characterisation of OM separated by SEC

Organic matter extracted from depth samples of NE cores B and E, and porewater DOM were fractionated by SEC. Each OM sample was passed through the SEC column in two separate runs, with 35 mg OM dissolved in 2 ml 0.1 M NaOH each time. The column mobile phase was 0.1 M NaOH, to ensure the OM remained soluble and because it is readily removed by cation exchange, as is described in section 4.2.2. Fractions from both runs were collected, combined, de-salted by cation exchange and freeze dried to generate enough material in each fraction for characterisation. The samples fractions were characterised by UV/Vis, FTIR and 1 and 2-dimensional NMR spectroscopy techniques.

4.4.1. UV/Vis analysis of SEC size fractions

Organic matter from different depths in the NE bog profile was analysed by UV/Vis after size fractionation by SEC. The intention of the analysis was twofold: Firstly, E2:E3, E4:E6,

$S_{275-295}$ SUVA 254 and SR values were calculated from the spectra in order to draw conclusions about the character of OM in size fractions based on the reported interpretations of the parameters in the literature. Secondly, the results of UV/Vis analysis were compared with the results of NMR and FTIR analysis to verify the OM characteristics influencing the UV/Vis parameters. This helps with interpretation of UV/Vis results for similar samples, as the results of analysis of soil OM are relatively less common in the literature than those of DOM.

The analysis was undertaken on 1 mg of OM accurately weighed to 4 decimal places and dissolved in 0.01 M NaOH to make a final solution concentration of 100 mg OM L^{-1}. The DOC concentrations (mg C L^{-1}) used to calculate the SUVA 254 were calculated using the results of C, H, N, S analysis of fractions F1 – F4 from the 15 – 20 cm sample from NE core E (section 4.4.2). The E2:E3, E4:E6, E2:E3, E4:E6, $S_{275-295}$, SUVA 254 and SR were calculated from the UV/Vis spectra (the description of these parameters is given in section 2.4.6). Freeze-dried material from these fractions was also subjected to a humic acid:fulvic acid separation and the ratio of these operationally defined sub-fractions was compared with the results of UV characterisation. The results are presented in figure 4.4. Correlations between UV/Vis parameters were calculated using the Spearman's rank correlation.

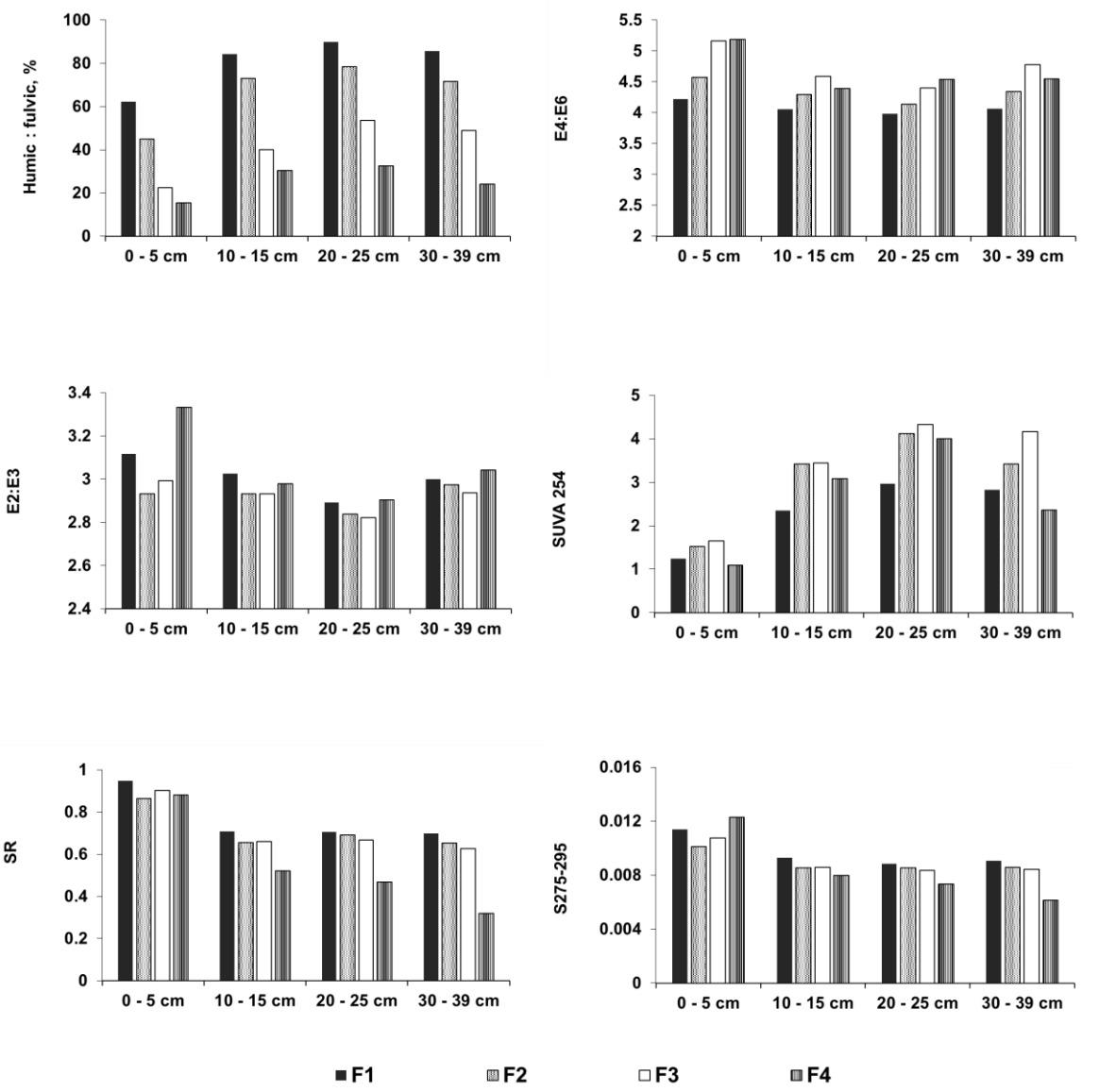

Figure 4.4. Results of UV/Vis analysis of OM in SEC fractions from 4 different depths of NE bog core B.

Consistent trends are evident in the results of UV/Vis analysis of SEC fractionated OM from different depths in the bog profile. The percentage of humic acid:fulvic acid decreases from F1 – F4, in all four samples from different depths in the bog, showing the increasingly fulvic acid character of the smaller size fractions. This is consistent with the description of the relatively large size of humic acids compared to fulvic acids. The E4:E6 ratio which is

sometimes described as the "index of humification" (Stevenson, 1982), increases from F1 – F4 and is strongly inversely correlated to the humic acid content ($\rho = 0.89$, $p = < 0.001$).

The E2:E3 ratio has its highest values in F1 and F4 for all samples and lower values in F2 and F3. This pattern is inversely correlated to the results of the SUVA 254 ($\rho = 0.76$, $p = 0.001$). The SUVA 254 and E2:E3 ratio are reported to have positive and negative correlations, respectively, with aromaticity. Therefore, these results are an indication that the F2 and F3 have greater aromatic content than F1 and F4.

The decrease in SR and $S_{275\text{-}295}$ from F1 to F4 in three out of four samples is in agreement with the results of Helms *et al.*, (2008) who recommend the use of $S_{275-295}$ as an indicator of molecular weight. The E2:E3 ratio shows a poor relationship with molecular weight, suggesting that molecular weight is not a major influence on this parameter, and that aromaticity is more important. This is in agreement with Helms *et al.*, (2008) who found a poor relationship between E2:E3 and molecular weight. This is clarified and expanded in the results of ^{1}H NMR analysis (section 4.4.4).

The consistent trends seen in the results of analysis of samples from different depths in the bog, e.g. the decrease in humic:fulvic ratio seen in F1 – F4 in all four depth samples, highlights the reproducibility of SEC as a method of OM fractionation.

There are also trends seen in different fractions with depth in the profile. For example, the SUVA 254 of F1 in each of the 0 – 5, 10 – 15 and 20 – 25 cm samples increases with depth. This is indicative of an increase of aromaticity with depth, as was seen in the analysis of total OM samples in section 3.4.1.2. The same increase with depth is seen in each of the other fractions, F2, F3 and F4 from the 0 – 5 cm sample to the 20 -25 cm sample. This shows where the sample originated in the depth profile influences the character of the OM in separated SEC fractions.

The results show that the fractionation by SEC was effective at separating OM with different properties and that the results are reproducible with different samples. The origin of the sample within the bog depth profile as well as the separation by SEC influences the results of UV/Vis analysis.

4.4.2. Elemental analysis of OM in SEC fractions

The C and H concentration of OM in SEC fractions from NE core E 20 – 25 cm sample was analysed uisng an elemental analyser (Carlo Erba NA 2500). The results were used to calculate the H/C ratios, presented below (figure 4.5).

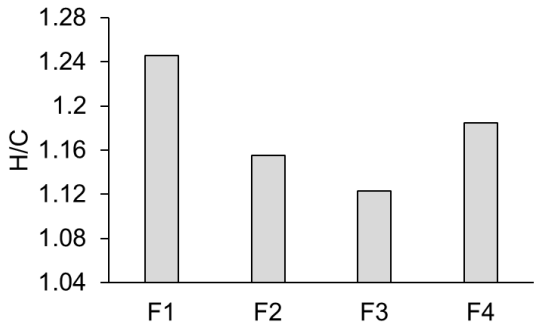

Figure 4.5. H/C ratios of SEC fractions F1 – F4 for OM from NE core E, 20 – 25 cm.

The results of elemental analysis show a lower H/C ratio in F2 and F3 compared to F1 and F4. A lower H/C ratio is indicative of increased aromaticity (Rice and MacCarthy, 1991). This suggests higher aromaticity in F2 and F3, a result which is in agreement with the analysis of SEC fractions by UV/Vis spectroscopy (section 4.4.1).

4.4.3. FTIR analysis of SEC fractions

Isolated SEC fractions were analysed using FTIR in two ways. Fractions separated from NE core B 0-5 cm sample were analysed by transmission FTIR using the KBr pellet method (section 2.4.7.1) while SEC fractions from 3 depths in NE core E were analsyed using FTIR-ATR. Samples from NE core B were fractionated into 4 fractions, (e.g. section 4.3.1) while samples from NE core E were separated into 5 fractions, with the smallest fraction divided into F4a and F4b, as described in figure (4.2).

The results of analysis of fractions of the NE core B 0 – 5 cm sample separated into 4 fractions by SEC and analysed by transmission FTIR are presented below, in figure 4.6.

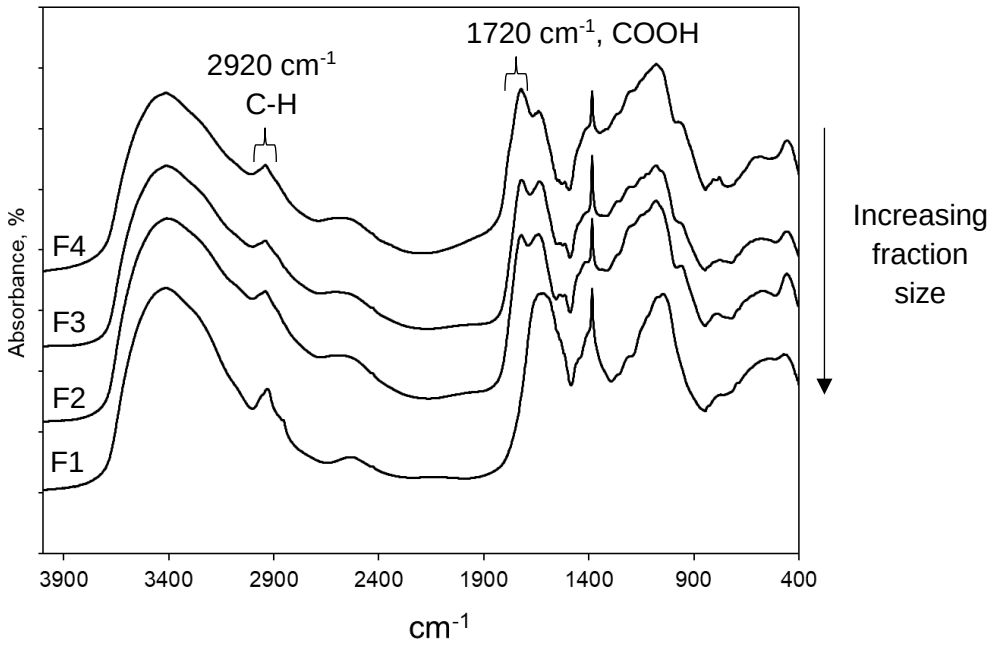

Figure 4.6. Transmission FTIR spectra of SEC fractions F1 – F4 of the NE core B 0-5 cm depth sample.

Figure 4.6 shows the transmission FTIR spectra of SEC fractions from NE core B, 0-5 cm depth. Two changes are obvious in the spectra from F1 – F4. Firstly, the sharp peak at 1720 cm^{-1} decreases in intensity from small to large SEC fractions (F4 – F1) and is not present at all in the largest fraction (F1). This shows the presence of carboxylic acids in the smaller size fraction OM. The second major spectral change is the increase in prominence of the peak at 2920 cm^{-1}, due to the C-H stretch of methyl groups, with SEC size fraction. This is indicative of increased amounts of aliphatic chain structures in the largest size fraction which decreases to the smallest fraction.

Figure 4.7 shows the results of FTIR-ATR analysis of SEC fractions from the 5 – 10 cm depth of NE core E. The spectra were obtained by FTIR-ATR and then had an ATR correction applied (Essential FTIR, Operant LLC, Virginia USA) for ease of comparison to the results of transmission FTIR analysis. The smallest fraction is divided into F4a and F4b, giving a total of 5 fractions.

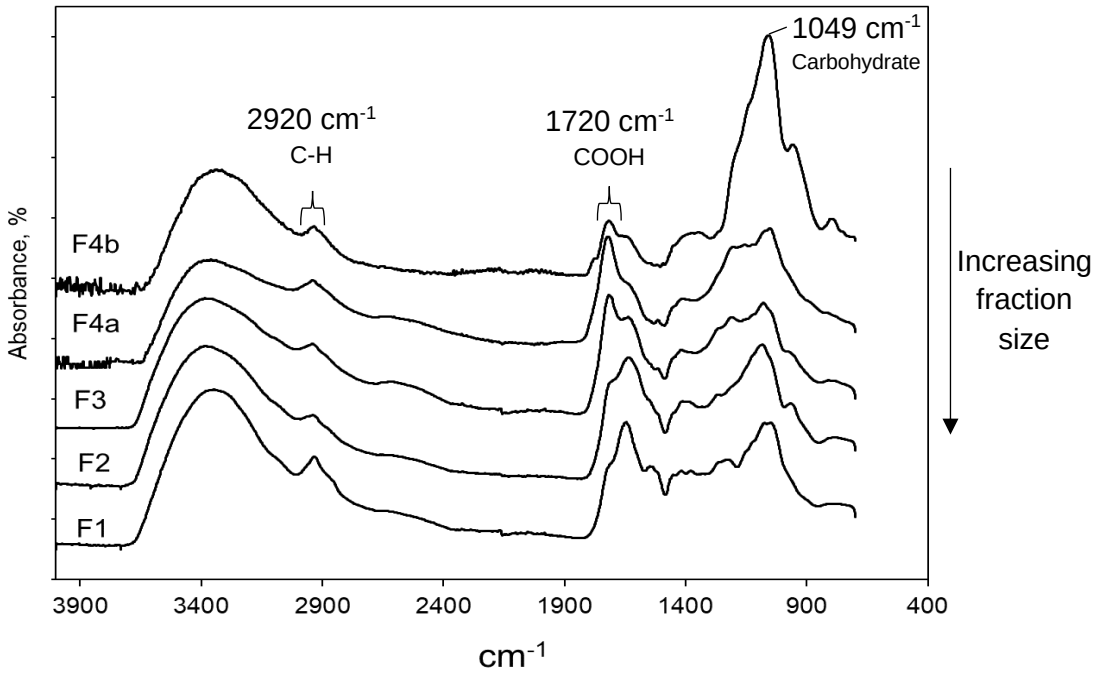

Figure 4.7. FTIR-ATR spectra of SEC fractions F1 – F4b of the NE core E 5-10 cm depth sample.

In the results of analysis of OM in SEC fractions by FTIR-ATR, in figure 4.7, the increase of the peak at 1709 cm^{-1} and decrease of the peak at 2920 cm^{-1} with decreasing fraction size from F1 – F4a is evident. This is similar to the result observed in figure 4.6, however in this case a further difference is seen due to the splitting of F4 into two fractions, F4a and F4b. The smallest fraction, F4b, shows a considerable increase in the peak at 1049 cm^{-1}, which is caused by the absorbance of carbohydrate OM. This is also seen in other samples from different depths of the same core (NE core E) fractionated by SEC and analysed by FTIR-ATR, shown in figure 4.8.

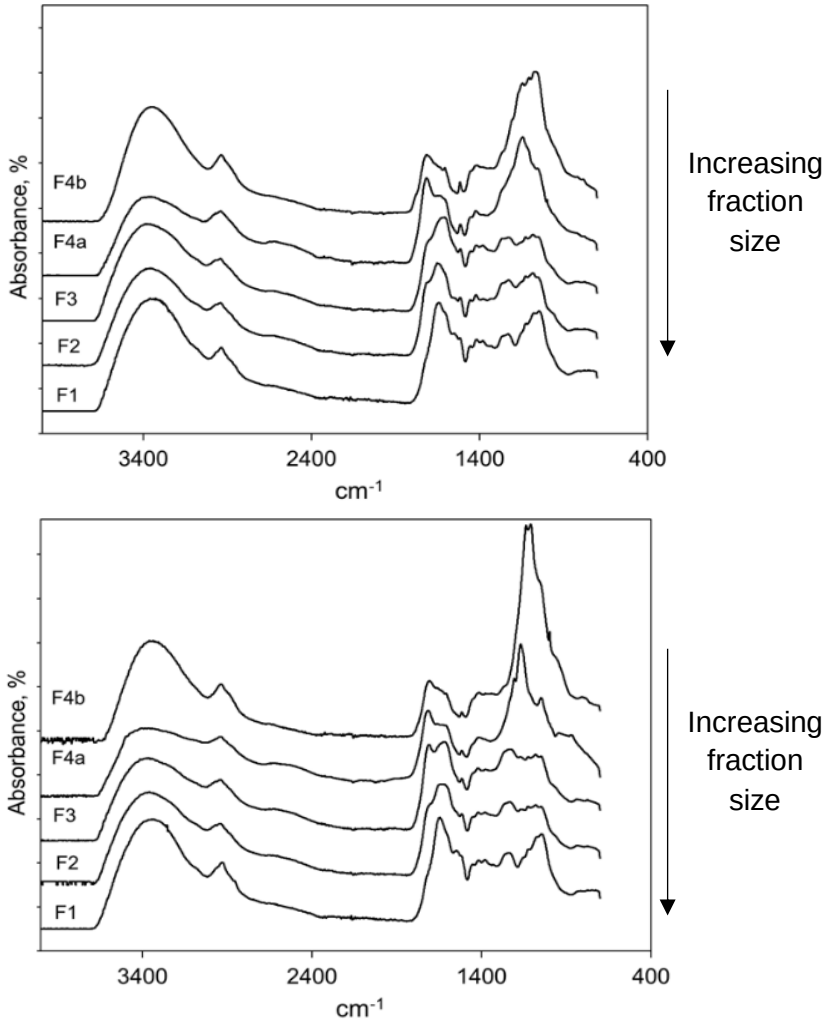

Figure 4.8. FTIR-ATR spectra of SEC fractions F1 – F4b of the NE core E 25 - 30 cm (top) and 40 – 45 cm (bottom) depth samples.

The smallest fraction, F4b, from the 25 – 30 and 40 – 45 cm depth samples of NE core E shows a more pronounced peak at 2920 cm^{-1} than F2 – F4a in each case. This suggests that there is an increase of aliphatic CH_2 in F4b with increased depth.

Overall, the most significant features of the FTIR spectra are the increase in carboxylic acid from F1 – F4a, the increased amount of aliphatic CH_2 in F1 and the large amount of carbohydrate OM in F4b, indicated by the peak around 1049 cm^{-1}. The relationship of these results with those of NMR and UV/Vis are discussed in section (4.4.5).

4.4.4. NMR analysis of SEC fractions

Size exclusion chromatography fractions from NE cores B and E were analysed by ^{1}H NMR and integrated to measure the proportion of ^{1}H in four major regions: aromatic, carbohydrate, functionalised aliphatic and unfunctionalised aliphatic. Closer inspection of the spectra also reveals information which is not evident from looking at the integrals alone. 2D NMR methods, COSY (correlation spectroscopy) and HSQC (heteronuclear single quantum coherence spectroscopy), helped to deconvolute overlapping peaks within the complex mixture to further investigate differences between the largest and smallest OM fractions. The analysis of SEC fractions from NE core B were carried out by weighing approximately 12 mg of extracted sample from four depths in the core and dissolving in 600 µL 0.05 M NaOD (deuterated NaOH). The integration of regions of the ^{1}H NMR spectra show the relative proportion of different components of the OM in each SEC fraction. Figure 4.9 shows the relative proportion of ^{1}H in each integrated NMR region for OM in SEC fractions. The samples originated from four depths in NE core B.

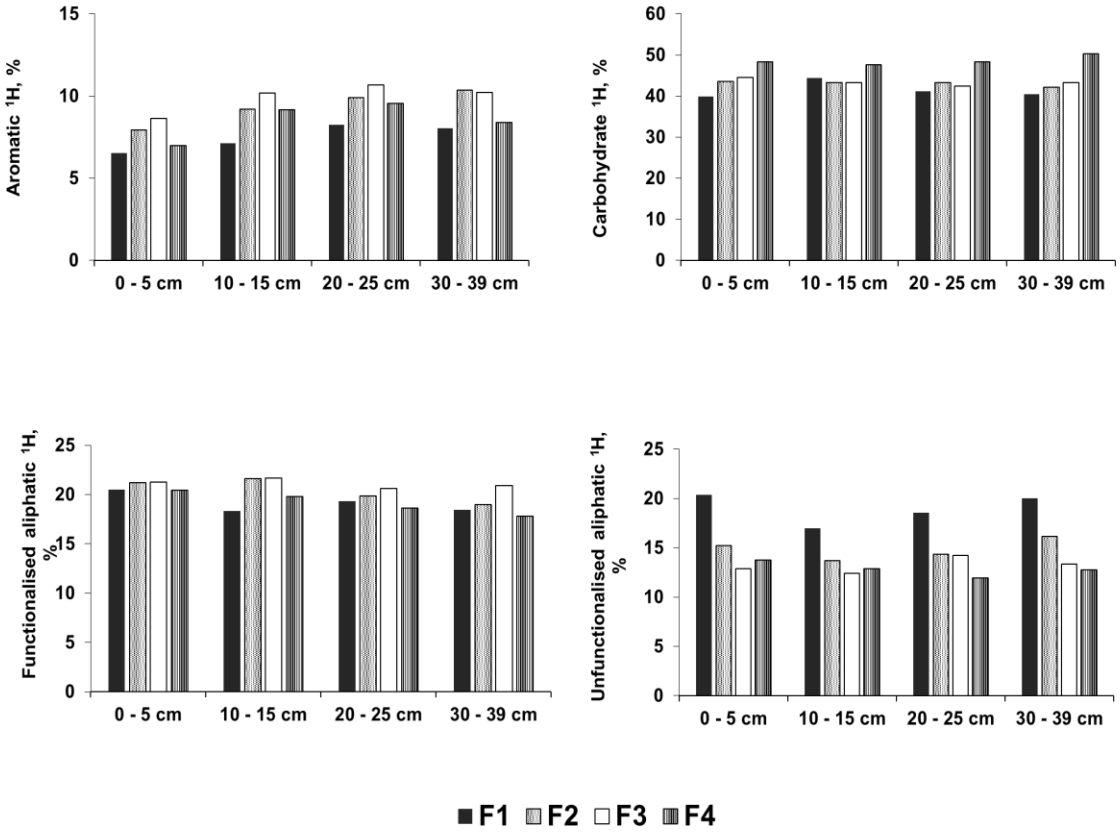

Figure 4.9. Relative intensity of integrated regions of the ^{1}H NMR spectra of SEC fractions, F1 – F4, of depth samples from NE core B.

There are consistent trends in each integral region between the samples from different depths. The content of aromatic ^{1}H is relatively low in F1 and F4 and higher in F2 and F3, with the highest value in F3 in three out of four samples. The carbohydrate region is lowest in F1 and highest in F4, with the intermediate fractions being more variable. Finally, the unfunctionalised aliphatic component of the OM is highest in F1 relative to the other fractions. The results of the analysis of SEC fractions were compared by ANOVA using Minitab statistical software (e.g. the aromatic region for all four F1 depth samples compared to the aromatic region for all four F2 samples). The statistical comparison shows significant differences between the fractions in all four NMR integrated regions ($p < 0.05$).

Organic matter extracted from four depths of NE core E were separated into 5 fractions by SEC which were analysed by ^{1}H NMR. Splitting F4 into two fractions (F4a and F4b) decreased the total amount of OM available for analysis, so only around 5 or 6 mg was available for NMR analysis, however the results of integration of NMR spectra measured on lower OM concentration are still comparable, as long as the spectra are of good quality, as it is only a semi quantitative method of analysis. As in the results of FTIR analysis, there are clear differences between F4a and F4b, as can be seen in figure 4.10

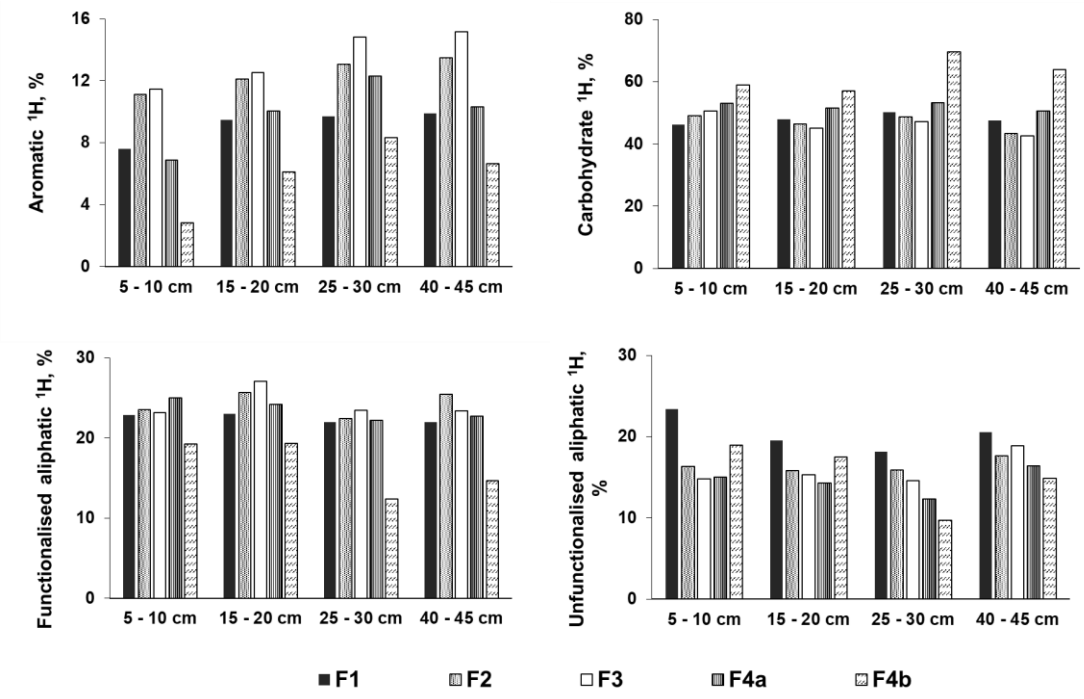

Figure 4.10. Relative intensity of integrated regions of the ^{1}H NMR spectra of SEC fractions, F1 – F4b, of depth samples from NE core E.

The results of ^{1}H NMR analysis of NE core E are very similar to those of NE core B, with an increase then decrease of aromatic ^{1}H from F1 – F4b, overall increase of carbohydrate from F1 – F4b, variable functionalised aliphatic region and decrease in unfunctionalised aliphatic material from F1. The main differences seen in the smallest fraction, F4b, compared to F1 – F4a is the very low aromatic component and very high carbohydrate component.

Important results from the analysis of integrals from both sets of SEC separated OM are the relatively low concentration of aromatic ^{1}H in in the largest fraction, F1, and the inversely high concentration of unfunctionalised aliphatic material in the same fraction. The mid, F2 and F3, are relatively high in aromatic OM and the smallest fractions, F4a and F4b, are low in aromatic material with a large increase in carbohydrate OM from F4a to F4b.

Closer examination of the ^{1}H NMR spectra reveals further information which is not evident from looking at the integrals alone. The spectra for SEC fractions from NE core E, 15 – 20 cm are shown in figure 4.11, with specific peaks within the aliphatic region highlighted in the expanded region underneath the full spectra.

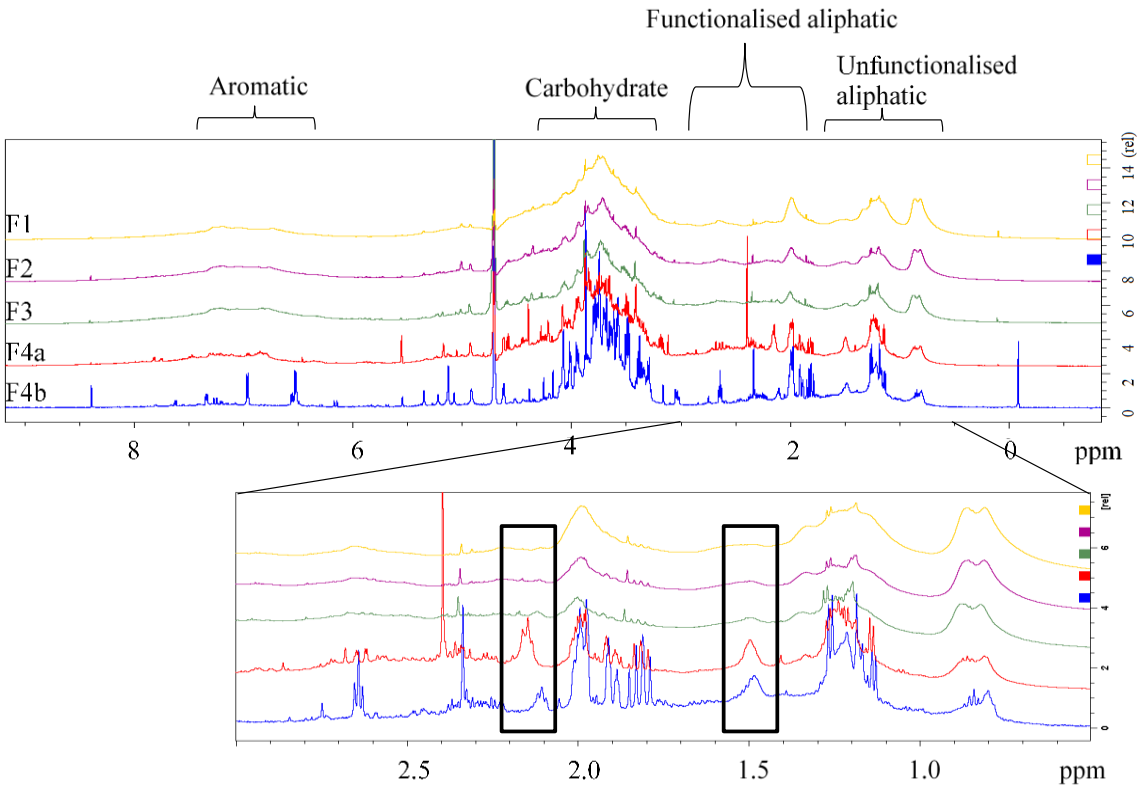

Figure 4.11. ^{1}H NMR spectra of OM from NE core E, 15 – 20 cm separated into SEC size fractions. Black boxes highlight peaks in the expanded view which are discussed below.

Changes in the intensity of integrated regions between SEC fractions can be seen in the spectra in figure 4.11, but other variations between fractions are also evident. Firstly, the smaller fractions have many sharp peaks, while the early eluting fractions have relatively smooth spectra. Peak broadening can occur as molecules aggregate, for example by H bonding, while small molecules exhibit many sharp peaks. The high intensity of the carbohydrate region of F4b and small aromatic region are clear from the comparison of the spectra. Also, the decrease in unfunctionalized aliphatic material from F1 – F4b can be attributed to the decrease in the large peak at around 0.8 ppm, which is identified as methyl, mainly from peptide by Simpson *et al.*, (2011).

The expanded section of figure 4.11 shows the aliphatic region of the spectra from around 3.0 to 0.5 ppm. Within this region it is possible to see the appearance of peaks from F1 to

F4a and 4b, highlighted by the black boxes. These two peaks match the chemical shifts of peaks identified by Simpson *et al.*, (2011), as methyl groups positioned β (around 2.1 ppm) and γ (around 1.5 ppm) to COOH groups. The γ methyl group, being further from the functional group, is located upfield on the ^{1}H NMR axis compared to the β methyl group as it is less de-shielded due to its further proximity to the strongly electronegative O atoms. This allocation is confirmed by the examination of the 2D COSY NMR spectrum, fig 4.12.

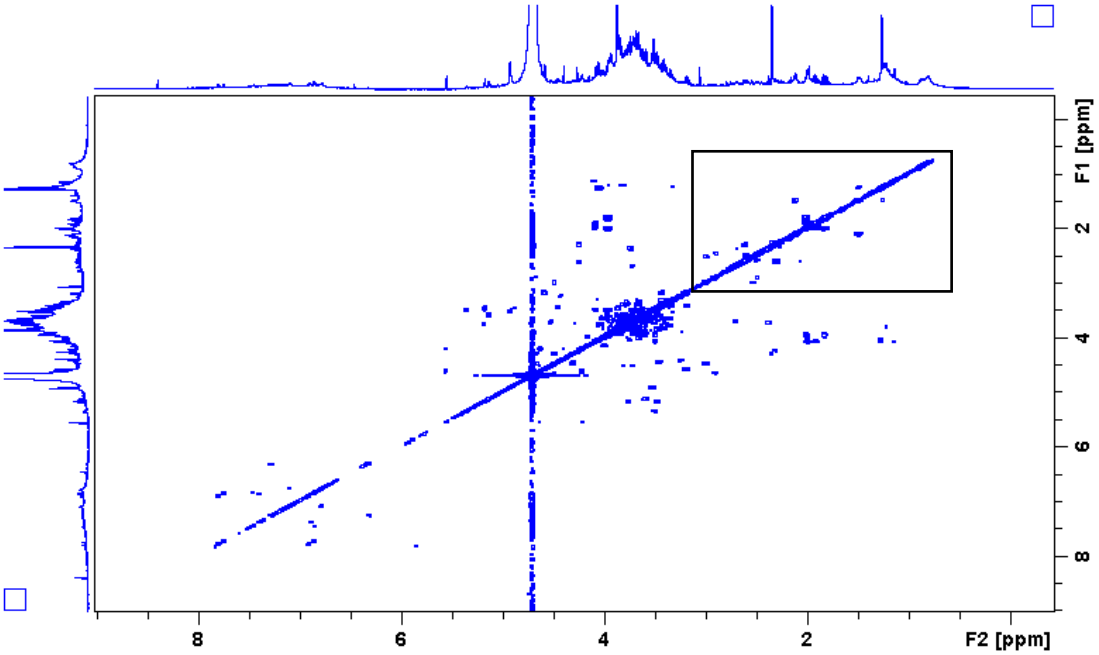

Figure 4.12. 2D COSY NMR spectrum of OM from NE core B, 10 – 15 cm F4 (smallest size fraction). The black box indicates the region expanded in figure 4.13.

Peaks on the COSY spectrum arise when protons have spin-spin coupling, indicating they are spatially close to one another on a molecule, usually within around two or three bonds distance. COSY NMR is useful for indicating which peaks in complex spectra are linked, thereby helping to identify functional groups due to the increase in intensity of peaks related to protons occupying different positions around the functional group. Model compounds of known structure can be used to identify regions of the COSY spectra related to particular functional groups or compound classes (Hertkorn, 2006). The box in figure 4.12 indicates a region of the spectrum which is expanded in figure 4.13.

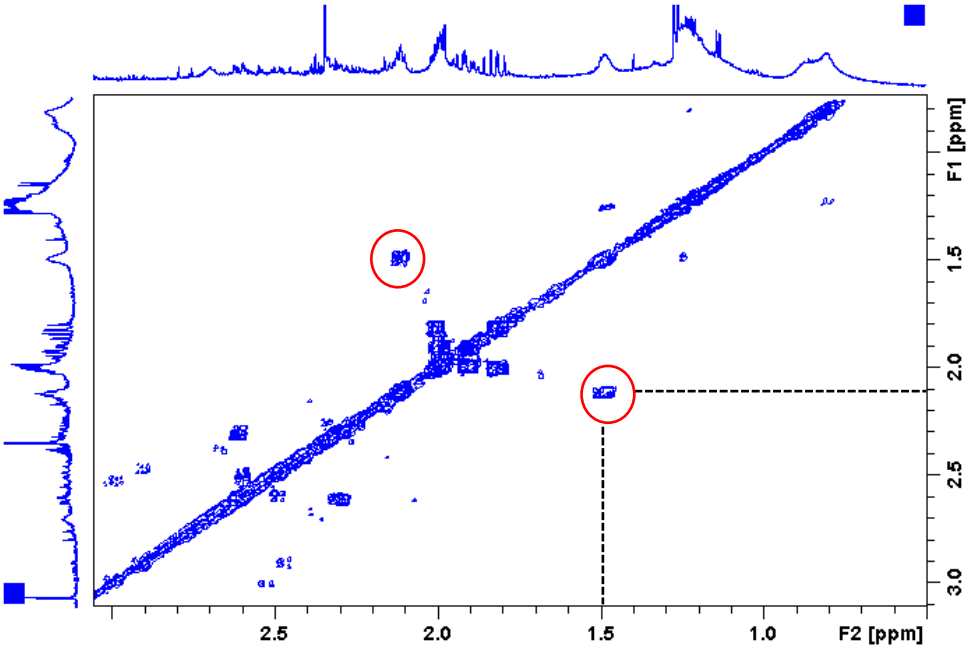

Figure 4.13. Expanded section of 2D COSY NMR spectrum of OM from NE core B, 10 – 15 cm F4 (smallest size fraction) seen in figure 4.12. The red circles indicate the cross peaks arising from spin-spin coupling between ^{1}H on methyl groups in β and γ position to a functional group.

The expanded region of the COSY spectrum lies within the region of intra functionalised aliphatic molecules, β to heteroatoms (Hertkorn, 2006). The peaks highlighted with the red circles are the same as those identified in the expanded section of the ^{1}H NMR spectra in figure 4.11. The fact that the peaks in the ^{1}H spectra exhibit a cross peak in the COSY spectrum shows that they are they arise due to ^{1}H in close proximity to each other and which share a functional group. This is good evidence that the identification of these peaks as methyl β and γ to COOH is correct, and the fact that the peaks only appear in the smaller SEC fractions demonstrates the higher COOH concentration in these fractions.

Further information can be obtained by using a HSQC experiment, which is a 2D NMR experiment using ^{1}H and ^{13}C nuclei. The peaks shown on a HSQC spectrum appear where a C-H bond occurs. The HSQC experiment provides greater resolution than a 1D ^{1}H NMR by deconvoluting overlapping peaks (as does the COSY spectrum). A further benefit of the HSQC experiment is the ability to distinguish C which is bonded to an odd or even number of H atoms. Groups containing CH or CH_3 are shown in the opposite phase to CH_2 groups (positive phase vs. negative phase). This can be seen in figure 4.14, showing the HSQC spectrum of the same sample seen in figures 4.12 and 4.13, F4 of bog core B 10 – 15 cm.

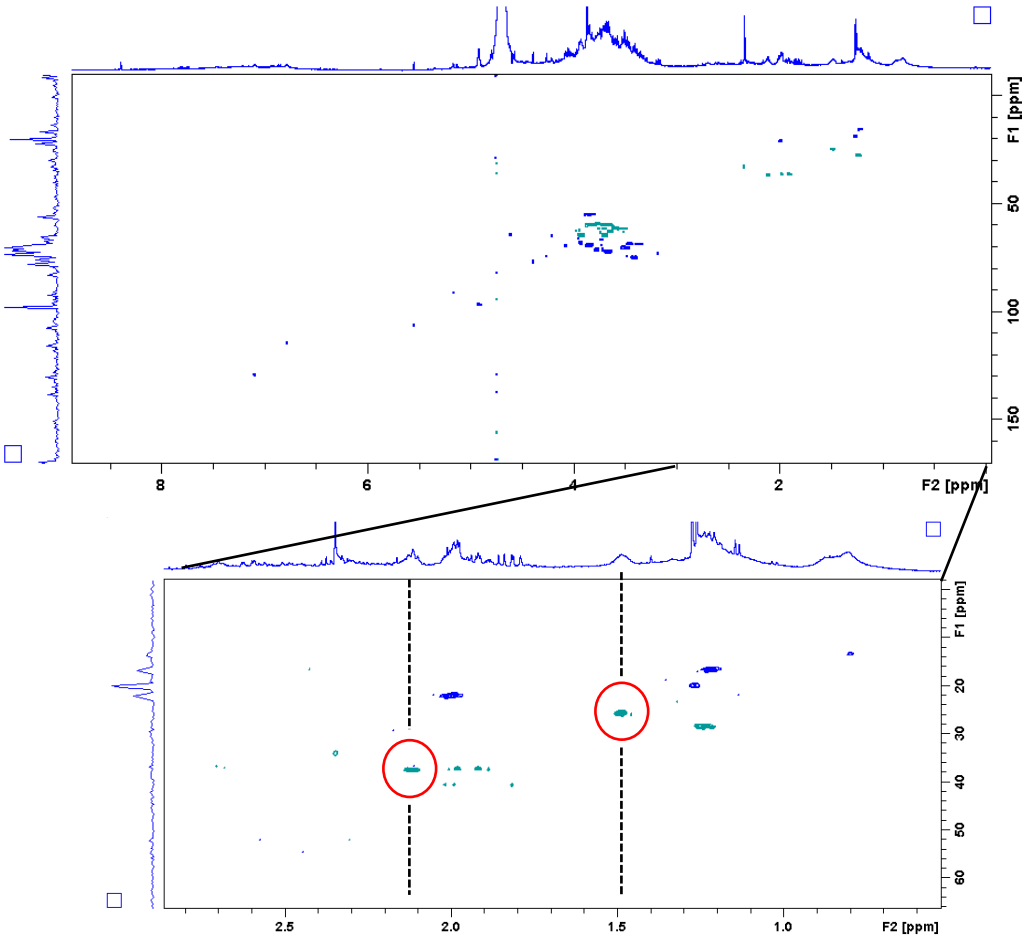

Figure 4.14. 2D HSQC NMR spectrum of OM from NE core B, 10 – 15 cm F4 (smallest size fraction) seen in figures 4.11 – 4.13. The red circles indicate the cross peaks arising from CH_2 methyl groups in β and γ position to a functional group. Negative phase peaks are coloured green (CH_2) and positive phase peaks are coloured blue (CH and CH_3).

The signal to noise ratio of HSQC spectra are limited by the low natural abundance of ^{13}C, therefore high sample concentration or large numbers of scans are required to increase signal. However, despite the relatively low intensity because of the limited sample available, there is still useful information to be gleaned from the spectrum.

In the expanded section of figure 4.14 the red circles indicate the peaks in the ^{1}H spectrum with resonances at around 1.5 and 2.1 ppm, the same peaks as are highlighted in the COSY spectrum and ^{1}H spectra in figures 4.11 – 4.13. These cross peaks fall within the aliphatic region of the ^{13}C spectrum on the y-axis (47.0 – 0 ppm, Hertkorn, 2006). The green colour of the peaks indicate that they are negatively phased, which means they arise from CH_2 groups. Combining this information with the results of the COSY analysis lends further confidence to the identification of the peaks as methyl groups with β and γ structural position to a carboxylic acid.

These cross peaks are not seen on the COSY or HSQC spectra of the largest SEC fraction (F1), indicating the increased presence of aliphatic carboxylic acid molecules in the smallest size fractions. This is in agreement with the results of FTIR analysis, which show larger peaks relating to COOH groups in the smallest SEC fractions F4 and F4a compared to F1 – F3 (figure 4.6 and 4.7, section 4.4.3). Figure 4.15 below, shows some potential structures of molecules which could give rise to the observed NMR peaks.

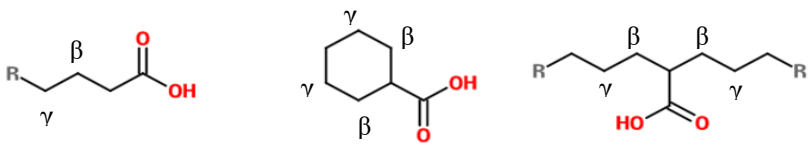

Figure 4.15. Possible molecular constituents which could be responsible for the peaks observed on 1 and 2D NMR spectra in figures 4.11 – 4.14. The CH_2 groups responsible for the peaks at ~2.1 ppm and ~1.5 ppm (on the ^{1}H spectra) are indicated by β and γ respectively.

4.4.5. Conclusions from the characterisation of SEC fractions

The analysis of SEC fractions by UV/Vis, FTIR and NMR spectroscopies shows clear evidence that OM isolated in different size fractions by SEC has very different physical structure and properties, other than molecular size. The largest fraction, F1, has the most humic character and contains larger amounts of unfunctionalised aliphatic material, indicated by the integrated region of NMR spectra and the pronounced peak at 2920 cm^{-1} in FTIR spectra. The mid fractions, F2 and F3 have the most aromatic character, first indicated by the E2:E3 and SUVA 254 UV/Vis parameters and H/C ratio and confirmed by the integration of ^{1}H NMR spectra. Finally, in the region of the smallest size fractions, F4a and F4b, the OM is over 60 % fulvic in character and has relatively high concentrations of carbohydrate, shown by NMR analysis and the peak at 1049 cm^{-1} in FTIR spectra. The small fractions also have high relative concentrations of carboxylic acid functionality, shown by the large increase in the peak at 1709 cm^{-1} in the FTIR spectra and confirmed by the appearance of coupled peaks in the 2D COSY and HSQC spectra, first identified in the ^{1}H NMR spectra.

The results can also be used to assess the influence of OM properties on the UV/Vis parameters investigated. The application of the Spearman's rank correlation to assess the similarity of results of UV/Vis and NMR analysis identifies the UV/Vis results which are linked to OM properties. As is noted in section 4.4.1, there is a strong inverse correlation between the E4:E6 ratio and the humic acid content. E4:E6 and the percent humic are also correlated with molecular weight (ρ = -0.78, and 0.84 respectively, $p < 0.001$). When the results of analysis of NMR regions are included it is clear that the SUVA 254 and E2:E3 ratio are strongly linked to aromaticity (ρ = -0.67 and 0.90, respectively, $p < 0.005$). The unfunctionalized aliphatic region is strongly correlated with molecular size (ρ = 0.88, $p < 0.001$).

4.5. Characterisation of humic and fulvic acid fractions

Humic and fulvic acid fractions separated from extracted OM from NE core E were analysed by UV/Vis and ^{1}H NMR for comparison with isolated size fractions and total OM samples. The results show considerable compositional differences between the two fractions. The results of the analysis of humic and fulvic acid fractions from all depths of NE core E by UV/Vis and NMR and are presented below (figures 4.16 and 4.17).

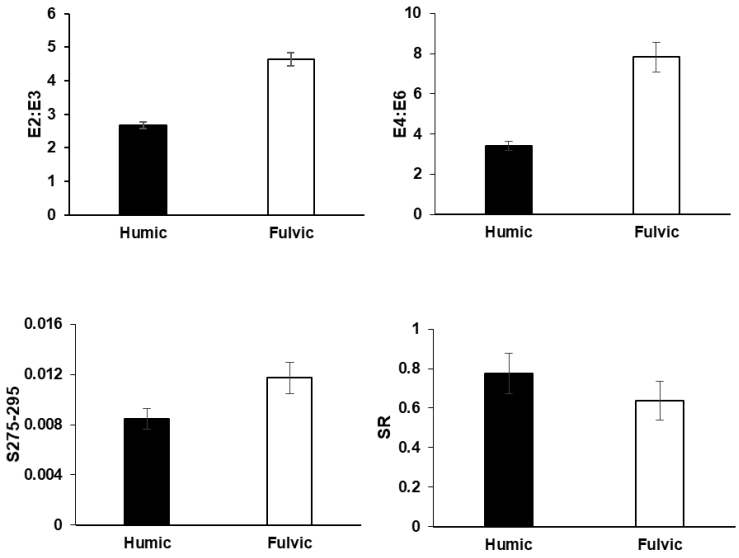

Figure 4.16. UV/Vis parameters of humic and fulvic acid samples extracted and fractionated from NE bog core E samples. Error bars show the standard deviation of 9 replicates.

The results of analysis of humic and fulvic acid fractions by UV/Vis show there are significant differences between humic acid and fulvic acid samples in all four parameters shown in figure 4.16. The E2:E3 and E4:E6 are both lower in the humic acid samples than the fulvic acid samples. These trends agree with those in the literature for the comparison of humic and fulvic acids and OM of fulvic or humic character (e.g. Stevenson, 1982; Chen *et al.*, 2011; Purmalis & Klavins, 2013). The results of the measurement of $S_{275\text{-}295}$ shows

an increase between humic and fulvic acids. This is opposite to what would be expected, as this parameter tends to decrease with decreasing molecular weight, as is seen in section 4.4.1 (Helms *et al.*, 2008). The SR shows a higher value in the humic acid samples than the fulvic acid samples as is expected based on the molecular weight of the fractions.

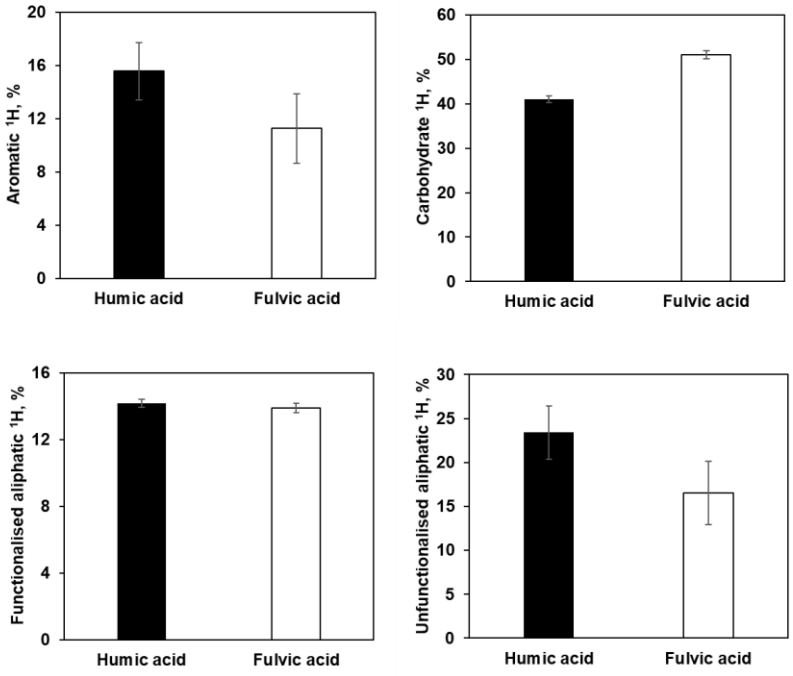

Figure 4.17. ^{1}H NMR parameters of humic and fulvic acid samples extracted and fractionated from NE bog core E samples. Error bars show the standard deviation of 9 replicates.

The results of ^{1}H NMR analysis return significant differences between humic and fulvic acids in aromatic, carbohydrate and unfunctionalised aliphatic composition ($p < 0.05$). Humic acids have higher aromaticity and unfunctionalised aliphatic content, while the fulvic acids have higher carbohydrate composition.

Comparison of these results (figure 4.17) with those of SEC of the same samples (figures 4.4 and 4.9) shows that there are similarities and differences in the two methods of OM

fractionation. The smallest fractions from SEC (F4) have the highest fulvic acid composition and, like the separated fulvic acids, have a corresponding high carbohydrate ^{1}H content.

The early eluting SEC fraction (F1) has the highest humic acid content, and, like the separated humic acid, has the highest unfunctionalised aliphatic ^{1}H content. However, the early eluting fraction does not contain the highest aromatic content, which is seen in F3 in 7 out of 8 separated samples, and F2 in the other sample. Humic acids are frequently described as having larger molecular weight than fulvic acids, and while this generality holds true in these results (early eluting fractions are more humic than later eluting fractions) the fractions isolated by SEC are not simply separated into humic and fulvic fractions. Greater separation is achieved by SEC, with intermediate eluting fractions (F2 and F3) that are neither solely humic nor fulvic acid and have high aromaticity.

4.6. Varying NaOH concentration extraction of NOM

Extractions using four concentrations of NaOH (0, 0.01, 0.1 and 1.0 M) were undertaken on depth samples from bog core E. Samples were shaken in a ratio of 1 g dried and ground soil sample to 10 ml extractant (thoroughly degassed). The samples were shaken for four hours under an atmosphere of N_2 gas. After centrifugation (8300 g, 20 minutes) and filtration (0.45 µm syringe filters) an aliquot of the solutions containing NaOH was diluted to 0.01 M (NaOH conc.) with DI water and 0.01 M NaOH, in order to be within the linear range of the UV/Vis spectrophotometer (below an absorbance of 1.5). The samples extracted with DI water had a 2 times dilution applied with DI water for the same reason. These aliquots were then analysed by UV/Vis while the remainder of the solutions were desalted by cation exchange and freeze dried. The OM recovered was then analysed by ^{1}H NMR.

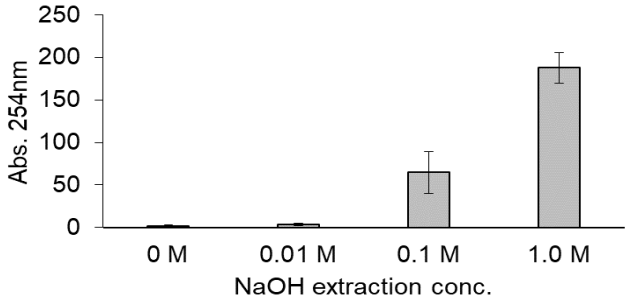

Figure 4.18. Dilution corrected absorbance at 254 nm of solutions extracted with varying concentrations of NaOH from 0 – 1.0 M. The absorbance is used as a proxy for OM concentration in solution. (Peacock *et al.*, 2014) Error bars show the standard deviation of 9 replicates.

Figure 4.18 shows the dilution corrected absorbance of the extraction solutions. The absorbance of the solution extracted with 1.0 M NaOH is over two orders of magnitude higher than that extracted with 0.0 M NaOH (DI water). The 1.0 M solution extracts up to 75 % of the total organic matter (by LOI %) as is shown in section 4.8.

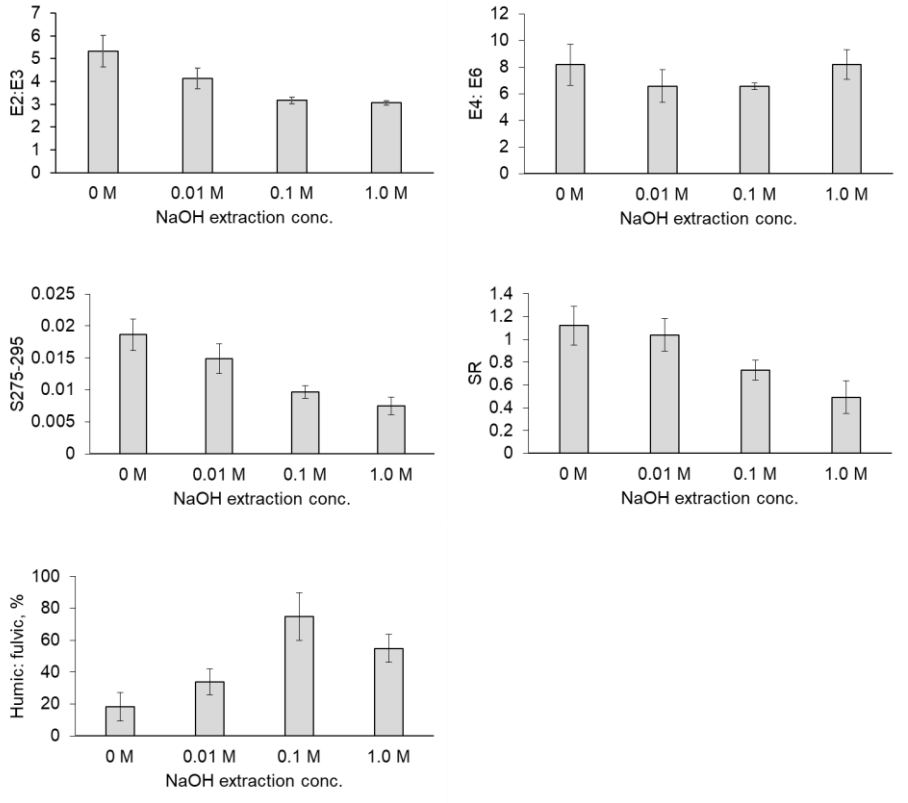

Figure 5.19. Analysed UV/Vis parameters of samples extracted with NaOH solutions of varying concentration from 0 – 1.0 M. Error bars show the standard deviation of 9 replicates.

The UV/Vis analysis parameters of the extracted solutions are shown in figure 4.19. The E2:E3, $S_{275-295}$ and SR all decrease with increasing extractant concentration. Based on the results of the characterisation of SEC fractions (section 4.4.1) these results could indicate a decrease in molecular weight or increase of aromaticity. There is no significant trend seen in the E4:E6 with different extraction solution. There is an increase in the humic:fulvic acid ratio of the samples from 0 to 0.1 M, followed by a slight decrease to the sample extracted with 1.0 M NaOH solution. This decrease in humic:fulvic acid ratio at the highest NaOH concentration is perhaps an indication that OM has been oxidised by the very high pH, despite degassing of solutions and extracting under N_2. These results point to 0.1 M NaOH as the most suitable extractant to use for its ease of desalting and lack of OM sample alteration which was potentially observed in the highest concentration extractant.

The figure below (4.20) shows the results of ^{1}H NMR analysis of the same samples.

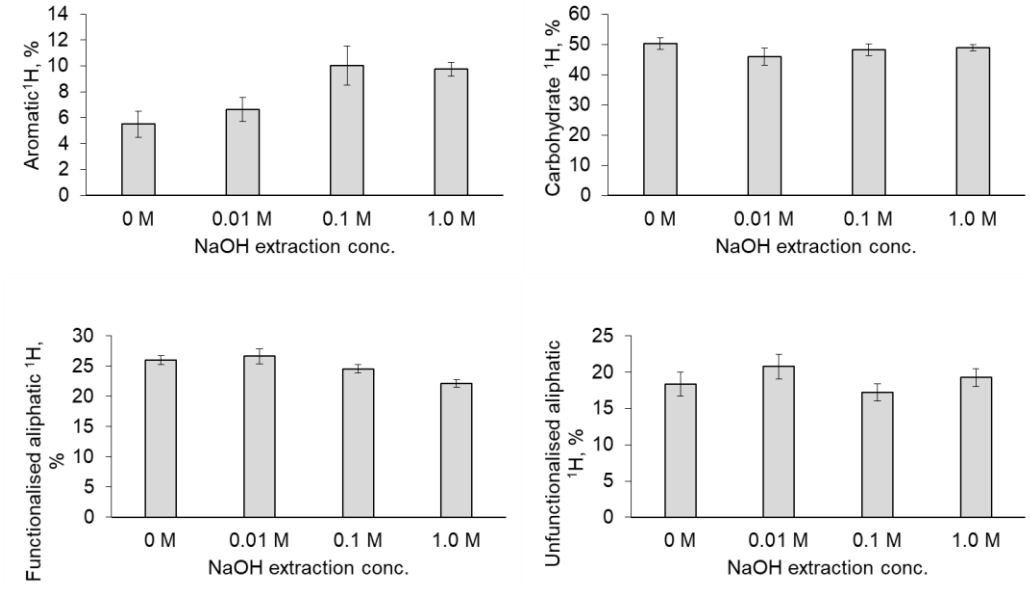

Figure 4.20. Relative intensity of ^{1}H NMR integrated regions in OM extracted with varying concentrations of NaOH, 0 – 1.0 M. Error bars show the standard deviation of 9 replicates.

Two major changes in the OM composition are evident with the increase of NaOH concentration (figure 4.20): the increase of aromatic content and decrease of functionalised aliphatic material. There is no trend in the data for carbohydrate or unfunctionalised aliphatic components.

The results of UV/Vis and NMR characterisation of OM extracted with increasing concentration of NaOH show that the higher concentration NaOH solutions are able to access pools of recalcitrant OM which is not readily extracted with lower NaOH concentrations. The material extracted by higher concentration NaOH has more aromatic character and lower amounts of functional groups.

Figure 4.21 shows the SEC elution profiles of OM extracted with different conc. NaOH. (Sephadex, G75, 35 cm, 2 ml min $^{-1}$, 0.1 M NaOH eluent).

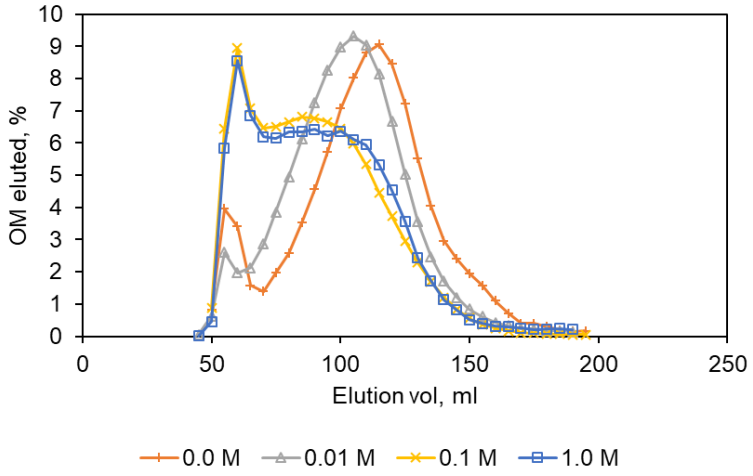

Figure 4.21. SEC elution profiles of OM extracted with 0, 0.01, 0.1 and 1.0 M NaOH, measured by absorbance at 254 nm. (Sephadex, G75, 35 cm, 2 ml min $^{-1}$, 0.1 M NaOH eluent)

The elution profiles show that the OM extracted with higher concentrations of NaOH has greater amounts of OM eluting in the large size fractions, while the OM extracted with DI water predominantly elutes in the smaller size fractions.

4.6.1. Comparison of DI water-extracted OM and pore water OM

Organic matter extracted with DI water (as seen in section 4.6) is compared with pore water OM from the Needles Eye bog. The aim of the comparison was to investigate the compositional differences and similarities in order to see whether extractions with DI water yields OM with similar properties to that found in porewater. Similarity of OM properties would suggest that extracting peat samples with DI water would be a good representation of OM and associated metals found in pore waters.

The SEC elution profiles DI water extracted OM and porewater extracted OM are presented in figure 4.22.

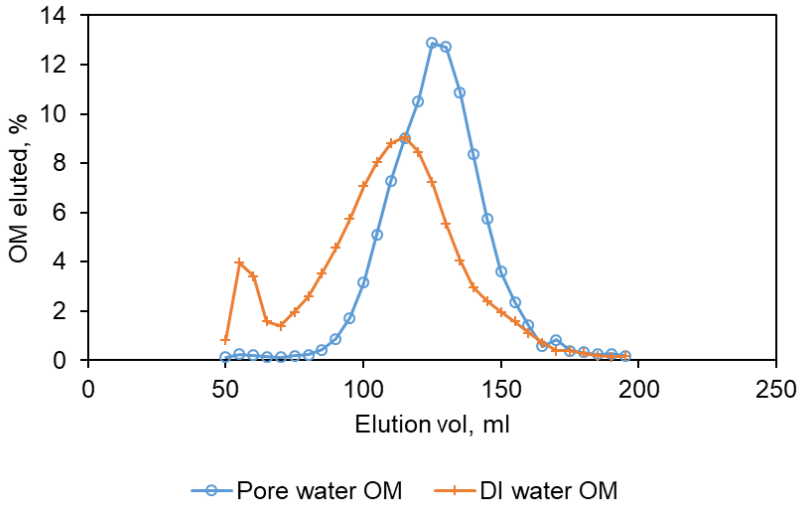

Figure 4.22. SEC elution profiles of OM extracted with DI water and OM from porewater measured by absorbance at 254 nm. (Sephadex, G75, 35 cm, 2 ml min $^{-1}$, 0.1 M NaOH eluent)

The SEC elution profiles (figure 4.22) show that the main peak of the porewater OM elution profile elutes around 15 ml after the main peak of the DI water extracted OM. The DI water extracted OM also exhibits a peak of large molecules at around 55 ml not seen in the porewater OM. This indicates that the porewater OM is composed of smaller molecules than DI water extracted OM.

The pore water OM also has compositional differences to the OM extracted with DI water, as can be seen in the ^{1}H NMR profiles shown in figures 4.23 and 4.24.

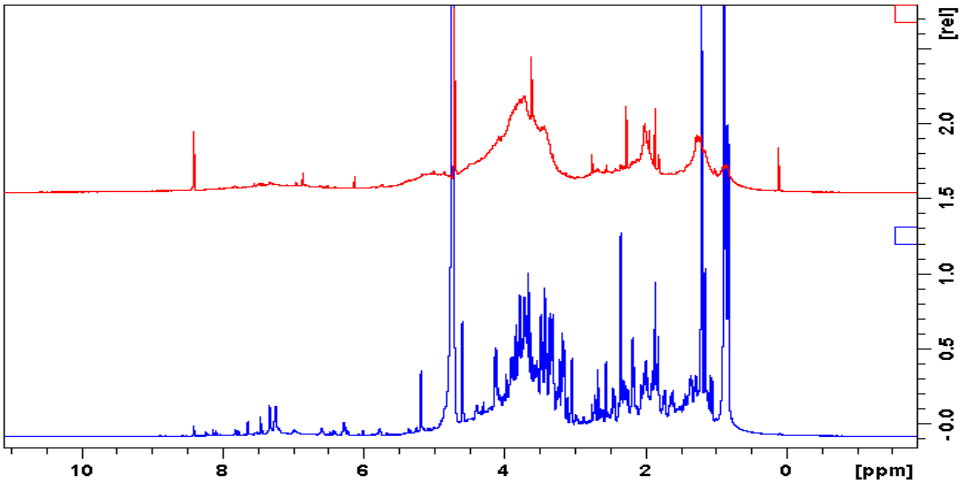

Figure 4.23. ^{1}H NMR spectra of DI water extracted OM (top, red) and porewater OM (bottom, blue) both from NE bog core E 10 – 15 cm sample.

The spectra of pore water OM and OM extracted with DI water, are shown in figure 4.23. It is evident that there are many more sharp peaks in the porewater OM compared to DI water-extracted OM, and so it clearly contains more discrete small molecules than the DI water-extracted OM.

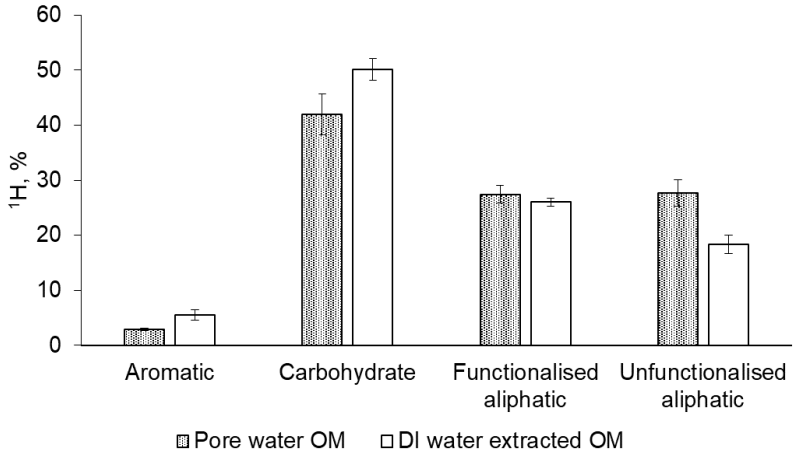

Figure 4.24. Intensity of ^{1}H NMR integrated regions in spectra of DI water extracted OM and porewater OM. Error bars show the standard deviation of 8 replicates for pore water OM and 9 replicates for DI water extracted OM.

This agrees with the SEC elution profiles of the different samples in figure 4.22 which shows that the DI water-extracted OM contains more, larger size components.

From the integrated regions of the porewater OM and water extracted OM, in figure 4.24, it is clear that pore water OM has less aromatic and carbohydrate components but a relatively higher proportion of functionalised and unfunctionalised aliphatic material. Water extractable OM has sometimes been used to represent DOC in soil (e.g. Corvasce *et al.*, 2006; Guigue *et al.*, 2014), however the results presented above suggest that there are significant differences beteen soil porewater DOC and water extracted DOC. The differences between the two types of OM could be significant when assessing the OM-facilitated transport of potentially toxic elements like U.

4.7. Analysis of metals in SEC fractions

Metals were analysed using ICP-MS in fractions separated by SEC in order to obtain results which could be interpreted alongside the results of organic matter characterisation in the context environmental mobility of U.

Two challenges encountered in the analysis of metals in SEC fractions are the dilution effect of the fractionation process and the high salt concentration of the matrix (0.1 M NaOH). Initially ICP-OES was used to analyse metals in SEC fractions as it has good tolerance for high salt solutions and is still effective with solutions of up to 10 – 30% total dissolved solids (Tyler, 2001). However, despite the high U concentration in bulk soil samples from the Needle's Eye site (section 3.2.1), after fractionation the concentrations in fractions were close to or below the LOD for the instrument of 0.39 mg L^{-1}. For this reason, ICP-MS was required. This meant, however, that the samples required a 10 times dilution to lower the concentration of NaOH before analysis. Despite the dilution stage, the increase in sensitivity with ICP-MS compared to ICP-OES meant the results of analysis of metals in SEC fractions were, for the most part, well above the LOQ (0.29 μg L^{-1}, n = 17).

Another challenge in the analysis of metals associated with fractionated OM is the harsh chemical conditions used which can alter the speciation and association of metals. Previous

work in which researchers have analysed U in SEC size fractions have yielded complex and sometimes contradictory results. Uranium has been found in different points of the elution profile in different experiments. In some cases the majority of U elutes in the region of small organic molecules close to the elution limit of the column (Sadi *et al.*, 2002), while in others the U elutes with the largest size fraction suggesting that it is bound to large organic molecules. The experiments presented below use varying SEC column conditions by changing the eluent used to investigate the effect on the association of U and other metals with OM.

Metals were analysed in SEC fractions of OM extracted using 0.1 M NaOH from four depths of bog core E. These are the same samples for which the results of OM characterisation has already been shown in section 4.4. As is described in section 4.4, the SEC column was eluted with 0.1 M NaOH in order to keep the OM in solution and for ease of de-salting prior to OM characterisation.

Figure 4.26 shows that the results for the metals analysed could be separated into two distinct groups: Fe, Mn, Pb and Cu are found in their highest concentration in the early eluting large size fraction (F1), while U, Al and As have their highest concentrations in the late eluting small size fractions (F4a and F4b). In this simplified elution profile (of only 5 fractions) none of the metals closely match the OM elution profile. The elution profiles are in agreement with other published results of experiments using HP-SEC, gel filtration SEC, asymmetrical field flow fractionation and ultrafiltration showing U and As eluting in the smaller size fractions and Pb and Fe eluting in larger size fractions (Zhang *et al.*, 1997; Sadi *et al.*, 2002; Bolea *et al.*, 2006; Bolea, Laborda and Castillo, 2010; Kozyatnyk *et al.*, 2016). However, results of other studies have shown that U is often found associated with larger size humic substances and colloidal particles in the environment (Graham *et al.*, 2000; Laborda *et al.*, 2008; Phrommavanh *et al.*, 2013; Xu, 2013). The results of these studies show that the fractionation of U in the environment is highly dependent on the local

chemical conditions. This is also seen in the results of the ultrafiltration of pore waters from the site shown in section 3.7, where the colloidal:truly dissolved U changes with depth in the bog profile.

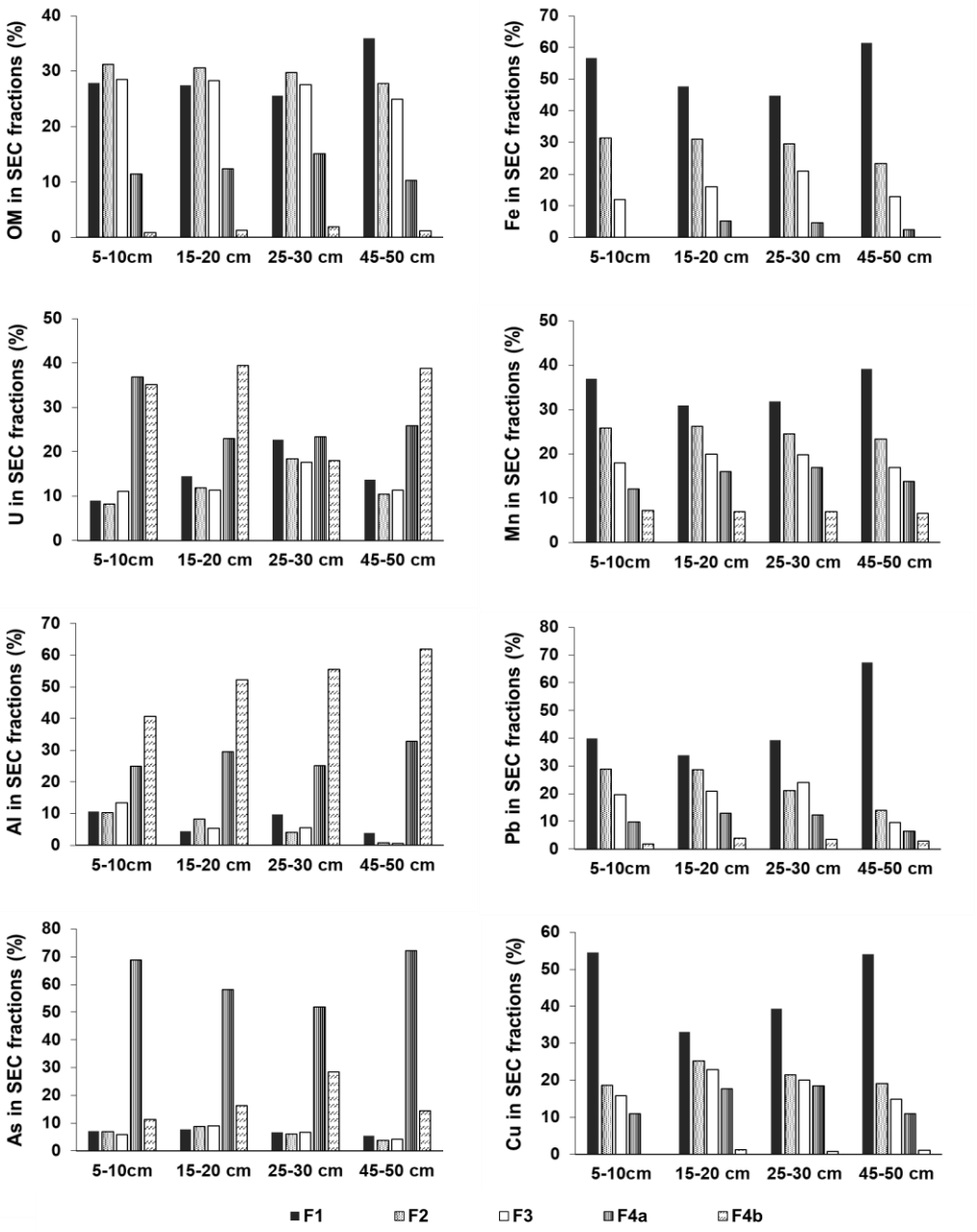

Figure 4.26 Metals in SEC fractions of 4 depth samples from bog core E analysed by ICP-MS. The column used was 35 cm length Sephadex G75 eluted with 0.1 M NaOH. Fractions were analysed directly from the column after 10 times dilution with DI water.

A further SEC experiment was undertaken in order to further investigate the association of U and other metals with NOM under different conditions.

Tests on the solubility of OM showed that it would remain in solution at pH values around neutral if it is first dissolved in 0.1 M NaOH and slowly adjusted downwards with small volumes of HCl solutions (0.01 – 0.1 M). Trying to re-dissolve OM in solutions of pH 7 leads to incomplete dissolution and addition of HCl too fast causes some humic acid to precipitate which may then not go back into solution without increasing the solution pH. By slow addition of HCl and allowing the solution to equilibrate as functional groups slowly protonate, it is possible to obtain a solution of OM which remains in solution at pH 7. By this method it is possible to carry out SEC experiments at pH 7 using DI water and NaCl solutions as the eluent. With DI water as the eluent metals can be analysed by ICP-MS and OM can be freeze dried for characterisation by NMR without the need to first de-salt the sample. The profiles below show the elution profiles of metals and OM obtained using 0.1 M NaOH, 0.1 M NaCl, 0.01 M NaCl and DI water as the column eluents. The profiles were analysed in 10 ml volume fractions. The OM used in the experiments below is from the 6 – 8 cm depth of bog core A which was extracted with 0.1 M NaOH and de-salted by cation exchange before freeze drying.

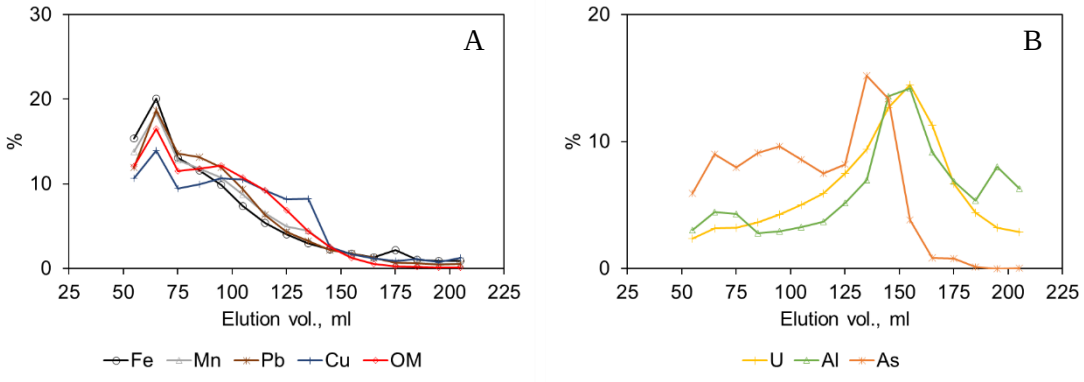

Figure 4.27. SEC elution profiles of OM and metals eluted with 0.1 M NaOH. OM elution profile measured by absorbance at 254 nm.

Sephadex G75, 35 cm length, flow rate = 2 ml min^{-1}

Three different elution profiles can be seen in the results in figure 4.27, which are in agreement with those in figure 4.26. The metals are shown on two separate axes and are grouped according to those with similar elution profiles for clarity. In figure 4.27 A it can be seen that Fe, Mn, Pb and Cu follow the elution profile of OM with early elution followed by a tail of decreasing molecular size. The profiles of U, Al and As, shown in figure 4.27 B, show some elution with large OM sizes but are dominated by elution in the small size fraction of the profile, with U and Al eluting just after the peak of As. The percentage of As in the large to medium size fraction of the elution profile (from around 50 – 125 ml) and the peak before the elution limit of the column suggests there is some interaction of As with OM or Fe oxides.

Using 0.1 M NaCl at pH 7 as the eluent changes the elution profiles (figure 4.28).

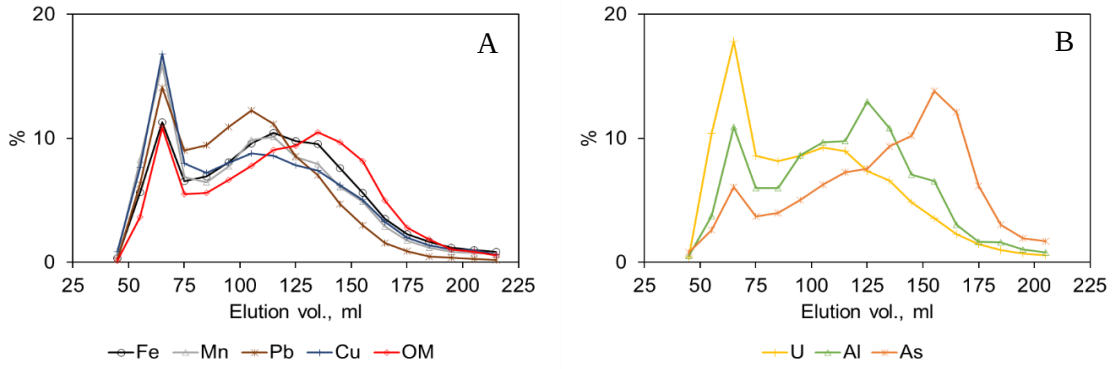

Figure 4.28. SEC elution profiles of OM and metals eluted with 0.1 M NaCl (pH 7). OM elution profile measured by absorbance at 254 nm. Sephadex G75, 35 cm length, flow rate = 2 ml min^{-1}

The elution profile of OM eluted with 0.1 M NaCl has a greater amount of OM in the tail after the peak of excluded OM. As is seen in figure 4.27 with 0.1 M NaOH as the eluent, the elution profiles of Fe, Mn, Pb and Cu are similar to that of OM. There is a major change in the profile of U, (figure 4.28 B), which much more closely follows the OM profile, with no evidence of a peak near the elution limit of the column as was seen in figure (4.27 B).

The profile of Al has also changed, being similar to the OM profile, whereas the As profile still has its major peak near the elution limit of the column.

Uranium and Pb share a secondary maximum concentration (after the main peak) at 105 ml, with a decrease which occurs before the secondary peak of OM. This shows a preference of both U and Pb for larger OM. As is shown below, in figure 4.29, this OM is dominated by humic acid character, while the later eluting fraction is predominantly of fulvic acid character. The fulvic acid content was analysed by measuring the UV/vis spectrum of the OM after acidification to pH 1 (to precipitate humic acid), centrifuging and filtering through 0.45 µm syringe filters leaving only fulvic acid in solution. The absorbance at 254 nm was compared to that of the original fraction before acidification.

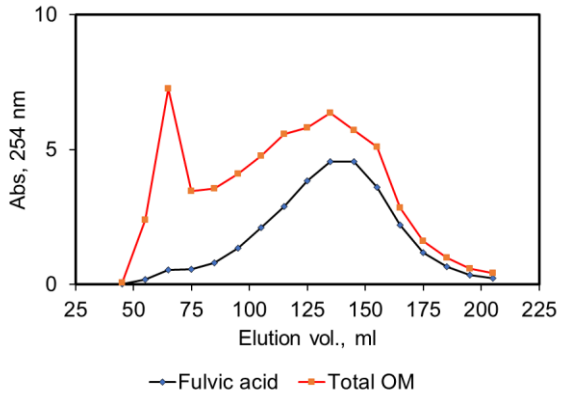

Figure 4.29. SEC elution profiles of total OM and the fulvic acid component of bog A 4 – 6 cm sample, with 0.1 M NaCl as the eluent. The elution profiles are measured by absorbance at 254 nm.

The figures below show the results of SEC fractionation using 0.01 M NaCl (figure 4.30) and DI water (figure 4.31) as the eluent.

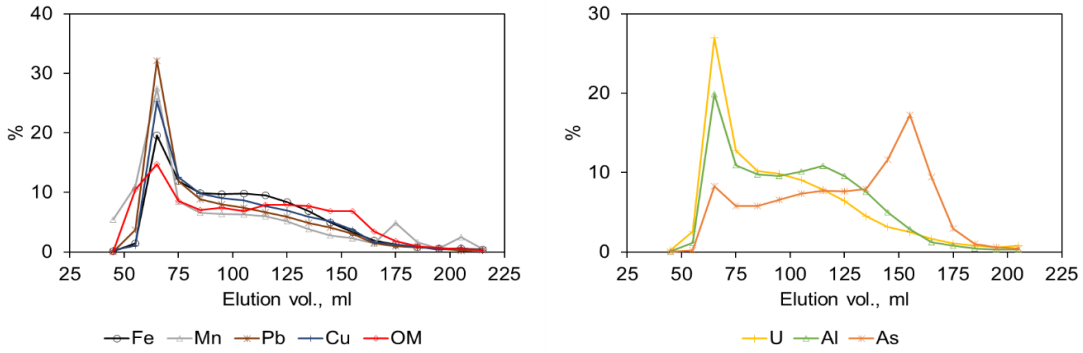

Figure 4.30. SEC elution profiles of OM and metals eluted with 0.01 M NaCl (pH 7). OM elution profile measured by absorbance at 254 nm. Sephadex G75, 35 cm length, flow rate = 2 ml min^{-1}

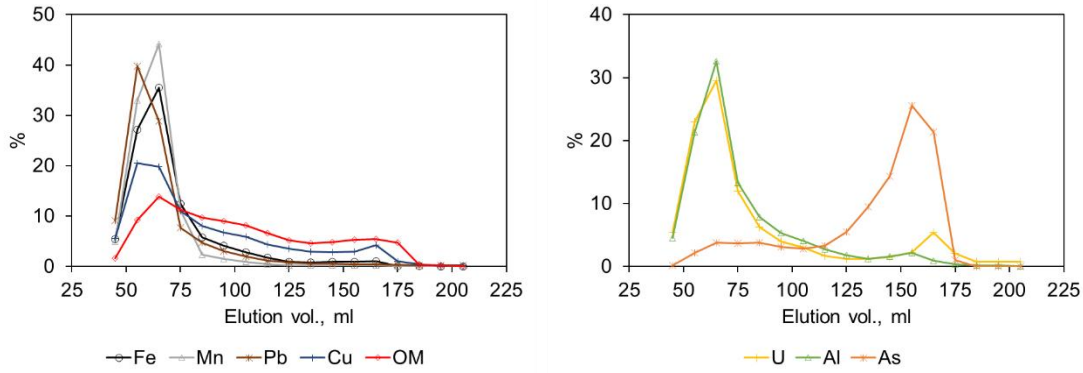

Figure 4.31 SEC elution profiles of OM and metals eluted with DI water. OM elution profile measured by absorbance at 254 nm. Sephadex G75, 35 cm length, flow rate = 2 ml min^{-1}

The profiles of the metals eluted with 0.01 M NaCl shows a continuation of the trend seen between the 0.1 M NaOH and 0.1 M NaCl, with Fe, Pb, Mn, Cu, U and Al showing affinity for the early eluting OM while As has a major peak in the small molecule size zone of the elution profile. There is a decrease in the prominence of the early eluting peak at around 65 ml in the OM elution profile and an elongation of the tail of medium to small molecular size OM.

A major change is seen in the profile of OM eluted with DI water, with a further decrease in the early eluting large molecule peak and an increase of material in the small size fractions. In this case none of the metals analysed follow the OM elution profile very closely, and all but As are associated with the large, early eluting OM. The main peak of As is still found at or very near the elution limit of the column, suggesting it is free in solution and not associated with OM. The results of analysis metal SEC elution profiles with different eluents shows the changing association of U with OM. It is associated with large size fractions at neutral pH but it appears to be dissociated from OM at high pH when 0.1M NaOH is used as the eluent.

Analysis of the OM fractions eluted with DI water by ^{1}H NMR (figure 4.32) shows similar trends to those of fractions eluted with 0.1 M NaOH (figure 4.9).

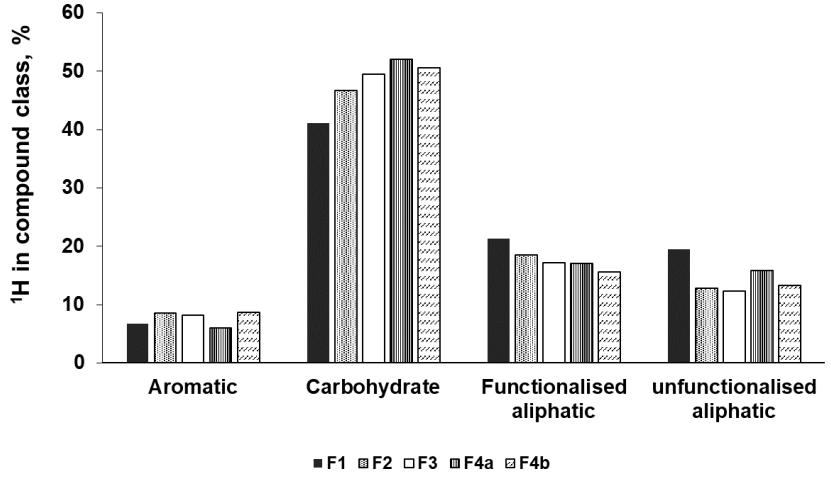

Figure 4.32. Intensity of integrated regions of the ^{1}H NMR spectra of OM in SEC fractions eluted with DI water. The OM sample is from NE core A, 4 – 6 cm sample, as is used in figures 5.27 – 5.31.

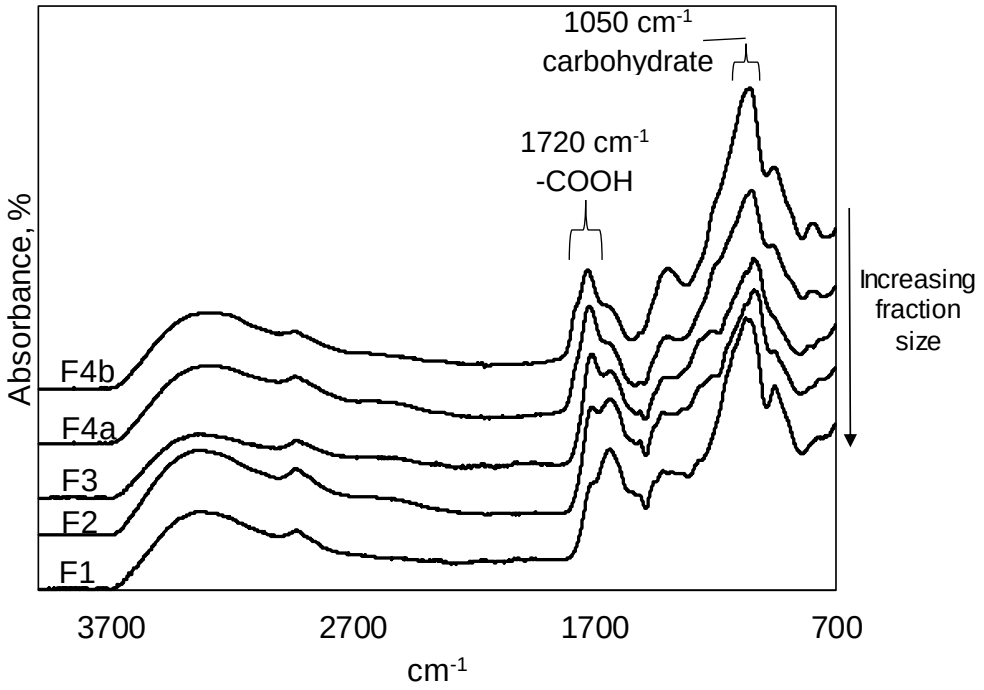

Figure 4.33. FTIR-ATR spectra of OM in SEC fractions eluted with DI water. OM was collected, cation exchanged to remove inorganics and freeze dried before analysis. The OM sample is from NE core A, 4 – 6 cm sample, as is used in figures 4.27 – 4.32.

The results of ^{1}H NMR and FTIR analysis (figures 4.31 and 4.32) demonstrate the increase of carbohydrate from F1 to F4a and F4b. Analysis by ^{1}H NMR also shows that unfunctionalised aliphatic OM is at its highest concentration in the largest fraction F1. The increase of ^{1}H in the aromatic region between F1 and F2 followed by the decrease to F4a is also the same trend as shown previously, however the apparent increase of aromatic material in fraction F4b marks a difference between the use of different eluents. ^{1}H NMR also shows more functionalised aliphatic material in F1 than was seen in the analysis of samples eluted with 0.1 M NaOH (figures 4.9 and 4.10), however the FTIR results clearly show the increase of carboxyl functionality from F1 – F4b, which was the same trend as was seen in the samples eluted with 0.1 M NaOH (figure 4.8). This apparent inconsistency between the two analysis techniques is likely to be due to the semi-quantitative nature of the ^{1}H NMR technique, as the dominance of the carbohydrate peak in the later fractions reduces the prominence of the functionalised aliphatic signal. On examination of the NMR spectra the peaks at 2.1 and 1.5 ppm relating to CH_2 β and γ to functional groups, identified in figure 4.11, were also evident in fractions F4a and F4b of the sample eluted with water and were not present in F1 – F3. This is further evidence of the increase of carboxylic functionality from F1 – F4b. Overall the trends are the same as those seen in the analysis of fractions eluted with 0.1 M NaOH, showing the robust nature of this method of fractionation. It is clear that the change in column conditions, not organic matter character is the driving force behind the changing elution profile of U in the different column runs. It also appears that the high pH rather than variable ionic strength is the main influencing factor.

The elution profiles of OM in the different experiments show that increasing the background ionic strength and pH encourage the OM to elute earlier, in larger size fractions. This is indicative of intermolecular bonding being encouraged by the high background salt concentration, as has been seen in other studies (Chin and Gschwend,

1991; Oste, Temminghoff and Van Riemsdijk, 2002; Gavrilescu, 2014). Although the high pH keeps the OM in solution it also appears to cause it to elute earlier. This effect could possibly be caused by repulsion between the gel beads and OM at high pH values, or it could be that the increase in negative surface charge in the OM at high pH encourages intermolecular bonding by bridging with Na^+ or protons.

4.8. Variable pH extractions of metals from soil samples from the Needle's Eye bog

Based on the results of the column experiments, the role of pH on the solubility of U and other metals in samples from the site was investigated further in a batch extraction experiment. Soil amples from two depth sections of bog core E (15 – 20 cm and 35 – 40 cm) were shaken with varying concentrations of HCl or NaOH in a constant ratio of 1 g ground and sieved (2 mm) soil sample to 10 ml extractant. The concentrations used were 1.0, 0.1, 0.01, 0.001 and 0.0 M HCl or NaOH. The samples were shaken for 4 hours on an end over end shaker before centrifugation for ten minutes at 8300 g and filtration with a 0.45 µm syringe filter. Metals in the resulting solutions were analysed by ICP-MS, with the high concentration extractant solutions diluted to 0.01 M to avoid excess salt concentration. The OM concentration was measured by UV/Vis absorbance at 254 nm. The results are shown below (figure 4.34).

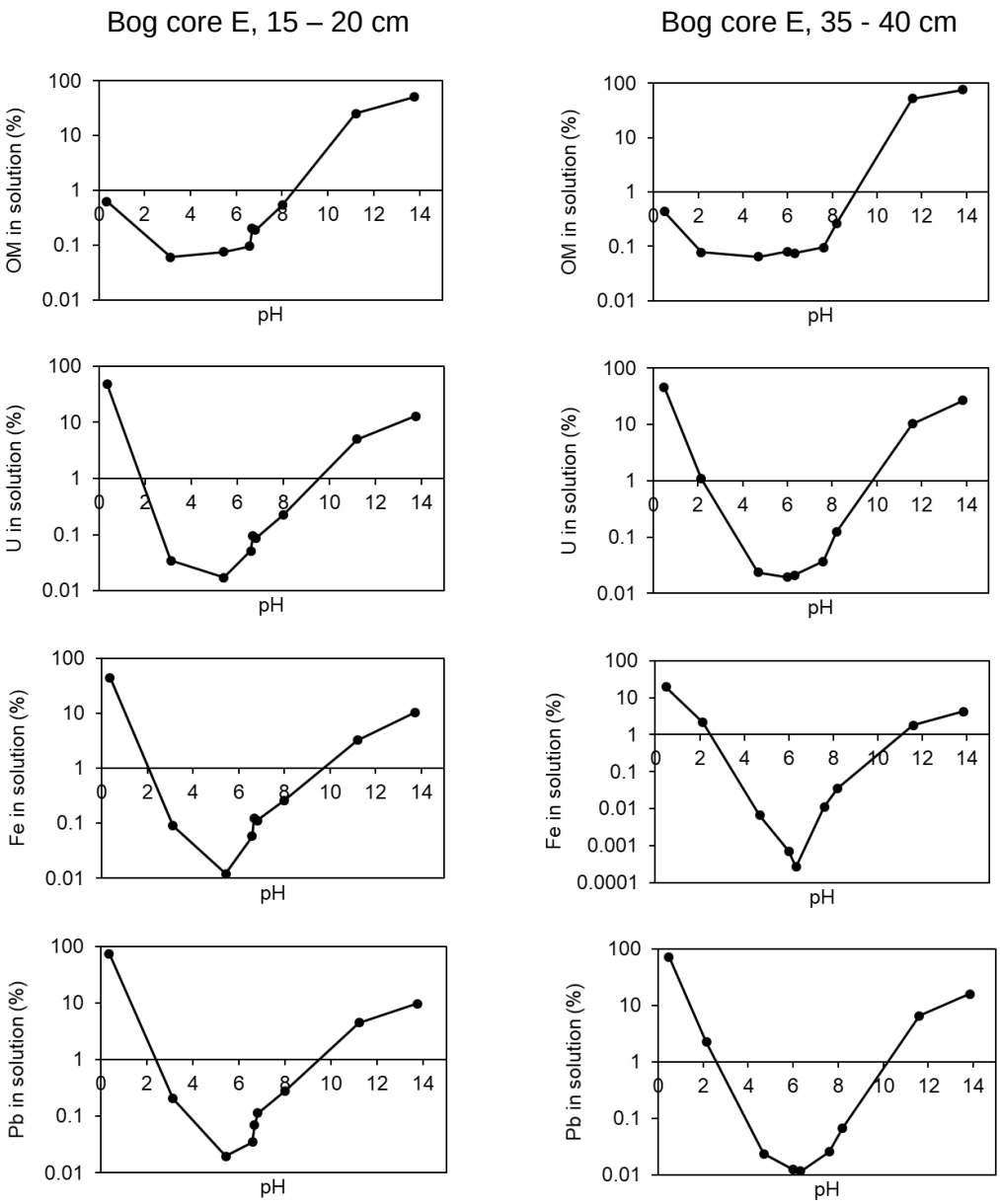

Figure 4.33. Percentage of total metals and OM released into solution using extractants of different pH.

The results of the extraction experiment (figure 4.33) reiterate the pH dependence of U mobility, with less than 0.1 % of the total U extracted into solution between pH 3 and 8. This is in agreement with the results of other studies which show that the binding of U on humic substances, soils and minerals is strong at neutral to low pH values (Li, Victor and Chakrabarti, 1980; Waite *et al.*, 1994; Echevarria, Sheppard and Morel, 2001). Above pH 8 there is a release of U into solution. From this experiment it is not possible to judge whether U and OM are associated although the increase of U in solution occurs at the same time as the large increase of OM in solution. However, when the results of the SEC experiment in section 4.7 are taken into consideration it seems likely that the U is not associated with OM at high pH values. The character of OM released into solution using these different extractants has been discussed in more detail in section 4.6.

The results of these experiments show how the mobility of U is greatly influenced by the local chemical environment, and in particular pH. At pH values from around 4 – 8 the U is associated with the solid phase and the OM is largely immobile. Increasing the pH leads to an increase of OM dissolution and an increase of U mobility. The SEC experiments show that U at high pH is not associated with OM, and is most likely in the form of $UO_2(CO_3)_2^{2-}$, $UO_2(CO_3)_3^{4-}$ or $Ca_2UO_2(CO_3)_3$ which dominate in solution above pH 8. The negative charge of this U anion is likely to be repelled by the negative charge of the OM surfaces, inhibiting binding. The pH dependence of the binding of U in these results is very similar to that seen in the results of experiments investigating the adsorption of U onto ferrihydrite, granite, hematite and ultrafiltration membranes (Waite *et al.*, 1994; Murphy, Lenhart and Honeyman, 1999; Semiao, Rossiter and Schafer, 2010; Fan *et al.*, 2014) which show strong adsorption of U onto Fe oxides and OM at near neutral pH values, but decreased adsorption at higher pH in the presence of CO_2. These results are in agreement with those of Stockdale & Bryan, (2012) who showed that around 10 % of U remains associated with OM at a pH of around 12.9.

The combination of OM characterisation techniques and U analysis shows that in a pH range of around 3.5 – 8 U is associated with “large” OM fractions which have a largely aliphatic and humic acid character, with relatively low amounts of carbohydrate material and aromatic components compared to the fractions which have less affinity for binding U.

4.9. Influence of redox chemistry on U association with OM

Iron oxides and hydroxides are well known for their ability to associate with OM and bind U. In an environmental setting it is often difficult to distinguish the influence of Fe (hydr)oxides and OM on U binding and immobilisation. The results of the SEC studies in section 4.7 show that under neutral pH and oxic conditions the U and Fe are found in the same large fractions associated with OM.

As is shown in section 3.7.3, the conditions in the Needle’s Eye bog are highly reducing particularly below a depth of around 20 cm. In order to investigate the influence of reducing conditions on the interaction of U, Fe and OM a further SEC experiment was undertaken using 0.05 M hydroxyl ammonium chloride as the eluent, (adjusted to pH 7 with ammonium hydroxide and hydrochloric acid solutions) as it is a strong reducing agent. The OM sample was dissolved in 0.05M hydroxyl ammonium chloride at alkaline pH and adjusted down to pH 7 with solutions of HCl.

Using hydroxylammonium chloride as the eluent significantly changes the SEC elution profiles of OM and metals.

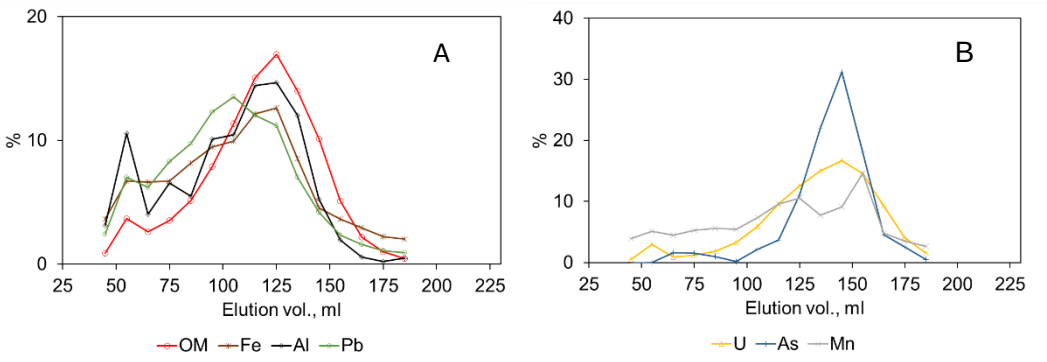

Figure 4.34. SEC elution profiles of OM and metals eluted with 0.05 M hydroxylammonium chloride (pH7). OM elution profile measured by absorbance at 254 nm. Sephadex G75, 35 cm length, flow rate = 2 ml min^{-1}

An obvious difference between these profiles and those shown in section 4.7 is the decrease of the early eluting peak of molecules excluded from the internal porosity of the gel beads. The OM profile is dominated by a large, broad peak at around 125 ml with Pb and Fe showing a similar profile. This suggests that the "large" molecules seen previously have been disaggregated and dispersed throughout the smaller column fractions. This could have been achieved by the reduction of Fe(III) oxides, which are poorly soluble and likely to form colloidal aggregates with OM in solution, to Fe(II) which is more soluble. This could also explain the dispersal of OM observed. The continued association of Fe and OM suggests that the reducing conditions have caused partial reduction of Fe and Mn oxides and partial dispersal of Fe-OM aggregates, causing them to decrease in size and elute in the mid-size range of the column. The profile of Mn in figure 4.34 B has two peaks, one at around 125 ml eluting with the peak of OM and the second at around 160 ml, near to the elution limit of the column. The two peaks of the Mn elution profile is indicative of incomplete reduction of Mn oxides causing some Mn to be associated with OM and some to be truly dissolved in solution as Mn(II).

As in section 4.7, the As present is still found near the permeation limit of the column, likely to be freely in solution rather than associated with OM, with the peak of As

concentration occuring at 145 ml. The peak of U occurs at the same point, 20 ml after the main peak of OM. suggesting that it is not as strongly associated with the OM in the presence of hydroxylammonium hydrochloride as other metals, such as Pb and Cu appear to be.

Taken alongside the results of the SEC experiment shown in section 4.7, it is apparent that aerobic conditions are favourable for U binding to the large OM fractions. The experiment shows that the use of hydroxylammonium chloride as the eluent affects the elution of OM, shifting the OM elution profile to smaller size fractions. This is possibly due to the disaggregation of Fe-OM colloids in the strongly reducing conditions.

4.10. Profiles of DI water-extractable U and other metals

The results of the above experiments (sections 4.7 and 4.8) show that at neutral to acidic pH values U is associated with larger OM fractions and is less mobile. Therefore, extraction with DI water and analysis of U and other metals provides an indication of the changing OM association with depth at the site. The results of analysis of metals extracted by DI water are shown in figure 4.35.

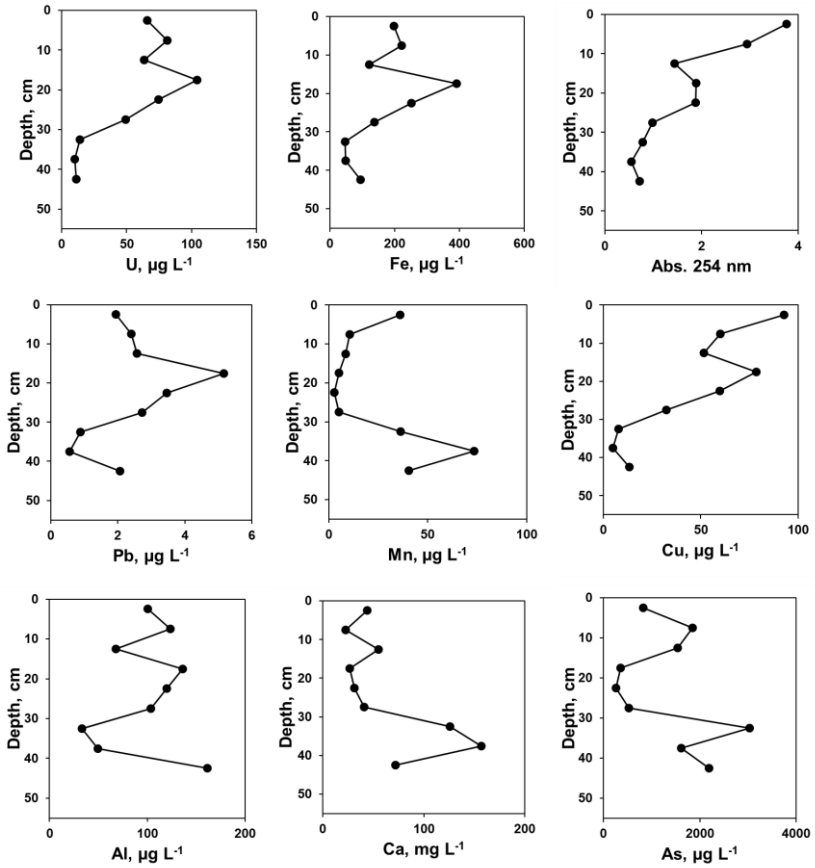

Figure 4.35. Profiles of water extractable OM and metals in samples from NE core E.

The profiles of metals extractable with DI water (figure 4.35) are similar to the solid phase concentration profiles shown in section 3.2. The statistical relationship between the metals and OM extracted are summarised in the dendrogram in figure 4.36.

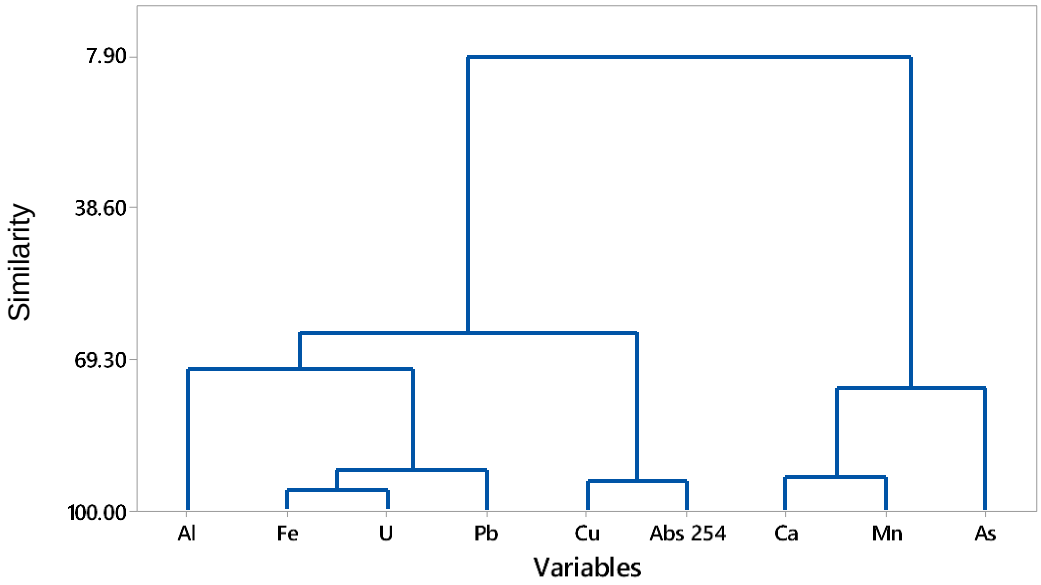

Figure 4.36. Dendrogram showing the associations between water-extractable elements and OM (measured by the absorbance at 254 nm) from the NE bog core E. Strong correlation is indicated by close proximity on the x axis and short height of connecting bars.

Figure 4.36 shows the relationship between DI water extractable metals and OM. A shorter height on the y axis and closer proximity on the x axis indicate a strong positive correlation. Spearman's rank test was used to analyse the correlation between two variables. The statistical analysis shows a strong relationship between U and Fe ($\rho = 0.917$, $p = 0.001$) with Pb showing a similarly strong correlation ($\rho = 0.8$, $p = 0.01$). The relationship between U and the absorbance at 254 nm (as a proxy for OM concentration) is also significant ($\rho = 0.883$, $p = 0.002$). Copper has the closest relationship with OM concentration ($\rho = 0.967$, $p < 0.001$). The results of this extraction and analysis mirror those of the SEC experiments in section 4.7, showing a strong relationship between U, Fe and OM and a very strong association of Cu with OM.

4.11. Conclusions from the fractionation and characterisation of OM and U

4.11.1. Conclusions relating to OM characterisation

The results of characterisation of OM using spectroscopic analyses show that the fractionation techniques applied were successful in separating OM with different structural and functional characteristics. The combined use of NMR, UV/Vis and FTIR made it possible to confirm compositional differences between isolated fractions in a way that would not have been possible using individual techniques. Conclusions that can be drawn from the use of specific OM characterisation techniques are as follows:

The E2:E3 ratio and SUVA 254 are significantly correlated with OM aromaticity while $S_{275\text{-}295}$, SR and E4:E6 are correlated with molecular weight and humic acid content. These results are in agreement with the findings of other studies into the information derived from SUVA 254 (Weishaar *et al.*, 2003; Fernández-Romero *et al.*, 2016) E2:E3 (Peuravuori and Pihlaja, 1997) E4:E6 (Chen, Senesi and Schnitzer, 1977; You, Yin and Allen, 1999) and spectral slopes (Helms *et al.*, 2008; Fichot and Benner, 2012). Analysis by NMR and FTIR show that small OM fractions have large amounts of carbohydrate and highly functionalised aliphatic material. These fractions show fulvic acid behaviour in relation to changes in pH. Large fractions which exhibit humic acid behaviour have large amounts of unfunctionalised aliphatic component, while intermediate fractions have the most aromatic character.

The extraction of OM from samples using varying concentrations of NaOH releases OM of different characteristics due to the changing pH conditions. An increase in NaOH concentration released a greater total concentration of OM into solution which had increasingly humic, aromatic and larger size characteristics. This novel approach to OM extraction and simple preparation procedure proved to be an effective way to generate OM fractions with different chemical properties.

Characterisation of OM extracted with DI water and porewater DOM from the same samples showed that extracted OM was significantly different to pore water DOM, having larger molecular weight, higher aromaticity and fewer oxygen-containing functional groups. Akkanen *et al.*, (2005) and Chen, Lee and Hur, (2015) demonstrated how porewater sampling methods influence the characteristics of DOM collected, and these results again highlight the sensitivity of water soluble OM in soils to the extraction technique used.

The combination of UV/vis, FTIR, single and multi-dimensional NMR spectroscopic analysis techniques with OM fractionation has facilitated the identification of compositional differences between isolated fractions.

4.11.2. Conclusions relating to the interaction of U and OM

Results of combined SEC, ICP-MS and organic characterisation techniques demonstrate that under aerobic conditions U has a preferential association with OM of aliphatic and humic acid character and large molecular size. The binding of U to OM is most favourable at neutral pH (between 4 and 8), with lower and higher pH values resulting in increased mobilization of U. At pH > 8 uranyl carbonate species become important and compete with OM, causing U to be released into solution (Stockdale and Bryan, 2012). In highly reducing conditions OM and Fe are less able to form colloids and disaggregate into smaller size entities and their association with U is less clear.

Depth profiles (Chapter 3) showed that there was a zone of significantly elevated U concentration between 5 and 25 cm depth (zone B, figure 4.70). Conditions in zone B are highly favourable for U binding to OM, with a pH range of around 5.5 – 6.5, largely aliphatic and functional group rich OM and changing redox conditions with oxic water flowing into the bog. These characteristics explain the factors involved in concentrating U in the bog and enabling accumulation over time. Uranium from the mineralization in the

cliff is transported in aerobic, high pH porewaters to the bog. The change to lower pH and variable redox conditions then results in a change in speciation from soluble dissolved calcium uranyl carbonates to an association with OM of a predominantly aliphatic and humic character. Uranium remains as U(VI) in the bog as the calcium uranyl carbonate speciation inhibits reduction (Brooks *et al.*, 2003). The presence of DOM in solution also promotes the oxidation of U(IV) to U(VI) if oxygen is available (Gu *et al.*, 2005) so the oxic water flow conditions identified by Fe(II): Fe(III) analysis is also conducive to U(VI) remaining stable. The flow of oxic water promotes oxidation of Fe and Mn, forming mixed aggregate colloids containing U, Fe, Mn, Al and OM. This association was also seen in SEC experiments at neutral pH with water as the column eluent. Organic characterisation showed that the type of OM that U associated with had a humic acid character and is less soluble and more likely to precipitate. The precipitation of these colloids is a likely mechanism of transfer of U from solution to the solid phase.

Deeper in the bog (zone C) the conditions are less favourable for U binding, with highly reducing conditions, a lower pH of 4.5 – 5.7 and more humified OM with higher aromaticity and lower functional group content. These conditions are concurrent with a decrease in soil U concentration.

A variety of chemical factors influence the U binding at the site, with changes influencing the mobility of U. In experiments undertaken at chemical conditions similar to those in the natural environment U, Fe and OM are closely associated, resulting in decreased U mobility. An increase of pH would result in release of U into solution, both associated with OM and freely dissolved. This is in agreement with Stockdale and Bryan, (2012) who reported that at high pH U could be found in solution as an inorganic species or a humic complex.

This leads to an important conclusion relating to the long-term geological sequestration of nuclear waste in a deep geological repository. The use of cement in the construction of a deep geological repository would locally increase pH. The results presented here demonstrate that in a highly organic soil an increase in pH will cause a significant increase in the mobility of U.

5. Incorporation of anthropogenic radiocarbon into the organic matter within coastal sediments of SW Scotland

5.1. Introduction

The following chapter reports the results of an investigation into the origin and fate of organic matter associated with anthropogenic ^{14}C in sediments of the Southwick Merse, Dumfries and Galloway, SW Scotland. Work, since the late 1970's, has shown that sediments around the Solway coast maintain a time integrated discharge record of ^{137}Cs and ^{241}Am discharged from the Sellafield nuclear facility, NW England, which has proven useful in establishing the accumulation rate of the sediments (Aston and Stanners, 1979; Allan, 1993; MacKenzie *et al.*, 2004; Harvey, Hansom and MacKenzie, 2007). Radiocarbon discharged from Sellafield into the Irish Sea has also been shown to be incorporated in both the organic and inorganic fractions of Southwick Merse sediments (MacKenzie *et al.*, 2004). However, the origin and characteristics of sediment organic matter incorporating ^{14}C has, to date, not been investigated. This study has combined geochemical analysis, organic matter extraction, separation and characterisation techniques, and analysis of ^{14}C and ^{13}C in order to:

i) establish a chronology of sediment accumulation

ii) investigate the concentration of ^{14}C in extracted natural organic matter with depth

iii) examine the changes in organic matter characteristics with depth related to source material and ageing processes

iv) separate, identify and characterise fractions of NOM which incorporate anthropogenic ^{14}C

The results are based on the analysis of two cores collected on 28/10/13 (Merse core A, 96 cm in 2 cm increments) and 06/02/17 (Merse core B, 160 cm in 5 cm increments).

5.2. Geochemical profiles for sediments from the Southwick Merse

5.2.1. Elemental and LOI profiles of Merse core A

Figure 5.1 shows the LOI, Fe and Mn concentration profiles of core A.

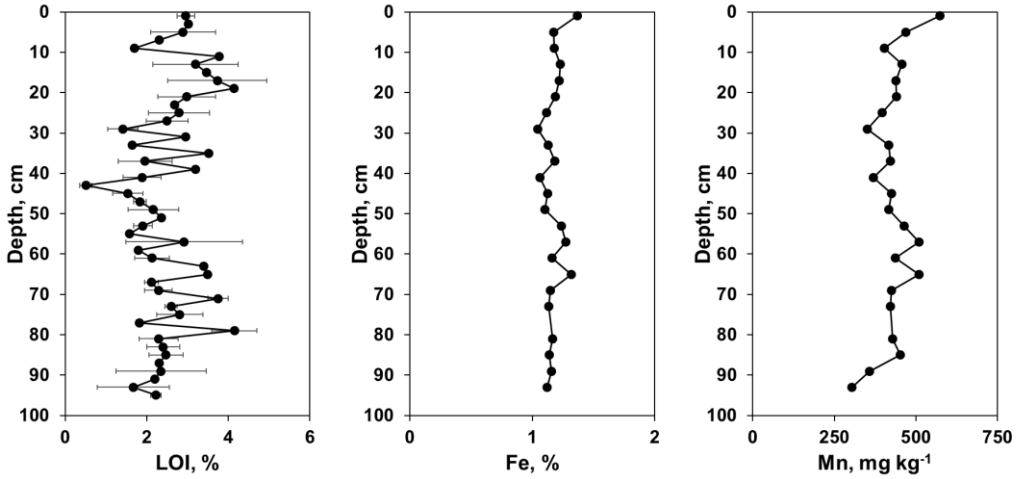

Figure 5.1. Geochemical depth profiles of Southwick Merse core A

The LOI profile shows that the total OM content of the sediment is low, as is typical of coastal sediments, with less than 5% organic matter throughout the profile. This is consistent with previous work at the site (Harvey, Hansom and MacKenzie, 2007). There is also no significant change in organic matter content with depth.

The Fe and Mn concentrations also show very little variation with depth, with relatively low concentration. The profiles offer no evidence of changes in redox chemistry with depth over the length of the core, perhaps due to the twice daily inundation with aerobic, saline water which occurs at the area of the site where the core was collected. It is noteworthy that in core B there was a distinct colour at a depth of around 100 – 110 cm of red/brown to grey/black indicates a change from oxic to reducing conditions at this depth.

5.2.2. Characterisation of extracted organic matter

Organic matter extracted from core A was analysed by ^{1}H NMR, FTIR and UV/Vis spectroscopy.

5.2.2.1. UV/Vis spectroscopy

The UV/Vis spectra were measured in samples shaken overnight (around 16 hours) under an N_2 atmosphere in degassed 0.1 M NaOH then filtered through glass fibre filter papers (Whatman, GF/A). Samples had a 10 times dilution applied before analysis to keep the absorbance within the instrument linear range (below absorbance of 1.5). Figure 5.2 shows the E2:E3 and E4:E6 ratios.

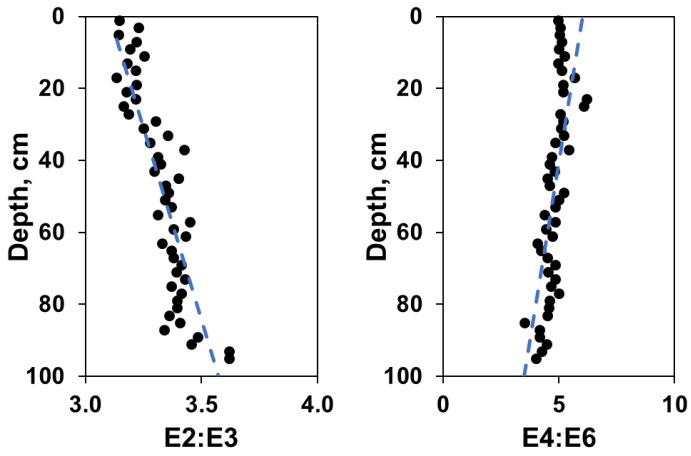

Figure 5.2. UV/Vis parameters E2:E3 and E4:E6 for extracted OM samples from the Southwick Merse core A.

As is shown in figure 5.2, the E2:E3 ratio increases linearly with depth (R^2 = 0.74), suggesting a decrease in aromaticity and molecular size (Peuravuori and Pihlaja, 1997; Minor *et al.*, 2014; See also sections 4.4.1 and 4.5). The E4:E6 ratio, on the other hand, shows a decrease with depth from ~5 to ~4. The E4:E6 ratio has an inverse relationship with humification, suggesting increasingly humified and larger size organic matter with

depth. The E4:E6 ratio of humic acids is usually <5, while fulvic acids have a value of > 5 (Stevenson, 1982; See also sections 4.4.1 and 4.5).

The situation is further complicated by the results of the analysis of the spectral slopes, $S_{350\text{-}400}$ and $S_{275\text{-}295}$, and the SR (figure 5.3).

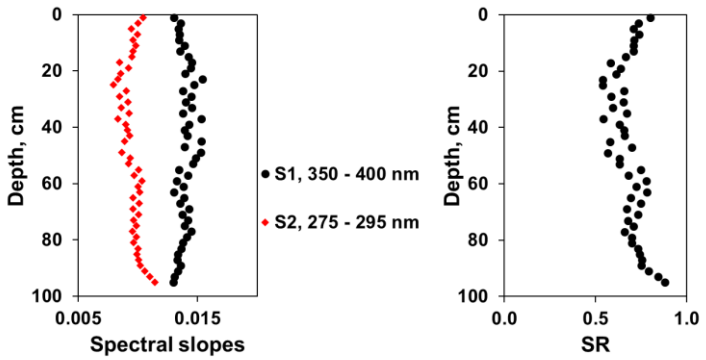

Figure 5.3. UV/Vis parameters $S_{350\text{-}400}$, $S_{275\text{-}295}$ and SR for extracted OM samples from the Southwick Merse core A.

The SR and $S_{275\text{-}295}$ show similar variation with depth ($R^2 = 0.94$), with an initial decrease to a depth of around 20 cm followed by an increase over the remainder of the profile.

The $S_{275\text{-}295}$ is inversely correlated to molecular weight and aromaticity (Helms *et al.*, 2008; See also sections 4.4.1 and 4.5). The increase in $S_{275\text{-}295}$ below a depth of 20 cm ($R^2 = 0.62$) is similar to the increase in E2:E3 ratio ($\rho = 0.44$, $p < 0.002$), and also suggests a decrease in aromaticity with depth below 20 cm. The origin of organic matter also influences its spectroscopic properties, with terrestrial organic matter generally having lower SR and $S_{275\text{-}295}$ than marine organic matter (Helms *et al.*, 2008; Fichot and Benner, 2012; Song *et al.*, 2014). This would indicate an increase in organic matter of marine origin between 20 and 96 cm.

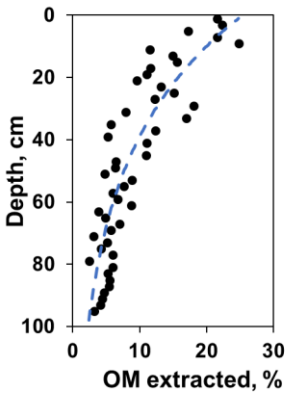

Figure 5.4. Percentage of total OM extracted by 0.1 M NaOH

The percentage of total extractable organic matter (figure 5.4) decreases with depth, suggesting an increase of recalcitrant humin material. The decrease fits a logarithmic trend ($R^2 = 0.75$) and is likely to be related to the ageing of organic matter with depth, with more labile extractable organic matter stabilized by microbial degradation processes over time. The decrease in extractable organic matter with depth could also be due to regular tidal inundation, as the core was collected from the bank of a tidal creek. The samples from deeper down the core are inundated daily, potentially causing the leaching of soluble organic components, while the samples from higher up the core are only inundated during the highest tides. This effect would cause extractable organic components to be washed out of the sediment at depths subject to daily inundation, while the less frequent inundation higher up in the core allows them to accumulate. The ageing and humification effect and tidal washing effect are both likely to impact the composition of OM in the core.

The results of UV/Vis analysis indicate the varied processes affecting the organic matter throughout the core, with ageing and microbially driven humification, organic matter origin and regular tidal inundation all influencing the organic matter characteristics. The UV/vis results provide a good starting point for describing the characteristics of the organic matter but do not allow for a detailed interpretation due to the low resolution of the technique. The results of UV/Vis analysis complement the results of FTIR, ^{1}H NMR and carbon isotope analysis presented below.

5.2.2.2. FTIR spectroscopy

Organic matter extracted from Merse core A with 0.1 M NaOH, dialysed against DI water (3500 MWCO) and freeze dried was analysed by FTIR-ATR spectroscopy. The results (figure 5.5) show variations in oxygen containing functional groups, aromatic and aliphatic content with depth.

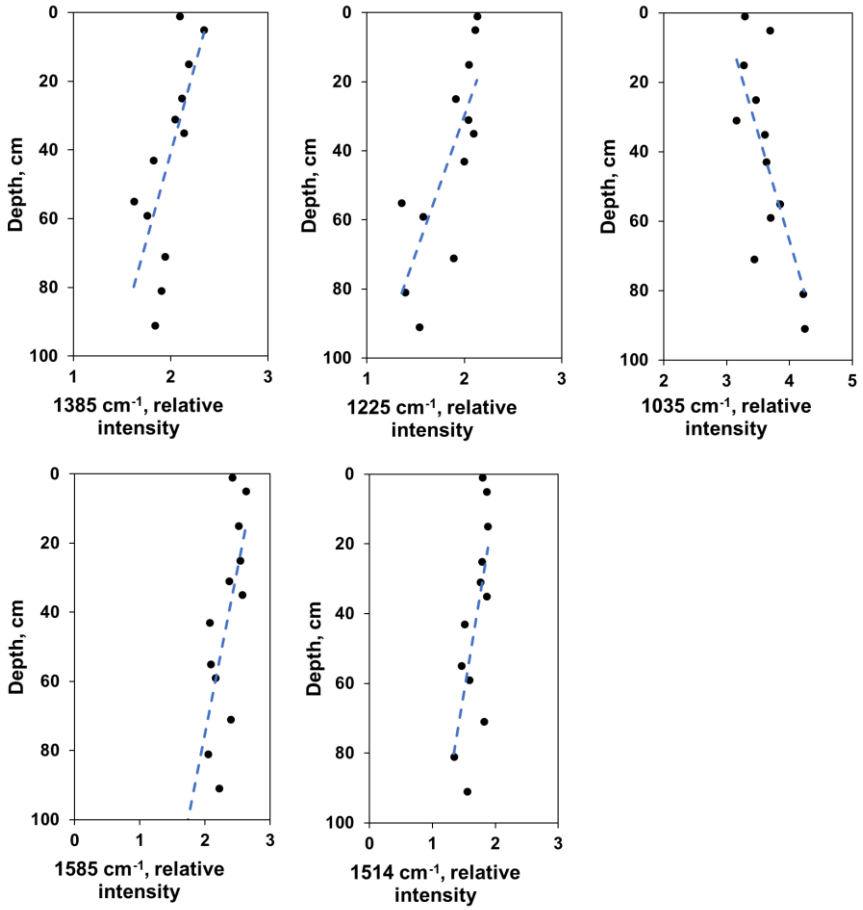

Figure 5.5. Results of FTIR-ATR analysis of OM extracted from various depths of Merse core A.

The FTIR peaks at 1385 and 1225 cm^{-1} show decreases with depth. These peaks are attributed to the absorbance of carboxylate functional groups. The peaks at 1585 and 1514 cm^{-1} also show a decreasing trend which can be attributed to aromatic structures or oxygen containing functional groups (section 2.4.7.1). Finally, the dominant peak at 1035 cm^{-1}, which is associated with the absorbance of carbohydrate and aliphatic structures shows an

overall increase with depth. The decrease in carboxylate functional groups could be caused by the humification process of the OM as it ages, while the decrease in aromaticity and increase in aliphatic structures is more likely to be an effect of the organic matter source, with organic matter of marine origin being dominant at depth. These trends in the FTIR results, while not strong, are consistent with those obtained via UV/Vis spectroscopic analysis of the same OM extracts.

5.2.2.3. ^{1}H NMR spectroscopy

Extracted and freeze-dried organic matter samples were analysed by ^{1}H NMR. The integrated area of major regions of the spectra are directly proportional to the amount of ^{1}H in different major chemical environments: aromatic, carbohydrate, oxygen rich aliphatic and unfunctionalized aliphatic. The figure below shows the variation of these regions in the analysed samples with depth.

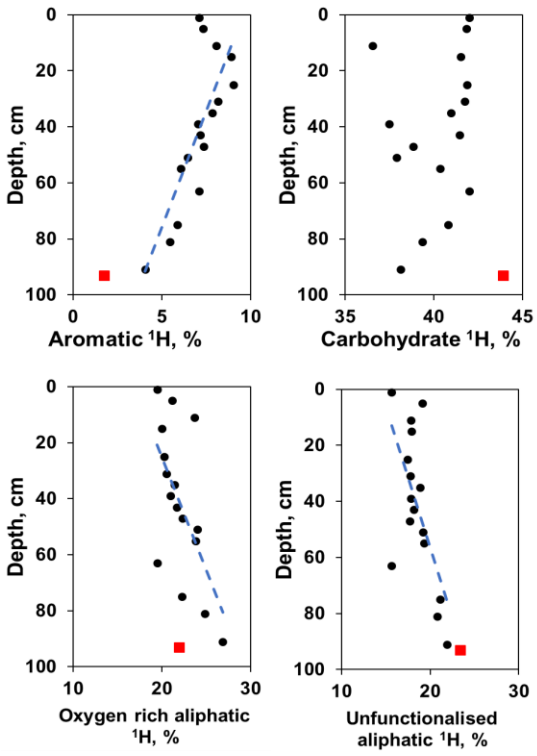

Figure 5.6. Intensity of ^{1}H NMR integrated regions of OM extracted from various depths of Merse core A. The red square on each profile indicates the result of ^{1}H NMR analysis of particulate organic carbon (POC) collected from the Irish Sea, also analysed as part of this study.

The spectra of the extracted OM samples are typical of those of soil or sediment OM, comprised of material which is humified and relatively unreactive compared with dissolved organic matter found in surface waters or the marine environment. Figure 5.6 shows that there is an overall decrease of aromatic functionality with depth, while functionalised and unfunctionalised aliphatic material increases with depth. This is contrary to the increased aromaticity of humic acids compared to fulvic acids and the increasing aromaticity of OM in depth profiles of soil (Stevenson, 1982; Rice and MacCarthy, 1991; Gressel *et al.*, 1996; Gondar *et al.*, 2005; Chang *et al.*, 2013). The reason for this is the changing origin of organic matter with depth in a system with two distinct inputs, as is discussed in section 5.2.2.4. There is a change in the profile shape at ~20 – 30 cm, with the aromatic and unfunctionalised aliphatic showing the greatest decrease and increase, respectively, below this depth. This is indicative of a transition to a different OM composition at this point as was also shown in the results of UV/Vis analysis (section 5.2.2.1).

Figure 5.6 shows that the carbohydrate region remains the largest fraction of the organic matter throughout the core but does not show any trend with depth.

The red square on each graph shows the result of NMR analysis of extracted organic matter from Irish Sea suspended particulate material, also analysed as part of this study. Suspended particulate organic matter becomes incorporated into coastal sediments as they accumulate. The suspended particulate organic matter has a low percentage of aromatic material and high percentages of carbohydrate and unfunctionalised aliphatic components relative to the sediment organic matter. The oxygen rich OM content of the Irish Sea suspended particulate material is very close to the average content of the sediment samples (mean = ~22.0 ± 2.1%, value of suspended particulate organic matter = ~22.0%). The profiles of the aromatic and unfunctionalised aliphatic organic matter components tend towards the values of the Irish Sea suspended particulate organic matter, suggesting an

increase in organic matter of marine origin with depth. The links between the results of UV/Vis and NMR analysis are discussed in section 5.2.2.5.

Further evidence for the variation in organic matter character with depth being due to the increasingly marine origin is provided by the results of analysis of $\delta^{13}C$, below.

5.2.2.4. $\delta^{13}C$ as a tracer of organic matter origin

In their study of the Southwick Merse sediments MacKenzie *et al.* (2004) demonstrated the use of $\delta^{13}C$ to investigate the origin of sediment organic matter at the Southwick Merse. The $\delta^{13}C$ of organic matter depends upon its origin. Values of $\delta^{13}C$ from -18 to -22‰ are typical of Irish Sea POC while the $\delta^{13}C$ of OM from a terrigenous source can vary from -24 to -32‰ (Gulliver, 2002; MacKenzie *et al.*, 2004; Muir *et al.*, 2017). Analysis of flora at Southwick Merse showed that it has a $\delta^{13}C$ of -28.4‰, while Irish Sea suspended POM had a value of -21.6‰ (Gulliver, 2002; MacKenzie *et al.*, 2004). More recently, $\delta^{13}C$ values of -20.0 and -21.9‰ have been measured in the Irish Sea POC, and, as in past studies, it is significantly enriched in ^{14}C (Wolstenholme *et al.*, 1998; Muir *et al.*, 2017).

These values can be used to assess the contribution of marine and terrigenous organic matter throughout the profile of the core, as is shown in figure 5.7.

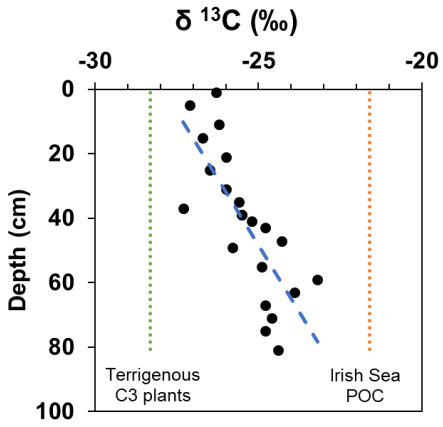

Figure 5.7. Changing $\delta^{13}C$ of extracted OM samples with depth. The green and orange dashed lines show the $\delta^{13}C$ results of analysis of terrigenous C3 plants from the Southwick Merse and Irish Sea POC, respectively (Mackenzie *et al.*, 2004).

The $\delta^{13}C$ values used to distinguish marine and terrigenous origin OM are those of MacKenzie *et al.*, (2004) as the terrigenous material analysed was from the same site as the current samples and the marine value is very similar to that recently measured for Irish Sea

eastern basin POC.

The analysis of extracted organic matter throughout the core shows a linear increase of $\delta^{13}C$ with depth linear trend ($R^2 = 0.58$, $p = 0.001$). These results are in agreement with those of MacKenzie *et al.*, (2004) and show the increase of organic matter of marine origin with depth from ~30% to ~60% of the total. The results in figure 5.7 show an overall positive linear trend with depth, but the increase in $\delta^{13}C$ is most pronounced below a depth of ~30 cm to a depth of ~60 cm. This is similar to the change of profile shape of the E2:E3 and E2:E4 ratios and $S_{275-295}$ UV/Vis parameters and also the aromatic and unfunctionalised aliphatic ^{1}H NMR regions. These results show the binary OM inputs at the site, with terrigenous OM being dominant from the surface to ~30 cm, followed by a mixed transition zone to OM of marine origin below ~60 cm.

The results of $\delta^{13}C$ analysis can be compared to the results of the other organic matter characterisation techniques employed to assess how the origin of the organic matter affects its composition.

5.2.2.5. Comparison of characterisation methods

To investigate trends between different characterisation parameters cluster analysis and linear correlation analysis using a Spearman's rank correlation were carried out.

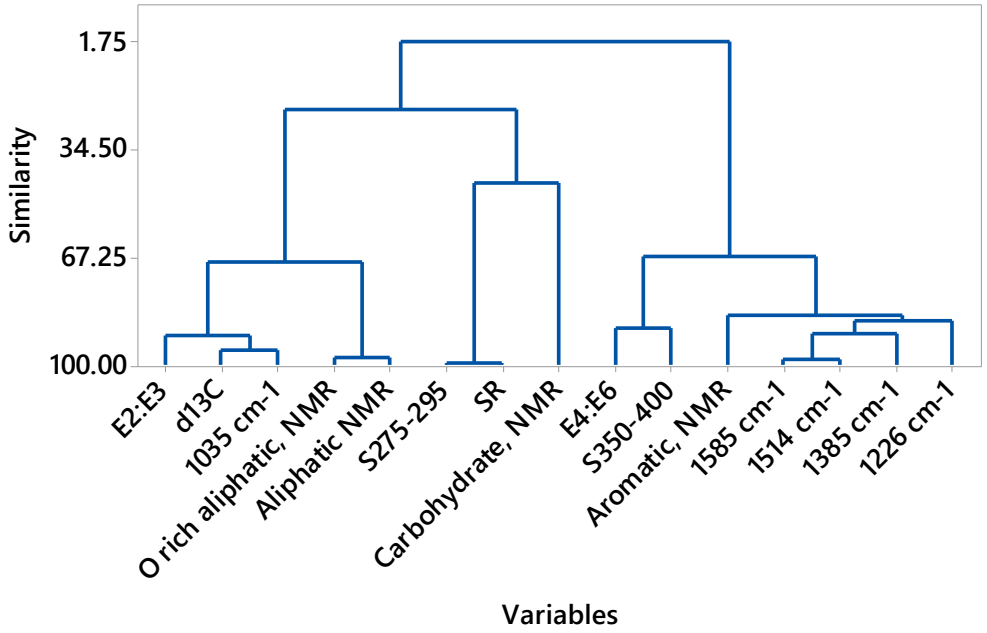

Figure 5.8. Dendrogram showing the results of cluster analysis of the results of OM characterisation analysis. Strong correlation is indicated by close proximity on the x axis and short height of connecting bars.

Figure 5.8 shows the results of cluster analysis of parameters from ^{1}H NMR, FTIR and UV/Vis analysis. Variables which have a stronger correlation are closer together on the x axis, with the height of the vertical lines joining them indicating the strength of the correlation. The results are divided into three main groups. The far left of the dendrogram shows the strong correlation between aliphatic character, from both NMR and FTIR, and origin of OM, shown by the δ^{13}C. The E2:E3 ratio from UV/vis is also in this region, suggesting a strong link between the value of the ratio and the origin of OM.

From the mid region of the dendrogram it can be seen that the carbohydrate region measured by NMR is not strongly correlated to any of the other variables. The SR and S_{275-}

$_{295}$ from UV/Vis analysis are strongly related to each other, as noted in section 5.2.2.1, showing that $S_{275-295}$ is the dominant parameter in the calculation of SR. Although not clear from the cluster analysis, the SR has a weak inverse correlation to aromaticity by NMR (ρ = -0.55, P = 0.05).

The E4:E6 ratio and $S_{350-400}$ from UV/Vis analysis show similar trends with depth. The E4:E6, like the E2:E3, has been previously observed to be inversely correlated to aromaticity; however, the opposite is true in this case. The reason for this discrepancy is not clear from the statistical analysis, but is possibly related to the variation in molecular weight with depth, as is discussed below, in section 5.3.1.

The third cluster is on the right of the dendrogram and consists of the aromaticity measured by NMR and FTIR (1514 and 1585 cm^{-1}) and the content of oxygen functional groups measured by FTIR (1385 and 1226 cm^{-1}). The fact that these FTIR parameters occur together and the fact that they are also all significantly negatively correlated with the absorbance at 1035 cm^{-1} suggests that the increase of the large peak at 1035 cm^{-1} with depth dominates the spectrum, causing the other peaks to decrease relative to it, as it is only a semi-quantitative technique.

Variables which are far away from each other on the x axis are negatively correlated, for example the E2:E3 and aromaticity by NMR, (ρ = -0.71, P = 0.01).

The results show that characterisation of OM using various spectroscopic techniques has proved to be an effective way of discerning the origin of OM in the sediments. The statistical analysis helps to clarify the characterisation of the OM in depth profiles by highlighting the main factors influencing the variation with depth. The most important change with depth is the increase in OM of marine origin. This in turn is the cause of the decrease in aromaticity and increase in aliphatic character with depth.

The same spectroscopic techniques used to characterise the OM of Merse core A have been applied to Merse core B (Johnston, 2017). The results agree with those presented here, showing a decrease in aromaticity and increase in E2:E3 ratio with depth. The similarity between the results shows that core B is very similar to core A, indicating that there has been little disruption in accumulation processes or mixing at the site in the approximately three years between the two cores being collected.

5.2.3. ^{14}C in extracted organic matter

Figure 5.9 shows the discharges of ^{14}C from Sellafield nuclear reprocessing facility into the Irish Sea from 1985 – 2013 (BNFL, 1985 - 1989; MAFF, 1990 - 1995; RIFE, 1996 - 2014).

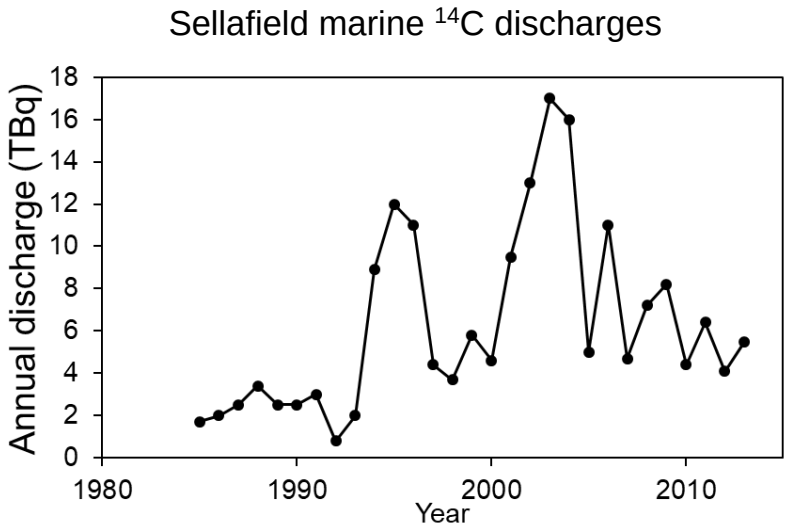

Figure 5.9. Annual ^{14}C liquid effluent discharge profile from 1985-2013. (BNFL, 1985 - 1989; MAFF, 1990 - 1995; RIFE, 1996 - 2014)

There is a large increase in marine ^{14}C discharge in 1993 when the main route of disposal was changed from atmospheric to marine discharge, causing a peak in 1995 and a second peak in 2003. The increase in ^{14}C discharge was evident in the organic component of Southwick Merse sediments when investigated in cores collected in 1994 and 2002 (MacKenzie *et al.*, 2004).

The profile ^{14}C in OM samples from Merse core A analysed by AMS is shown below, in figure 5.10.

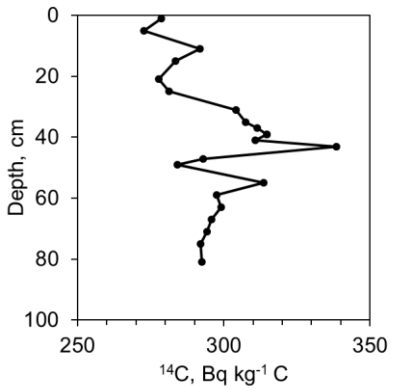

Figure 5.10. Specific activity of ^{14}C (Bq kg C^{-1}) in OM extracted from various depths of Merse core A.

The analysis of ^{14}C in extracted organic matter with depth (Figure 5.10) shows that ^{14}C is enhanced relative to the marine and terrestrial biota background level of ~240 – 250 Bq kg^{-1} C (Eisenbud and Gesell, 1997; Cook *et al.*, 1998; Gulliver *et al.*, 2001). The maximum measured specific activity occurs at a depth of 42 – 44 cm and represents a change in the profile from overall increase in ^{14}C concentration from the surface. The increase of ^{14}C from the surface to 44 cm is correlated with the increase in $\delta^{13}C$ in the same samples (ρ = 0.63, n = 13, p <0.02), suggesting that it is related to the change in organic matter origin with depth, with organic matter of a more marine origin having an elevated concentration of ^{14}C. Below 44 cm the ^{14}C and $\delta^{13}C$ are not related, which shows a decrease in the ^{14}C concentration of the organic matter of marine origin below the peak at 42 – 44 cm.

If it is assumed that the enrichment in ^{14}C in the core above background level is solely due to the input of ^{14}C enriched marine organic matter, then it is possible to calculate the enrichment in the marine fraction of the organic matter using the results of $\delta^{13}C$ analysis. This calculation has been undertaken in three steps. Firstly, the concentration of excess (above background level) ^{14}C (Bq kg^{-1} C) is calculated by equation 5.1:

$$Excess^{14}C\ (Bq\ kg^{-1}\ C)\ = Measured\ ^{14}C\ (Bq\ kg^{-1}\ C) - 250\ (Bq\ kg^{-1}\ C)$$

Equation 5.1

The approximate background ^{14}C concentration is 250 Bq kg^{-1}. The change in ^{14}C specific activity due to decay with depth is negligible (<0.4 Bq kg^{-1} C) over the duration of the approximate calculated age of the core (section 5.2.4).

The percentage of marine organic matter with depth can be calculated from the $\delta^{13}C$ results by equation 5.2:

$$Marine\ OM\ \% = \frac{(measured\ \delta^{13}C - terrestrial\ \delta^{13}C)}{(marine\ \delta^{13}C - terrestrial\ \delta^{13}C)} \times 100 \qquad \textit{Equation 5.2}$$

The marine and terrestrial $\delta^{13}C$ signatures are -21.6 and -28.3 respectively (MacKenzie *et al.*, 2004).

Assuming all the excess ^{14}C in the sediment organic matter is due to inputs of enriched marine organic matter, the enrichment of ^{14}C in the marine fraction of the organic matter is calculated by equation 5.3:

$$Excess\ carbon\ in\ marine\ OM\ (Bq\ kg^{-1}C) = \frac{Excess\ ^{14}C\ (Bq\ kg^{-1}C)}{marine\ OM\ \%} \times 100 \qquad \textit{Equation 5.3}$$

As an example, the sample at 4 – 6 cm has an excess ^{14}C activity of 22.8 Bq kg^{-1} C. The sample OM is 17.9 % marine, and the excess ^{14}C is assumed to be in the marine OM, therefore 22.8 Bq kg^{-1} total C is actually 22.8 Bq in 17.9 % of the total C, or 0.179 kg. Therefore, the excess ^{14}C in the marine OM is 22.8 Bq in 0.179 kg, which is equal to 127.3 Bq kg^{-1} C.

By this method, the excess ^{14}C in marine origin organic matter throughout the core can be calculated, giving rise to the profile shown in figure 5.11.

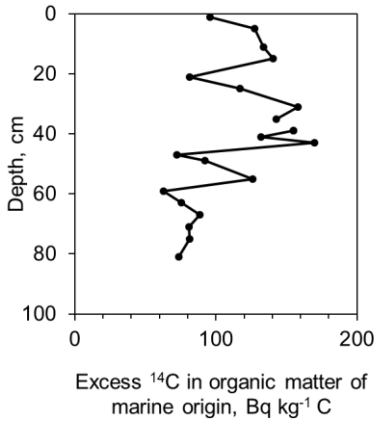

Figure 5.11. Calculated specific activity of ^{14}C (Bq kg C^{-1}) in OM of marine origin based on the $\delta^{13}C$.

When the origin of the organic matter is taken into account, as in figure 5.11, there is a significant overall decrease in the activity of ^{14}C in the marine derived OM with depth ($p < 0.05$). Transforming the ^{14}C excess data from Bq kg^{-1} of total C to Bq kg^{-1} of marine origin C does not alter the presence of the broad peak between the depths of 31 – 43 cm. However, there is a difference from the surface to the mid-point of the core where it appears that the enhanced ^{14}C activity of the marine organic matter is diluted by the input of terrigenous organic matter.

The decrease in ^{14}C concentration below 44 cm could be related to a period of relatively low discharge between 1997 and 2000, or before 1992, or the profile could be unrelated to the peak discharges. In order to examine the relationship between the enrichment of sediment organic matter and liquid ^{14}C effluent discharge from Sellafield it is necessary to establish a chronology of the sediment core, as is described in the following section.

5.2.4. Establishing a chronology of Southwick Merse core A

Establishing a chronology of the Southwick Merse sediment profile allows comparison of peaks and troughs in the measured specific activities with those of the Sellafield liquid effluent ^{14}C discharge. Previous studies of the site have successfully calculated chronologies and sedimentation rates using the unique discharge peaks of ^{137}Cs and ^{241}Am from Sellafield which are preserved in accumulated sediments (Kershaw *et al.*, 1990; Allan, 1993; MacKenzie *et al.*, 1994, 2004; Harvey and Allan, 1998), however, continued accumulation naturally buries the peaks deeper into the sediment and Harvey *et al.*, (2007) had difficulties in deriving chronologies from cores collected at the Southwick Merse around 2005. Verifying the chronologies derived from Sellafield radionuclides by ^{210}Pb analysis is also problematic around the coast of the Irish Sea due to inputs of ^{210}Pb and ^{226}Ra from anthropogenic sources (Kershaw *et al.*, 1990).

In this study, the accumulation of Sellafield-derived ^{137}Cs and ^{241}Am and natural ^{210}Pb were analysed in an attempt to establish a sediment chronology.

5.2.4.1. Gamma spectroscopy of Merse core A

Table 5.1 shows the results of analysis of Merse core A by gamma spectroscopy. It did not reveal any peaks related to the input of Sellafield derived radionuclides, nor was there a decrease of excess ^{210}Pb with depth which would be indicative of a stable chronology. This was consistent with the results of Harvey *et al.*, (2007) who were unable to calculate a chronology or accumulation rate in 5 out of ten 1-m length cores collected at the Southwick Merse in around 2005. The measurement of excess ^{210}Pb also show no sign of steady accumulation and is likely to have been influenced by anthropogenic inputs of

anthropogenic ^{210}Pb and ^{226}Ra into the Irish Sea (McCartney, Kershaw and Allington, 1990).

Table 5.1. Results of analysis of total sediment samples of Merse core A by gamma spectrometry

	Depth (cm)	^{210}Pb ($Bqkg^{-1}$)	Supported ^{210}Pb ($Bq\ kg^{-1}$)	Excess ^{210}Pb ($Bq\ kg^{-1}$)	^{137}Cs ($Bq\ kg^{-1}$)	^{241}Am ($Bq\ kg^{-1}$)
Measured energy		(46 keV)	Average of ^{214}Pb (295 and 352 keV) and ^{214}Bi (609 keV)	Total ^{210}Pb minus supported ^{210}Pb	(662 keV)	(60 keV)
	0 - 2	26 ± 3	30 ± 2	4	105 ±1	182 ± 2
	10 - 12	27 ± 2	24 ± 2	-3	95 ± 1	165 ± 2
	26 - 28	25 ± 3	30 ± 2	5	67 ± 1	129 ± 2
	38 - 40	23 ± 3	28 ± 2	5	78 ± 1	152 ± 2
	40 - 42	26 ± 3	27 ± 3	1	78 ± 1	150 ± 2
	42 - 44	23 ± 4	29 ± 3	6	78 ± 1	156 ± 2
	42 - 44	21 ± 3	27 ± 2	6	77 ± 1	149 ± 2
	44 - 46	25 ± 3	26 ± 3	2	84 ± 1	161 ± 2
	60 - 62	25 ± 4	26 ± 3	1	102 ± 2	188 ± 2
	80 - 82	18 ± 4	25 ± 3	7	105 ± 2	169 ± 2
	86 - 88	15 ± 3	27 ± 2	12	169 ± 2	264 ± 3
	88 - 90	20 ± 5	28 ± 3	8	136 ± 2	217 ± 3
	90 - 92	25 ± 6	25 ± 4	0	135 ± 3	216 ± 3
	92 - 94	19 ± 5	27 ± 4	8	144 ± 3	242 ± 3
	94 - 96	17 ± 3	25 ± 3	8	121 ± 2	191 ± 2

A second, longer core was collected in order to see whether it was possible to locate the maxima of Sellafield derived ^{137}Cs and ^{241}Am at a depth below the maximum extent of Merse core A.

Again, no distinct high activity peaks were seen in this core, however the Cs:Am ratio increased below a depth of 120 cm (figure 5.12).

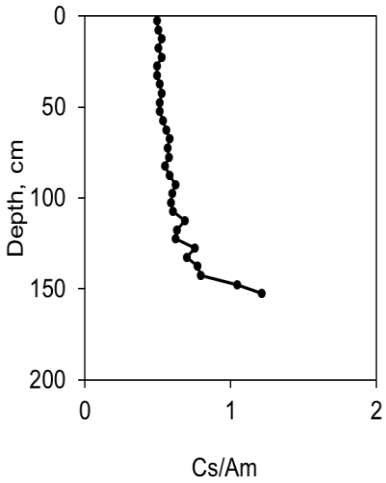

Figure 5.12. Cs/Am ratio measured in Merse core B.

Two previous studies based at the Southwick Merse have reported the Cs/Am ratios of samples in cores which could be identified as having been collected in close proximity to those of the current study (Allan, 1993; Moyes, 1995). The results from the previous studies have been added onto the Cs/Am profile of Merse core B where they overlap, as is shown in figure 5.13.

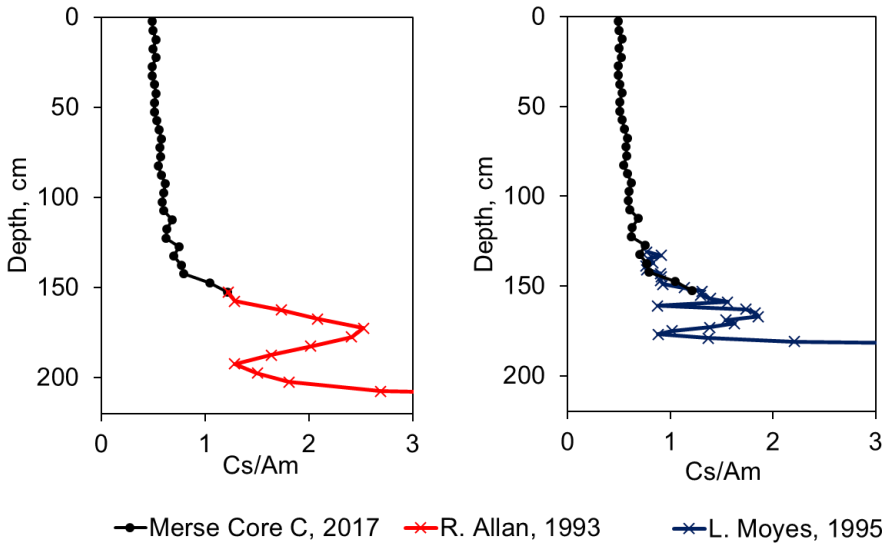

Figure 5.13. Cs/Am ratio of Merse core B with the results of analysis by Allan, (1993) and Moyes, (1995) added at the point of closest cross over.

Both of the previous data sets have been corrected for decay over the last 23 and 26 years respectively and have been added on to the current profile to give the best possible overlap of data. There are one and eleven overlapping points in the data from Allan, (1993) and Moyes, (1995) respectively with one and six points, respectively, from Merse core B. The two overlapping data sets can be used to make a qualitative estimate of the sediment accumulation rate from 1993 or 1995 to 2017.

Based on the data from Allan, (1993), Merse core B has a date of around 1991 at a depth of 155 – 160 cm. The data from Moyes, (1995), give the depth of 130 – 135 cm a date of around 1994. These depths can be used to calculate an accumulation rate for the area of 5.87 and 5.76 cm yr^{-1}, based on the data from Allan (1993) and Moyes (1995), respectively. These values are close to each other and higher than those calculated by Allan (1993) and Moyes (1995), of 2.95 and 2.5 cm yr^{-1} respectively, but within the range seen at the site in other studies. Harvey *et al.*, (2007) directly measured an accumulation rate of up to 9.3 cm yr^{-1} at the Southwick water riverbank, and rates of 5.1 and 6.3 cm yr^{-1} nearby, with measurements of ^{137}Cs and ^{241}Am suggesting accumulation rates in excess of 4 cm yr^{-1}.

Although this method of calculating the sedimentation rate is by no means ideal, it does appear to be a useful estimate, and fits in well with those measured in previous studies. The average of the two accumulation rates has been used to calculate a chronology with depth of Merse core A, shown in figure 5.14.

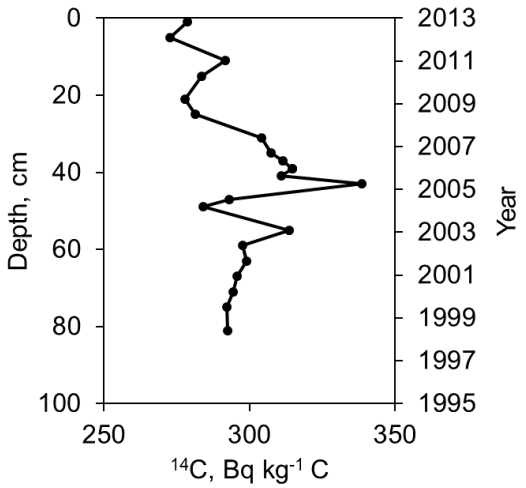

Figure 5.14. Specific activity of ^{14}C in OM samples from Merse core A with the date estimated from the calculated accumulation rate of 5.82 cm yr^{-1}.

The main ^{14}C peak is at between 30 and 44 cm in Merse core A. The corresponding date range, calculated using the average accumulation rate of 5.82 cm yr^{-1}, is 2005 – 2008. The peak in maximum ^{14}C effluent discharge occurred in 2003 - 04, as is shown in figure 5.9. This represents a delay in incorporation into sediments of around 2 – 4 years which is in agreement with previous studies of Sellafield derived radionuclides that suggest a lag time from release to sediment incorporation of 1.5 to 3.7 years (Aston and Stanners, 1982; Jones, Roberts and Miller, 1988; Kershaw *et al.*, 1990; Marsden *et al.*, 2006).

Using the broad ^{14}C peak of Merse core A at 42 – 44 cm to estimate the accumulation rate, with a 2 year lag time (Marsden *et al.*, 2006), gives a result of 5.5 cm yr^{-1}. This is similar to the estimates from the Cs/Am ratio and is a corroboration of the calculated chronology.

The results of this study, taken together with previous investigations at the site, show that the sedimentation rate at the Southwick Merse is highly variable both spatially and temporally, with a range of around 2 – 9 cm yr^{-1}. This also shows that there is potential for Sellafield ^{14}C effluent discharges to be used to calculate sedimentation rates around the Irish Sea. Although complicated by the mixing of marine and terrigenous C, the

measurement of $\delta^{13}C$ can be used to deconvolute the origin of deposited organic matter. Also, unlike ^{137}Cs and ^{241}Am in previous studies, the depth distribution of ^{14}C does not so clearly match the peaks and troughs of temporal discharges from Sellafield. This could be due to the complex mixing processes involved in transferring inorganic forms of ^{14}C to organic C which can be deposited in a particulate form.

5.3. Fractionation of Southwick Merse organic matter

Extracted organic matter from the top, middle and bottom of Merse core A was fractionated by size exclusion chromatography (SEC) and characterised by UV/vis, FTIR and ^{1}H NMR and analysed for ^{14}C activity and $\delta^{13}C$ by AMS.

5.3.1. Characterisation of size fractionated OM

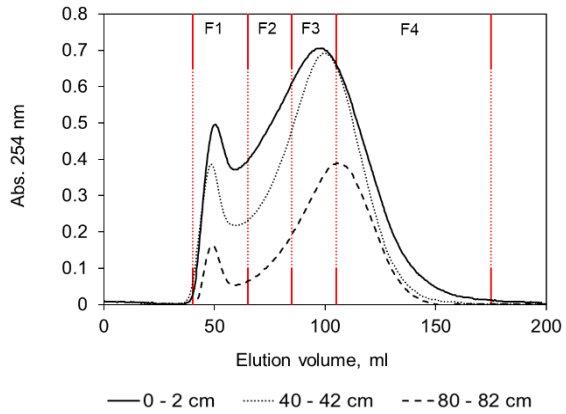

Figure 5.15. Elution profiles of OM extracted from three depths of Merse core A measured by absorbance at 254 nm. The elution fractions shown are the same as those described in Section 4.3. (Sephadex G75, eluted with 0.1 M NaOH, 2 ml min $^{-1}$).

Figure 5.15 shows the SEC elution profiles of three extracted OM samples with depth (25 mg OM dissolved in 2 ml of 0.1 M NaOH). The elution profile was monitored by continuous UV/Vis absorbance measured at 254 nm. The samples were divided into four fractions, indicated on the figure by F1 – F4, with F1 being the "largest" and F4 the "smallest". The second peak is larger than the first in all three cases, however this is not simply an effect of concentration, the wavelength chosen also influences the observed profile. The wavelength of 254 nm is the region of the UV/vis absorbance spectrum strongly associated with the absorbance of aromatic molecules, so the relatively large peak of "small" molecules is actually due to the higher concentration of aromatic moieties in this

fraction. This effect is shown for the 80 – 82 cm depth elution profile in figure 5.16, where the elution profile measured at 254 nm is compared to that measured at 465 nm, a wavelength less strongly influenced by aromaticity of the sample, and is confirmed by the results of characterisation of the fractions throughout this section.

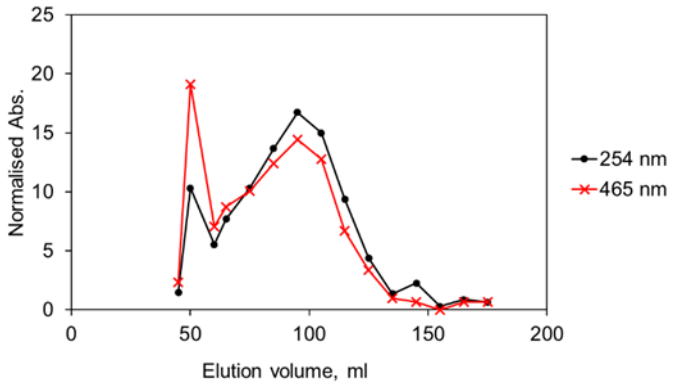

Figure 5.16. Elution profiles of OM extracted from 80 – 82 cm of Merse core A measured by absorbance at 254 (black) and 465 nm (red). (Sephadex G75, eluted with 0.1 M NaOH, 2 ml min $^{-1}$).

Figure 5.16 shows the comparison of elution profiles of extracted OM from 80 – 82 cm measured by UV/Vis at 254 and 465 nm (from the same spectra). The profile measured at 465 nm has a much higher absorbance in the largest fraction (around 50 ml elution volume), suggesting that the relatively low absorbance at 254 nm at this point is not due to low OM concentration but low OM aromaticity. Similarly, the relatively high absorbance in the peak of the smallest fraction (~90 – 150 ml elution volume) is indicative of increased OM aromaticity in this fraction. This is also the reason why the overall absorbance of the elution profiles of the three samples decreases with depth, because, as is shown in section 5.2.2, the aromaticity of the samples decreases with depth.

Figure 5.17, below, shows the changes of UV/Vis parameters between SEC fractions and between samples from different depths.

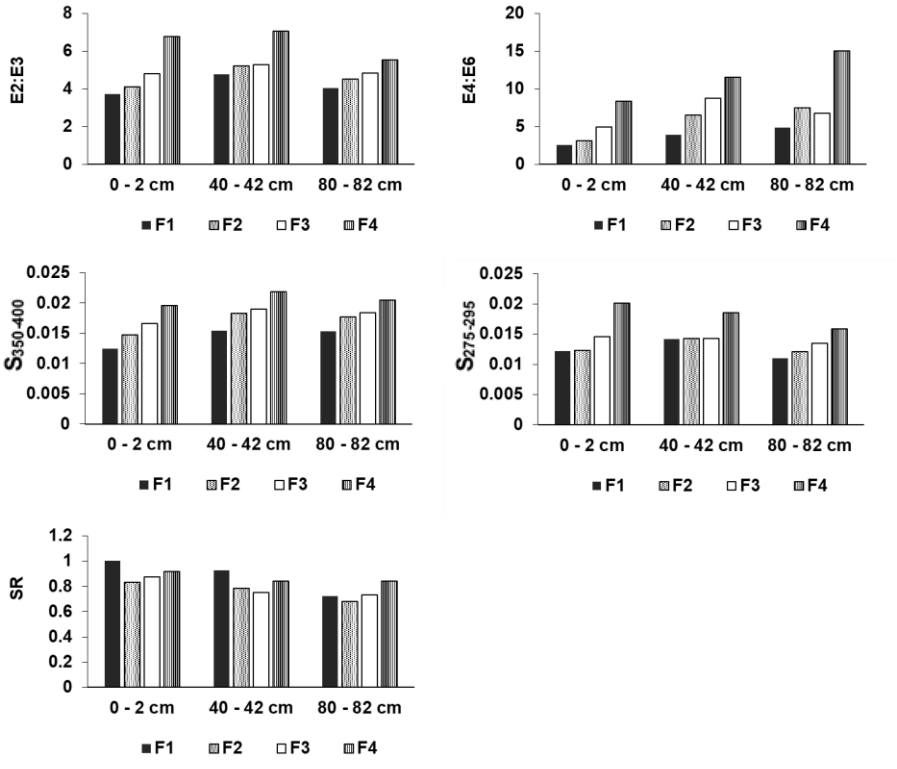

Figure 5.17. Results of the UV/Vis analysis of SEC fractions of OM from three depths in Merse core A.

The E2:E3, E4:E6, $S_{350-400}$ and $S_{275-295}$ all increase as the molecular size decreases, the SR, however shows no trend between fractions in the three samples. An interpretation of the results in relation to the other characterisation techniques is given at the end of the section.

Organic matter collected from SEC fractions was de-salted by cation exchange, freeze dried and anlaysed by FTIR. From the results of analysis by FTIR, the clearest trend between fractions is the increase of the peak at 1720 cm^{-1} in the two smaller fractions relative to the first two fractions. This can be seen in figure 5.18, below.

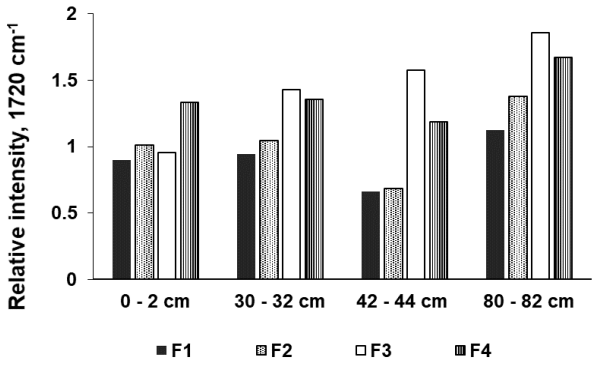

Figure 5.18. Results of the FTIR analysis of SEC fractions of OM from four depths in Merse core A.

In all cases the first fraction has the lowest peak at this point in the spectrum. This peak is attributed to the C=O group of -COOH functional groups, showing an increase in carboxyl functionality in the smaller fractions. Other changes seen in the results of FTIR analysis from large to small fractions were the general decrease in the peak at 2920 cm^{-1}, caused by the asymmetric stretch of CH in CH_2, and the decrease in the peak at 1630 cm^{-1}, which is attributed to the carboxylate or aromatic functionality. However, the between-fraction changes at these wavenumbers were not as clear as the increase in intensity at 1720 cm^{-1}.

The spectral changes from large to small fractions were generally similar to those seen in the analysis of material from the Needle's Eye bog (section 4.4), but unfortunately due to low sample amounts it was not possible to do more replicates to establish the reproducibility of the variations in OM composition observed for the saltmarsh samples.

The analysis of SEC fractions by ^{1}H NMR provided further information about the composition of the size fractions, as can be seen in figure 5.19.

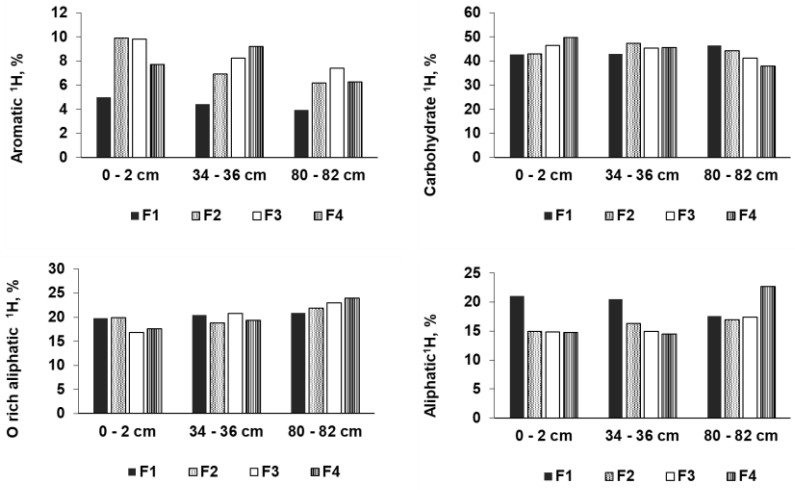

Figure 5.19. Percentage of ^{1}H in integrated regions of the ^{1}H NMR spectra of OM collected from SEC fractions of three Merse core A depth samples.

The main difference evident is the low aromaticity of F1 compared to the smaller size fractions. In the samples from 0 – 2 and 34 – 36 cm there is a peak in aliphatic organic matter in the first fraction, while the deepest fraction has an increased aliphatic character in the smallest fraction. There is also an increase in the oxygen rich aliphatic OM from F1 to F4 in the deepest sample. The area of the integrated peaks allows for comparison of the relative contribution of different types of OM in each sample.

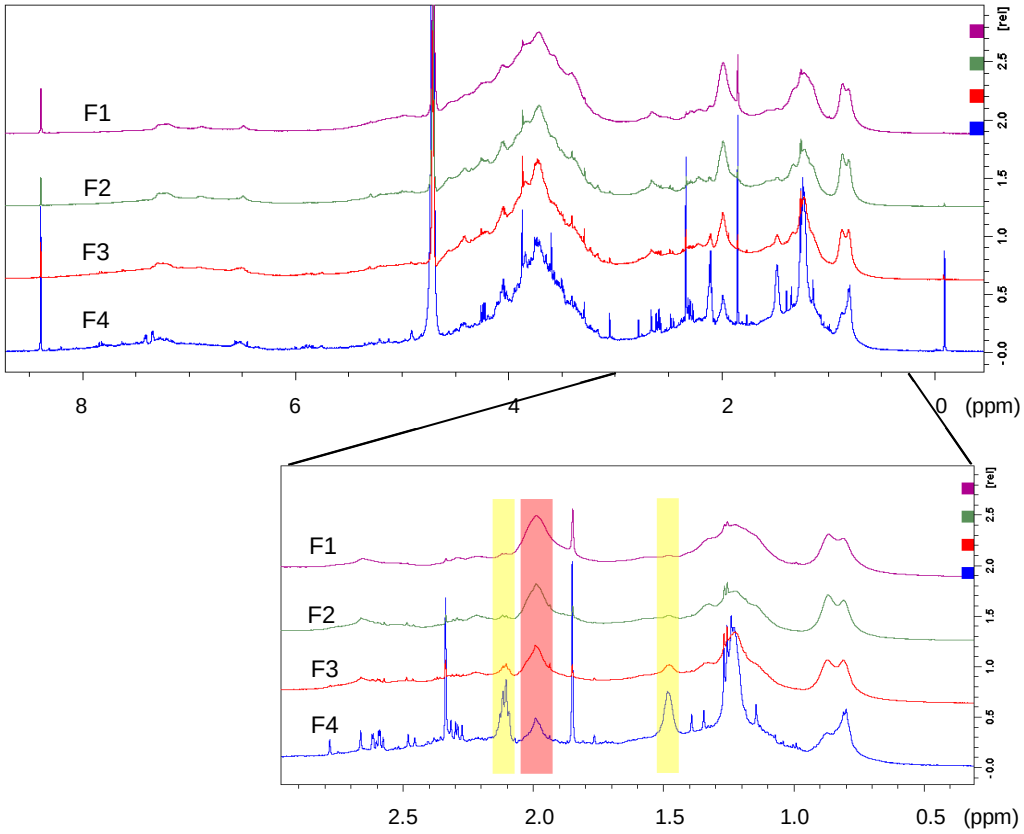

Figure 5.20. ^{1}H NMR spectra of SEC fractionated OM from the 80 – 82 cm depth sample of Merse core A. The spectra of decreasing size fractions F1 – F4 are shown. The expanded section shows the aliphatic region of the spectra in more detail. The yellow and red bands highlight peaks which change in intensity from F1 – F4.

The NMR spectra of the SEC fractions (figure 5.20) have similar major features with different intensities, shown by the area of integrated regions in figure 5.19. However, by examining the aliphatic region (enlarged section at the bottom of figure 5.20) peaks which change on transition from the small to large fractions are revealed. The yellow bands highlight the peaks which increase in intensity from F1 – F4. The analysis of COSY and HSQC spectra of SEC fractions of Needle's Eye bog OM (section 4.4), and comparison to similar studies on NOM in the literature (Hertkorn *et al.*, 2002; Simpson, Kingery and Hatcher, 2003; Hertkorn, 2006; Simpson *et al.*, 2007; Simpson, McNally and Simpson, 2011) makes it possible to identify these peaks as CH_2 groups positioned β (peak at around 2.1 ppm) and γ (peak at around 1.5 ppm) to COOH functional groups. This corroborates

the results of FTIR analysis which showed an increase in carboxylic functional groups from F1 – F4.

The slightly broader peak highlighted in red at around 2 ppm can be attributed to amino acid side chains (Simpson *et al.*, 2007; Simpson, McNally and Simpson, 2011). The decrease of this peak could suggest a change in the amount of microbially derived OM present from F1 – F4. More detailed characterisation experiments would need to be applied in order to confirm this as the explanation for the decrease of the peak. This could be achieved by calibration of the NMR techniques with model compounds.

The same features are evident, albeit less prominently, in the SEC fractions of the samples from 0 – 2 cm and 34 – 36 cm in the sediment profile, as can be seen in figure 5.21.

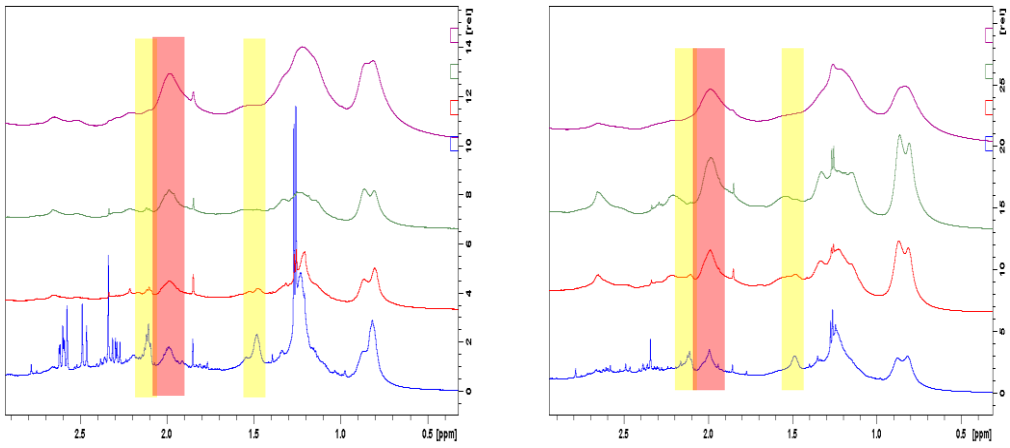

Figure 5.21. Aliphatic region of ^{1}H NMR spectra of SEC fractionated OM from the 0 – 2 cm (left) and 34 – 36 cm (right) depth samples of Merse core A. The spectra of decreasing size fractions F1 – F4 are shown from top to bottom. The yellow and red bands highlight peaks which change in intensity from F1 – F4, described above.

The main observations from the FTIR and NMR characterisation of OM SEC fractions are that there is an increase of aromatic character from F1 – F4 and a concurrent increase of aliphatic carboxylate functionality. The E2:E3 and E4:E6 ratio, $S_{350\text{-}400}$ and $S_{275\text{-}295}$ parameters measured by UV/vis all increased with decreasing SEC size fraction. These parameters have been shown to be inversely related to molecular weight and aromaticity, or degree of humification (Stevenson, 1982; Helms *et al.*, 2008; Chen *et al.*, 2011; See also section 4.4). In this case it appears that molecular weight is the dominant characteristic in these parameters, as there is a clear inverse relationship from F1 to F4. The increase of aromaticity from F1 – F4 does not cause a decrease in the UV/Vis E2:E3, E4:E6, or $S_{275\text{-}295}$.

5.3.2. ^{14}C and $\delta^{13}C$ analysis of fractionated OM

Figure 5.22 shows the ^{14}C specific activity of the OM of sediment samples which have undergone 0.1 M NaOH extraction (recalcitrant OM) compared to the extractable OM from the same samples.

The sediment samples were prepared from samples which had been extracted with 0.1 M NaOH then rinsed well with DI water, dried, washed with 2 M HCl for at least four hours to purge any carbonate present, rinsed with DI water once more and re-dried before preparation for analysis by AMS. Thus, the sediment ^{14}C activity and $\delta^{13}C$ results are of the recalcitrant organic fraction.

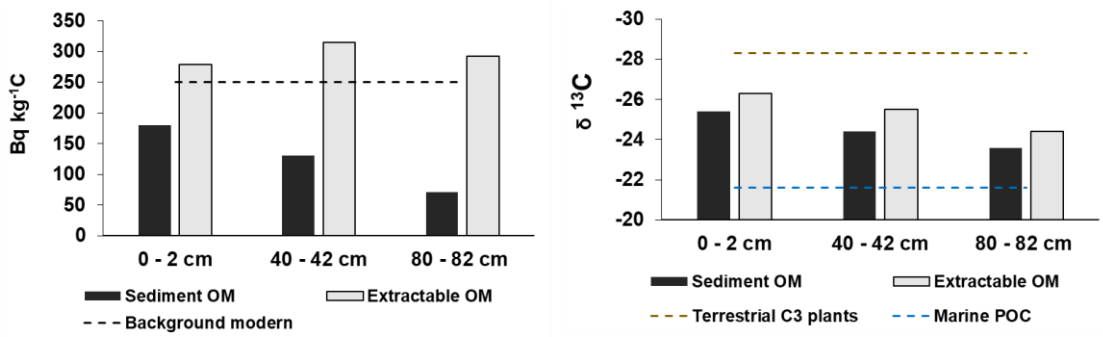

Figure 5.22. Specific activity of ^{14}C and $\delta^{13}C$ in recalcitrant OM (not extracted by 0.1 M NaOH) and extracted OM from three depths in Merse core A. The specific activity of ^{14}C is compared to the background modern activity of 250 Bq kg^{-1} and the $\delta^{13}C$ results are compared to those of marine POC and terrestrial C3 plants from the Southwick Merse. (MacKenzie et al., 2004)

It can be seen in figure 5.22 that the sediment OM has a much lower ^{14}C specific activity than the extractable OM, and is in fact depleted relative to the background modern level of around 250 Bq kg^{-1} C. This indicates that that the less extractable sediment OM is composed of old organic matter compared to the extractable OM. There is also a steady decrease with depth between the three sediment samples, indicating ageing with depth in the profile. These results are comparable with those of MacKenzie *et al.*, (2004) who also found depleted ^{14}C specific activities which decreased with depth in samples of total sediment OM. The results show that the extractable OM is enriched in ^{14}C relative to the sediment OM which has implications for the potential transfer of anthropogenic ^{14}C between environmental pools, as the more labile, extractable organic matter is a favourable substrate for microbial respiration.

The $\delta^{13}C$ of the sediment OM has a more marine POC signature than the extractable OM, and, like the extractable OM, the sediment OM has a more marine signature with depth. Again, this result is in agreement with MacKenzie *et al.*, (2004).

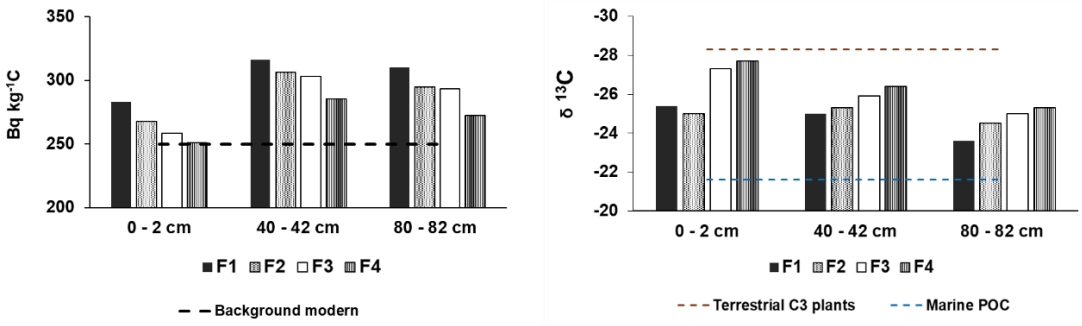

Figure 5.23. Specific activity of ^{14}C and $\delta^{13}C$ in SEC fractionated OM from three depths in Merse core A. The specific activity of ^{14}C is compared to the background modern activity of 250 Bq kg^{-1} and the $\delta^{13}C$ results are compared to those of marine POC and terrestrial C3 plants from the Southwick Merse (MacKenzie et al., 2004).

Figure 5.23 shows the ^{14}C specific activity of size fractions separated by SEC, with F1 being the largest fraction and F4 the smallest. There is a clear decrease of ^{14}C from the largest to smallest fraction in each sample. This is accompanied by a trend from marine to terrigenous $\delta^{13}C$ signal from the large to small fractions in all three examples. This is in agreement with the results of Malik *et al.*, (2012) who also found more negative $\delta^{13}C$ values in the small size fractions of fresh-water, coastal and marine OM separated by HPLC-SEC. The decrease in ^{14}C activity with increasingly terrigenous $\delta^{13}C$ signature, shown in figure 5.23, is as would be expected from a source of marine OM with enhanced ^{14}C activity.

5.3.3. Conclusions relating to the analysis of ^{14}C in OM

This work represents a novel application of fractionation, characterisation and isotope analysis techniques to investigate the incorporation of anthropogenic ^{14}C into OM and assess its potential for remobilization after deposition in sediments.

The comparison of extractable and recalcitrant OM shows that the extractable OM is considerably enriched with ^{14}C and the recalcitrant OM is formed of old OM which is likely to have been stabilized by humification processes over time. Within the extractable OM, the OM of marine origin, identified by the $\delta^{13}C$ signature, from shallower depths in the profile has elevated ^{14}C activity compared to that found at depth. There is a considerable dilution effect near the surface due to inputs of terrigenous OM. The results from the analysis both of depth profiles and SEC fractions show that OM with a more marine $\delta^{13}C$ signature has low aromaticity. The results of SEC analysis show that this material is found in the larger OM size fractions and is relatively enriched in ^{14}C, confirming that OM of more marine origin is enriched with ^{14}C relative to OM of terrigenous origin. The fact that the highest ^{14}C activity is in the larger size fractions suggests that, of the extractable OM, it is in the less labile fraction. This is backed up by the decrease in extractable OM with depth, contrary to the increase of marine origin OM and also the more marine $\delta^{13}C$ of recalcitrant OM relative to extractable OM. This evidence shows that OM of marine origin is quite unreactive once it reaches coastal sediments, probably because it has already undergone a significant amount of microbial degradation in the marine environment before being deposited in sediment. Should erosion and redistribution of sediments occur, it is unlikely that this ^{14}C enriched OM would act as a transferrable source of ^{14}C due to its apparent resistance to weathering processes.

6. Conclusions

The work undertaken in this study has highlighted the pivotal role organic matter plays in influencing the mobility of radionuclides in the environment. This role has been demonstrated for two radionuclides of very different properties and behaviour, U and ^{14}C, in two distinct environmental settings. The project objectives have been achieved by combining targeted organic and inorganic analysis techniques applied in the field and in the laboratory. The conclusions relating to objectives i. to iii. (Section 1.10) are summarised below:

i) Investigate geochemical characteristics of the Needle's Eye bog, determine geochemical influences on U accumulation and identify the oxidation state and speciation of U.

Analysis of transect samples showed that the point of highest U accumulation occurred where U rich porewaters enter the highly organic, low pH and predominantly reducing zone of the bog, ~17 m from the cliff. The zone of solid phase U enrichment between ~10 and 30 cm in the core profile was accompanied by variable redox conditions in the porewaters. This was indicated by the presence of high concentrations of Fe(III) coinciding with the predominantly colloidal U and Fe, isolated by ultrafiltration. Below a depth of ~30 cm, U showed less colloidal association and the dominant Fe species found in the porewaters was Fe(II). This point also marked the decrease in solid phase U enrichment. The correlation between U and Ca soil concentrations in all four cores analysed and in the soils and porewaters of the transect samples highlights the close relationship between U and Ca at the site, with U remaining in solution thanks to the formation of calcium uranyl carbonate species until reaching the bog where the pH decreases and U becomes associated with OM and Fe colloids while Ca remains truly dissolved in solution. The analysis of porewaters in transects and in depth profiles has built on previous work at the site and corroborates the

mechanism proposed by Xu, (2013) whereby the formation of these Fe-OM colloids facilitates the removal of U to the solid phase. The mechanism of colloid formation leading to U removal from solution, previously observed at a site polluted with depleted uranium from weapons testing (Graham *et al.*, 2011), could be important at other sites in which the accumulation of U by OM has been observed (e.g. Read *et al.*, 1993; Li *et al.*, 2015).

This study has confirmed, by the use of XANES, that U(VI) was present in the bog despite the prevailing reducing conditions, as was first demonstrated by Xu, (2013). Furthermore, EXAFS analysis demonstrated that the U(VI) was directly bound to the oxygen functional groups of OM. This is the first time the direct binding of U(VI) with OM has been proven at this site. The association of U(VI) (Read *et al.*, 1993; Regenspurg *et al.*, 2010; Li *et al.*, 2014; Li *et al.*, 2015) and U(IV) (Bone *et al.*, 2017) with OM has been previously observed in the environment and this study again highlights the importance of OM in immobilising U under the highly variable redox conditions prevalent at the Needle's Eye, shown by the Fe(II):Fe(III) ratio in porewaters.

For the first time, organic matter characterisation techniques were applied at the site. The combination of a suite of analytical methods have enhanced the understanding of the OM properties and structure in depth profiles and in a transect across the site. The OM from transect samples showed changes in composition consistent with zonation across the site. The transition from bog to saltmarsh manifested in OM by the development of more humic acid and aromatic composition while the OM within the bog had a higher concentration of carboxyl functionality, indicated by the FTIR band at 1720 cm^{-1}. In OM from depth profile samples an increase of aromaticity and decrease of oxygen rich functionalities was indicative of NOM humification and ageing processes with depth (Stevenson, 1982; Zech, Haumaier and Kogel-Knaber, 1989). The application of bomb pulse ^{14}C dating confirmed the ageing of OM with depth and facilitated the calculation of an accumulation rate of 0.28 ± 0.09 cm $year^{-1}$, which compares favourably with the accumulation rates of four Scottish

bogs (average 0.22 ± 0.01 cm $year^{-1}$) reported by Cloy *et al.*, (2009) . Schmeide *et al.*, (2003) reported that the complexation of U(VI) by humic acids was predominantly via carboxylic acid functional groups, suggesting that the NOM in the upper region of the bog, which is relatively enriched in carboxyl functional groups compared to lower down the profile, is favourable for binding U. Further evidence for the association of U and OM with depth in the profile was shown by the analysis of O/C ratio in soil samples from core E which correlated strongly with the soil U concentration ($\rho = 0.95$, $p<0.001$) which is in agreement with the results of EXAFS, showing the direct binding of U with oxygen functional groups of NOM.

ii) Investigate the composition of NOM in separated fractions and identify and characterise those which bind U

Organic matter from the site was successfully separated into fractions of distinct composition and properties, with differences in aromaticity, oxygen functional group content and solubility evident, as demonstrated by UV/vis, FTIR and NMR spectroscopic analysis and the humic: fulvic acid ratio. Early eluting size exclusion chromatography (SEC) fractions had an apparent mass of >100kDa, by comparison with ultrafiltration, greater humic acid character, relatively low aromaticity and carboxylic acid content and a higher aliphatic content compared to smaller fractions. The latest eluting fractions had a mass of <3 kDa and had high concentrations of carboxylic acid functional groups and fulvic acid character. Intermediate fractions, with an apparent mass of ~100 – 3 kDa had a relatively high aromaticity compared to earlier and later eluting fractions. The results of UV/vis analysis were compared with FTIR and NMR to improve the interpretation of results obtained by UV/vis. The E2:E3 ratio and SUVA 254 were correlated with aromaticity while the spectral slope $S_{275-295}$, spectral slope ratio (SR) and E4:E6 were influenced by molecular weight and degree of humification. These results are in agreement with the findings of other studies into the information derived from SUVA 254 (Weishaar

et al., 2003; Fernández-Romero *et al.*, 2016) E2:E3 (Peuravuori and Pihlaja, 1997) E4:E6 (Chen, Senesi and Schnitzer, 1977; You, Yin and Allen, 1999) and spectral slopes (Helms *et al.*, 2008; Fichot and Benner, 2012).

Analysis of U in SEC fractions showed that at neutral pH, similar to that seen in the bog, U was associated with "large" OM size fractions which have high contributions from aliphatic components and show humic acid characteristics. Iron was also found in the same fraction, implying the formation of Fe-OM aggregates. The interaction of U with Fe and OM is well documented (e.g. Waite *et al.*, 1994; Lenhart and Honeyman, 1999; Bargar *et al.*, 2000) and the results of SEC experiments corroborated the proposed mechanism of U removal to the solid phase in the bog, with disaggregation of Fe-OM colloids under reducing conditions and aggregation and incorporation of U under oxic conditions. pH was shown to be an important variable when considering the mobility of U, as batch extractions of soil from the site at different pH demonstrated the release of U from soil at high and low pH. The elution of U through SEC columns was also dependent on pH. Uranium eluted in the largest SEC fraction at neutral pH but eluted in the smallest SEC fraction at high pH. This is in agreement with Stockdale and Bryan, (2012), who demonstrated the release of U into solution at high pH, with only ~10% remaining associated with humic substances at pH 12.9.

iii) Investigate the accumulation of anthropogenic ^{14}C in sediment NOM and identify and characterise the fractions of NOM which incorporate ^{14}C

In sediments at the Southwick Merse, anthropogenic ^{14}C was found to accumulate in 0.1 M NaOH extractable OM. The marine or terrigenous origin of this sediment OM was first identified by spectroscopic analysis techniques and confirmed by $\delta^{13}C$ analysis. Characterisation of OM showed that terrigenous OM, indicated by the $\delta^{13}C$ signature, had

higher aromaticity while OM of marine origin was more aliphatic. The variation of OM origin with depth identified by MacKenzie *et al.*, (2004) was confirmed by this study, and the change in OM composition with depth was identified as being due to the changing origin of the OM with depth. Separation of extracted OM of marine or terrigenous origin was achieved by SEC. Organic matter of marine origin was found in the larger size fractions and was again shown to be more aliphatic, while terrigenous OM eluted in the smaller SEC size fractions and had more aromatic structure. The OM eluting in the large SEC fractions was enriched with anthropogenic ^{14}C demonstrating the incorporation of Sellafield discharged ^{14}C into marine organic matter. These results show that marine OM enriched with anthropogenic ^{14}C and deposited into sediments is relatively large and less mobile.

Overall, the results of this study highlight the importance of NOM in soils and sediments as a substrate for binding and incorporating U and ^{14}C respectively, with both these radionuclides found associated with larger, less functional group rich and less mobile NOM fractions in this study. This suggests that at these sites the radionuclides will remain stable for as long as conditions remain favourable, and also that similar organic soils and accreting coastal sediments are likely to be effective sinks for both U and ^{14}C rspectively. However, changes in geochemical conditions at both sample sites could cause remobilisation of U and ^{14}C associated with OM. A relatively small increase in pH in the bog, for example caused by seawater inundation if sea levels were to rise, could lead to mobilisation of U by creating conditions favourable for maintaining calcium uranyl carbonates in solution (Gorman-lewis, Burns and Fein, 2007). The coastal sediments of the Solway coast are highly dynamic and although in some areas sediment has been accumulating for tens of thousands of years (McMillan *et al.*, 2011), in others, and notably around the Southwick Merse, erosion and redeposition occur (Cutts and Hemingway, 1996; Harvey, Hansom and MacKenzie, 2007). A large erosion and redeposition event could cause the re-distribution of ^{14}C incorporated in sediments over a wide area. Furthermore, a greater increase in pH to

>10 would facilitate the dissolution and mobilisation of OM and the radionuclides associated with it in both sample sites examined. Organic matter found in this study to be enriched in ^{14}C was alkali soluble while recalcitrant OM was not enriched. Similarly, high pH was shown to release U from the organic soil and this U was likely to be largely freely dissolved in solution with a small percentage associated with OM (Stockdale and Bryan, 2012). This has serious implications for the mobility of these radionuclides around a deep geological repository due to the localised increase of pH caused by the use of cementitious construction materials (Jacques *et al.*, 2010). Remobilisation by these mechanisms could cause U and ^{14}C to come into contact with vulnerable receptors, therefore U and ^{14}C associated with NOM should not be considered to be irreversibly immobilised.

7. Further work

Based on the findings of this investigation, it is clear that NOM in soils and sediments is an important substrate for accumulation of radionuclides and heavy metals. The Needle's Eye Natural Analogue site presents a unique set of conditions for the investigation of the influence of OM, redox chemistry, pH and water flow on natural decay series nuclides. Analysis of ^{226}Ra at the site could yield an important insight into its mobility and associations in the environment. Isotopes of Ra are of interest in radiological risk assessment due to their relatively long half-lives, short lived daughter nuclides and high mobility in the environment (Fesenko *et al.*, 2014).

Now the geochemical behaviour of ^{14}C and U have been defined there is an opportunity for further research into their potential transfer into biota. The interaction of microbes and plants with OM could be an important factor in the fate of radionuclides at these Natural laboratory sites and also could act as a pathway for radionuclides to reach potentially vulnerable receptors.

The unusual redox conditions found in the Needles Eye bog has been hypothesised to be related to the subsurface flow of oxic, Ca and U bearing water from the cliff. An investigation of the hydrogeochemistry of the site, such as subsurface flow paths and flow rates, is necessary to confirm the source of the variable soil chemical conditions.

Colloid formation has been implicated as a mechanism of transferring U to the solid phase in the Needle's Eye Bog, however the formation and behaviour of colloids at the site is still poorly understood. Further investigation into colloid formation, characterisation and stability in solution at the site would provide useful information on the colloid mediated transport or accumulation of U, other radionuclides and potentially toxic elements. This information would be applicable to other instances of colloid facilitated transport or immobilisation in contaminated sites.

References

Abdulla, H. A. N., Minor, E. C., Dias, R. F. and Hatcher, P. G. (2010) 'Changes in the compound classes of dissolved organic matter along an estuarine transect: A study using FTIR and ^{13}C NMR', *Geochimica et Cosmochimica Acta*. 74(13), pp. 3815–3838. doi: 10.1016/j.gca.2010.04.006.

Adam, P., Bertness, M., Davy, A. and Zedlar, J. (2008) 'Saltmarsh', in Polunin, N. V. C. (ed.) *Aquatic Ecosystems. Trends and Global Prospects*. Cambridge: Cambridge University Press, pp. 157–171. Available at: https:/www.cambridge.org/core.

Aitken, U., Takeshita, K., Matsura, S., Foundation, S. and Ikeya, M. (1980) 'Isotopic Disequilibrium of Uranium : Alpha-Recoil Damage and Preferential Solution Effects', (1), pp. 979–981.

Akkanen, J., Lyytikäinen, M., Tuikka, A. and Kukkonen, J. V. K. (2005) 'Dissolved organic matter in pore water of freshwater sediments: Effects of separation procedure on quantity, quality and functionality', *Chemosphere*, 60(11), pp. 1608–1615. doi: 10.1016/j.chemosphere.2005.02.045.

Allan, R. L. (1993) *Distribution, Geochemistry and Geochronology of Sellafield Waste in Contaminated Solway Firth Floodplain Deposits*. PhD Thesis, University of Glasgow.

Alloway, B. (2013) 'Uranium', in Alloway, B. (ed.) *Heavy Metals in Soils: Trace metals and metalloids and their availability*. 3rd edn. Dordrecht, Heidelberg, New York, London: Springer, pp. 565–577. doi: 10.1007/978-94-007-4470-7.

Ammann, A. A. (2007) 'SPECIAL FEATURE : Inductively coupled plasma mass spectrometry (ICP MS): a versatile tool', *Journal of Mass Spectrometry*, 42, pp. 419–427. doi: 10.1002/jms.

Andrews, J. E., Samways, G. and Shimmield, G. B. (2008) 'Historical storage budgets of organic carbon, nutrient and contaminant elements in saltmarsh sediments: biogeochemical context for managed realignment, Humber Estuary, UK.', *The Science of the Total Environment*, 405(1–3), pp. 1–13. doi: 10.1016/j.scitotenv.2008.07.044.

Appel, C., Ma, L. Q., Rhue, R. D. and Kennelley, E. (2003) 'Point of zero charge determination in soils and minerals via traditional methods and detection of electroacoustic mobility', *Geoderma*, 113(1–2), pp. 77–93. doi: 10.1016/S0016-7061(02)00316-6.

Arai, Y. (2010) 'Arsenic and Antimony', in Hooda, P. (ed.) *Trace Elements in Soils*. 1st edn. Chichester: Blackwell Publishing, John Wiley and Sons, pp. 383–400.

ARPANSA (2005) *Naturally-Occurring Radioactive Material (NORM) in Australia : Issues for Discussion*. Report by the Radiation Health & Safety Advisory Council.

Artz, R. R. E., Chapman, S. J., Jean Robertson, A. H., Potts, J. M., Laggoun-Defarge, F., Gogo, S., Comont, L., Disnar, J. R. and Francez, A. J. (2008) 'FTIR spectroscopy can be used as a screening tool for organic matter quality in regenerating cutover peatlands', *Soil Biology and Biochemistry*, 40(2), pp. 515–527. doi: 10.1016/j.soilbio.2007.09.019.

Aston, S. R. and Stanners, D. A. (1979) 'The determination of estuarine sedimentation by $^{134}Cs/\ ^{137}Cs$ and other artificial radionuclide profiles', *Estuarine and Coastal Marine Science*, 9, pp. 529–541.

Aston, S. R. and Stanners, D. A. (1982) 'The transport to and deposition of americium in intertidal sediments of the Ravenglass estuary and its relationship to plutonium', *Environmental Pollution. Series B, Chemical and Physical*, 3(1), pp. 1–9. doi: 10.1016/0143-148X(82)90038-6.

Atkins, P. (2006) *Physical Chemistry*. 8th edn. Oxford: Oxford University Press.

Babula, P., Adam, V., Opatrilova, R., Zehnalek, J. and Kizek, R. (2010) 'Uncommon Heavy Metals, Metalloids and Their Plant Toxicity: A review', in *Organic Farming, Pest Control and Remediation of Soil Pollutants*. doi: 10.1007/978-1-4020-9654-9.

Bakatula, E. N., Richard, D., Neculita, C. M. and Zagury, G. J. (2018) 'Determination of point of zero charge of natural organic materials', *Environmental Science and Pollution Research*. Environmental Science and Pollution Research, 25(8), pp. 7823–7833. doi: 10.1007/s11356-017-1115-7.

Balonov, M., Dubourg, M., Efremenkov, V., Gilpin, J., Mishin, E., Rabun, R., Wong, P. and Wright, M. (2004) 'Production and Emission Pathways', in *Management of Waste Containing Tritium and Carbon-14*. Vienna: IAEA, pp. 11–37.

Banning, A., Demmel, T., Rüde, T. R. and Wrobel, M. (2013) 'Groundwater uranium origin and fate control in a river valley aquifer.', *Environmental Science & Technology*, 47(24), pp. 13941–8. doi: 10.1021/es304609e.

Bargar, J. R., Reitmeyer, R., Lenhart, J. J. and Davis, J. A. (2000) 'Characterization of U(VI)-carbonato ternary complexes on hematite: EXAFS and electrophoretic mobility measurements', *Geochimica et Cosmochimica Acta*, 64(16), pp. 2737–2749. doi: 10.1016/S0016-7037(00)00398-7.

Basham, I., Milodowski, A., Hyslop, E. and Pearce, J. (1991) *The location of uranium in source rocks and sites of secondary deposition at the Needle's Eye natural analogue site, Dumfries and Galloway*. Luxembourg: Commission of the European Communities. Report EUR 13279.

Battin, T. J., Luyssaert, S., Kaplan, L. A., Aufdenkampe, A. K., Richter, A. and Tranvik, L. J. (2009) 'The boundless carbon cycle', *Nature Geoscience*. Nature Publishing Group, 2(9), pp. 598–600. doi: 10.1038/ngeo618.

Bayliss, C. R. and Langley, K. F. (2003a) ‘Chapter 1 – Setting the Scene’, in *Nuclear Decommissioning, Waste Management, and Environmental Site Remediation*, pp. 1–21. doi: 10.1016/B978-075067744-8/50004-7.

Bayliss, C. R. and Langley, K. F. (2003b) ‘Chapter 2 – Ionising Radiation and its Control’, in *Nuclear Decommissioning, Waste Management, and Environmental Site Remediation*, pp. 23–40. doi: 10.1016/B978-075067744-8/50005-9.

Begg, F. H., Cook, G. T., Baxter, M. S., Scott, E. M. and Mccartney, M. (1992) ‘Anthropogenic radiocarbon in the eastern Irish Sea and Scottish coastal waters’, *Radiocarbon*, 34(3), pp. 707–716.

Behrends, T. and Van Cappellen, P. (2005) ‘Competition between enzymatic and abiotic reduction of uranium(VI) under iron reducing conditions’, *Chemical Geology*, 220(3–4), pp. 315–327. doi: 10.1016/j.chemgeo.2005.04.007.

Bell, J. N. B. and Shaw, G. (2005) ‘Ecological lessons from the Chernobyl accident.’, *Environment International*, 31(6), pp. 771–7. doi: 10.1016/j.envint.2005.05.026.

Bell, N. G. A., Graham, M. C. and Uhrín, D. (2016) ‘Isotope-filtered nD NMR spectroscopy of complex mixtures to unravel the molecular structures of phenolic compounds in tagged soil organic matter’, *The Analyst*. Royal Society of Chemistry, 141(15), pp. 4614–4624. doi: 10.1039/C6AN00999A.

Bell, N. G. A., Murray, L., Graham, M. C. and Uhrín, D. (2014) ‘NMR methodology for complex mixture “separation”.’, *Chemical Communications (Cambridge, England)*, 50(14), pp. 1694–7. doi: 10.1039/c3cc48907h.

Bell, N. G. A, Michalchuk, A. A. L., Blackburn, J. W. T., Graham, M. C. and Uhrín, D. (2015) ‘Isotope-Filtered 4D NMR Spectroscopy for Structure Determination of Humic

Substances.', *Angewandte Chemie (International ed. in English)*, 54(29), pp. 8382–5. doi: 10.1002/anie.201503321.

Benner, R. (2004) 'What happens to terrestrial organic matter in the ocean?', *Marine Chemistry*, 92, pp. 307–310. doi: 10.1016/S0146-6380(97)00066-1.

Biester, H., Knorr, K. H., Schellekens, J., Basler, A. and Hermanns, Y. M. (2014) 'Comparison of different methods to determine the degree of peat decomposition in peat bogs', *Biogeosciences*, 11(10), pp. 2691–2707. doi: 10.5194/bg-11-2691-2014.

Blackburn, J. W. T., Kew, W., Graham, M. C. and Uhrín, D. (2017) 'Laser Desorption/Ionization Coupled to FTICR Mass Spectrometry for Studies of Natural Organic Matter', *Analytical Chemistry*, 89(8), pp. 4382–4386. doi: 10.1021/acs.analchem.6b04817.

Blair, D. (2013) *Carbon and contaminant trace metal biogeochemistry in surficial organic-rich terrestrial systems*. PhD Thesis, University of Edinburgh.

BNFL (1985) *Annual Report on Radioactive Discharges and Monitoring of the Environment, 1985 - 1989*. Risley.

Bojanowski, R., Radecki, Z., Campbell, M. J., Burns, K. I. and Trinkl, A. (2001) Report on the Intercomparison Run for the Determination of Radionuclides in IAEA-326 and IAEA-327. IAEA/AL/10. Vienna: IAEA.

Bolea, E., Gorriz, M. P., Bouby, M., Laborda, F., Castillo, J. R. and Geckeis, H. (2006) 'Multielement characterization of metal-humic substances complexation by size exclusion chromatography, asymmetrical flow field-flow fractionation, ultrafiltration and inductively coupled plasma-mass spectrometry detection: A comparative approach', *Journal of Chromatography A*, 1129(2), pp. 236–246. doi:0.1016/j.chroma.2006.06.097.

Bolea, E., Laborda, F. and Castillo, J. R. (2010) 'Metal associations to microparticles, nanocolloids and macromolecules in compost leachates: Size characterization by asymmetrical flow field-flow fractionation coupled to ICP-MS', *Analytica Chimica Acta*, 661(2), pp. 206–214. doi: 10.1016/j.aca.2009.12.021.

Bone, S. E., Dynes, J. J., Cliff, J. and Bargar, J. R. (2017a) 'Uranium(IV) adsorption by natural organic matter in anoxic sediments', *Proceedings of the National Academy of Sciences*, 114(4), pp. 711–716. doi: 10.1073/pnas.1611918114.

Bordelet, G., Beaucaire, C., Phrommavanh, V. and Descostes, M. (2013) 'Sorption Properties of Peat for U(VI) and ^{226}Ra in U Mining Areas', *Procedia Earth and Planetary Science*. Elsevier B.V., 7(Vi), pp. 85–88. doi: 10.1016/j.proeps.2013.03.121.

Boss, C. and Fredeen, K. (2004) *Concepts, Instrumentation and Techniques in Inductively Coupled Plasma Optical Emission Spectroscopy*. 3rd edn. Shelton: Perkin Elmer.

Bots, P., Morris, K., Hibberd, R., Law, G. T. W., Mosselmans, J. F. W., Brown, A. P., Doutch, J., Smith, A. J. and Shaw, S. (2014) 'Formation of stable uranium(VI) colloidal nanoparticles in conditions relevant to radioactive waste disposal', *Langmuir*, 30(48), pp. 14396–14405. doi: 10.1021/la502832j.

Bourdon, B., Turner, S., Henderson, G. M. and Lundstrom, C. C. (2003) 'Introduction to U-series Geochemistry', *Reviews in Mineralogy & Geochemistry*, 52(1), pp. 1–24. doi: 10.2113/0520001.

Bracke, G. and Müller, W. (2008) 'Contribution to a more realistic approach in assessing the release of C-14 from low-level radioactive waste repositories', *Journal of Contaminant Hydrology*. Elsevier B.V., 102(3–4), pp. 210–216. doi: 10.1016/j.jconhyd.2008.09.014.

Brady, N. and Weil, R. (1996) 'Soil Organic Matter', in Kupchik, A. and Carnis, M. (eds)

The Nature and Properties of Soils. London: Prentice-Hall International, pp. 361–398.

Braithwaite, a and Livens, F. (1997) 'Kinetically controlled release of uranium from soils', *European Journal of Soil Science*, (December), pp. 661–673. doi: 10.1111/j.1365-2389.1997.tb00566.x.

Braithwaite, R. and Knight, J. (1990) 'Rare minerals , including several new to Britain , in supergene alteration of U - C u - A s - B i - C o mineralisation near Dalbeattie , south Scotland', *Mineralogical Magazine*, 54, pp. 129–131.

Brooks, S. C., Fredrickson, J. K., Carroll, S. L., Kennedy, D. W., Zachara, J. M., Plymale, A. E., Kelly, S. D., Kemner, K. M. and Fendorf, S. (2003) 'Inhibition of bacterial U(VI) reduction by calcium', *Environmental Science and Technology*, 37(9), pp. 1850–1858. doi: 10.1021/es0210042.

Brugge, D. and Buchner, V. (2011) 'Health effects of uranium: new research findings.', *Reviews on Environmental Health.*, 26 231(4), pp. 231–349.

Bryan, N. D., Abrahamsen, L., Evans, N., Warwick, P., Buckau, G., Weng, L. and Van Riemsdijk, W. H. (2012) 'The effects of humic substances on the transport of radionuclides: Recent improvements in the prediction of behaviour and the understanding of mechanisms', *Applied Geochemistry*. 27(2), pp. 378–389. doi: 10.1016/j.apgeochem.2011.09.008.

Burd, F. (1989) *The Saltmarsh Survey of Great Britain*. Nature Conservancy Council Report Number 17, Peterborough.

Busetti, F., Berwick, L., McDonald, S., Heitz, A., Joll, C. A., Loh, J. and Power, G. (2014) 'Physicochemical Characterization of Organic Matter in Bayer Liquor', *Industrial & Engineering Chemistry Research*, 53(15), pp. 6544–6553. doi: 10.1021/ie4028268.

Chang, R. R., Mylotte, R., McInerney, R., Tzou, Y. M. and Hayes, M. H. B. (2013) 'A comparison of the compositional differences between humic fractions isolated by the IHSS and exhaustive extraction procedures', *Functions of Natural Organic Matter in Changing Environment*, 9789400756, pp. 141–145. doi: 10.1007/978-94-007-5634-2_25.

Charlesworth, M. E., Service, M. and Gibson, C. E. (2006) 'The distribution and transport of Sellafield derived ^{137}Cs and ^{241}Am to western Irish Sea sediments.', *The Science of the Total Environment*, 354(1), pp. 83–92. doi: 10.1016/j.scitotenv.2004.12.062.

Chen, H., Zheng, B., Song, Y. and Qin, Y. (2011) 'Correlation between molecular absorption spectral slope ratios and fluorescence humification indices in characterizing CDOM', *Aquatic Sciences*, (73), pp. 103–112. doi: 10.1007/s00027-010-0164-5.

Chen, J., Gu, B., Leboeuf, E. J., Pan, H. and Dai, S. (2002) 'Spectroscopic characterization of the structural and functional properties of natural organic matter fractions.', *Chemosphere*, 48(1), pp. 59–68. Available at: www.ncbi.nlm.nih.gov/pubmed /12137058.

Chen, J., Gu, B., Royer, R. A. and Burgos, W. D. (2003) 'The roles of natural organic matter in chemical and microbial reduction of ferric iron', *Science of the Total Environment*, 307(1–3), pp. 167–178. doi: 10.1016/S0048-9697(02)00538-7.

Chen, M., Lee, J. and Hur, J. (2015) 'Effects of sampling methods on the quantity and quality of dissolved organic matter in sediment pore waters as revealed by absorption and fluorescence spectroscopy', *Environmental Science and Pollution Research*, 22(19), pp. 14841–14851. doi: 10.1007/s11356-015-4656-7.

Chen, Y., Senesi, N. and Schnitzer, M. (1977) 'Information provided on humic substances by E4/E6 ratios.', *Soil Science Society of America Journal*, (41), p. 352–358.

Chew, M. (2013) ‘Investigation of uranium redox chemistry and complexation across the pH range by cyclic voltammetry’. PhD Thesis, Loughborough University.

Chikaraishi, Y., Yamada, Y. and Naraoka, H. (2005) ‘Hydrogen and carbon isotope fractionation during lipid biosynthesis of terrestrial plants’, *Limnology and Oceanography*, 50(6), pp. 1763–1770.

Chin, Y. and Gschwend, P. M. (1991) ‘The abundance , distribution , and configuration of porewater organic colloids in recent sediments’ *Geochimica et Cosmochimica Acta*, 55(5), pp.1309-1317.

Christl, I. and Kretzschmar, R. (2001) ‘Interaction of copper and fulvic acid at the hematite-water interface’, *Geochimica et Cosmochimica Acta*, 65(20), pp. 3435–3442. doi: 10.1016/S0016-7037(01)00695-0.

Clark, M. J. (1986) ‘Fallout from Chernobyl’, *Journal of the Society of Radiological Protection*, 6, p. 157.

Cloy, J. M., Farmer, J. G., Graham, M. C. and Mackenzie, A. B. (2009) ‘Retention of As and Sb in ombrotrophic peat bogs: Records of As, Sb, and Pb deposition at four Scottish sites’, *Environmental Science and Technology*, 43(6), pp. 1756–1762. doi: 10.1021/es802573e.

Collingridge, D. (1984) ‘Lessons of nuclear power US and UK history’, *Energy Policy*, 12(1), pp. 46–67. doi: 10.1016/0301-4215(84)90087-9.

Come, B. and Chapman, N. (1985) *Natural Analogue Working Group, First Meeting Brussels, November 5 - 7, 1985*. Luxembourg: Commission of the European Communities.

Conte, P. and Piccolo, A. (1999) ‘Conformational arrangement of dissolved humic substances. Influence of solution composition on association of humic molecules’,

Environmental Science and Technology, 33(10), pp. 1682–1690. doi: 10.1021/es9808604.

Cook, G., Scott, E. and Harkness, D. (2010) 'Radiocarbon as a Tracer in the Global Carbon Cycle', in Froehlich, H. (ed.) *Radioactivity in the Environment*. Amsterdam, p. 10:89-137.

Cook, G. T., Begg, F. H., Naysmith, P., Scott, E. M. and McCartney, M. (1995) 'Anthropogenic ^{14}C marine geochemistry in the vicinity of a nuclear fuel reprocessing plant', *Radiocarbon*, 37(2), pp. 459–467.

Cook, G. T., Mackenzie, a B., Naysmith, P. and Anderson, R. (1998) 'Natural and Anthropogenic ^{14}C in the UK Coastal Marine Environment', *Journal of Environmental Radioactivity*, 40(1), pp. 89–111.

Cook, G. T., MacKenzie, A. B., Muir, G. K. P., MacKie, G. and Gulliver, P. (2004) 'Sellafield-derived anthropogenic ^{14}C in the Marine Intertidal Environment of the NE Irish Sea', *Radiocarbon*, 46(2), pp. 877–883.

Corvasce, M., Zsolnay, A., D'Orazio, V., Lopez, R. and Miano, T. M. (2006) 'Characterization of water extractable organic matter in a deep soil profile', *Chemosphere*, 62(10), pp. 1583–1590. doi: 10.1016/j.chemosphere.2005.07.065.

Covelo, E. F., Vega, F. A. and Andrade, M. L. (2007) 'Competitive sorption and desorption of heavy metals by individual soil components', *Journal of Hazardous Materials*, 140, pp. 308–315. doi: 10.1016/j.jhazmat.2006.09.018.

Cumberland, S. A., Douglas, G., Grice, K. and Moreau, J. W. (2016) 'Uranium mobility in organic matter-rich sediments : A review of geological and geochemical processes', *Earth Science Reviews*. 159, pp. 160–185. doi: 10.1016/j.earscirev.2016.05.010.

Currie, K. I., Brailsford, G., Nichol, S., Gomez, A., Sparks, R., Lassey, K. R. and Riedel, K. (2009) 'Tropospheric 14CO2 at Wellington, New Zealand: the world's longest record',

Biogeochemistry, 104(1–3), pp. 5–22. doi: 10.1007/s10533-009-9352-6.

Cutts, N. and Hemingway, K. (1996) 'The Solway Firth: broad scale habitat mapping', *Scottish Natural Heritage. Research, Survey and Monitoring Report No. 46*. Edinburgh: SNH, p. 214.

D'Andrilli, J., Chanton, J. P., Glaser, P. H. and Cooper, W. T. (2010) 'Characterization of dissolved organic matter in northern peatland soil porewaters by ultra high resolution mass spectrometry', *Organic Geochemistry*. 41(8), pp. 791–799. doi: 10.1016/j.orggeochem.2010.05.009.

Dalzell, B. J., Minor, E. C. and Mopper, K. M. (2009) 'Photodegradation of estuarine dissolved organic matter: a multi-method assessment of DOM transformation', *Organic Geochemistry*., 40(2), pp. 243–257. doi: 10.1016/j.orggeochem.2008.10.003.

Deditius, A. P., Utsunomiya, S. and Ewing, R. C. (2008) 'The chemical stability of coffinite, $USiO_4.nH_2O$; $0 < n < 2$, associated with organic matter: A case study from Grants uranium region, New Mexico, USA', *Chemical Geology*, 251(1–4), pp. 33–49. doi: 10.1016/j.chemgeo.2008.02.009.

DEFRA (2011) *Environmental Permitting Guidance Radioactive Substances Regulation*. London: DEFRA. Available at: www.defra.gov.uk/environment/policy/permits.

DEFRA (2013) *Environmental Permitting Guidance Core guidance For the Environmental Permitting (England and Wales) Regulations 2010*. London: DEFRA. Available at: http://archive.defra.gov.uk/environment/policy/permits/guidance.htm#ep.

DEFRA, BERR and DOENI (2008) *Managing Radioactive Waste Safely: A Framework for Implementing Geological Disposal*. Belfast: The Stationary Office. Report Cm 7386

Dhillon, G. S., Gillespie, A., Peak, D. and Van Rees, K. C. J. (2017) 'Spectroscopic

investigation of soil organic matter composition for shelterbelt agroforestry systems', *Geoderma*. Elsevier B.V., 298, pp. 1–13. doi: 10.1016/j.geoderma.2017.03.016.

Dias da Cunha, K. M., Henderson, H., Thomson, B. M. and Hecht, A. a (2014) 'Ground water contamination with ^{238}U, ^{234}U, ^{235}U, ^{226}Ra and ^{210}Pb from past uranium mining: cove wash, Arizona.', *Environmental Geochemistry and H ealth*, 36(3), pp. 477–87. doi: 10.1007/s10653-013-9575-2.

Dick, D., Santos, J. and Ferranti, E. (2003) 'Chemical characterization and infrared spectroscopy of soil organic matter from two southern Brazilian soils', *Revista Brasileira de Ciência do Solo*, 27(3), pp. 29–39. doi: 10.1590/S0100-06832003000100004.

Dobbs, R. A., Wise, R. H. and Dean, R. B. (1972) 'The use of ultra-violet absorbance for monitoring the total organic carbon content of water and wastewater', *Water Research*, 6(10), pp. 1173–1180. doi: 10.1016/0043-1354(72)90017-6.

Drever, J. (1997) 'Heavy Metals and Metalloids', in *The Geochemistry of Natural Waters, Surface and Groundwater Environments*. 3rd edn. Upper Saddle River, New Jersey, pp. 189–192.

Duarte, R. M. B. O., Barros, A. C. and Duarte, A. C. (2012) 'Resolving the chemical heterogeneity of natural organic matter: new insights from comprehensive two-dimensional liquid chromatography.', *Journal of chromatography.*, 1249, pp. 138–46. doi: 10.1016/j.chroma.2012.06.022.

Dunbar, E., Cook, G. T., Naysmith, P., Tripney, B. G. and Xu, S. (2016) 'AMS ^{14}C Dating at the Scottish Universities Environmental Research Centre (SUERC) Radiocarbon Dating Laboratory', *Radiocarbon*, 58(01), pp. 9–23. doi: 10.1017/RDC.2015.2.

Echevarria, G., Sheppard, M. I. and Morel, J. L. (2001) 'Effect of pH on the sorption of

uranium in soils', *Journal of Environmental Radioactivity*, 53(2), pp. 257–264. doi: 10.1016/S0265-931X(00)00116-8.

Edwards, K. (1968) Isotopic Analysis of Uranium in Natural Waters by Alpha Spectrometry. *Geological Survey Water-Supply Paper 1696-F*, Washington.

Edzwald, J. K., Becker, W. C. and Wattier, K. L. (1985) 'Surrogate Parameters for monitoring organic matter and THM precursors', *Journal of the American Waterworks Association*, 77(4), pp. 122–132.

Eisenbud and Gesell, T. (1997) 'Chapter 6 – Natural Radioactivity', in *Environmental Radioactivity*. 4th edn. San Diego, pp. 134–200. doi: 10.1016/B978-012235154-9/50010-4.

Eisenbud, M. and Gesell, T. (1997a) 'Experience with radioactive contamination due to accidents', in *Environmental Radioactivity from Natural, Industrial & Military Sources*, pp. 378–437.

Eisenbud, M. and Gesell, T. (1997b) 'Radiological Assessment and Its Application to Dose Reconstruction', in *Enviromental Radioactivity*. 4th edn. San Diego, pp. 470–493.

Enev, V., Pospíšilová, L., Klučáková, M., Liptaj, T. and Doskočil, L. (2014) 'Spectral characterization of selected humic substances', *Soil and Water Research*, 9(1), pp. 9–17.

Environment Agency (2007) *Soil Guideline Values for inorganic arsenic in soil*. Bristol. Science Report SC050021/ arsenic SGV, Available at: www.environment-agency.gov.uk/clea.

EPA (1996) 'Method 3052: Microwave assisted acid digestion of siliceous and organically based matrices', pp. 1–20. Available at: http://www.epa.gov/osw/hazard/testmethods/sw846/pdfs/3052.pdf.

Eriksson, G. (1979) ‘An algorithm for the computation of aqueous multi-component, multiphase equilibria’, *Analytica Chimica Acta*. Elsevier, 112(4), pp. 375–383. doi: 10.1016/S0003-2670(01)85035-2.

Ewing, R. C., Runde, W. and Albrecht-Schmitt, T. E. (2010) ‘Environmental impact of the nuclear fuel cycle : Fate of actinides’, *Materials Research Society Bulletin*, 35(November), pp. 859–866.

Fabry, V. J., Seibel, B. A., Feely, R. A., Fabry, J. C. O. and Fabry, V. J. (2008) ‘Impacts of ocean acidification on marine fauna and ecosystem processes’, *ICES Journal of Marine Science*, 65(3), pp. 414–432. doi: 10.1093/icesjms/fsn048.

Falso, M. J. S. and Buchholz, B. A. (2013) ‘Bomb pulse biology’, *Nuclear Instruments and Methods in Physics Research, Section B: Beam Interactions with Materials and Atoms*., 294, pp. 666–670. doi: 10.1016/j.nimb.2012.08.045.

Fan, Q. H., Hao, L. M., Wang, C. L., Zheng, Z., Liu, C. L. and Wu, W. S. (2014) ‘The adsorption behavior of U(VI) on granite’, *Environmental Science: Processes & Impacts*, 16(3), p. 534. doi: 10.1039/c3em00324h.

Fan, X., Song, J. and Peng, P. (2012) ‘Comparison of isolation and quantification methods to measure humic-like substances (HULIS) in atmospheric particles’, *Atmospheric Environment*., 60, pp. 366–374. doi: 10.1016/j.atmosenv.2012.06.063.

FAO (2006) *Guidelines for Soil Description*. 4th edn. Rome: Food and Agricuture Organisation of the United Nations. doi: 10.2165/00115677-199701040-00003.

Farmer, J. G., Eades, L. J. and Graham, M. C. (1999) ‘The lead content and isotopic composition of british coals and their implications for past and present releases of lead to the uk environment’, *Environmental Geochemistry and Health*, 21:257–272.

Favas, P. J. C., Pratas, J., Mitra, S., Sarkar, S. K. and Venkatachalam, P. (2016) 'Biogeochemistry of uranium in the soil-plant and water-plant systems in an old uranium mine', *Science of the Total Environment.*, 568, pp. 350–368. doi: 10.1016/j.scitotenv.2016.06.024.

Fernández-Romero, M. L., Clark, J. M., Collins, C. D., Parras-Alcántara, L. and Lozano-García, B. (2016) 'Evaluation of optical techniques for characterising soil organic matter quality in agricultural soils', *Soil and Tillage Research.*, 155, pp. 450–460. doi: 10.1016/j.still.2015.05.004.

Fesenko, S., Carbalho, F., Martin, P., Moore, W. . and Yankovich, T. (2014) 'Radium in the Environment', in *The Environmental Behaviour of Radium,*.Technical reports series number 476., Vienna: IAEA, pp. 33–104.

Fichot, C. G. and Benner, R. (2012) 'The spectral slope coefficient of chromophoric dissolved organic matter ($S_{275-295}$) as a tracer of terrigenous dissolved organic carbon in river-influenced ocean margins', *Limnology and Oceanography*, 57(5), pp. 1453–1466. doi: 10.4319/lo.2012.57.5.1453.

Fox, P. M., Davis, J. A., Kukkadapu, R., Singer, D. M., Bargar, J. and Williams, K. H. (2013) 'Abiotic U(VI) reduction by sorbed Fe(II) on natural sediments', *Geochimica et Cosmochimica Acta.*, 117, pp. 266–282. doi: 10.1016/j.gca.2013.05.003.

Fredrickson, J., Kostandarithes, H., Li, S., Plymale, A. and Daly, M. (2000) 'Reduction of Fe(III), Cr(VI), U(VI), and Tc(VII) by Deinococcus radiodurans R1', *Applied and Environmental Microbiology*, 66(5), pp. 2006–2011. doi: 10.1128/AEM.66.5.2006-2011.2000.

Frenkel, a I. and Korshin, G. V (2001) 'Studies of Cu(II) in soil by X-ray absorption spectroscopy', *Canadian Journal of Soil Science*, 81(3), pp. 271–276. doi: 10.4141/S00-

073.

Fujitake, N., Kusumoto, A., Tsukamoto, M., Noda, Y., Suzuki, T. and Otsuka, H. (1999) ‘Properties of soil humic substances in fractions obtained by sequential extraction with pyrophosphate solutions at different pHs’, *Soil Science and Plant Nutrition*, 49(3), pp. 347–353. doi: 10.1080/00380768.2003.10410019.

Gadde, R. R. and Laitinen, H. A. (1974) ‘Studies of Heavy Metal Adsorption by Hydrous Iron and Manganese Oxides’, *Analytical Chemistry*, 46(13), pp. 2022–2026.

Garrels, R. M. (1953) ‘Some Thermodynamic Relations Among the Uranium Oxides and Their Relation to the Oxidation State of the Uranium Ores of the Colorado Plateaus’, *American Minerologist*, 38, pp. 1251–1265.

Gauthier, T. D. (2001) ‘Detecting trends using spearman’s rank correlation coefficient’, *Environmental Forensics*, 2(4), pp. 359–362. doi: 10.1080/713848278.

Gavrilescu, M. (2014) *Colloid-Mediated Transport and the Fate of Contaminants in Soils, The Role of Colloidal Systems in Environmental Protection.*, pp. 397-451, doi: 10.1016/B978-0-444-63283-8.00017-X.

Giovanela, M., Crespo, J. S., Antunes, M., Adamatti, D. S., Fernandes, A. N., Barison, A., da Silva, C. W. P., Guégan, R., Motelica-Heino, M. and Sierra, M. M. D. (2010) ‘Chemical and spectroscopic characterization of humic acids extracted from the bottom sediments of a Brazilian subtropical microbasin’, *Journal of Molecular Structure.*, 981(1–3), pp. 111–119. doi: 10.1016/j.molstruc.2010.07.038.

Gondar, D., Iglesias, A., López, R., Fiol, S., Antelo, J. M. and Arce, F. (2006) ‘Copper binding by peat fulvic and humic acids extracted from two horizons of an ombrotrophic peat bog’, *Chemosphere*, 63(1), pp. 82–88. doi: 10.1016/j.chemosphere.2005.07.003.

Gondar, D., Lopez, R., Fiol, S., Antelo, J. M. and Arce, F. (2005) 'Characterization and acid-base properties of fulvic and humic acids isolated from two horizons of an ombrotrophic peat bog', *Geoderma*, 126(3–4), pp. 367–374. doi: 10.1016/j.geoderma.2004.10.006.

Goodsite, M. E., Rom, W., Heinemeier, J., Lange, T., Ooi, S., Appleby, P. G., Shotyk, W., Van Der Knapp, W. O., Lohse, C. and Hansen, T. S. (2001) 'High-resolution AMS ^{14}C dating of post-bomb peat archives of atmospheric pollutants', *Radiocarbon*, 43(28), pp. 495–515. doi: 10.1017/S0033822200041163.

Gorman-Lewis, D., Burns, P. C. and Fein, J. B. (2007) 'Review of uranyl mineral solubility measurements', *Journal of Chemical Thermodynamics*, 40, pp. 335–352. doi: 10.1016/j.jct.2007.12.004.

Goslar, T., Van Der Knaap, W. O., Hicks, S., Andric, M., Czernik, J., Goslar, E., Räsänen, S. and Hyötylä, H. (2005) 'Radiocarbon Dating of Modern Peat Profiles: Pre-and Post-Bomb ^{14}C Variations in the Construction of Age-Depth Models', *Radiocarbon*, 47(1), pp. 115–134.

Graham, M. C., Oliver, I. W., Mackenzie, A. B., Ellam, R. M. and Farmer, J. G. (2008) 'An integrated colloid fractionation approach applied to the characterisation of porewater uranium-humic interactions at a depleted uranium contaminated site.', *The Science of the Total Environment*, 404(1), pp. 207–17. doi: 10.1016/j.scitotenv.2008.05.042.

Graham, M. C., Oliver, I. W., MacKenzie, A. B., Ellam, R. M. and Farmer, J. G. (2011) 'Mechanisms controlling lateral and vertical porewater migration of depleted uranium (DU) at two UK weapons testing sites.', *The Science of the Total Environment.*, 409(10), pp. 1854–66. doi: 10.1016/j.scitotenv.2011.01.011.

Graham, M. C., Vinogradoff, S. I., Abbott, A. and Farmer, J. G. (2000) 'Application of gel

electrophoretic techniques to the investigation of actinide-humic interactions in soils', *Radiochimica Acta*, 88(9–11), pp. 775–778. doi: 10.1524/ract.2000.88.9-11.775.

Gramss, G. and Voigt, K. D. (2014) 'Forage and rangeland plants from uranium mine soils: Long-term hazard to herbivores and livestock?', *Environmental Geochemistry and Health*, 36(3), pp. 441–452. doi: 10.1007/s10653-013-9572-5.

Gray, J., Jones, S. and Smith, A. (1992) 'Discharges to the environment from the Sellafield Site ', *Journal of Radiological Protection : Official Journal of the Society for Radiological Protection*, 15(2), pp. 99–131.

Gressel, N., McColl, J. G., Preston, C. M., Newman, R. H. and Powers, R. F. (1996) 'Linkages between phosphorus transformations and carbon decomposition in a forest soil', *Biogeochemistry*, 33(2), pp. 97–123. doi: 10.1007/BF02181034.

Gu, B. and Chen, J. (2003) 'Enhanced microbial reduction of Cr(VI) and U(VI) by different natural organic matter fractions', *Geochimica et Cosmochimica Acta*, 67(19), pp. 3575–3582. doi: 10.1016/S0016-7037(03)00162-5.

Gu, B. H., Schmitt, J., Chen, Z. H., Liang, L. Y. and McCarthy, J. F. (1994) 'Adsorption and Desorption of Natural Organic-Matter on Iron-Oxide - Mechanisms and Models', *Environmental Science & Technology*, 28(1), pp. 38–46. doi: 10.1021/es00050a007.

Gu, B., Yan, H., Zhou, P., Watson, D. B., Park, M. and Istok, J. (2005) 'Natural humics impact uranium bioreduction and oxidation', *Environmental Science and Technology*, 39(14), pp. 5268–5275. doi: 10.1021/es050350r.

Guigue, J., Mathieu, O., Lévêque, J., Mounier, S., Laffont, R., Maron, P. A., Navarro, N., Chateau, C., Amiotte-Suchet, P. and Lucas, Y. (2014) 'A comparison of extraction procedures for water-extractable organic matter in soils', *European Journal of Soil Science*,

65(4), pp. 520–530. doi: 10.1111/ejss.12156.

Gulliver, P. (2002) *PhD Thesis*. University of Glasgow.

Gulliver, P., Cook, G. T., Mackenzie, A. B., Naysmith, P. and Anderson, R. (2001) 'Transport of Sellafield derived ^{14}C from the Irish Sea through the North channel', *Radiocarbon*, 43(2B), pp. 869–877.

Gustafsson, J. P. (2014) 'Visual Minteq 3.1'. Stockholm. Available at: https://vminteq.lwr.kth.se/.

Hackney, C. T. and Haines, E. B. (1980) 'Stable Carbon Isotope Composition of Fauna and Organic Matter Collected in a Mississippi Estuary', *Estuarine and coastal marine science*, 10, pp. 703–708.

Hanrahan, G. (2012) 'Soil Chemistry', in *Key Concepts in Environmental Chemistry*. Oxford: Academic Press, Elsevier, pp. 245–262.

Hansom, J. D. (2007) 'Solway firth (north shore)', *Coastal Geomorphology of Great Britain*, 28(1962), pp. 1–8.

Hart, H., Craine, L. E., Hart, D. J. and Hadad, C. M. (2007) *Organic Chemistry, A Short Course*. 12th edn. Edited by R. Stratton, R. Lombard, and M. Bridges. Boston.

Harvey, M. M. and Allan, R. L. (1998) 'The Solway Firth saltmarshes', *Scottish Geographical Magazine*, 114(1), pp. 42–45. doi: 10.1080/00369229818737026.

Harvey, M. M., Hansom, J. D. and MacKenzie, a B. (2007) 'Constraints on the use of anthropogenic radionuclide-derived chronologies for saltmarsh sediments.', *Journal of Environmental Radioactivity*, 95(2–3), pp. 126–48. doi: 10.1016/j.jenvrad.2007.02.005.

Hayes, M. H. B. (2006) 'Solvent Systems for the Isolation of Organic Components from

Soils', *Soil Science Society of America Journal*, 70(3), p. 986. doi: 10.2136/sssaj2005.0107.

Hayes, M. H. B., Swift, R. S., Wardle, R. E. and Brown, J. K. (1975) 'Humic materials from an organic soil: A comparison of extractants and of properties of extracts', *Geoderma*, 13(3), pp. 231–245. doi: 10.1016/0016-7061(75)90020-8.

Hedges, J. I., Keil, R. G. and Benner, R. (1997) 'What happens to terrestrial organic matter in the ocean?', *Organic Geochemistry*, 27(5–6), pp. 195–212. doi: 10.1016/S0146-6380(97)00066-1.

Heier, K. (1965) 'Radioactive elements in the continental crust', *Nature*, 208, pp. 479–480.

Helms, J. R., Stubbins, A., Ritchie, J. D., Minor, E. C., Kieber, D. J. and Mopper, K. (2008) 'Absorption spectral slopes and slope ratios as indicators of molecular weight, source, and photobleaching of chromophoric dissolved organic matter', *Limonology and Oceanography*, 53(3), pp. 955–969. doi: 10.4319/lo.2008.53.3.0955.

Helmy, A. K., Ferreiro, E. A. and Bussetti, S. G. D. E. (1994) 'Cation Exchange Capacity and Condition of Zero Charge of Hydroxy-a1 Montmorillonite', *Clay Minerals*, 42(4), pp. 444–450. doi: 10.1346/CCMN.1994.0420410.

Hering, J. G. and Morel, F. M. (1988) 'Humic acid complexation of calcium and copper.', *Environmental Science & Technology*, 22(10), pp. 1234–7. doi: 10.1021/es00175a018.

Herres, W. and Gronholz, J. (1989) 'Understanding FTIR data processing', Bruker Analytic, Wikingerstr.

Hertkorn, N. (2006) *Molecular level structural analysis of natural organic matter and of humic substances by NMR spectroscopy: A Habilitationsschrift*. Thesis, Technischen Universität München-Weihenstephan.

Hertkorn, N., Harir, M., Koch, B. P., Michalke, B. and Schmitt-Kopplin, P. (2013) 'High-field NMR spectroscopy and FTICR mass spectrometry: Powerful discovery tools for the molecular level characterization of marine dissolved organic matter', *Biogeosciences*, 10(3), pp. 1583–1624. doi: 10.5194/bg-10-1583-2013.

Hertkorn, N., Permin, A, Perminova, I., Kovalevskii, D., Yudov, M., Petrosyan, V. and Kettrup, A (2002) 'Comparative analysis of partial structures of a peat humic and fulvic acid using one- and two-dimensional nuclear magnetic resonance spectroscopy.', *Journal of Environmental Quality*, 31(2), pp. 375–87. doi: 10.2134/jeq2002.3750.

Hidaka, H. and Kikuchi, M. (2010) 'SHRIMP in-situ isotopic analyses of REE, Pb and U in micro-minerals bearing fission products in the Oklo and Bangombé natural reactors: A review of a natural analogue study for the migration of fission products', *Precambrian Research*., 183(1), pp. 158–165. doi: 10.1016/j.precamres.2010.07.012.

Hodge, E., McDonald, J., Fischer, M., Redwood, D., Hua, Q., Levchenko, V., Drysdale, R., Waring, C. and Fink, D. (2011) 'Using the ^{14}C Bomb Pulse to Date Young Speleothems', *Radiocarbon*, 53(02), pp. 345–357. doi: 10.1017/S0033822200056605.

Holden, N. E. (1981) 'The Uranium Half-Lives : A Critical Review', National Nuclear Data Centre Information Analysis Report. Brookhaven Natonal Laboratory, Upton, New York

Hooker, P. (1991) *The Geology, Hydrogeology, and Geochemistry of the Needle;s Eye natural analogue site*. Brussels: Commission of the European communities, EUR-13434.

Hua, Q., Barbetti, M. and Rakowski, A. (2013) 'Atmospheric radiocarbon for the period 1950–2010', *Radiocarbon*, 55(4), pp. 2059–2072.

Huang, P.-T., Patel, M., Santagata, M. C. and Bobet, A. (2009) 'Classification of Organic Soils', *Soil Science Society of America Journal*, B7(1), p. 108. doi:

10.2136/sssaj1926.0361599500B700010022x.

Hyun, S. P., Davis, J. A. and Hayes, K. F. (2014) ‘Abiotic U(VI) reduction by aqueous sulfide’, *Applied Geochemistry*. 50, pp. 7–15. doi: 10.1016/j.apgeochem.2014.07.021.

IAEA (1999) *Use of Natural Analogues To Support Radionuclide Transport models for Deep Geological Repositries for long lived radioactive wastes*. Vienna: IAEA-TECDOC-1109.

IAEA (2002) ‘Using Isotopes to Understand the Oceans and Climate Change’, *Encyclopedia of Atmospheric Sciences*, pp. 1–10. Available at: https://www.iaea.org/About/Policy/GC/GC51/GC51InfDocuments/English/gc51inf-3-att3_en.pdf.

IAEA (2003) *Scientific and Technical Basis for the Geological Disposal of Radioactive Wastes*. Vienna: International Atomic Energy Agency, STI/DOC/010/413.

IAEA (2009) *Classification of Radioactive Waste*. Vienna: IAEA, General Safety Guide No. GSG-1.

IAEA (2010) *Analytical Methodology for the Determination of Radium Isotopes in Environmental Samples, IAEA Analytical Quality in Nuclear Applications Series*. Vienna, IAEA/AQ/19.

Ingri, N., Kakolowicz, W., Sillén, L. G. and Warnqvist, B. (1967) ‘High-speed computers as a supplement to graphical methods—V: Haltafall, a general program for calculating the composition of equilibrium mixtures’, *Talanta*. 14(11), pp. 1261–1286. doi: 10.1016/0039-9140(67)80203-0.

Jackson, B. P., Ranville, J. F., Bertsch, P. M. and Sowder, A. G. (2005) ‘Characterization of colloidal and humic-bound Ni and U in the “dissolved” fraction of contaminated

sediment extracts', *Environmental Science and Technology*, 39(8), pp. 2478–2485. doi: 10.1021/es0485208.

Jacques, D., Wang, L., Martens, E. and Mallants, D. (2010) 'Modelling chemical degradation of concrete during leaching with rain and soil water types', *Cement and Concrete Research*., 40(8), pp. 1306–1313. doi: 10.1016/j.cemconres.2010.02.008.

Jamet, P., Hooker, P. J., Schmitt, J. M., Ledoux, E. and Escalier Des Orres, P. (1993) 'Hydrogeochemical modelling of an active system of uranium fixation by organic soils and sediments (Needle's Eye, Scotland)', *Mineralium Deposita*, 28(1), pp. 66–76. doi: 10.1007/BF00199011.

Jawinski, E. B. (2002) 'Electrospray Ionization Fourier Transform Ion Cyclotron Resonance Mass Spectrometry (ESI FT-ICR MS): Characterization of Complex Environmental Mixtures', *Environmental Forensics*, 3, pp. 207–216. doi: 10.1006/enfo.2002.0109.

Jenner, G., Longerich, H., Jackson, S. and Fryer, B. (1990) 'ICP-MS — A powerful tool for high-precision trace-element analysis in Earth sciences: Evidence from analysis of selected U.S.G.S. reference samples', *Chemical Geology*, 83(1–2), pp. 133–148. doi: 10.1016/0009-2541(90)90145-W.

Johnson, W. H., Buck, B. J., Brogonia, H. and Brock, A. M. Y. L. (2004) 'Variations in Depleted Uranium Sorption and Solubility with Depth in Arid Soils', *Soil and Sediment Contamination*, 13(6), pp. 533–544. doi: 10.1080/10588330490519428.

Johnston, H. (2017) The Molecular Scale Characterisation of Saltmarsh Organic Matter and ^{14}C Availability., BSc Dissertation, University of Edinburgh.

Jones, A., Jones, K., Holmes, S., Ewers, L. and Cabianca, T. (2013) 'Assessing the possible

radiological impact of routine radiological discharges from proposed nuclear power stations in England and Wales.', *Journal of Radiological Protection : Official Journal of the Society for Radiological Protection*, 33(1), pp. 163–74. doi: 10.1088/0952-4746/33/1/163.

Jones, D. G., Roberts, P. D. and Miller, J. M. (1988) 'The distribution of gamma-emitting radionuclides in surface subtidal sediments near the Sellafield plant', *Estuarine, Coastal and Shelf Science*, 27(2), pp. 143–161. doi: 10.1016/0272-7714(88)90087-X.

Jones, M. N. and Bryan, N. D. (1998) 'Colloidal properties of humic substances', *Advances in Colloid and Interface Science*, 78(1), pp. 1–48. doi: 10.1016/S0001-8686(98)00058-X.

Jungner, H., Sonninen, E., Possnert, G. and Tolonen, K. (1995) 'Use of bomb-produced ^{14}C to evaluate the amount of CO_2 emanating from two peat bogs in Finland', *Radiocarbon*, 37(2), p. 567–573 ST–Use of bomb–produced C–14 to evaluat.

Keith, S., Doyle, J. and Harper, C. (2012) *Toxicological profile for Radon*. Atlanta: Agency for Toxic Substances and Disease Registry (US). Available at: https://www.ncbi.nlm.nih.gov/books/NBK158792/.

Kelly, S. D. (2010) *Synchrotron-Based Techniques in Soils and Sediments, Developments in Soil Science*. Elsevier (Developments in Soil Science). doi: 10.1016/S0166-2481(10)34014-1.

Kelly, S. D., Hesterberg, D. and Ravel, B. (2008) 'Analysis of Soils and Minerals Using X-ray Absorption Spectroscopy', *Methods of Soil Analysis*, Part 5. M(SSSA Book Series no. 5), pp. 387–463. doi: 10.2136/sssabookser5.5.c14.

Kennedy, J. and Atkinson, G. (2006) *A History of Marchon Works at Whitehaven, Industrial History of Cumbria*. Available at: http://www.cumbria-industries.org.uk/a-z-of-

industries/chemicals/a-history-of-marchon-works-at-whitehaven/ (Accessed: 15 August 2018).

Kershaw, P. J., Woodhead, D., Allington, D. and Lovett, M. (1990) 'A Sediment History of Sellafield Discharges', *Journal of Environmental Radioactivity*, 12, pp. 201–241.

Kim, S., Kramer, R. W. and Hatcher, P. G. (2003) 'Graphical method of analysis of ultrahigh-resolution broadband mass spectrometry of natural organic matter, the Van Krevelen diagram', *Analytical Chemistry*, 75(20), pp. 5336–5344.

Kinniburgh, D. and Cooper, D. (2011) *PhreePlot, Creating graphicaloutput with PHREEQC*. Centre for Ecology and Hydrology, Bangor.

Kirby, H. W. (1954) 'Decay and Growth Tables for Naturally Occurring Radioactive Series', *Analytical Chemistry*, 26(6), pp. 1063–1071. doi: 10.1021/ac60090a035.

Kiss, K., Szalai, Z., Jakab, G., Madarász, B. and Zboray, N. (2014) 'Soil Carbon'. A. E. Hartemink and K. McSweeney (Eds). Cham: Springer International Publishing, pp. 127–136. doi: 10.1007/978-3-319-04084-4.

Kostich, M. S., Flick, R. W., Batt, A. L., Mash, H. E., Boone, J. S., Furlong, E. T., Kolpin, D. W. and Glassmeyer, S. T. (2017) 'Aquatic concentrations of chemical analytes compared to ecotoxicity estimates', *Science of the Total Environment*. 579, pp. 1649–1657. doi: 10.1016/j.scitotenv.2016.06.234.

Kozyatnyk, I., Bouchet, S., Bjorn, E. and Haglund, P. (2016) 'Fractionation and size-distribution of metal and metalloid contaminants in a polluted groundwater rich in dissolved organic matter', *Journal of Hazardous Materials*, 318, pp. 194–202. doi: 10.1016/j.jhazmat.2016.07.024.

Kurttio, P., Harmoinen, A., Saha, H., Salonen, L., Karpas, Z., Komulainen, H. and

Auvinen, A. (2006) ‘Kidney Toxicity of Ingested Uranium From Drinking Water’, *American Journal of Kidney Diseases*, 47(6), pp. 972–982. doi: 10.1053/j.ajkd.2006.03.002.

Kurttio, P., Salonen, L., Ilus, T., Pekkanen, J., Pukkala, E. and Auvinen, A. (2006) ‘Well water radioactivity and risk of cancers of the urinary organs’, *Environmental Research*, 102(3), pp. 333–338. doi: 10.1016/j.envres.2005.12.010.

Kuss, H.-M. (1992) ‘Applications of microwave digestion technique for elemental analyses’, *Fresenius’ Journal of Analytical Chemistry*, 343(9–10), pp. 788–793. doi: 10.1007/BF00633568.

Laborda, F., Bolea, E., Górriz, M. P., Martín-Ruiz, M. P., Ruiz-Beguería, S. and Castillo, J. R. (2008) ‘A speciation methodology to study the contributions of humic-like and fulvic-like acids to the mobilization of metals from compost using size exclusion chromatography-ultraviolet absorption-inductively coupled plasma mass spectrometry and deconvolution an’, *Analytica Chimica Acta*, 606(1), pp. 1–8. doi: 10.1016/j.aca.2007.10.048.

Landais, P. (1996) ‘Organic geochemistry of sedimentary uranium ore deposits’, *Ore Geology Reviews*, 11(1–3), pp. 33–51. doi: 10.1016/0169-1368(95)00014-3.

Landry, C. and Tremblay, L. (2012) ‘Compositional Differences between Size Classes of Dissolved Organic Matter from Freshwater and Seawater Revealed by an HPLC-FTIR System’, *Environmental Science & Technology*, 46(3), pp. 1700–1707. doi: 10.1021/es203711v.

Langmuir, D. (1997) ‘Actinides and Their Daughter and Fission Products’, in McConnin, R. (ed.) *Aqueous Environmental Geochemistry*. New Jersey: Prentice HAll, pp. 486–542.

Lead, J. R., Davison, W., Hamilton-Taylor, J. and Buffle, J. (1997) 'Characterizing Colloidal Material in Natural Waters', *Aquatic Geochemistry*, 3, pp. 213–232. doi: 10.1023/A:1009695928585.

Leenheer, J. a (2009) 'Systematic Approaches to Comprehensive Analyses of Natural Organic Matter', *Annals of Environmental Science*, 3, pp. 1–130.

Lemotte, P. K. and Little, J. B. (1984) 'DNA Damage Induced in Human Diploid Cells by Decay of Incorporated Radionuclides. *Cancer Research.* 44:1337–1342.

Lenhart, J. J., Cabaniss, S. E., MacCarthy, P. and Honeyman, B. D. (2000) 'Uranium (VI) complexation with citric, humic and fulvic acids', *Radiochimica Acta*, 88(6/2000), p. 345. doi: 10.1524/ract.2000.88.6.345.

Lenhart, J. J. and Honeyman, B. D. (1999) 'Uranium(VI) sorption to hematite in the presence of humic acid', *Geochimica et Cosmochimica Acta*, 63(19–20), pp. 2891–2901. doi: 10.1016/S0016-7037(99)00269-0.

Lesher, E. K. and Honeyman, B. D. (2009) 'Analysis of pH Dependent Uranium (VI) Sorption to Nanoparticulate Hematite by Flow Field-Flow Fractionation - Inductively Coupled Plasma Mass Spectrometry', 43(14), pp. 5403–5409.

Lesher, E. K., Honeyman, B. D. and Ranville, J. F. (2013) 'Detection and characterization of uranium-humic complexes during 1D transport studies', *Geochimica et Cosmochimica Acta*. Elsevier Ltd, 109, pp. 127–142. doi: 10.1016/j.gca.2013.01.014.

Levin, I. and Kromer, B. (2004) 'The Tropospheric $^{14}CO_2$ Level In Mid-Latitudes of The Northern Hemisphere (1959–2003)', *Radiocarbon*, 46(3), pp. 1261–1272. doi: 10.2458/azu_js_rc.46.4181.

Levy, R. (1980) 'Precipitation of carbonates in soils in contact with waters undersaturated

or oversaturated in respect to calcite', *Journal of Soil Science*, 31: 41–51.

Lewis, R. J. (2007) *Gel Filtration*. Amersham Pharmacia Biotech. doi: 10.1002/9780470114735.hawley07722.

Li, D., Kaplan, D. I., Chang, H. S., Seaman, J. C., Jaffé, P. R., Koster Van Groos, P., Scheckel, K. G., Segre, C. U., Chen, N., Jiang, D. T., Newville, M. and Lanzirotti, A. (2015) 'Spectroscopic evidence of uranium immobilization in acidic wetlands by natural organic matter and plant roots', *Environmental Science and Technology*, 49(5), pp. 2823–2832. doi: 10.1021/es505369g.

Li, D., Seaman, J. C., Chang, H.-S., Jaffe, P. R., Koster van Groos, P., Jiang, D.-T., Chen, N., Lin, J., Arthur, Z., Pan, Y., Scheckel, K. G., Newville, M., Lanzirotti, A. and Kaplan, D. I. (2014) 'Retention and chemical speciation of uranium in an oxidized wetland sediment from the Savannah River Site.', *Journal of environmental radioactivity*, 131, pp. 40–6. doi: 10.1016/j.jenvrad.2013.10.017.

Li, W., Victor, D. and Chakrabarti, C. (1980) 'Effect of pH and Uranium Concentration on Interaction of Uranium(VI) and Uranium(IV) with Organic Ligands in Aqueous Solutions', *Analytical Chemistry*, 52, pp. 520–523.

Liger, E., Charlet, L. and Van Cappellen, P. (1999) 'Surface catalysis of uranium(VI) reduction by iron(II)', *Geochimica et Cosmochimica Acta*, 63(19–20), pp. 2939–2955. doi: 10.1016/S0016-7037(99)00265-3.

Lu, Y., Li, X., Mesfioui, R., Bauer, J. E., Chambers, R. M., Canuel, E. A. and Hatcher, P. G. (2015) 'Use of ESI-FTICR-MS to characterize dissolved organic matter in headwater streams draining forest-dominated and pasture-dominated watersheds', *PLoS ONE*, 10(12), pp. 1–21. doi: 10.1371/journal.pone.0145639.

Lv, J., Zhang, S., Wang, S., Luo, L., Cao, D. and Christie, P. (2016) 'Molecular-Scale Investigation with ESI-FT-ICR-MS on Fractionation of Dissolved Organic Matter Induced by Adsorption on Iron Oxyhydroxides', *Environmental Science and Technology*, 50(5), pp. 2328–2336. doi: 10.1021/acs.est.5b04996.

Maberly, S. C., Raven, J. A. and Johnston, A. M. (1992) 'Discrimination between ^{12}C and ^{13}C by marine plants', *Oecologia*, 91, pp. 481–492.

MacGregor, K. (2016) *Spatial and temporal variations in potentially toxic elements (Sb, Pb, Cu and Zn) and PAH concentrations and associations in run-off from urban and rural areas of Scotland*. PhD Thesis, University of Edinburgh.

MacKenzie, A. B., Cook, G. T., Barth, J., Gulliver, P. and McDonald, P. (2004) '^{14}C and $\delta^{13}C$ characteristics of organic matter and carbonate in saltmarsh sediments from south west Scotland', *Journal of Environmental Monitoring*, 6(5), pp. 441–447. doi: 10.1039/b315766k.

MacKenzie, A. B., Hardie, S. M. L., Farmer, J. G., Eades, L. J. and Pulford, I. D. (2011) 'Analytical and sampling constraints in ^{210}Pb dating', *Science of the Total Environment*. Elsevier B.V., 409(7), pp. 1298–1304. doi: 10.1016/j.scitotenv.2010.11.040.

Mackenzie, A. B., Hooker, P. J., Scott, R. D. and Houston, C. M. (1989) *Natural Decay Series Radionuclide Studies at the Needle's Eye Natural Analogue Site*. Brussels: Commission of the European Communities.

Mackenzie, A. B. and Scott, R. D. (1993) 'Sellafield waste radionuclides in Irish Sea intertidal and salt marsh sediments', *Environmental Geochemistry and Health*,15, pp. 173–184.

MacKenzie, A. B., Scott, R. D., Allan, R. L., Ben Shaban, Y. A., Cook, G. T. and Pulford,

I. D. (1994) ‘Sediment radionuclide profiles: Implications for mechanisms of Sellafield waste dispersal in the Irish Sea’, *Journal of Environmental Radioactivity*, 23(1), pp. 39–69. doi: 10.1016/0265-931X(94)90504-5.

MacKenzie, A. B., Scott, R. D., Houston, C. and Hooker, P. J. (1991a) *Natural Decay Series Radionuclide Studies at the Needle's Eye Natural Analogue Site II, 1989 - 1991*. Brussels: Commission of the European Communities.

MacKenzie, A. B., Scott, R. D. and Williams, T. M. (1987) ‘Mechanisms of northwards dispersal of Sellafield waste’, *Nature*, 329, pp. 42–45.

MacKenzie, A. B., Whitton, A. M., Shimmield, T. M., Jemielita, R. A., Scott, R. D. and Hooker, P. J. (1991) *Natural analogue decay series radionuclide studies at the Needle's eye natural analogue site, II, 1989-1991*.

MAFF (1992) *Radioactivity in Surface and Coastal Water of the British Isles, 1990 to 1994. Aquatic Environment Monitoring Report No. 29, 34, 38, 42, 45*. Lowestoft.

Magnusson, Å. (2007) *14-C Produced by Nuclear Power Reactors – Generation and Characterization of Gaseous, Liquid and Solid Waste*. PhD Theisis, Lund University.

Mahieu, N., Powlson, D. S. and Randall, E. W. (1999) ‘Statistical Analysis of Published ^{13}C CPMAS NMR Spectra of Soil Organic Matter’, *Soil Science Society of America Journal*, 63, pp. 307–319.

Malik, A., Scheibe, A., Lokabharathi, P. A. and Gleixner, G. (2012) ‘Online stable isotope analysis of dissolved organic carbon size classes using size exclusion chromatography coupled to an isotope ratio mass spectrometer’, *Environmental Science and Technology*, 46(18), pp. 10123–10129. doi: 10.1021/es302467y.

Mao, L., Young, S. D. and Bailey, E. H. (2015) ‘Lability of copper bound to humic acid.’,

Chemosphere. 131, pp. 201–208. doi: 10.1016/j.chemosphere.2015.03.035.

Marsden, O. J., Abrahamsen, L., Bryan, N. D., Philip Day, J., Keith Fifield, L., Gent, C., Goodall, P. S., Morris, K. and Livens, F. R. (2006) 'Transport and accumulation of actinide elements in the near-shore environment: field and modelling studies', *Sedimentology*, 53(1), pp. 237–248. doi: 10.1111/j.1365-3091.2005.00761.x.

Masscheleyn, P. H. (1991) 'Effect of Redox Potential and pH on Arsenic Speciation and Solubility in a Contaminated Soil', *Environmental Science and Technology* (25), pp. 1414–1419.

Matilainen, A., Gjessing, E. T., Lahtinen, T., Hed, L., Bhatnagar, A. and Sillanpää, M. (2011) 'An overview of the methods used in the characterisation of natural organic matter (NOM) in relation to drinking water treatment.', *Chemosphere*. Elsevier Ltd, 83(11), pp. 1431–42. doi: 10.1016/j.chemosphere.2011.01.018.

McCarthy, J. F. and McKay, L. D. (2004) 'Colloid Transport in the Subsurface', *Vadose Zone Journal*, 3, p. 326. doi: 10.2136/vzj2004.0326.

McCartney, M., Kershaw, P. J. and Allington, D. J. (1990) 'The Behaviour of ^{210}Pb and ^{226}Ra in the Eastern Irish Sea', *Journal of Environmental Radioactivity*, 12, pp. 243–265.

McCurdy, E., Potter, D. and Woods, G. (2006) 'Unmatched Removal of Spectral Interferences in ICP-MS Using the Agilent Octopole Reaction System with Helium Collision Mode', pp. 1–8. Available at: http://www.agilent.com/cs/library/applications/5989-4905EN.pdf.

McKenna, P. and Longworth, R. D. (1995) 'Residual Chernobyl fallout and Sellafield pollutants found on the Isle of Man.', *The Science of the Total Environment*, 173–174, pp. 7–14. Available at: http://www.ncbi.nlm.nih.gov/pubmed/8560234.

McKinney, M. and Schoch, R. (2003) ‘The Soil of the Earth’, in *Environmental Science Systems and Solutions*. 3rd edition. Boston, Toronto, London, Singapore: Jones and Bartlett Publishers, pp. 325–330.

McMillan, A. A., Merritt, J. W., Auton, C. A. and Golledge, N. R. (2011) *The Quaternary geology of the Solway. Research Report RR/11/04*. Keyworth, Nottingham. doi: 10.1002/jqs.2932.

Mead, R. N., Mullaugh, K. M., Brooks Avery, G., Kieber, R. J., Willey, J. D. and Podgorski, D. C. (2013) ‘Insights into dissolved organic matter complexity in rainwater from continental and coastal storms by ultrahigh resolution Fourier transform ion cyclotron resonance mass spectrometry’, *Atmospheric Chemistry and Physics*, 13(9), pp. 4829–4838. doi: 10.5194/acp-13-4829-2013.

Megens, L., Van Der Plicht, J., De Leeuw, J. W. and Smedes, F. (2002) ‘Stable carbon and radiocarbon isotope compositions of particle size fractions to determine origins of sedimentary organic matter in an estuary’, *Organic Geochemistry*, 33(8), pp. 945–952. doi: 10.1016/S0146-6380(02)00060-8.

Mibus, J., Sachs, S., Pfingsten, W., Nebelung, C. and Bernhard, G. (2007) ‘Migration of uranium(IV)/(VI) in the presence of humic acids in quartz sand: A laboratory column study’, *Journal of Contaminant Hydrology*, 89(3–4), pp. 199–217. doi: 10.1016/j.jconhyd.2006.08.005.

Miller, J. M. and Taylor, K. (1966) ‘Uranium Mineralisation near Dalbeattie, Kicudbrightshire.’, *Bulletin of the Geological Survey of Great Britain*, (25), pp. 1–18.

Miller, W., Alexander, R., Chapman, N., McKinley, I. and Smellie, J. (1994) *Technical report 93-03 - Natural analogue studies in the geological disposal of radioactive wastes*, *Studies in Environmental Science 57*. Amsterdam, London, New York, Tokyo: Elsevier.

Minor, E. C., Swenson, M. M., Mattson, B. M. and Oyler, A. R. (2014) 'Structural characterization of dissolved organic matter: A review of current techniques for isolation and analysis', *Environmental Science. Processes & Impacts*. Royal Society of Chemistry, 16, pp. 2064–2079. doi: 10.1039/c4em00062e.

Mossini, E., Macerata, E. and Giola, M. (2015) 'Review of international normatives for natural radioactivity determination in building materials', *Nukelonika*, 60, pp. 597–602. doi: 10.1515/nuka-2015-0101.

Moyes, L. N. (1995) *Undergraduate thesis, BSc Environmental Chemistry*. University of Edinburgh.

Muir, G. K. P., Tierney, K. M., Cook, G. T., MacKinnon, G., Howe, J. A., Heymans, J. J., Hughes, D. J. and Xu, S. (2017) 'Ecosystem uptake and transfer of Sellafield-derived radiocarbon (14C). Part 1. The Irish Sea', *Marine Pollution Bulletin*. 114(2), pp. 792–804. doi: 10.1016/j.marpolbul.2016.10.072.

Munier-Lamy, C., Adrian, P., Berthelin, J. and Rouiller, J. (1986) 'Comparison of binding abilities of fulvic and humic acids extracted from recent marine sediments with UO_2^{2+}', *Organic Geochemistry*, 9(6), pp. 285–292. doi: 10.1016/0146-6380(86)90109-9.

Murphy, R. J., Lenhart, J. J. and Honeyman, B. D. (1999) 'The sorption of thorium (IV) and uranium (VI) to hematite in the presence of natural organic matter', *Colloids and Surfaces A: Physicochemical and Engineering Aspects*, 157(1–3), pp. 47–62. doi: 10.1016/S0927-7757(99)00115-6.

Murray, R. L. and Holbert, K. E. (2015) 'Radioactivity', in *Nuclear Energy*. 7th edn. London: Elsevier, pp. 31–46. doi: 10.1016/B978-0-12-416654-7.00003-4.

Naganuma, K., Okazaki, M., Yonebayashi, K., Kyuma, K., Vijarnsorn, P., Bakar, Z. A.,

Yonebayashi, K., Kyuma, K., Vijarnsorn, P. and Bakar, Z. A. (1993) 'Surface charge and adsorption characteristics of copper and zinc on tropical peat soils', *Soil Science and Plant Nutrition*, 39(3), pp. 455–462. doi: 10.1080/00380768.1993.10419786.

NDA and DECC (2014) *Radioactive Wastes in the UK : A Summary of the 2013 Inventory*. NDA/ST/STY (14) 0006. Moor Row, Cumbria.

Neagoe, A., Iordache, V. and Fa, I. C. (2012) 'The Role of Organic Matter in the Mobility of Metals in Contaminated Catchments', in *Bio-Geo Interactions in Metal-Contaminated Soils*, pp. 297–325. doi: 10.1007/978-3-642-23327-2.

Nedveckaite, T., Gudelis, A and Vives i Batlle, J. (2013) 'Impact assessment of ionizing radiation on human and non-human biota from the vicinity of a near-surface radioactive waste repository.', *Radiation and Environmental Biophysics*, 52(2), pp. 221–34. doi: 10.1007/s00411-013-0459-8.

Newsome, L., Morris, K. and Lloyd, J. R. (2014) 'The biogeochemistry and bioremediation of uranium and other priority radionuclides', *Chemical Geology*. 363, pp. 164–184. doi: 10.1016/j.chemgeo.2013.10.034.

Niemeyer, J., Chen, Y. and Bollag, J.-M. (1992) 'Characterization of Humic Acids, Composts, and Peat by Diffuse Reflectance Fourier-Transform Infrared Spectroscopy', *Soil Science Society of America Journal*, 56(1), pp. 135–140. doi: 10.2136/sssaj1992.03615995005600010021x.

NIST (2009) *Certificate of Analysis, Standard Reference Material 2710a*. National Institute of Standards and Technology Special Publication 260-172

Noseck, U., Tullborg, E.-L., Suksi, J., Laaksoharju, M., Havlová, V., Denecke, M. A. and Buckau, G. (2012) 'Real system analyses/natural analogues', *Applied Geochemistry*. 27(2),

pp. 490–500. doi: 10.1016/j.apgeochem.2011.09.017.

Oliver, I. W., Graham, M. C., Mackenzie, A. B., Ellam, R. M. and Farmer, J. G. (2008) ‘Distribution and partitioning of depleted uranium (DU) in soils at weapons test ranges - investigations combining the BCR extraction scheme and isotopic analysis.’, *Chemosphere*, 72(6), pp. 932–9. doi: 10.1016/j.chemosphere.2008.03.029.

Oliver, I. W., Graham, M. C., MacKenzie, A. B., Ellam, R. M. and Farmer, J. G. (2007) ‘Assessing depleted uranium (DU) contamination of soil, plants and earthworms at UK weapons testing sites.’, *Journal of Environmental Monitoring : JEM*, 9(7), pp. 740–8. doi: 10.1039/b700719a.

Oren, A. and Chefetz, B. (2012) ‘Sorptive and Desorptive Fractionation of Dissolved Organic Matter by Mineral Soil Matrices’, *Journal of Environment Quality*, 41(2), p. 526. doi: 10.2134/jeq2011.0362.

Osman, K. T. (2013) ‘Wetland Soils’, in *Soils: Principles, Properties and Management*. Dordrecht: Springer, pp. 1–271. doi: 10.1007/978-94-007-5663-2.

Oste, L. A., Temminghoff, E. J. M. and Van Riemsdijk, W. H. (2002) ‘Solid-solution partitioning of organic matter in soils as influenced by an increase in pH or Ca concentration’, *Environmental Science and Technology*, 36(2), pp. 208–214. doi: 10.1021/es0100571.

Ouatmane, A., Hafidi, M. and Gharous, M. El (1999) ‘Complexation of calcium ions by humic and fulvic acids’, *Analusis*, 27(5), pp. 428–432. Available at: http://analusis.edpsciences.org/index.php?option=com_article&access=standard&Itemid=129&url=/articles/analusis/pdf/1999/05/m140599.pdf.

Owen, D. E. and Otten, J. (1995) ‘Mountain wetlands: Efficient uranium filters – potential

impacts.', *Ecological Engineering*, 5, pp. 77–93.

Pansu, M. and Gautheyrou, J. (2006) 'Quantification of Humic Compounds', in *Handbook of Soil Analysis: Mineralogical, Organic and Inorganic Methods*. New York: Springer, pp. 371–396.

Peacock, M., Evans, C. D., Fenner, N., Freeman, C., Gough, R., Jones, T. G. and Lebron, I. (2014) 'UV-visible absorbance spectroscopy as a proxy for peatland dissolved organic carbon (DOC) quantity and quality: considerations on wavelength and absorbance degradation.', *Environmental Science. Processes & Impacts*, pp. 10–12. doi: 10.1039/c4em00108g.

Peacock, M., Freeman, C., Gauci, V., Lebron, I. and Evans, C. D. (2015) 'Investigations of freezing and cold storage for the analysis of peatland dissolved organic carbon (DOC) and absorbance properties', *Environmental Science: Processes & Impacts*. Royal Society of Chemistry, 17, pp. 1290–1301. doi: 10.1039/C5EM00126A.

Pédrot, M., Dia, A., Davranche, M., Bouhnik-Le Coz, M., Henin, O. and Gruau, G. (2008) 'Insights into colloid-mediated trace element release at the soil/water interface', *Journal of Colloid and Interface Science*, 325(1), pp. 187–197. doi: 10.1016/j.jcis.2008.05.019.

Peel, H. R., Martin, D. P. and Bednar, A. J. (2017) 'Extraction and characterization of ternary complexes between natural organic matter, cations, and oxyanions from a natural soil', *Chemosphere*. Elsevier Ltd, 176, pp. 125–130. doi: 10.1016/j.chemosphere.2017.02.101.

Perkin Elmer Life and Analytical Sciences (2005) 'FT-IR Spectroscopy Attenuated Total Reflectance (ATR)', *Technical Report*, pp. 1–5. Available at: https://shop.perkinelmer.com/content/TechnicalInfo/TCH_FTIRATR.pdf.

Perminova, I. V., Hatfield, K. and Hertkorn., N. (2002) *The use of humic substances to remediate polluted environment: From theory to practice*. NATO Science Series IV. Earth and Environmental Sciences – Vol. 52.

Peuravuori, J. and Pihlaja, K. (1997) 'Molecular size distribution and spectroscopic properties of aquatic humic substances', *Analytica Chimica Acta*, 337(2), pp. 133–149. doi: 10.1016/S0003-2670(96)00412-6.

Phrommavanh, V., Leermakers, M., de Boissezon, H., Nos, J., Koko, M.-B. and Descostes, M. (2013) 'Characterizing the Transport of Natural Uranium and its Decay Product 226Ra, Downstream from Former Mines in France', *Procedia Earth and Planetary Science*. 7(0), pp. 693–696. doi: 10.1016/j.proeps.2013.03.064.

Piccolo, A. (2002) 'The supramolecular structure of humic substances: a novel understanding of humic chemistry and implications in soil science', *Advances in Agronomy*, 75, pp. 57–134. doi: http://dx.doi.org/10.1016/S0065-2113(02)75003-7.

Piccolo, A., Nardi, S. and Concheri, G. (1996a) 'Macromolecular changes of humic substances induced by interaction with organic acids', *European Journal of Soil Science*, 47(3), pp. 319–328. doi: 10.1111/j.1365-2389.1996.tb01405.x.

Piccolo, A., Nardi, S. and Concheri, G. (1996b) 'Micelle-like formation of humic substances as revealed by size exclusion chromatography', *Chemosphere*, 33(4), pp. 595–602.

Piotrowska, N., Blaauw, M., Mauquoy, D. and Chambers, F. M. (2011) 'Constructing deposition chronologies for peat deposits using radiocarbon dating', *Mires and Peat*, 7(10), pp. 1–14. doi: 10.1111/j.1365-2486.2009.01920.x.

Pokrovsky, O. S., Dupré, B. and Schott, J. (2005) Fe-Al-organic colloids control of trace

elements in peat soil solutions: Results of ultrafiltration and dialysis, *Aquatic Geochemistry*. 11:241–278. doi: 10.1007/s10498-004-4765-2.

Polubesova, T. and Chefetz, B. (2014) 'DOM-Affected Transformation of Contaminants on Mineral Surfaces: A Review', *Critical Reviews in Environmental Science and Technology*, 44(3), pp. 223–254. doi: 10.1080/10643389.2012.710455.

Ponthieu, M., Juillot, F., Hiemstra, T., van Riemsdijk, W. H. and Benedetti, M. F. (2006) 'Metal ion binding to iron oxides', *Geochimica et Cosmochimica Acta*, 70(11), pp. 2679–2698. doi: 10.1016/j.gca.2006.02.021.

Pospíšilová, L., Komínková, M., Zítka, O., Kizek, R., Barančíková, G., Litavec, T., Lošák, T., Hlušek, J., Martensson, A. and Liptaj, T. (2015) 'Fate of humic acids isolated from natural humic substances', *Acta Agriculturae Scandinavica, Section B — Soil & Plant Science*. Taylor & Francis, 65(6), pp. 517–528. doi: 10.1080/09064710.2015.1030442.

Prat, O., Vercouter, T., Ansoborlo, E., Fichet, P., Perret, P., Kurttio, P. and Salonen, L. (2009) 'Uranium speciation in drinking water from drilled wells in Southern Finland and its potential links to health effects', *Environmental Science and Technology*, 43(10), pp. 3941–3946. doi: 10.1021/es803658e.

Puigdomenech, I. (2013) 'Hydra-Medusa Speciation Software'. Available at: https://www.kth.se/che/medusa/.

Pulford, I. D. (2010) 'Gold and Uranium', in Hooda, P. S. (ed.) *Trace Elements in Soil*. Chichester: Blackwell Publishing, JohnWiley and Sons, pp. 551–566. doi: 10.1017/CBO9781107415324.004.

Pulford, I. D. and Flowers, H. (2006a) 'Sediments - Processes', in *Environmental Chemistry at a Glance*. 1st edn. Oxford: Blackwell publishing Ltd., pp. 40–41.

Pulford, I. D. and Flowers, H. (2006b) ‘Soil Horizons and Soil Profiles’, in *Environmental Chemistry at a Glance*. 1st edn. Oxford: Blackwell Publishing, pp. 30–31.

Purmalis, O. and Klavins, M. (2012) ‘Formation and Changes of Humic Acid Properties during Peat Humification Process within Ombrotrophic Bogs’, *Open Journal of Soil Science*, 02(02), pp. 100–110. doi: 10.4236/ojss.2012.22015.

Purmalis, O. and Klavins, M. (2013) ‘Comparitive study of peat humic acids by using UV spectroscopy’, *Proceedings of the First Annual Interdiscinary Conference, AIIC*. 24-26 April, Azores, Portugal.

Ramsey, C. B. (1994) ‘Analysis of chronological information and radiocarbon calibration: the program OxCal’, *Archaeological Computing Newsletter*, 41(11), p. e16. Available at: https://c14.arch.ox.ac.uk/oxcal.html.

Ramsey, C. B. (2008) ‘Deposition models for chronological records’, *Quaternary Science Reviews*, 27(1–2), pp. 42–60. doi: 10.1016/j.quascirev.2007.01.019.

Ramsey, C. B. (2009) ‘Bayesian Analysis of Radiocarbon Dates’, *Radiocarbon*, 51(1), pp. 337–360. doi: 10.2458/azu_js_rc.v51i1.3494.

Ranville, J. F., Hendry, M. J., Reszat, T. N., Xie, Q. and Honeyman, B. D. (2007) ‘Quantifying uranium complexation by groundwater dissolved organic carbon using asymmetrical flow field-flow fractionation’, *Journal of Contaminant Hydrology*, 91(3–4), pp. 233–246. doi: 10.1016/j.jconhyd.2006.11.002.

Rashid, M. (1985) ‘Diagenetic Transformations of Humic Compounds’, in *Geochemistry of Marine Humic Compounds*. New York: Springer, pp. 188–212.

Rawlins, B., McGrath, S., Scheib, A., Breward, N., Cave, M., Lister, T., Ingham, M., Gowing, C. and Carter, S. (2012a) *The Advanced Soil Geochemical Atlas of England and*

Wales. Keyworth: British Geological Survey. Available at: http://resources.bgs.ac.uk/ebooks/AdvancedSoilGeochemicalAtlasEbook/pubData/source/Advanced Soil Geochemical Atlas of England and Wales.pdf.

Raymond, P. A and Bauer, J. E. (2001) 'Riverine export of aged terrestrial organic matter to the North Atlantic Ocean.', *Nature*, 409(6819), pp. 497–500. doi: 10.1038/35054034.

Read, D., Bennet, D. G., Hooker, P. J., Ivanovich, M., Longworth, G., Milodowski, A. E. and Noy, D. J. (1993) 'The migration of uranium into peat-rich soils at Broubster, Caithness, Scotland, UK', *Journal of Contaminant Hydrology*, 13, pp. 291–308.

Regenspurg, S., Margot-Roquier, C., Harfouche, M., Froidevaux, P., Steinmann, P., Junier, P. and Bernier-Latmani, R. (2010) 'Speciation of naturally-accumulated uranium in an organic-rich soil of an alpine region (Switzerland)', *Geochimica et Cosmochimica Acta*. 74(7), pp. 2082–2098. doi: 10.1016/j.gca.2010.01.007.

Renshaw, J. C., Butchins, L. J. C., Livens, F. R., May, I., Charnock, J. M. and Lloyd, J. R. (2005) 'Bioreduction of uranium: environmental implications of a pentavalent intermediate.', *Environmental Science & Technology*, 39(15), pp. 5657–60. Available at: http://www.ncbi.nlm.nih.gov/pubmed/16124300.

Rice, J. A. and MacCarthy, P. (1991) 'Statistical Evaluation of the Elemental Composition of Humic Substances', *Organic Geochemistry*, 17(5), pp. 635–648. doi: 10.1016/0146-6380(91)90006-6.

RIFE (1996) 'Radioactivity in Food and the Environment. Annual reports, 1 - 19, 1996 - 2014'.

Ritcey, G. (1996) 'Mining and Milling Uranium Ore', in Wilson, P. D. (ed.) *The Nuclear Fuel Cycle*. Oxford: Oxford University Press, pp. 18–40.

Ritchie, J. D. and Perdue, M. E. (2003) 'Proton-binding study of standard and reference fulvic acids, humic acids, and natural organic matter', *Geochimica et Cosmochimica Acta*, 67(1), pp. 85–93. doi: 10.1016/S0016-7037(02)01044-X.

Rodriguez, F. J., Schlenger, P. and Garcia-Valverde, M. (2016) 'Monitoring changes in the structure and properties of humic substances following ozonation using UV-Vis, FTIR and ^{1}H NMR techniques', *Science of the Total Environment*. 541, pp. 623–637. doi: 10.1016/j.scitotenv.2015.09.127.

Le Roux, G. and Marshall, W. A. (2011) 'Constructing recent peat accumulation chronologies using atmospheric fall-out radionuclides', *Mires and Peat*, 7, pp. 1–14. Available at: http://connection.ebscohost.com/c/articles/69615500/constructing-recent-peat-accumulation-chronologies-using-atmospheric-fall-out-radionuclides.

Rumble, J. (2017) 'Nuclear and Particle Physics: Table of the isotopes', in *Handbook Of Chemistry and Physics Online*. 98th edn. CRC press. Available at: http://hbcponline.com/faces/contents/InteractiveTable.xhtml?tableId=643&search=true.

Sadi, B. B. M., Wrobel, K., Wrobel, K., Kannamkumarath, S. S., Castillo, J. R. and Caruso, J. A. (2002) 'SEC-ICP-MS studies for elements binding to different molecular weight fractions of humic substances in compost extract obtained from urban solid waste', *Journal of Environmental Monitoring*, 4(6), pp. 1010–1016. doi: 10.1039/b206985g.

Sasao, E., Ota, K., Iwatsuki, T., Niizato, T., Arthur, R. C., Stenhouse, M. J., Zhou, W., Metcalfe, R., Takase, H. and Mackenzie, A. B. (2006) 'An overview of a natural analogue study of the Tono Uranium Deposit , central Japan'. *Geochemistry: Exploration, Environment, Analysis*, 6, pp. 5–12

Schaller, J., Weiske, A., Mkandawire, M. and Dudel, E. G. (2008) 'Enrichment of uranium in particulate matter during litter decomposition affected by Gammarus pulex L.',

Environmental Science and Technology, 42(23), pp. 8721–8726. doi: 10.1021/es801456q.

Schijf, J. and Zoll, A. M. (2011) 'When dissolved is not truly dissolved-The importance of colloids in studies of metal sorption on organic matter', *Journal of Colloid and Interface Science*. 361(1), pp. 137–147. doi: 10.1016/j.jcis.2011.05.029.

Schmeide, K., Sachs, S., Bubner, M., Reich, T., Heise, K. H. and Bernhard, G. (2003) 'Interaction of uranium(VI) with various modified and unmodified natural and synthetic humic substances studied by EXAFS and FTIR spectroscopy', *Inorganica Chimica Acta*, 351(1), pp. 133–140. doi: 10.1016/S0020-1693(03)00184-1.

Schnitzer, M. (1982) 'Organic matter characterization', in Page, A. L., Miller, R. H., and Keeny, D. R. (eds) *Methods of Soil Analysis, Part 2: Chemical and Microbiological Properties*. Madison Wisc.: American Society of Agronomy, pp. 581–594.

Schulten, H. and Schnitzer, M. (1993) 'A State of the Art Structural Concept for Humic Substances', *Naturwissenschaften*, 30, pp. 29–30.

Schwab, G. M. and Philinis, J. (1947) 'Reactions of Iron Pyrite: Its Thermal Decomposition, Reduction by Hydrogen and Air Oxidation', *Journal of the American Chemical Society*, 69(11), pp. 2588–2596. doi: 10.1021/ja01203a007.

Schwertmann, U. (1982) 'The Point of Zero Charge of Natural and Synthetic Ferrihydrites and Its Relation to Adsorbed Silicate', *Clay Minerals*, 17(4), pp. 471–476. doi: 10.1180/claymin.1982.017.4.10.

Scott, R. D., MacKenzie, A. B., Ben-Shaban, Y. A., Hooker, P. J. and Houston, C. M. (1991) 'Uranium transport and retardation at the Needle's Eye analogue site, South West Scotland', *Radiochimica Acta*, 52/53, pp. 357–365. doi: 10.1524/ract.1991.5253.2.357.

Scottish Natural Heritage (2017) *Citation: Upper Solway flats and marshes site of special*

scientific interest, Dumfries and Galloway. Available at: http://gateway.snh.gov.uk/sitelink/siteinfo.jsp?pa_code=1583#features.

Sellafield Ltd (2011) *Monitoring our Environment Discharges and Monitoring in the United Kingdom Annual Report 2011*. Nuclear Decomissioning Authority. Available at: http://www.sellafieldsites.com/wp-content/uploads/2012/08/Sellafield_Report_2011_800K1.pdf.

Semiao, A., Rossiter, H. and Schafer, A. (2010) 'Impact of organic matter and speciation on the behaviour of uranium in submerged ultrafiltration', *Journal of Membrane Science*, 44, pp. 174–180. doi: 10.1016/j.memsci.2009.10.056.

Settimio, L., McLaughlin, M. J., Kirby, J. K., Langdon, K. A., Janik, L. and Smith, S. (2015) 'Complexation of silver and dissolved organic matter in soil water extracts', *Environmental Pollution*. 199, pp. 174–184. doi: 10.1016/j.envpol.2015.01.027.

Sheppard, S., Evenden, W. and Anderson, A. (1992) 'Multiple assays of uranium toxicity in soil', *Environmental Toxicology and Water Quality*, 7(3), pp. 275–294.

Simpson, A. J., Kingery, W. L. and Hatcher, P. G. (2003) 'The identification of plant derived structures in humic materials using three-dimensional NMR spectroscopy', *Environmental Science and Technology*, 37(2), pp. 337–342. doi: 10.1021/es025956j.

Simpson, A. J., Kingery, W. L., Hayes, M. H., Spraul, M., Humpfer, E., Dvortsak, P., Kerssebaum, R., Godejohann, M. and Hofmann, M. (2002) 'Molecular structures and associations of humic substances in the terrestrial environment', *Naturwissenschaften*, 89(2), pp. 84–88. doi: 10.1007/s00114-001-0293-8.

Simpson, A. J., McNally, D. J. and Simpson, M. J. (2011) 'NMR spectroscopy in environmental research: From molecular interactions to global processes', *Progress in*

Nuclear Magnetic Resonance Spectroscopy, 58(3–4), pp. 97–175. doi: 10.1016/j.pnmrs.2010.09.001.

Simpson, A. J., Simpson, M. J., Smith, E. and Kelleher, B. P. (2007) 'Microbially derived inputs to soil organic matter: Are current estimates too low?', *Environmental Science and Technology*, 41(23), pp. 8070–8076. doi: 10.1021/es071217x.

Skoog, D., West, D., Holler, J. and Crouch, S. (2004) *Fundamentals of Analytical Chemistry*. 8th edn. Edited by S. Kiselica and A. White. London: Thomson, Brooks/Cole.

Smedley, P. L., Smith, B., Abesser, C. and Lapworth, D. (2006) *Uranium occurrence and behaviour in British groundwater*, *Uranium*. Keyworth. BGS Commissioned Report CR/06/050N, Available at: http://nora.nerc.ac.uk/7432/.

Sohrabi, M., Parsouzi, Z., Amrollahi, R., Khamooshy, C. and Ghasemi, M. (2013) 'Public exposure from environmental release of radioactive material under normal operation of unit-1 Bushehr nuclear power plant', *Annals of Nuclear Energy*, 55, pp. 351–358. doi: 10.1016/j.anucene.2012.12.002.

Song, K., Li, L., Tedesco, L., Clercin, N., Li, L. and Shi, K. (2014) 'Spectral characterization of colored dissolved organic matter for productive inland waters and its source analysis', *Chinese Geographical Science*, 25(3), pp. 295–308. doi: 10.1007/s11769-014-0690-5.

Sposito, G. (1998) 'On points of zero charge', *Environmental Science and Technology*, 32(19), pp. 2815–2819. doi: 10.1021/es9802347.

Steelink, C. (2002) Investigating Humic Acids in Soils. *Analytical Chemistry*, June, pp. 327 - 333

Stenson, A. C. (2009) 'Fourier transform ion cyclotron resonance mass spectral

characterization of metal-humic binding.', *Rapid Communications in Mass Spectrometry : RCM*, 23(4), pp. 465–76. doi: 10.1002/rcm.3889.

Stenson, A. C., Marshall, A. G. and Cooper, W. T. (2003) 'Exact Masses and Chemical Formulas of Individual Suwannee River Fulvic Acids from Ultrahigh Resolution Electrospry Ionization {F}ourier transform Ion Cyclotron Resonance Mass Spectra', *Analytical Chemistry*, 75(6), pp. 1275–1284.

Stevenson, F. J. (1982) *Humus Chemistry: Genesis, Composition, Reactions*. New York, Chichester, Brisbane, Toronto, Singapore: John Wiley and Sons Inc.

Stockdale, A. and Bryan, N. D. (2012) 'Uranyl binding to humic acid under conditions relevant to cementitious geological disposal of radioactive wastes', *Mineralogical Magazine*, 76(December), pp. 3391–3399. doi: 10.1180/minmag.2012.076.8.52.

Stumm, W. and Morgan, J. (1970) *Aquatic Chemistry: Chemical Equilibria and Rates in Natural Waters*. 3rd edn. Hoboken, NY, USA: John Wiley & Sons.

Sulzberger, B. and Durisch-Kaiser, E. (2009) 'Chemical characterization of dissolved organic matter (DOM): A prerequisite for understanding UV-induced changes of DOM absorption properties and bioavailability', *Aquatic Sciences*, 71(2), pp. 104–126. doi: 10.1007/s00027-008-8082-5.

Sundquist, E. T., Ackerman, K. V, Parker, L. and Huntzinger, D. N. (2009) 'An Introduction to Global Carbon Cycle Management', *Carbon sequestration and its role in the global carbon cycle*, pp. 1–23. US Geological Survey Report. doi: 10.1029/2009GM000914.

Suzuki, Y. and Suko, T. (2006) 'Geomicrobiological factors that control uranium mobility in the environment: Update on recent advances in the bioremediation of uranium-

contaminated sites', *Journal of Mineralogical and Petrological Sciences*, 101(6), pp. 299–307. doi: 10.2465/jmps.060322.

Tack, F. (2010) 'Trace Elements: General Soil Chemistry, Principles and Processes', in *Trace Elements in Soil*. 1st edn. Chichester: Blackwell Publishing, Alloway B.J (ed.) pp. 9–32.

Takala, M. and Manninen, P. (2006) *Sampling and Analysis of Groundwater Colloids – a literature review*. Working report, 2006 - 15, Posiva, Olkiluoto.

Taylor, D. and Taylor, S. (1997) 'Environmental uranium and human health', *Review of Environmental Health.*, 12(3), pp. 147–57.

Taylor, R. and Bar-Yosef, O. (2014) *Radiocarbon Dating: An Archeological Perspective*. 2nd edn. New York: Routledge.

Tfaily, M. M., Cooper, W. T., Kostka, J. E., Chanton, P. R., Schadt, C. W., Hanson, P. J., Iverson, C. M. and Chanton, J. P. (2014) 'Organic matter transformation in the peat column at Marcell Experimental Forest: Humification and vertical stratification', *Journal of Geophysical Research: Biogeosciences*, 119, pp. 661–675. doi: 10.1002/2013JG002492.

Thomson, J., Dyer, F. . and Croudace, I. W. (2002) 'Records of radionuclide deposition in two salt marshes in the United Kingdom with contrasting redox and accumulation conditions', *Geochimica et Cosmochimica Acta*, 66(6), pp. 1011–1023.

Thorn, K., Folan, D. and MacCarthy, P. (1989) Characterization of the International Humic Substances Society Standard and Reference Fulvic and Humic Acids by Solution State Carbon-13 (^{13}C) and Hydrogen-1 (^{1}H) Nuclear Magnetic Resonance Spectrometry', *Water-Resources Investigations Report 89-4196 (USGS)*, 13, p. 99.

Tierney, K. M., Muir, G. K. P., Cook, G. T., MacKinnon, G., Howe, J. A., Heymans, J. J.

and Xu, S. (2015) ‘Accumulation of Sellafield-derived radiocarbon (14C) in Irish Sea and West of Scotland intertidal shells and sediments’, *Journal of Environmental Radioactivity*. 151, pp. 321–327. doi: 10.1016/j.jenvrad.2015.10.029.

Tierney, K., Muir, G. K. P., Cook, G. T., MacKinnon, G., Howe, J. A., Heymans, J. J., Hughes, D. J. and Xu, S. (2017) ‘Ecosystem uptake and transfer of Sellafield-derived radiocarbon (14C). Part 2. The West of Scotland’, *Marine Pollution Bulletin*. 115, pp. 57–66. doi: 10.1016/j.marpolbul.2016.10.072.

Till, J. E. (2008) ‘The Radiological Assessment Process’, in Till, J. E. and Grogan, H. (eds) *Radiological Risk Assessment and Environmental Analysis*. 1st edn. Oxford: Oxford University Press, pp. 1–47. doi: 10.1093/acprof:oso/9780195127270.003.0001.

Tinnacher, R. M., Nico, P. S., Davis, J. A and Honeyman, B. D. (2013) ‘Effects of fulvic acid on uranium(VI) sorption kinetics.’, *Environmental Science & Technology*, 47(12), pp. 6214–22. doi: 10.1021/es304677c.

Tinti, A., Tugnoli, V., Bonora, S. and Francioso, O. (2015) ‘Recent applications of vibrational mid-infrared (IR) spectroscopy for studying soil components: A review’, *Journal of Central European Agriculture*. 16(1), pp. 1–22. doi: 10.5513/JCEA01/16.1.1535.

Todorov, T., Wolf, R. and Adams, M. (2014) *Multi-Elemental Analysis of Aqueous Geological Samples by Inductively Coupled Plasma-Optical Emission Spectrometry*. USGS Open File Report 2014-1067. Available at: http://dx.doi.org/10.3133/ofr20141067.

Tokarev, I., Zubkov, A. A., Rumynin, V. G., Polyakov, V. A., Kuznetsov, V. Y. and Maksimov, F. E. (2006) ‘Origin of high $^{234}U/^{238}U$ ratio in post-permafrost aquifers’, in Merkel, B. J. and Hasche-berger, A. (eds) *Uranium in the Environment : Mining impact and consequences*. Berlin, Heidelberg, New York: Springer, pp. 847–856.

Tremblay, L. B. (2006) *The ultrahigh resolution mass spectrometry of natural organic matter from different sources*. PhD Thesis, Florida State University.

Trubetskaya, O., Shaloiko, L., Demin, D., Marchenkov, V., Proskuryakov, I., Coelho, C. and Trubetskoj, O. A. (2011) 'Combining electrophoresis with detection under UV light and multiple ultrafiltration for isolation of humic fluoresence frations', *Analytica Chimica Acta*, 690, pp. 263–268.

Trubetskaya, O., Trubetskoi, O., Borisov, B. and Ganzhara, N. (2011) 'Electrophoresis and size-exclusion chromatography of humic substances extracted from detritus and soils of different geneses', *Eurasian Soil Science*, 41(2), pp. 171–175. doi: 10.1134/S1064229308020087.

Trubetskoj, O. A., Hatcher, P. G. and Trubetskaya, O. E. (2010) '1 H-NMR and 13 C-NMR spectroscopy of chernozem soil humic acid fractionated by combined size-exclusion chromatography and electrophoresis', *Chemistry and Ecology*, 26(4), pp. 315–325. doi: 10.1080/02757541003785825.

Trubetskoj, O. A., Trubetskaya, O. E., Afanas'eva, G. V., Reznikova, O. I. and Saiz-Jimenez, C. (1997) 'Polyacrylamide gel electrophoresis of soil humic acid fractionated by size-exclusion chromatography and ultrafiltration', *Journal of Chromatography A*, 767(1–2), pp. 285–292. doi: 10.1016/S0021-9673(97)00019-8.

Twardowski, M. S., Boss, E., Sullivan, J. M. and Donaghay, P. L. (2004) 'Modeling the spectral shape of absorption by chromophoric dissolved organic matter', *Marine Chemistry*, 89(1–4), pp. 69–88. doi: 10.1016/j.marchem.2004.02.008.

Tyler, G. (2001) *ICP-OES , ICP-MS and AAS Techniques Compared, Technical note 05: ICP Optical Spectroscopy*. Edison, NJ.

UNSCEAR (2008) *Sources and effects of ionizing radiation*. New York: United nations publication. Report to the General Assembly with Scientific Annexes. Official Records of the General Assembly, Sixty-third Session, Supplement No. 46. doi: 10.1097/00004032-199907000-00007.

US Department of Energy (2017) *US Department of Energy, Waste Isolation Pilot Plant*. Available at: http://www.wipp.energy.gov/index.htm (Accessed: 15 February 2017).

US National Research Council/ National Academy of Sciences (1957) *The Disposal of Radioactive Waste on Land*. Publication. Washington DC: National Research Council.

Veeramani, H., Scheinost, A. C., Monsegue, N., Qafoku, N. P., Kukkadapu, R., Newville, M., Lanzirotti, A., Pruden, A., Murayama, M. and Hochella, M. F. (2013) 'Abiotic reductive immobilization of U(VI) by biogenic mackinawite', *Environmental Science and Technology*, 47(5), pp. 2361–2369. doi: 10.1021/es304025x.

Vepraskas, M. J. and Lindbo, D. L. (2012) 'Redoximorphic Features as Related to Soil Hydrology and Hydric Soils', *Hydropedology*, pp. 143–172. doi: 10.1016/B978-0-12-386941-8.00005-8.

Vindedahl, A. M., Strehlau, J. H., Arnold, W. A. and Penn, R. L. (2016) 'Organic matter and iron oxide nanoparticles: aggregation, interactions, and reactivity', *Environmental Sciience: Nano*. Royal Society of Chemistry, 3, p. DOI: 10.1039/C5EN00215J. doi: 10.1039/C5EN00215J.

Vintró, L. L., Smith, K. J., Lucey, J. A. and Mitchell, P. I. (2000) 'The environmental impact of the Sellafield discharges', pp. 1–27.Available from: http://citeseerx.ist.psu.edu/viewdoc/download?doi=10.1.1.366.4067&rep=rep1&type=pdf

Viollier, E., Inglett, P. W., Hunter, K., Roychoudhury, A. N. and Cappellen, P. Van (2000)

‘The ferrozine method revisited : Fe(II)/ Fe(III) determination in natural waters’, *Applied Geochemistry*,15, pp. 785–790.

Viseu, M., Carvalho, F. P. and Oliveira, J. M. (2016) ‘Radioactivity and Water Quality in Areas of Old Uranium’, *Water, Air, & Soil Pollution*. 227: 252 doi: 10.1007/s11270-016-2948-2.

Vodyanitskii, Y. N. and Shoba, S. A. (2015) ‘Biogeochemistry of carbon, iron, and heavy metals in wetlands (Analytical review)’, *Moscow University Soil Science Bulletin*, 70(3), pp. 89–97. doi: 10.3103/S0147687415030072.

Waite, T. D., Davis, J. A., Payne, T. E., Waychunas, G. A. and Xi, N. (1994) ‘Uranium (VI) adsorption to ferrihydrite: Application of a surface complexation’, *Geochimica et Cosmochimica Acta*, 58(24), pp. 5465–5478.

Wallbridge, S., Banford, A. and Azapagic, A. (2012) ‘Life cycle environmental impacts of decommissioning Magnox nuclear power plants in the UK’, *The International Journal of Life Cycle Assessment*, 18(5), pp. 990–1008. doi: 10.1007/s11367-012-0534-4.

Wang, J., Liu, J., Chen, Y., Song, G., Chen, D., Xiao, T., Li, H., Wang, C. and Jiang, F. (2016) ‘Preliminary results of spatial distribution of uranium and thorium in soil profiles near a uranium industrial site, Guangdong province, China’, *Nukleonika*, 61(3), pp. 367–371. doi: 10.1515/nuka-2016-0061.

Wang, Y., Frutschi, M., Suvorova, E., Phrommavanh, V., Descostes, M., Osman, a. a. a., Geipel, G. and Bernier-Latmani, R. (2013) ‘Mobile uranium(IV)-bearing colloids in a mining-impacted wetland.’, *Nature Communications*. 4(2942), pp. 1–9. doi: 10.1038/ncomms3942.

Warren, L. and Haack, E. (2001) ‘Biogeochemical controls on metal behavior in freshwater

environments', *Earth-Sciences Reviews*, 54, pp. 261–320.

Watson, S. J., Jones, A. L., Oatway, W. B. and Hughes, J. S. (2005) *Ionising Radiation Exposure of the UK Population : 2005 Review*, *Health Protection Agency*. Oxfordshire: Health Protection Agency Radiation protection division. Report HPA-RPD-001

Weishaar, J., Aiken, G., Bergamaschi, B., Fram, M., Fujii, R. and Mopper, K. (2003) 'Evaluation of specific ultra-violet absorbance as an indicator of the chemical content of dissolved organic carbon', *Environmental Science and Technology*, 37(20), pp. 4702–4708. doi: 10.1021/es030360x.

WHO (2012) *Uranium in Drinking-water*, *Guidelines for Drinking-water Quality*. Geneva. WHO/SDE/WSH/03.04/118/Rev/1

Wilkin, R. T. (2006) *Mineralogical preservation of solid samples collected frm anoxic subsurface environments*, *Ground Water Issue*. UNited State Environmental Protection Agency, EPA/600/R-06/112

Williams, G. M., Hooker, P. J. and Brightman, M. A. (1990) *Field studies about radionuclide migration, natural analogues and faults in clays*. Commission of the European Communities Report EUR 13022

Wilson, P. D. (1996) *The Nuclear Fuel Cycle, From Ore to Waste*. Edited by W. P.D. Oxford: Oxford University Press.

Winde, F., Erasmus, E. and Geipel, G. (2017) 'Uranium contaminated drinking water linked to leukaemia - Revisiting a case study from South Africa taking alternative exposure pathways into account', *Science of the Total Environment*. Elsevier B.V., 574, pp. 400–421. doi: 10.1016/j.scitotenv.2016.09.035.

Wolstenholme, A., Mackenzie, A. B., Cook, G. T., Naysmith, P., Meadows, P. S. and

McDonald, P. (1998) ‘The Behaviour of Sellafield-Derived 14-C in the Northeast Irish Sea’, *Radiocarbon*, 40(1), pp. 447–458.

Woods, G. C., Simpson, M. J., Kelleher, B. P., Mccaul, M. and Kingery, W. L. (2010) ‘Online High-Performance Size Exclusion Chromatography - Nuclear Magnetic Resonance for the Characterization of Dissolved Organic Matter’, E*nvironmental Science and Technology*, 44(2), pp. 624–630.

Xia, K., Bleam, W. and Helmke, P. (1997) ‘Studies of the nature of Cu^{2+} and Pb^{2+} binding sites in soil humic substances using X-ray absorption spectroscopy’, *Geochimica et Cosmochimica*, 61(11), pp. 2211–2221.

Xu, X. (2013) *Uranium Associations and Migration Behaviour at the Needle’s Eye Natural Analogue Site in SW Scotland*. PhD Thesis, University of Edinburgh.

Yafa, C., Farmer, J. G., Graham, M. C., Bacon, J. R., Barbante, C., Cairns, W. R. L., Bindler, R., Renberg, I., Cheburkin, a, Emons, H., Handley, M. J., Norton, S. a, Krachler, M., Shotyk, W., Li, X. D., Martinez-Cortizas, A, Pulford, I. D., MacIver, V., Schweyer, J., Steinnes, E., Sjøbakk, T. E., Weiss, D., Dolgopolova, A and Kylander, M. (2004) ‘Development of an ombrotrophic peat bog (low ash) reference material for the determination of elemental concentrations.’, *Journal of Environmental Monitoring*, 6(5), pp. 493–501. doi: 10.1039/b315647h.

Yang, Y., Saiers, J. E. and Barnett, M. O. (2013) ‘Impact of interactions between natural organic matter and metal oxides on the desorption kinetics of uranium from heterogeneous colloidal suspensions’, *Environmental Science and Technology*, 47(6), pp. 2661–2669. doi: 10.1021/es304013r.

Yang, Y., Saiers, J. E., Xu, N., Minasian, S. G., Tyliszczak, T., Kozimor, S. A., Shuh, D. K. and Barnett, M. O. (2012) 'Impact of natural organic matter on uranium transport through saturated geologic materials: From molecular to column scale', *Environmental Science and Technology*, 46(11), pp. 5931–5938. doi: 10.1021/es300155j.

Yim, M. S. and Caron, F. (2006) 'Life cycle and management of carbon-14 from nuclear power generation', *Progress in Nuclear Energy*, 48(1), pp. 2–36. doi: 10.1016/j.pnucene.2005.04.002.

Yoshioka, S. and Kitano, Y. (1985) 'Transformation of aragonite to calcite through heating', *Geochemical Journal*, 19, pp. 245–249.

You, S.J., Yin, Y. and Allen, H. E. (1999) 'Partitioning of organic matter in soils: effects of pH and water/soil ratio', *The Science of the Total Environment*, 227(2), pp. 155–160. doi: 10.1016/S0048-9697(99)00024-8.

Zaccone, C., Lobianco, D., Shotyk, W., Ciavatta, C., Appleby, P. G., Brugia, E., Casella, L., Miano, T. M. and Orazio, V. D. (2017) 'Highly anomalous accumulation rates of C and N recorded by a relic, free-floating peatland in Central Italy',*Nature: Scientific Reports*, (February), pp. 1–10. doi: 10.1038/srep43040.

Zamora, M. L., Tracy, B. L., Zielinski, J. M., Meyerhof, D. P. and Moss, M.A (1998) 'Chronic ingestion of uranium in drinking water: a study of kidney bioeffects in humans.', *Toxicological Sciences: An Official Journal of the Society of Toxicology*, 43(1), pp. 68–77. doi: 10.1006/toxs.1998.2426.

Zech, W., Haumaier, L. and Kogel-Knaber, I. (1989) 'Changes in Aromaticity and Carbon Distribution of Soil Organic Matter Due to Pedogenesis', *The Science of the Total Environment*, 81/82, pp. 179–186.

Zhang, Y. J., Bryan, N. D., Livens, F. R. and Jones, M. N. (1997) 'Selectivity in the complexation of actinides by humic substances.', *Environmental Pollution*, 96(3), pp. 361–7. Available at: http://www.ncbi.nlm.nih.gov/pubmed/15093402.

Zhou, P. and Gu, B. (2005) 'Extraction of oxidized and reduced forms of uranium from contaminated soils: Effects of carbonate concentration and pH', *Environmental Science and Technology*, 39(12), pp. 4435–4440. doi: 10.1021/es0483443.

Zoppi, U., Skopec, Z., Skopec, J., Jones, G., Fink, D., Hua, Q., Jacobsen, G., Tuniz, C. and Williams, A. (2004) 'Forensic applications of ^{14}C bomb-pulse dating', *Nuclear Instruments and Methods in Physics Research, Section B: Beam Interactions with Materials and Atoms*, 223–224(SPEC. ISS.), pp. 770–775. doi: 10.1016/j.nimb.2004.04.143.